THE IMPACT OF MICROBIAL CHELATES ON MINERAL WEATHERING AND MICROBIAL METABOLIC ACTIVITY

by
Ezra Kulczycki

A thesis submitted in partial fulfillment
of the requirements for the Doctor of
Philosophy degree in geology
in the Graduate College of
The University of Kansas

May 2010

Thesis Committee:

_____

Jennifer A. Roberts, Thesis Supervisor

_____

David A. Fowle

_____

G. L. Macpherson

_____

Stephen T. Hasiotis

_____

William C. Johnson

Date Defended: _____

Graduate College
The University of Kansas

CERTIFICATE OF APPROVAL

PH.D. THESIS

This is to certify that the Ph.D. thesis of

Ezra Kulczycki

has been approved by the Examining Committee
for the thesis requirement for the Doctor of Philosophy
degree in geology at the May 2010 graduation.

Thesis Committee:

Jennifer A. Roberts, Thesis Supervisor

David A. Fowle

G. L. Macpherson

Stephen T. Hasiotis

William C. Johnson

Date Approved: _____

ACKNOWLEDGMENTS

Upon completion of my PhD I wish to acknowledge those who have helped me along the way. First off, my sincere thanks and appreciation goes to my advisor, Jennifer A. Roberts, for all of her support and guidance. In addition to raising the bar and challenging me to be a better scientist, she has effectively led by example how to succeed in Academia. Secondly, I wish to acknowledge David A. Fowle for the valuable expertise and resources provided to me. Thirdly, the remaining members of my committee, Gwendolyn L. Macpherson, Stephen T. Hasiotis, and William C. Johnson deserve thanks for their efforts. All have challenged me to attain a higher standard of scholastics, which I am grateful for. In addition, I must thank my collaborators, who played a key role in several publications, of which include David W. Graham and Charles W. Knapp. The funding to support my research was provided by multiple sources, which includes NSF Biogeosciences (EAR 0433980 awarded to Roberts and Graham), NSF Low Temperature Geochemistry and Geobiology (EAR 0750009 awarded to Fowle, Roberts and Graham), and the KU Geology Associates (Fowle).

In addition, I wish to thank the members of my lab group who have shared in the pursuit of knowledge or supported me with research efforts. In some cases there were components of my dissertation could not be completed without the assistance of my peers in the lab. Certainly the opportunity to bounce ideas, consult on technical issues, and blow off steam down at the pub was much appreciated. Deserving of mention includes the following: Paul Kenward, Arne Sturm, Karla Leslie, and Melissa Marietta. This acknowledgment should also be extended to the friends I made at KU outside of the lab. What a tremendous experience my time in Lawrence has been! For all of the great memories, Kansas will always occupy a special place in my heart.

And of course, I must thank my family for all of their patience and moral support along the way.

ABSTRACT

Ezra Kulczycki, PhD

Department of Geology, June 2010

University of Kansas

Geological materials are composed of elements, which can be released into the environment by dissolution or desorption processes and directly impact the metabolic activity of microorganisms. If subjected to environmental stress, microorganisms can adapt by applying unique strategies to safeguard their survival or perpetuate their ecological role in a given habitat. Microbial chelate production improves the chances of obtaining key metals that regulate enzymatic activity. In this dissertation, geochemical controls such as mineral solubility and desorption of nutrients from clays are examined with respect to their influence upon metabolic activity. In turn, the impact of microorganisms upon mineral weathering is investigated with respect to mineral composition and cellular design. A relationship between geologic host materials and biological activity is purported.

The role of microorganisms upon mineral weathering was investigated by collecting soil samples from the tropical rainforest of Barro Colorado Island, Panama. Microorganisms can utilize specific chelating agents to mobilize metals of nutritive benefit, i.e., siderophores for Fe^{3+} (*Pseudomonas putida*), and methanobactin for Cu (*Methylosinus trichosporium* OB3b). Enhanced Fe^{3+} solubility from minerals of a Panamanian soil was demonstrated in abiotic and biotic microcosms supplemented with the siderophore, desferrioxamine. Similarly, Cu and SiO_2 solubility was enhanced by methanobactin in increasing concentrations, provided that Cu was present in the mineral

phase. To evaluate the vital effect upon Cu leaching from mineral sources, rates of mineral weathering were compared with rates of CH_4 oxidation in the presence of *Methylosinus trichosporium* OB3b. The results indicate that methanotroph activity is sensitive to variations in solid phase Cu concentration provided that Cu is being made bioavailable. A final study investigating how NH_4^+ and Cu desorption from montmorillonite impacts methanotrophy showed that rates of CH_4 oxidation were inhibited by the release of these nutrients in excess amounts.

Microorganisms are sensitive to a diverse assortment of geological materials provided that key nutrients such as Fe, Cu or inorganic-N are present and made bioavailable by mineral dissolution or desorption processes. The efficiency of enzyme activity is controlled by both mineral composition and surrounding geochemical processes. In addition, microorganisms actively participate in the promotion of metal solubility from mineral sources. The findings of this dissertation illustrate that biological and geochemical processes are tied together and are responsible for driving metal cycling in soil environments. Furthermore, a novel linkage between mineral weathering and carbon cycling is revealed, and hinges upon the activity of methanotrophs and their requirement for Cu.

TABLE OF CONTENTS

LIST OF TABLES

LIST OF FIGURES

CHAPTER 1

INTRODUCTION

This study examines the linkage between geochemical processes and biological activity with a focus on microbial weathering and the release key nutrients. A number of insoluble phases contain elements of nutritional value and only become bioavailable in the aqueous phase. Microorganisms also benefit from desorption of surface–sorbed nutrients, which are less available in when sorbed. Not only do microorganisms benefit from weathering processes that promote the bioavailability of chemical elements they also can directly influence these reactions. Colonization and attachment of microorganisms to the surface of the mineral allows them to exert a direct influence upon the solubility of target metals (Bennett et al., 1996, 2001). In soils, a diverse set of specific niches may exist where the community of microorganisms that is colonizing a rock's surface will be different from the inhabitants of the surrounding soil (Certini et al., 2004). Attachment to mineral surfaces is critical because a microenvironment that protects the bacteria against environmental stresses is created during the formation of a biofilm (Beveridge et al., 1997; Liermann et al., 2000; Ojeda et al., 2008). Within these microenvironments, inorganic nutrients can be extracted directly from the mineral matrix as well as being shared amongst the surrounding microorganisms (Bennett et al., 2001; Brown et al., 1994; Roberts Rogers et al., 2001; Roberts Rogers and Bennett, 2004; Rogers et al., 1998). Select microorganisms have evolved unique strategies to release metals and nutrients from typically insoluble phases and in this study the focus will be

upon the impact of microbial chelates upon mineral weathering and desorption of surface-sorbed phases.

Siderophores are Fe(III) chelating compounds with the capability of promoting mineral weathering, e.g., hydroxamates or catecholates. In pH neutral or alkaline environments, the microbial depency upon siderophores to deliver Fe^{3+} to the cell becomes heightened as Fe(III) is generally insoluble under these conditions and occur as iron oxyhydroxide minerals. With a high affinity and specificity for Fe(III) complexation, siderophores provide a highly efficient Fe acquisition system by means of mineral dissolution (Kraemer, 2004). An important setting for siderophore promoted iron dissolution is in the tropics where the soils are enriched in insoluble iron oxide and clay silicate mineral phases. However, siderophores are not the only active microbial chelate to be found in tropical soils nor is Fe the only metal of nutritive value to microorganisms. Copper mobility as influenced by methanobactin may be critical for sustaining methanotroph activity in the tropics. In this study, a novel linkage between mineral weathering and carbon cycling is investigated, and hinges upon the metabolic requirement for Cu by methanotrophs.

Copper is essential for the activation of key enzymes involved in biological CH_4 oxidation, e.g., soluble and particulate methane monooxygenase (sMMO and pMMO, respectively). If Cu availability is limited to insoluble phases, methanotrophs must find a way to release the Cu into solution. A novel acquistion system has been recognized in a Cu-chelating molecule called methanobactin, which is thought to be the linkage that drives methanotroph promoted mineral weathering. Since methanobactin has a high affinity for Cu ($\log K > 18$, Choi et al., 2006), the chelation of Cu by methanobactin has

been compared with siderophores and Fe(III) coordination (Balasubramanian and Rosenzweig, 2008; Hakemian et al., 2005; Kim et al., 2004). Siderophores have been demonstrated to promote mineral weathering during the formation and detachment of a surface complex with Fe(III) (Holmen and Casey, 1996; Kalinowski et al., 2000; Kraemer, 2004) and consequently, the role of methanobactin is being examined as a Cu-trafficking molecule with the capability of enhancing the rates of mineral weathering reactions. A direct linkage between rates of Cu solubility and rates of CH_4 oxidation by methanotrophs is implied. In addition, microorganisms such as methanotrophs may rely upon desorption processes from clay minerals during periods of inundation, which has profound implications regarding the cycling of nutrients in a tight niche environment.

The dissertation is written in eight chapters including this introduction as chapter 1. The second chapter introduces the field setting of the tropical rainforest on Barro Colorado Island (BCI), Panama, which provides an ideal opportunity to examine the role of siderophores as an Fe(III) acquisition system in soils enriched in insoluble Fe-containing minerals. Batch reactors are used to examine microbially promoted and siderophore-promoted mineral weathering mechanisms in terms of their impact upon the release of Fe and other elements.

Chapter 3 provides a background on methanotroph ecology. Similar to siderophore generating microorganisms, some methanotrophs will generate a chalkophore called methanobactin to traffic Cu back to the cell (Kim et al., 2004). The common practice of relying upon ligands to solubilize metals of nutritive benefit is investigated. This chapter establishes the presence of methanotrophs and methanobactin in the soils of BCI, and extends the relevance of both to any other natural setting.

Chapter 4 was originally published in Geobiology (Kulczycki et al., 2007) and examines methanobactin-promoted dissolution kinetics of manufactured silicate glass. Generally, the results of this investigation demonstrate that higher rates of weathering are associated with increasing methanobactin concentration. However, rates of weathering are inhibited high concentrations of methanobactin, especially with high Cu concentrations in the glass, which results in an increase in methanobactin sorption to the glass surface.

Chapter 5 was published in the Geomicrobiology Journal (Kulczycki et al., 2010) and examines the stimulation of methanotroph activity by Cu in synthetic silicate glass. A direct relationship between the Cu content of silicate glasses and rates of CH_4 oxidation by *M. trichosporium* OB3b is demonstrated. Consequently we can predict how efficiently methanotrophs will mitigate the flux of CH_4 from geologic settings according to the Cu content of the minerals present.

A more detailed presentation of the weathering data linked with the methanotroph stimulation study is provided in Chapter 6. In addition to Cu release, the solubility of other metals such as Al is enhanced by the presence of the microbial cells. Biophysical processes are thought to drive the flux of metals from the silicate glass by lowering solution saturation levels during uptake of metals onto the reactive cell wall.

In the environment, Cu is not the only influence on methanotroph metabolism. Methane oxidation rates are impacted by concentrations of dissolved oxygen, copper, pH and NH_4^+ (Graham et al., 1993; Hanson and Hanson, 1996; King and Schnell, 1994; Schnell and King, 1995). Chapter 7 provides background on the co-oxidation of CH_4 and NH_4^+ by methanotrophs, where competitive utilization of the key enzyme, pMMO, is

attributed to the inhibition of CH_4 oxidation that commonly occurs (King and Schnell, 1994; Schnell and King, 1994). Chapter 8 examines the impact of nutrient flux upon methanotrophy with a particular focus upon desorption of Cu and NH_4^+ from montmorillonite.

Collectively, the chapters of this dissertation show how geochemical processes can influence the activity of microorganisms and vice versa with broader implications for nutrient and carbon cycling in the environment. The mobilization of nutrients (e.g., Cu or Fe, etc.) can enhance the metabolic activity of microorganisms, which may result in the mitigation of greenhouse gases, such as CH_4, when methanotrophs are present. Microbial production of chelating agents provides a competitive advantage over other species particularly if direct contact or close proximity with the nutrient source is maintained (i.e., the mineral). As in the example of methanotrophs, the success of this species over others will promote continued leaching of Cu from minerals due to the vital effect associated with biological CH_4 oxidation. With the quantitative evidence for how solid phase Cu impacts methanotroph activity, we can use information pertaining to mineral sources of Cu (e.g., concentration, solubility, etc.) to predict the kinetics of CH_4 oxidation.

CHAPTER 2

SIDEROPHORE-PROMOTED MINERAL WEATHERING IN PANAMANIAN SOILS

ABSTRACT

This study provides a comparative analysis of abiotic and biotic mineral weathering processes in tropical soils. In many environments microorganisms rely on trace elements from minerals to support their nutrient demands. In highly weathered soil environments, nutrients are scarce in solution and their bioavailability from the mineral phase is limited, therefore, microorganisms may adapt by promoting the solubility of minerals in order to access the nutrients that are key to their survival. In circum-neutral pH conditions, microorganisms are often dependent upon ligand-promoted mechanisms of metal release. Fe acqusition from and weathering of Panamanian oxisols from Barro Colorado Island were investigated utilizing *Pseudomonas putida*, a siderophore-generating bacterium and the siderophore desferioxamine mesylate (DFAM) under acidic and neutral pH conditions. Iron release was enhanced by both *P. putida* and DFAM. The primary mechanism of mineral weathering was the formation and detachment of an Fe(III)-DFAM complex at the mineral surface. From a biophysical standpoint, the anionic surface functional groups that compose the outer cell wall membrane of *P. putida* can partition metals and generate a steeper ion gradient between the mineral and solution. The consequential decrease in solution saturation levels that heightens the disequilibrium between the water-rock interface may represent an additional mechanism of microbially promoted mineral weathering. This study illustrates how microorganisms cope under

nutrient limited conditions by enhancing the solubility of minerals and metals to release metals essential for metabolism.

INTRODUCTION

In warm and humid climates such as the tropics, highly weathered soils predominate. The accumulation of weathering byproducts in shallow sloping terrains often results in the formation of deep soil profiles. The depth of many tropical forested soils may be more than several meters because erosive processes such as glaciations have not disturbed the pedogenesis in these locations for several millions of years (Birkeland, 1999). These soils are also subject to extensive removal of cations and silica (SiO_2) from the soil profile as a result of the long period of uninterrupted weathering (White et al., 1998).

Silicon removal from tropical soils is more pronounced relative to other climate regimes due to high annual mean temperatures and rates of precipitation. Only primary silica minerals of low solubility will remain, i.e., quartz (Schlesinger, 1997). The typical mineral components of these soils are clay minerals and oxide minerals, and highly resistant primary minerals. Oxisols, typical of the soils found in tropical rainforests, are abundant in clay-size particles dominated by iron and aluminum oxides, and represent the most highly weathered soils in the 12-order classification system (Brady and Weil, 2002). While the abiotic processes that contribute to mineral weathering in tropical soils are widely accepted, the role of microorganisms needs further examination.

Bioavailability of Fe, and the role of Siderophores

Iron is a key nutrient for most living organisms, including a wide variety of microorganisms. Depending upon the redox conditions, iron will either donate or accept electrons via chemical reactions that help to sustain the energy requirements of local opportunistic microorganisms (Widdel et al., 1993; Hersman et al., 2000). The cycling of electrons may often be linked to mineral dissolution processes (Vorhies and Gaines, 2009). Reductive dissolution of minerals containing ferric iron (Fe-III) is a common process that contributes to Fe solubility in anoxic environments, where microorganisms can use ferric iron oxyhydroxide minerals as electron acceptors for the respiration of organic carbon compounds (Ehrlich, 1996; Bridge and Johnson, 1998; Santelli al., 2001). However, the solubility of Fe(III) bearing minerals (i.e., iron oxides) is generally low at aerobic, neutral pH conditions (Stumm and Morgan, 1996; Drever, 1997; Cornell and Schwertmann, 2003). Solubility products for Fe(III)-oxides under these conditions range from 10^{-44} to 10^{-39} (Schwertmann and Cornell, 1991), which limits the aqueous equilibrium concentration of Fe^{3+} to ~10^{-17} M (Russell et al., 1974). Under these conditions Fe may not necessarily be bioavailable and microorganisms must accommodate for its low availability (Leong and Neilands, 1976).

To enhance Fe(III) bioavailability in organic carbon-rich environments, a number of bacteria and fungi secrete organic molecules called siderophores that are capable of forming stable aqueous complexes with ferric iron (Loper and Henkels, 1999). The term siderophore comes from the Greek meaning “iron bearer” and denotes Fe(III)-specific ligands that are produced by aerobic microorganisms that grow under low iron concentrations (Neilands, 1995). Siderophores are much more effective at binding Fe(III)

in soils than low molecular weight organic acids (Kalinowski et al., 2000). Perrin (1979) reported association constants of oxalic and citric acids with Fe^{3+} to be $10^{7.6}$ and $10^{17.3}$, respectively. In general siderophores bind Fe^{3+} to form 1:1 complexes with formation constants that range from 10^{25} to 10^{35} (Hersman et al., 1995; Hider, 1984; Hughes and Poole, 1989; Kalinowski et al., 2000; Konhauser, 2007; Neilands, 1982; Page, 1993; Winkelmann, 1991). Generally, higher formation constants occur with increasing number of denta in siderophore-Fe(III) complex (Page, 1993).

There are two general groups of siderophores that include hydroxamates (from fungi and bacteria) and catecholates (from bacteria) (Kalinowski et al., 2000). Other types include carboxylates and pyoverdins. The desferrioxamine mesylate (DFAM) form used in this study is the methane sulfonate form of the hydroxamate siderophore desferrioxamine B (DFO-B) (figure 2.1). Hydroxamic acid is the functional group in hydroxamates and consists of a carbonyl oxygen combined with an amino group, which singly chelates Fe(III) to form a bidentate complex (figure 2.2a, from Kalinowski et al., 2000). Hexadentate 3:1 complexes are formed if a sufficient number of siderophores are available, and are associated with higher binding constants (as high as 10^{52}, Hersman et al., 1995; Hider, 1984; Hughes and Poole, 1989; Kalinowski et al., 2000; Konhauser, 2007; Winkelmann, 1991). When reacting trihydroxamate siderophores such as deferriferrioxamine with an iron oxide, only one Fe(III) center can be coordinated at a time (Cocozza et al., 2002).

The occurrence of siderophores is ubiquitous to soil and marine environments of circumneutral pH where the presence of ferric iron is typically limited to insoluble phases, i.e., oxides, oxyhydroxides and amorphous iron hydroxides (Kraemer, 2004). In

some cases, siderophores will promote the weathering of iron oxides by forming a surface complex with Fe^{3+}, which then detaches and is released into solution (Holmen and Casey, 1996; Kraemer, 2004). This process has important implications for the release and mobilization of micronutrients (such as P) as well as toxic trace elements from iron oxides in these soil regimes (Wichard et al., 2009; Kraemer; 2004; Markwiese and Colberg, 2000; Nair et al., 2007). Few studies have elucidated the mechanism(s) by which microorganisms obtain Fe in aerobic soil environments. However, some microorganisms generate pH gradients, or synthesize chelating ligands and polymeric materials, which may prove to be very important in the mobilization of these traditionally unavailable sources of major and trace nutrients (Brantley et al., 2001).

Once the siderophore has formed a complex with Fe^{3+} and the complex has detached from the mineral surface, it then becomes bioavailable. The Fe(III)-siderophore complex is taken up by the cell membrane of the bacteria where the Fe is reduced, released from the siderophore and transported into the cell (figure 2.2c, from Kalinowski et al., 2000; Liermann et al., 2000). The siderophore is either recycled or destroyed upon reduction (Kalinowski et al., 2000), and the reduced iron (Fe^{2+}) can act as an electron donor in electron transport chains (reproducing Fe(III) as an insoluble hydrous oxide or oxyhydroxide precipitate, e.g., secondary minerals such as hematite, Fe_2O_3; and goethite, FeO(OH) or mineraloids such as ferrihydrite, $Fe_2O_3.9H_2O$, provided that the pH remains circum-neutral).

Bacteria

Native microbial communities are capable of enhancing the weathering of minerals in a variety of environmental settings (Barker et al., 1998; Banfield et al., 1999; Welch and Ullman, 1999; Bennett et al., 2001; Maurice et al., 2001; Edwards et al., 2004; Neaman et al., 2005). The bacterium *Pseudomonas putida* chosen for this study is a gram-negative rod that inhabits a variety of soil and water environments. The cell wall of bacteria is composed of multiple anionic surface functional groups that are highly reactive toward cations (Beveridge, 1989; Beveridge and Graham, 1991; Beveridge, 1999; Shockman and Barrett, 1983; Langley and Beveridge, 1999), hence, the mobility of cations in soil environments is influenced by the mere presence of bacteria. In addition to possessing reactive cell wall components that protect the cell from toxic exposure, *Pseudomonas putida* will generate siderophores under conditions of limited ferric iron availability (Sher and Baker, 1982).

Bacteria may mediate mineral weathering reactions in a variety of ways (e.g., acid-base, redox, and ligand contributions) depending on the microbial community present and the geochemical setting (Barker et al., 1998; Banfield et al., 1999; Welch and Ullman, 1999; Bennett et al., 2001; Maurice et al., 2001; Welch and McPhail, 2003; Edwards et al., 2004; Neaman et al., 2005). For example, mineral weathering is often promoted during colonization and biofilm accumulation on mineral surfaces due to the formation and concentration of metabolic products, e.g., organic and inorganic acids (Welch and Ullman, 1993; Ullman et al., 1996; Ehrlich 1998; Banfield et al., 1999; Welch et al., 1999; Liermann et al., 2000; Welch and McPhail, 2003; Ehrlich, 2006). Cations are released during acidolysis of minerals as the protons associated with the

organic or inorganic acids lower the pH of the microenvironment solution. In other instances, oxidative or reductive dissolution might be the dominant weathering mechanism responsible for weakening chemical bonds at the mineral surface that allows microbes to access nutrients bound within (e.g. Fe, P, and trace elements) (Widdel et al., 1993; Vandevivere et al., 1994; Emerson and Moyer 1997; Bridge and Johnson, 1998; Ehrlich, 1998; Hersman et al., 2000; Brantley et al., 2001). In these circumstances, direct contact of the microbial membrane with the mineral surface is required for oxidoreduction reactions to occur unless the microbe is capable of electron cycling by use of exocellular nanowire appendages (Gorby et al., 2006). In addition, mineral dissolution is promoted in response to the microbial generation of ligands that specifically bind with ferric iron and liberate it from the mineral as an activated Fe(III)-ligand complex (Holmen and Casey, 1996; Hersman et al., 2000; Roberts Rogers et al., 2001; Kraemer, 2004). In general, chelating molecules will enhance mineral dissolution rates by forming strong bonds with cations at the mineral surface.

When microbes such as *P. putida* need to obtain iron for metabolic processes, they regulate siderophore production according to the iron availability in the soil environment (Kalinowski et al., 2000). Under conditions, as in this study, where siderophores are readily available, the microbes will cease siderophore production and utilize the existing siderophores in the surrounding environment. For example, Winkelmann (1991) showed that some species of *Arthrobacter* rely on a consortium of other siderophore-producing bacteria to obtain iron because they do not produce siderophores of their own.

A common consequence of mineral weathering is the release of major and trace elements that may either satisfy the nutritional needs of the local microbial community (Rogers et al., 1998; Bennett et al., 2001; Roberts Rogers et al., 2001; Roberts Rogers and Bennett 2004; Uroz et al., 2009) or trigger a toxic response if the quantity released exceeds acceptable concentrations (Bååth, 1989; Hiroki, 1992; Rajapaksha et al., 2004; Oliveira and Pampulha, 2006; Schaider et al., 2007). On a larger scale, the flux of elements from the dissolving minerals over geological time scales may evoke bulk geochemical perturbations (Berner et al., 1983; Berner, 1995).

The role of soil microorganisms as contributors to mineral weathering is essential for ecological sustenance, particularly in an environment such as a humid tropical forest where phosphorus is most often the limiting nutrient (Bala Krishna Prasad and Ramanathan, 2009). The limited supply of PO_4^{3-} in tropical soils (i.e., oxisols) is often made unavailable as it becomes tightly bound to the iron and aluminum oxides that predominate (Agbenin, 2003; Schwertmann and Herbillon, 1992; Tate and Salcedo, 1988). Hence, mineral weathering linked with phosphorus solubility becomes an essential mechanism for promoting the bioavailability of phosphorus (Tate and Salcedo, 1988). Whether microorganisms enhance mineral weathering deliberately to release valuable nutrients or if this is something that occurs indirectly in response to microbial activity is not entirely clear. Regardless, the degree to which microorganisms contribute to mineral weathering needs to be quantified to understand how biological activity can impact the mobilization of nutrients from mineral sources in tropical soils.

Increased biomass is related to nutrient availability (P, Fe, etc.) therefore, the microbial weathering of minerals likely results from nutrient scavenging (Roberts Rogers

and Bennett, 2004). Microorganisms will often release extracellular organic ligands (Welch et al., 1999) in order for their physiological functions to benefit from the mineral content (Barker et al., 1998; Bennett et al., 2001). Iron and other essential metallic elements may be solubilized for acquisition and utilization in the synthesis of metalloenzymes and other biomolecules (Kalinowski et al., 2000). The beneficial uptake of metal associated anions, e.g., phosphate, may coincide with these organic ligand driven dissolution processes (Rogers et al., 1998). Ferric iron and other oxidized forms of metallic elements are also solubilized for use as terminal electron acceptors (Kalinowski et al., 2000; Kraemer, 2004). Furthermore, the cell wall precipitates that impede nutrient transport or adsorb nutrient elements may be dissolved by extracellular organic ligands to benefit the physiological function of the cell (Stone, 1997). In contrast, toxic metals such as aluminum can exert an inhibitory effect upon microbial surface colonization, thus limiting any microbial weathering influences (Roberts Rogers and Bennett, 2004).

A symbiotic relationship exists between microorganisms and plants that hinges upon nutrient cycling and mineral solubility. As plants require cations such as PO_4^{3-}, Ca^{2+}, Mg^{2+}, and K^{+} for survival, their success is dependent upon the bioavailability of these nutrients. Plants are forced to rely on soil mycorrhizae and bacteria to promote mineral weathering in order to obtain nutrients from otherwise recalcitrant sources. While this dependency is common in most soil habitats, the extent to which plants rely upon microorganisms as agents of nutrient delivery is most critical in the tropics compared to other climates. Hence, the health of the microorganism becomes critical to the health of the plant, and the rainforest itself (Schwertmann and Herbillon, 1992).

The broad goal of this study was to address the influence of siderophore-promoted dissolution of natural iron oxides and concomitant release of trace elements. In particular, *Pseudomonas putida,* a microorganism known to generate siderophores, was investigated to assess its ability to promote the weathering of iron-rich minerals from a Panamanian soil as a function of pH, and in the absence of phosphorus. Macro- and micronutrients were monitored to see if microbial interactions with the solid phase lead to their release under initially nutrient-limited conditions in solution.

Field Setting

The soil samples for this study were collected from a site on Barro Colorado Island (BCI), Panama. The island is one of several, centrally located within the Panama Canal watershed, where Lake Gatun was created in response to the damming of the Chagres River in 1914 (figure 2.3). The island is 1,500 ha in area with the highest elevation at 164 m above sea level (Dietrich et al., 1996). Vegetation on the island is dominantly tropical, semideciduous moist forest. One hundred year-old regrowth forests that were cleared by the French during construction of the Panama Canal cover nearly half of the island (Dietrich et al., 1996), the other half has remained relatively undisturbed for as much as 200 to 400 years (Foster and Brokaw, 1996). In the interests of maintaining a biological inventory, BCI was declared a preserve in 1923 and has been protected under the supervision of the Smithsonian Tropical Research Institute since 1946 (Leigh, 1996). Since that time, the island has predominantly been used for biological and ecological research.

The annual climate data report on BCI for the year of 2005 indicates that the average daily maximum temperature was 28.3^{o}C and the total rainfall accumulation was 2419.8 mm (Paton, 2005). The meteorological year on BCI is divided into two seasons, a pronounced dry season that extends from mid-December to the end of April and a wet season that extends from May to mid-December. Total accumulated dry season precipitation for 2005 was 289.9 ± 173.8 mm while the total accumulated precipitation during the wet season was 2332.1 ± 380.3 mm (Paton, 2005). Relatively little variation in temperature is observed on BCI throughout the year.

The geology of this area consists of basaltic volcaniclastics, basaltic and andesitic lava flows, and marine sediments (Woodring, 1958). The age of the igneous rocks of this area are Oligocene to Miocene (Dietrich et al., 1996). The Bohio and Caimito Formations consist of flat-lying sedimentary rocks that have been capped by the younger volcanic andesite (Johnson and Stallard, 1989). The Bohio Formation is early Oligocene in age, and is exposed on the northwestern coast (including the sampling location, near the Miller lighthouse) and in the central part of BCI. Overlying the Bohio Formation is the Caimito Formation, which is late Oligocene in age and is divided into “marine” (southwest BCI) and “volcanic” facies (eastern BCI). Basalts and intruding andesitic dikes can also be found throughout the island, particularly in the Bohio Formation and the “volcanic” facies of the Caimito Formation (Johnson and Stallard, 1989). Recent tectonic activity (Pliocene epoch) is responsible for the rugged topography and diverse parent material on BCI. In fact it was only 3.5 million years ago that the Isthmus of Panama had formed a land bridge connecting the Americas (Coates et al., 1992).

The soil types on BCI differ in response to parent material (bedrock) and local geomorphology, resulting in a series of alternating sequences characteristic of a soil catena (Birkeland, 1999). On the steeper terrains, kaolinitic clays predominate with subordinate smectites (Baillie et al., 2007; Dietrich et al., 1996). Stony brown loams of shallow depths (< 1 m to saprolite) characterize the soils, which is suggestive of incomplete weathering in response to erosion (Baillie et al., 2007). On the terrains with gentler topography, kaolinitic clays and ferric sesquioxides predominate with subordinate gibbsite (Baillie et al., 2007; Dietrich et al., 1996). These soils are highly weathered with extensive red silty clays and clays that reach depths beyond 2 m (Baillie et al., 2007). Soil pedogenesis varies dramatically in flat versus steep terrains (Stallard, 1985). On gentler slopes where erosion is minimized, more extensive soil development is favored (Dietrich et al., 1996).

The soils in the flatter areas of BCI are generally much thicker and classified as oxisols as opposed to the thinner alfisols found along the steeper slopes. However, local variations in soil classes are common throughout (figure 2.4). The oxisols are abundant in kaolinite and Fe and Al oxide minerals while the alfisols have more base cations and a greater proportion of montmorillinite (Leigh, 1999). Saprolites can be found at greater depths within the C-horizon and are composed of a matrix of smectite, kaolinite, and Al and Fe sesquioxides that surrounds grains of quartz, plagioclase, magnetite, and ortho and clinopyroxene (Johnson and Stallard, 1989).

Gentle sloping terrain with a deeper impermeable layer can yield relatively sluggish saturated hydraulic conductivity (K_s) compared to steep gradient topography (Godsy et al., 2004). Such conditions favor longer pore water residence times and cause

the dissolved constituent concentrations to increase in response to mineral dissolution. The gentle topography of the soil sample location on Barro Colorado Island consists of thick deeply weathered soils characteristic of transport-limited settings (Johnson and Stallard, 1989).

METHODS

Field site description

Soil samples for this study were collected during the dry season (March 2005) from a forested site located on the northwest side of the island near the Miller lighthouse (9° 10'N, 79°51'W, 81 m above sea level, figure 2.5). The forest at the sampling collection site is a tall, young forest with an age ranging between 125 to 200 years (Foster and Brokaw, 1996). Topography at this site has narrow, gently sloping (9^{o}) ridges (Dietrich et al., 1982). The underlying parent material represents an exposed portion of the Bohio Formation, which contains basaltic clast conglomerates in a sandy volcaniclastic matrix (Woodring, 1958). The clast size ranges from 5 to 50 cm in diameter and consists of basaltic andesite (52-57 SiO_2 wt%) (Le Bas, 2000) with phenocrysts composed of plagioclase, hornblende or clinopyroxene (Wilson, 2005). The poorly sorted sandy matrix is made up of a mixture of rounded, altered volcanic lithic fragments, angular plagioclase, and minor amphibole and magnetite (Wilson, 2005). The soils of the Miller Forest are yellow-brown in color, less than 150 cm thick, and overly a layer of saprolite composed of boulder-sized chunks of fresh bedrock and thin weathering rinds. While the soils contain the occasional fresh gravel-sized rock, they are predominantly rich in clay (Dietrich et al., 1982).

There were numerous reasons for choosing this site location to collect samples from, which includes the following: (1) The site is a biological reserve, and has remained protected for nearly a century, (2) bedrock is of known composition (basaltic conglomerates), (3) surface vegetation is distinct and well defined, (4) limited topographic relief, which minimizes the effects of soil erosion (5) extensive soil

characterization has been performed on previously collected samples throughout the depth profile, e.g., soil moisture, particle size, organic matter, mineralogy, soil pH, total lipid biomass, extractable metals (major, trace, and rare earth elements, Wilson, 2005), and whole soil analysis (Wilson, 2005).

A trench was dug to collect soil samples since the clay proved to be inaccessible beyond 0.3 m when using the piston corer. Soils were examined using Munsell soil color charts (Munsell Color, 1994), hand texturing, and visual examination for root depth and structure characterization. The Munsell soil color chart encodes a hue with a letter abbreviation, e.g., YR – yellow red, and value with a number and chroma being the last number (i.e., for the sample collected at 65-70 cm depth, 7.5YR 4/6 is 7.5 hue (yellow red) value/chroma). A value of 0 represents absolute black while a 10 represents absolute white. Samples were collected from each soil horizon with modified 50-ml sterile syringes, which were used as horizontal mini-core devices. To prevent cross-contamination and maintain sterility, nitrile gloves were worn by sample-collectors and extraction equipment was cold-sterilized with ethanol prior to collection. Mini soil cores were placed in sterile sampling bags and returned to STRI where they were stored at -80^{o}C until being shipped to the Great Lakes Institute for Environmental Research (GLIER), University of Windsor, for continued storage at -80^{o}C. Some samples were shipped to the Department of Geology, University of Kansas, for microbial community structure analysis.

Sampling methods

The soil samples from the depth interval of 65-70 cm was selected because it represents a fraction from the C-horizon where the regolith had weathered in place and was rich in relatively insoluble iron oxides and silicate clays. In preparation for batch reactivity experiments, the soil size fraction was constrained between 75-212 μm by sieving and was then lyophilized for 24hrs (Modulyo D Thermo Savant freeze drier). Once dried, the soils were sterilized according to the chloroform technique (Kjoller et al., 2001) to remove activity of native microorganisms. The bulk mineral content of the soil sample was confirmed by X-ray diffraction (XRD) at the University of Windsor, Department of Earth Sciences using a Rigaku MiniFlex with a Cu Kα radiation source. Samples were scanned at 1^{o} per minute at 0.05^{o} intervals and peaks were identified using JADE software.

Minimal Media

Cultures were grown in a Fe-free modified M9 minimal medium (MM9) with the following composition: 125 g l^{-1} Na_2HPO_4, 30 g l^{-1} KH_2PO_4, 5 g l^{-1} NaCl, and 10 g l^{-1} NH_4Cl. In a given liter, 979 ml of M9 salts were supplemented with 1 ml of 1M $MgSO_4$, 10ml of 40% (w/v) glucose, and 10 ml of 0.5% (w/v) yeast extract; these solutions were prepared and sterilized separately. The siderophore desferrioxamine B (DFO-B) was added as its mesylate salt desferrioxamine mesylate (DFAM) to two separate media variants with a concentration of 200 μM. In total there were four variations of the minimal media. These include: minimal media; minimal media without phosphorus compounds; minimal media with DFAM; minimal media with DFAM but without

phosphorus compounds. The phosphorus depleted media variants were investigated to monitor microbial performance in the time course experiments without the provision of a key nutrient that is often limiting in the tropical soils.

Bacterial growth

A lyophilized culture of *Pseudomonas putida* was acquired from the DSMZ - Deutsche Sammlung von Mikroorganismen und Zellkulturen GmbH (German Collection of Microorganisms and Cell Cultures) and revived by growth in 3-ml of trypticase soy broth (TSB) with 0.5% yeast extract for 24-hr at 32^{o}C. The activated culture was then transferred to 1-L of TSB and incubated for an additional 24-hr to allow the bacteria to reach the late log phase of growth ($O.D._{600nm}$ > 0.8 absorbance units). The cells were separated from the nutrient medium by centrifugation, rinsed in 0.01 M $NaNO_3$ electrolyte three times and centrifuged again to remove the remaining electrolyte. The cell suspension was restored in 1-L of minimal media and the time course experiments were initiated.

Batch reactivity experiments

In order to quantify the microbial influence upon mineral weathering, a series of batch experiments were performed to compare iron release from Panamanian soil under abiotic vs. biotic conditions. The experiments were designed to test the extent that mineral weathering is enhanced by siderophores, *P. putida*, and *P. putida* + siderophores. Test tubes containing 0.1 g of soil and 15-ml solution were prepared in duplicate for each abiotic experimental variation (minimal media; minimal media without phosphorus

compounds; minimal media with DFAM; minimal media with DFAM but without phosphorus compounds, table 2.1) and repeated in a set of biotic experiments using *P. putida*. For each variation of media there was also a corresponding blank where soil was absent. Over a 35-day trial, test tube microcosms (duplicates of 8 (abiotic) to 10 (biotic)) were rotated end-over-end at 270 rpm and at room temperature ($25^{o}C$) and sacrificed for analysis at regular intervals until no microcosms remained.

Sample analysis consisted of collecting 1-ml of solution that would be set aside for enumerating cells (biotic experiments). In both biotic and abiotic experiments the samples were centrifuged for 10 minutes at 6000 rpm, and the supernatant was filtered with 0.2-µm nylon syringe filters and collected in clean test tubes. A 1-ml sample of filtered solution was acidified with HNO_3 (final solution pH < 2) and was analyzed for metals (Fe, Al, Si, and trace) by Inductively Coupled Plasma Optical Emission Spectroscopy (ICP-OES, IRIS #701776, Thermo Jarrell Ash Corporation). The pH and *Eh* of the remaining solution was recorded. A portion of the solid phase was stored in gluteraldehyde before preparing for electron microscopy by utilization of a rapid room temperature chemical fixation technique (Vandevivere and Bevaye, 1993). Scanning electron microscopy [SEM; Leo 1550 (Carl Zeiss SMT Inc., Thornwood, NY, USA) operated at an accelerating voltage of 10 kV] was performed on stub-mounted samples that were gold-sputter-coated for 1.5 minutes.

RESULTS

Classification of soil color using the Munsell soil color chart (Munsell, 1994) indicated that the soil sample was highly oxidized due to the red-yellow brown color. The

sample collected from the C-horizon falls under the sesquioxide clay classification (Munsell, 1994) and was massive, having very little structure. The description of the entire soil profile is the following: An A horizon extending down to 20 cm. A Bt horizon was evident between 20 cm and 35 cm, where whitish yellowish sand sized concretions first appear. The lower in depth, the more abundant and larger the concretions become (0.2 to 2 mm in diameter). This saprolitic layer is representative of a transition horizon between B and C to a depth of 60 cm. The sandier texture that predominates from 60 cm down to 100 cm is indicative of the C horizon as it contains a greater mixture of weathered regolith material. The yellowish hue to the brown soil increased with depth. The yellow nodules represent redoximorphic features found typically in environments that experience repeated wetting and drying conditions. These nodules may in fact be plinthites, which are composed of a mixture of iron-rich oxides, clay, and fine quartz (Davies, 1997; Aide et al., 2004).

Soil mineral content

Figure 2.6 illustrates the XRD scan results of the unreacted soil sample. The exact mineral composition of the soil sample is difficult to constrain since amorphous phases are likely present and the abundance of oxide minerals may mask other mineral peaks. The dominant mineral phases that were discernible in the scan include halloysite ($Al_2Si_2O_5(OH)_4$) with d-spacings at D_2 = 4.36Å, and D_3 = 3.35Å; magnetite (Fe_3O_4) with d-spacings at D_1 = 2.53Å, D_2 = 1.483Å, and D_3 = 1.614Å; maghemite (Fe_2O_3) with d-spacings at D_1 = 2.52Å, D_2 = 1.61Å, and D_3 = 2.95Å; and illite ($K_yAl_4(Si_{8-}$

$_y$,Al_y)$O_{20}(OH)_4$, usually with $1 < y < 1.5$, but always with $y < 2$) with d-spacings at D_1 = 4.43Å, D_2 = 2.56Å, and D_3 = 3.66Å.

Scanning Electron Microscopy

Dissaggregation of soil particles was confirmed by scanning electron microscopy within the first hour of reactivity (figure 2.7). The soil fragments varied in size ranging between 2-5 μm in diameter, and were smaller than the mesh size (75-212 μm) of the sieves used to constrain the grain size fragments. Considering the short reactivity period (< 1 hr), the small soil fragments were likely to be a consequence of particle disaggregation upon mixing with the acidic media solution (~ pH 4) rather than silicate/oxide precipitates that had formed in response to supersaturation. The fragments may also be the weathering products of a hydrolysis reaction.

Solution pH conditions

Over the 35-day period, the solution pH varied according to treatment, with acidic pH values in the P-depleted MM9 media treatments (biotic and abiotic), and neutral to slightly alkaline in the P-enriched MM9 media (figure 2.8). In the abiotic and biotic experiments using medias not buffered with phosphate, the variation between trends of solution pH was marginal (P-depleted pH range: 3.64-4.35; P-depleted + DFAM pH range: 3.58-4.08; P-depleted pH range: 3.92-4.54; P-depleted + DFAM pH range: 4.22-4.51). In abiotic experiments using medias that were buffered with phosphate, comparable solution pH ranges were observed between both media variants (P-enriched pH range: 7.11-7.25; P-enriched + DFAM pH range: 7.19-7.25). In the biotic experiments

using medias that were buffered with phosphate, the trend in solution pH was higher (greater than 1 pH unit) when adding DFAM to the P-enriched MM9 media (pH: 8.54-8.65) compared to no DFAM being present (pH: 7.25-7.41). There was, however, a significant difference between buffered and unbuffered media treatments (> 3 pH units regardless of the presence of DFAM or not), which was not surprising.

Phosphorus

The net concentrations of Al, Si, and Fe released from the soils were measured in both abiotic and biotic experiments, where net concentration represents the dissolved quantity analyzed after filtration. Results were dependent upon solution pH, the presence or absence of microbial populations and the addition of DFAM. In the biotic experiments, results also differed with respect to the media being used, MM9 P-enriched vs. MM9 P-depleted (no phosphorus). Phosphate in the media not only serves to buffer the solution pH but is also a limiting nutrient. Analysis of solution trace elements such as As, Cd, Cr, Cu, Mo, Ni, Pb, Se, Sn, and Zn were either at or below initial levels measured in blanks or were below detection. In both P-depleted media treatments, elemental phosphorus was initially below detection. However, within the first day phosphorus was detected at concentrations of 6 mmole L^{-1} or higher in the biotic treatments and 35 mmole L^{-1} or higher in the abiotic treatments, which would suggest that P had been released from the oxide minerals within the soil matrix (data not shown). A subsequent decline in abiotic and biotic phosphorus concentration was observed until no longer being detectable by day 5 of the trial. The formation of stable Fe- or Al-PO_4 mineral complexes (Vivianite or strengite, or variscite, respectively) would account for such a decline in phosphorus under

acidic pH conditions (Brady and Weil, 2002; Eby, 2004). The mean phosphorus concentration in the P-enriched treatments was 840 ± 60 mmole L^{-1}.

Fe release

Iron weathering from the soil minerals (magnetite and maghemite) was confirmed by an increase in the aqueous Fe concentration with time for all media variants (figure 2.9). The illite and halloysite minerals may also have been sources of Fe if Fe(III) substitution for Al(III) had occurred during diagenesis, which is not uncommon.

In the P-depleted media variants, the net release of Fe was significantly higher in both treatments spiked with DFAM (abiotic and biotic) vs. the corresponding treatments where DFAM was absent (figure 2.9a). The proton-promoted contribution to Fe release under acidic conditions (~ pH 4) was only evident in the late stage of the trial (35 days) for the abiotic treatments. However, the siderophore-promoted mechanism acted faster, and liberated comparatively more Fe into solution during the early stage of the trial. This was observed for both the abiotic and biotic treatments spiked with DFAM. The biotic treatment not spiked with DFAM appears to have liberated the least amount of Fe into solution.

In the P-enriched media variants, trends in net Fe release were distinct between the abiotic and biotic treatments (figure 2.9b). At circum-neutral pH, the contribution of a proton-promoted mechanism of weathering was expected to be negligible. In both abiotic treatments, an initial and rapid increase in aqueous Fe was shortly followed by a decrease. Following the precipitation event, increasing trends in Fe release were observed where higher saturation levels were permitted by the presence of DFAM compared to

abiotic treatments absent of DFAM. Biotic treatments (DFAM and no DFAM) had relatively overlapping trends in Fe release with each corresponding abioitc treatment. It would appear that another precipitation event (perhaps hematite precipitation) occurred in both abiotic treatments by the 35th day that was not observed in the biotic treatments.

Fe speciation: Fe(II) and Fe(III)

In addition to measuring aqueous Fe by ICP-OES, the Ferrozine method was applied to differentiate between the Fe redox couples (Stookey, 1970; Viollier et al., 2000). The presence of multivalent Fe-minerals such as magnetite provided a source of ferrous iron. Under oxic conditions, Fe reduction is not expected to be dominant, however, in a batch system, oxygen depletion will cause a temporal shift in redox conditions that may promote iron reduction. Soluble Fe^{2+} was consistently low in comparison to soluble Fe^{3+} for all treatments (figures 2.10 and 2.11). Significant increases in aqueous Fe^{2+} concentrations were only observed in the later stages (25 to 35 days) of the abiotic P-depleted experiments. Otherwise, soluble Fe was predominantly ferric throughout the 35-day reaction period for each of the treatments examined. In previous reports, reduction of Fe(III) does not occur until the siderophore-Fe(III) complex has been assimilated by the microbe (Leong and Neilands, 1976; Muller and Raymond, 1984; Neilands, 1995), which would favor the predominance of Fe(III) over Fe(II) in solution as observed in the biotic and DFAM-spiked treatments of this study. In some circumstances, however, extracellular iron reductases generated by siderophore-producing microbes will reduce Fe(III) in solution (Vartivarian and Cowart, 1999).

Al release

Aluminum weathering from the soil minerals (halloysite and illite) was confirmed by an increase in the aqueous Al concentration with time over the 35-day trial for all media variants (figure 2.12). In the P-depleted media variants, net Al release was highest in the abiotic control not spiked with DFAM, while the differences between the other P-depleted media treatments were marginal (figure 2.12a). Aqueous Al concentrations were consistently higher in the abiotic treatments compared to the corresponding biotic treatments (no DFAM, and DFAM-spiked), and the differences were more pronounced when DFAM was absent. Any variability in Al release from minerals may have been masked by cell wall sorption (anionic surface functional groups, Mera and Beveridge, 1993; Ferris, 1989; Hu and Boyer, 1996; Yee and Fein, 2001), since only aqueous Al was monitored.

In the P-enriched media variants, the non-linear trend in aqueous Al was noticeably lower in the *P. putida* + DFAM treatment when compared with the others (figure 2.12b). The distinctly lower aqueous Al trend observed for the *P. putida* + DFAM treatment correlates with higher solution pH conditions (figures 2.8 and 2.12b). Based on the solubility of Al in equilibrium with gibbsite, higher aqueous Al concentrations would be expected as the pH departs from neutrality (Nordstrom et al., 1990).

Si Release

Silicon weathering from the soil minerals (halloysite and illite, or perhaps from the Fe-oxides) was confirmed by an increase in the aqueous Si concentration with time over the 35-day trial for all media variants (figure 2.13). In the P-depleted media variants,

net Si release was higher in the abiotic controls compared to the corresponding biotic treatments (figure 2.13a). In the P-enriched media variants, the non-linear trends in net Si release were similar between treatments, with the exception of the biotic treatment spiked with DFAM, which was significantly lower than the rest (figure 2.13b). By the end of the trial (35-days), the biotic treatment spiked with DFAM had aqueous Si concentrations that were approximately 7 or 8 times lower than the other treatments. The lower Si solubility of the biotic treatment spiked with DFAM corresponds with an anomalously high solution pH compared to the other treatments (figure 2.8b).

Significantly higher trends in net Si release were observed in the P-enriched media treatments (figure 2.13b) compared to the corresponding P-depleted treatments (figure 2.13a). The sole exception to this relationship was with the biotic treatments spiked with DFAM. The differences in aqueous Si concentration between corresponding P-enriched and P-depleted treatments became more pronounced as time advanced to 35 days. This phenomenon is attributed to the higher solution pH (pH > 7) provided by the phosphate buffer in the media, where aqueous Si speciation (i.e., $Si(OH)_4$) is possible (Stumm and Morgan, 1996; Drever, 1997).

Release rates: Fe, Al, and Si

The observed change in aqueous metal concentration is best described by a first order rate expression, $M = M_0e^{-kt}$, where M is the concentration of the aqueous species, and M_0 is the concentration at time zero, k is the rate constant, and t is time. Instead of calculating the rate that a mineral is dissolved, the rate constant for metal release was calculated from the slope of the line when plotting $\ln[M]/[M]_0$ vs. time in days. In each

case (Fe, Al, and Si), initial rates were calculated from the linear trend observed within two days of reactivity (tables 2.2, 2.3, and 2.4). The observed decrease in weathering rates over time is attributed to either the formation of a diffusion-inhibiting leach layer or the formation of secondary precipitates on the mineral surface as equilibrium conditions are more closely achieved (Schott and Berner, 1983; Schott and Berner, 1985; Chou and Wollast, 1985).

The net Fe release rates for each media treatment (abiotic and biotic) are presented in table 2.2. In the P-depleted set of treatments, the addition of DFAM resulted in enhanced Fe release rates for both the abiotic ($r_{\text{Abiotic P-depleted+DFAM}} = 0.67 \pm 0.5\ d^{-1} > r_{\text{Abiotic P-depleted}} = 0\ d^{-1}$) and biotic treatments ($r_{\text{Biotic P-depleted+DFAM}} = 0.53 \pm 0.1\ d^{-1} > r_{\text{Biotic P-depleted+DFAM}} = 0.37 \pm 0.04\ d^{-1}$), indicating that siderophore-promoted mineral weathering was active. Considering that cell associated Fe was not measured, there is no point to compare abiotic and biotic rates or release. A fraction of the Fe^{3+} was likely bound to anionic surface functional groups of the *P. putida* cell wall or assimilated for cellular function, or both. Independent or combined effects would result in a low estimate of the amount of Fe that was released from the minerals when only analyzing the aqueous content.

In the P-enriched set of treatments, the calculated Fe release rates were similar between all treatments (table 2.2). Higher rates of Fe release were calculated for treatments spiked with DFAM compared to those that were not (for abiotic and biotic treatments), however, they were within error of one another. The impact of the siderophore-promoted mechanism of Fe release appears to be significant over longer time periods rather than the 2-day period with which the rates were calculated.

In abiotic media variants, Fe release rates were similar between P-enriched and P-depleted treatments spiked with DFAM (table 2.2). The presence of DFAM in the media overrides any contribution from the phosphate and as such, comparable Fe release rates were observed. However, when DFAM was absent, a higher rate of Fe release was observed in the P-enriched treatment. In the biotic media variants, again, Fe release rates were similar between P-enriched and P-depleted treatments spiked with DFAM (table 2.2). In the absence of DFAM, however, a higher rate of Fe release was observed in the P-enriched biotic media treatment.

Release rates for Al and Si are reported in tables 2.3 and 2.4, respectively. In the abiotic treatmens, a relatively higher rate of Al release was observed when the P-depleted media treatment was spiked with DFAM. However, DFAM's impact upon Si release rate was not significant. In the biotic P-depleted media treatment, it appears that DFAM did enhance the rate of Al release, however due to overlapping error bars, once again the impact of DFAM upon Si release rate cannot be considered statistically significant.

In P-enriched media, poor fits in trends of Al and Si release were observed for the abiotic treatment not spiked with DFAM within a 2-day time frame. As such abiotic rates of Al and Si release could not be calculated and no comparisons could be made with DFAM-spiked treatment. With *P. putida* present, DFAM did not enhance Al or Si release rates relative to the non-DFAM treatment. Therefore, siderophore-mediated Al weathering does not appear to be relevant at circum-neutral pH when *P. putida* is present.

DISCUSSION

Mineral weathering in the tropics is primarily influenced by the climate, which is characterized by relatively high mean annual temperatures and precipitation compared to other settings. In addition to the influences of climate, microorganisms make significant contributions to mineral weathering, particularly with respect to the mobilization of Fe in soils. In this study, the kinetics of mineral weathering in Panamanian soils was promoted by the presence of *P. putida*.

Reactivity at the mineral-solution interface can be caused by a number of factors. In strictly abiotic conditions, weathering is promoted when the solution in contact with the mineral is undersaturated with respect to elements at the surface (steady state steady flow). In equilibrium conditions, such as a void space filled with stagnant pore water, the rate of dissolution will slow down with time as the solution becomes more saturated with the dissolving elements. Upon reaching the saturation limit, a solid precipitate will form with a composition that reflects the solution. Only by flushing the pore water with a fresh solution that is undersaturated with respect to the mineral elements will continued dissolution be possible, a.k.a., *steady-state* conditions.

Mineral dissolution in the abiotic reactors used in these experiments was ultimately driven by thermodynamic equilibrium conditions representative of the solution pH and *Eh*. More CO_2 is expected to be present in the biotic systems compared to the abiotic systems due to microbial respiration, which can influence the solution pH. However, instead of observing a decrease in solution pH with time, as CO_2 reacts with H_2O to form carbonic acid, a subtle increase was observed, and this was true for all media variants (figure 2.8). Only when DFAM is present in the phosphate buffered media, does

the microbial presence appear to significantly raise the solution pH (> 1 pH unit) relative to the corresponding abiotic media. The minerals themselves would serve to buffer solution pH during reactivity. Equilibrium reactions between iron oxides and Fe^{3+}/Fe^{2+} would consume protons (Garrels and Christ, 1965), while the silicate mineral component of the soil (halloysite and illite) would buffer solution pH by providing a sink for protons and CO_2 during chemical weathering (Berner et al., 1983; Brady, 1991; Eby, 2004).

Fe release

Abiotic Fe release was controlled by solution pH and solubilization triggered by the formation of complexes with anionic chemical species. Fe solubility was proton-promoted in P-depledted abiotic treatments due to the acidic pH of these media solutions (figure 2.9a). However, the influence of chelates and phosphate complexes with Fe would account for the observed trends in Fe release in the P-enriched media treatments (figure 2.9b). In both abiotic P-enriched media treatments (DFAM and no DFAM), the initial release of Fe from the soil minerals is attributed to the formation of a soluble Fe-phosphate complex, which is highly favorable from a thermodynamic standpoint (K = 16 to 36 for various Fe^{2+}/Fe^{3+} phosphate complexes; Morel and Hering, 1993; Stumm and Morgan, 1995). However, saturation limits must have been exceeded, which would have caused these complexes to precipitate out of solution as mineral phases, and would account for the decline in aqueous Fe concentration that followed the initial rise. Other possible precipitates of Fe include (oxy)hydroxides and silicates (Morel and Hering, 1993; Stumm and Morgan, 1995).

Other factors influencing mineral dissolution with respect to Fe are the presence of *P. putida* cells, or siderophores, or both. Since *P. putida* derives energy from Fe in electron transport reactions (Loper and Henkels, 1999) the sustained release of Fe^{3+} from the soil minerals could be driven by metabolic activity. Iron dissolution kinetics was particularly enhanced by the heterologous siderophore, DFAM (table 2.2). This was expected since siderophores have a high affinity for Fe(III). Essentially the formation of a stable aqueous Fe-DFAM complex is thermodynamically favorable as the formation constant for molecules with three bidentate ligands is 10^{30} or greater (Neilands, 1995). While the individual *P. putida* cells were expected to generate their own siderophores (Sher and Baker, 1982), the amount that they could secrete en mass not was expected to be as high as the amount that was added (200 μM). Although Liermann et al. (2000) assumed that the likely siderophore concentration present in bacterial micro-niches found in natural soils to be as high as 240 μM. The equivalently high rates of Fe release that were observed in the abiotic and biotic treatments spiked with DFAM confirmed that a siderophore-promoted mechanism of Fe dissolution was active. In either case (abiotic or biotic), the rate of Fe release was higher than in biotic treatments not spiked with DFAM, regardless of whether the media was buffered with phosphate or not. It is most probable that ferric iron release from the iron containing soil minerals (e.g., magnetite and maghemite) was enhanced by the formation of a surface complex with the siderophore (self generated or heterologous) and the rate of release was controlled by the detachment of the Fe(III)-siderophore complex. Recent work by Kim et al. (2010) shows that Fe(III)-desferrioxamine B complexes are reduced by the fully reduced hydroquinone form of flavin mononucleotide (FMN_{HQ}) in the absence of strong Fe(II)-chelating agents.

Ligand-promoted mineral dissolution reaction rates are controlled by excess surface adsorbed ligands and the nature of the Fe(III)-ligand surface complexes (Furrer and Stumm, 1986). The dissolution reaction is promoted by the formation of a precursor complex by adsorption of the ligand, which polarizes the bonds between the iron ion and oxygen in the crystal lattice (Kraemer, 2004). Factors that make organic ligands effective promoters of iron oxide dissolution include (1) the tendency to form inner sphere surface complexes, (2) having a high affinity for adsorption in the neutral to alkaline pH-range, and (3) the tendency to form mononuclear multidentate surface species (Kraemer, 2004). Increasing denticity of coordinating ligands will improve the likelihood for inner sphere coordination of dissolved metal ions (Margerum et al., 1978). However, there is a limitation to the number of bonds that can form between an organic ligand and a single Fe(III) ion in the inner coordination sphere at the mineral surface. The effect on dissolution rate by a 5-member ring bidentate surface complex is higher than it is by a 6 or 7 member ring. Inhibition of oxide dissolution results from the simultaneous coordination of adjacent surface sites by a single ligand (Bondietti et al., 1993). Due the similarities in rate constants between desferrioxamine B (DFO-B) and acetohydroxamic acid (aHA), only a single hydroxamate group of the adsorbed DFO-B is likely participating in surface complexation to coordinate Fe(III) from iron oxides (Cocozza et al., 2002). This type of binding behavior makes DFAM an effective promoter of iron dissolution.

A number of factors that influence the conformation and bonding of adsorbed multidentate siderophores include steric constraints imposed by the surface and siderophore architecture, charge, and hydrophobicity. The DFO-B behaves as a cationic

species below pH 8 due to the protonated terminal amine group (pK_{a1} = 8.38) (Kraemer, 2004). The electophoretic mobilities of tropical soil clays have been shown to be more negative with increasing pH (Osei and Singh, 1999), hence DFAM sorption onto the minerals in this study would have been higher in the P-enriched treatments compared to the P-depleted treatments.

In addition to the action of siderophores, Fe release was likely influenced by the biophysical properties of the *P. putida* cells and would be masked if only analyzing for aqueous Fe. The anionic surface functional groups that make up the reactive cell wall components would provide additional binding sites for Fe and other cations (Yee and Fein, 2001; Wang et al., 2003; Ojeda et al., 2008) that were otherwise absent in the abiotic treatments. The fraction of Fe partitioned from solution onto the cell wall of *P. putida* was expected to be higher since electrostatic attraction between cations and anionic surface functional groups is consistently more pronounced at circum-neutral pH compared to acidic conditions (Mera and Beveridge, 1993; Ferris, 1989; Yee and Fein, 2001; Kulczycki et al., 2002). The combination of cell wall binding and assimilation of Fe may explain the initially lower aqueous Fe concentrations that were observed relative to the abiotic treatments. However, as time advanced, a continuous increase in aqueous Fe concentration was observed in both biotic treatments. Fe^{3+} assimilation by *P. putida* cells may account for the relatively diminished trends in aqueous Fe concentrations in the biotic treatments, especially since Fe is an essential nutrient (Bagg and Neilands, 1987; Madigan and Martinko, 2005). Since the cell-associated iron was not analyzed in these experiments we cannot make any claims regarding the total amount of Fe released from the soil minerals in the presence of *P. putida* or *P. putdia* + DFAM.

At neutral pH, lower *Eh* conditions (often negative) are required for iron (Fe^{2+}/Fe^{3+}) to remain stable as an aqueous species above 10^{-9} M (Stumm and Morgan, 1996). Therefore, the *Eh* must not have been low enough, and precipitation of an iron oxide or oxy(hydroxide) species was probable. Solution saturation state (SI = $\log(IAP/K_{sp})$) with respect to several Al, Si, and Fe containing phases was calculated using WEB-PHREEQ, an implementation of PHREEQC (Parkhurst, 1995). Supersaturation (positive SI) of numerous secondary mineral phases (Al-, Fe-oxides and aluminosilicate clay) was observed up to several orders of magnitude within the first 48 hours of the experiments for both the abiotic and biotic treatments, particularly with respect to gibbsite, goethite, hematite and kaolinite. The saturation indices for solution conditions at the end of the experiments (35 days) are given for each treatment in table 2.5. Based on the calculated SIs, hematite and goethite precipitation was likely to occur in each of the P-enriched media treatments (hematite SIs: 13.28-14.2; goethite SIs: 5.64-6.1) and the P-depleted biotic treatment that was spiked with DFAM (hematite SIs: 4.12, goethite SIs: 1.06). At these levels ferric iron was unlikely to remain in solution, unless it was complexed by a chelate such as DFAM. In unbuffered treatments, kaolinite precipitation was expected to occur since positive saturation indices were calculated (SIs: 1.62-3.86). With the exception of the P-enriched biotic treatment spiked with DFAM, gibbsite precipitation should also have occurred in each treatment (SIs: 0.13-1.52).

Fe redox couples: Fe(II) and Fe(III)

Determination of the Fe redox couples permitted the redox potential (*Eh*) to be calculated for specific sampling intervals in each of the treatments. The electron activity

(*pe*) in each solution had to be determined and then converted to *Eh*. In all treatments and sampling intervals, the average *Eh* was close to 0.8 V (which corresponds with a *pe* value of ~13.5), however, the range would vary from treatment to treatment (table 2.6). WEBPHREEQ simulations calculated the *pe* to be approximately 17, which corresponds with an *Eh* of 1.0 V. In either case, the calculated *Eh* values favor Fe^{3+}stability over Fe^{2+} (Drever, 1997).

Despite the favorable Eh conditions for Fe^{3+} stability, at pH values of ~4 and ~7, hematite or ferrihydrite stability is more favorable (Garrels and Christ, 1965). In addition, for media treatments buffered with phosphate, Fe^{3+}-phosphate complexes are also expected to form (Morel and Hering, 1993; Stumm and Morgan, 1995). Fe(II) was detected in the biotic P-enriched treatments, suggesting that magnetite dissolution was active for these treatments. The presence of DFAM did not enhance Fe^{2+} release, which confirms that the mechanism of Fe release by siderophores only applies to Fe^{3+}.

Si and Al release

Relatively lower aqueous Si concentrations were observed in the biotic experiments compared with abiotic treatments (figure 2.13). A likely explanation was that a fraction of the aqueous Si had been partitioned by anionic cell wall components of *P. putida* (Mera and Beveridge, 1993; Yee and Fein, 2001). Metal binding by bacterial cell wall components is typically more pronounced at higher pH (Mera and Beveridge, 1993; Ferris, 1989; Yee and Fein, 2001; Kulczycki et al., 2002), hence more Si binding was expected to occur in the P-enriched biotic treatments compared to the P-depleted ones. However, higher aqueous Si trends were observed in the abiotic pH-buffered

treatments compared with the corresponding acidic abiotic treatments, which would suggest that pH is an important factor. For quartz and amorphous silica in pure solutions, the pH has to increase beyond 9.83 before solubility increases (Rimstidt and Barnes, 1980). Previous work has demonstrated that siderophore-generating microorganisms were responsible for dissolving clays with trace quantities of iron and yielded higher growth rates compared to samples absent of clay (Maurice et al., 2001), further emphasizing how mineralogy can influence microbial activity and vice versa.

The stability of aqueous Al is controlled by pH, the presence or absence of *P. putida*, the presence or absence of DFAM, and the presence or absence of phosphate. Gibbsite solubility increases as the pH departs from neutrality, however the variability in aqueous Al concentration was negligible between corresponding abiotic treatments that differed only by the presence or absence of a phosphate buffer. The buffered treatments of neutral pH were expected to demonstrate lower aqueous Al concentrations if in equilibrium with gibbsite (Nordstrom et al., 1990). However soluble Al-phosphate complexes may have formed, which would account for the higher aqueous Al concentrations observed in the abiotic buffered treatment compared to the corresponding acidic treatment. The partitioning of Al by the *P. putida* cells in the biotic treatments was expected to occur at greater quantities with increasing pH, as described above for Si. The presence of DFAM in the biotic treatment buffered with phosphate diminishes the mobility of both Al and Si. These speculations are supported by the calculated saturation indices for gibbsite, kaolinite, and quartz in table 2.5. Perhaps the combination of phosphate, DFAM, and extracellular polymeric substances from *P. putida* poison the release of Al and Si from the soil minerals by steric hindrence.

Release rates: Fe, Al, and Si

The enhancement of Fe release by siderophores was confirmed in each media variety that had been spiked with DFAM, where relatively higher release rates were observed compared to the corresponding treatment not spiked with DFAM (table 2.2). In treatments not spiked with DFAM, the higher Fe release rates that were observed in both phosphorus buffered treatments (abiotic and biotic) are attributed to the formation of soluble Fe-phosphate complexes. In addition, the presence of *P. putida* cells resulted in higher release rates than corresponding abiotic treatments, and is attributed to both biophysical and metabolic processes, which are described in greater detail below.

Under abiotic conditions, Al release rates were lowest in the phosphorus buffered treatments, which was expected since at neutral pH gibbsite solubility is lowest (Nordstrom et al., 1990). The presence of *P. putida* cells yielded a relatively higher rate and is attributed to the binding of Al^{3+} by anionic surface functional groups on the cell wall membrane (Beveridge, 1989; Ferris, 1989; Mera and Beveridge, 1993; Beveridge, 1999; Yee and Fein, 2001). Otherwise lower rates of Al release were observed in biotic treatments compared to corresponding abiotic treatments, as determined by analysis of aqueous Al. Higher rates of Al release would be expected in the biotic treatments if cell associated Al was also quantified. The presence of DFAM yielded the highest rates of Al release at values that were comparable between each media variety. This finding strongly suggests that chelating molecules such as DFAM are capable of forming complexes with multiple metals.

Silicon release rates were higher in the P-enriched media treatments than the corresponding P-depleted treatments suggesting that pH did have an influence on Si

solubility. For quartz and amorphous silica, pH dependent solubility does not occur until values above 9.83 (Rimdstidt and Barnes, 1980). However, silicate minerals higher up the Goldich weathering series would be less resistant to weathering at neutral pH, i.e., clay minerals (Berner and Berner, 1996). As with Fe, and Al, the reported rates of Si release in the biotic treatments were lower than they would be if the cell associated Si had also been quantified. The influence of DFAM upon Si mobility is not clear.

Microbial-mineral interactions

The kinetics of mineral weathering with respect to all metals is influenced by the presence of *P. putida* cells. Their presence caused higher rates of Fe release compared to the corresponding abiotic media treatments (table 2.4), and can be attributed to a siderophore-promoted mechanism. In order to satisfy *P. putida's* energy requirements provided by ferric iron (Neilands, 1995; Neilands and Nakamura, 1991), independently manufactured and secreted siderophores would promote enhanced Fe release from the iron oxides. However, there may also be a passive role contributed by the anionic surface functional groups of the microbial cells that serves to influence mineral weathering rates.

Generic to all bacterial cell walls, gram-negative or gram-positive, is the presence of anionic surface functional groups that will electrostatically attract cations, and in enhanced quantities with elevated solution pH. As *P. putida* is a bacterium with gram-negative cell wall architecture, the outer membrane components in particular are reactive with metal ions (Beveridge, 1989; Ferris, 1989; Mera and Beveridge, 1993; Beveridge, 1999; Yee and Fein, 2001). Hence, the reactive surface functional groups will partition metals from solution as they are released from the mineral. Therefore, the presence of

microbial cells such as *P. putida* will be responsible for maintaining a concentration gradient between the mineral surface and the solution. Continued mineral dissolution will be promoted up until all the surface sites have been filled. Thereafter, the concentration gradient would diminish to the point at which the solution reaches it's saturation limit, provided that equilibrium conditions remain dominant. In addition to Fe, metals (e.g., Al, Si, and trace metals) would be released from the minerals and subsequently sequestered by the *P. putida* cells.

The degree to which microbial cells will be attracted to a mineral surface is also dependent upon electrostatic attraction between anion surface functional groups and the surface charge of the mineral at a given pH. Binding between minerals and bacteria will be enhanced by electrostatic attraction if the pH conditions are above the mineral net point of zero charge (n.p.z.c. or pH p.z.c.) where the surface charge is positive (Mera and Beveridge, 1993). The literature indicates that the pH p.z.c. for minerals identified in this study range between 6 and 7.1 for halloysite (Theng and Wells, 1995), 6 and 6.6 for maghemite (Vayssieres, 2009) and is 6.5 for magnetite (Milonjić et al., 1983). Therefore, a higher degree of electrostatic interaction between the *P. putida* cells and soil minerals would be expected to occur in the P-enriched media treatments where the solution pH was relatively neutral. Such an interaction would generate microbial-mineral composite structures (Small et al., 2001; Kulczycki et al., 2005) and eventually promote biofilm formation (Brown et al., 1994; Beveridge et al., 1997). In either case, the conditions that affect the metal flux from the mineral to solution would be altered. With biofilm development, protons consumed during mineral weathering would cause the pH of the local micro-environment to increase (Bland and Rolls, 2005).

In addition to physical processes such as electrostatic attraction, microbial cells may colonize and attach to a mineral surface to acquire nutrients (Rogers et al., 1998; Bennett et al., 2001; Roberts Rogers et al., 2001). The most obvious nutrient that would be obtained directly from the surface of either of the iron oxides is ferric iron. Under aerobic conditions, many microorganisms depend upon ferric iron as an electron acceptor to promote oxygen reduction for ATP synthesis, among other functions (Neilands, 1995). These circumstances are typically associated with circum-neutral pH conditions where the utilization of siderophores is necessary to form a stable aqueous complex with the ferric iron (Hersman et al., 1996; 2000; Maurice et al., 2000; Neilands, 1995).

The relative positions of the major cations (Fe, Al, and Si) within the mineral lattice may have had an influence on the observed weathering patterns. Higher Si solubility may destabilize Al-oxygen and Fe-oxygen bonds in the mineral framework and enhance the rate of Al and Fe release particularly if single oxygen atoms are shared by more than one individual cation. Desferioxamine itself (a hydroxamate) may have been responsible for the enhanced Al release rates that were observed in most of the treatments, since it is recognized as an Al(III) chelating ligand (Garrison and Crumbliss, 1987; Yokel, 2002). If the amount of DFAM was in excess of the quantity that actively complexed Fe(III), then the remainder could complex Al(III) as well. The only case where DFAM did not appear to enhance Al release was at circum-neutral pH when *P. putida* was present (i.e., P-enriched biotic treatments). However, Al accumulation by the cells may have masked the effect. Siderophore-mediated Al uptake by bacteria has been documented where Al absorption occurred through the siderophore transport receptor (Hu and Boyer, 1996). The similarity between Fe and Al ionic radii permits siderophore

coordination with Al, however the associated microbial uptake of Al has direct implications with respect to heavy metal toxicity under iron-deficient conditions.

SUMMARY

The release of Fe from the highly weathered Panamanian soil minerals was enhanced by DFAM and by the presence of *Pseudomonas putida*, suggesting a ligand-promoted mechanism of dissolution in both circum-neutral and acidic pH conditions. The major mineral sources of Fe were from magnetite and maghemite, while contributions from illite was suspected. Aluminum and Si release was controlled by both solution pH and the anionic cell wall components of *P. putida*. The electrostatic binding of metals generates a steep gradient between the mineral and solution, and promotes passive dissolution. Major source minerals include halloysite and illite. The release of Si and Al appears to be correlated and is attributed to the sharing of oxygen atoms in the mineral structure. In addition, the removal of Al or Si from the mineral structure during weathering could destabilize Fe from neighboring sites and promote further weathering.

Fe and Al were mobilized from highly weathered soil minerals by the siderophore-generating microorganism, *Pseudomonas putida*. Hence, this study illustrates the importance of microorganisms in the soil environment in terms of their contribution to the release of key nutrients and potentially toxic metals from minerals. The availability of mineral source nutrients is not only beneficial to the microorganisms themselves but also to plants that would otherwise be under stress in a low-nutrient soil environment. The ecological function that microorganisms serve is particularly critical to tropical soil settings where nutrients such as Fe and P are not readily available.

Table 2.1: Media variations for batch reactivity experiments.

Abiotic	**Biotic**
MM9	MM9
MM9 (no phosphate)	MM9 (no phosphate)
MM9 + DFAM	MM9 + DFAM
MM9 + DFAM (no phosphate)	MM9 + DFAM (no phosphate)

- Abiotic and biotic medias were prepared with 0.1 g of sterilized soil per 15-ml solution. *Pseudomonas putida* cells were suspended in medias for biotic reactors only.
- Each media variant (abiotic and biotic) had a corresponding blank that was absent of soil.

Table 2.2: Fe release rates

	[†]Abiotic			[§]Biotic		
Media Treatment	[e]Rate	[f]r^2	[g]MSE	[e]Rate	[f]r^2	[g]MSE
[a]P-depleted	0	---	---	0.37	0.903	0.04
[b]P-depleted + DFAM	0.67	0.724	0.5	0.53	0.856	0.1
[c]P-enriched	0.27	0.52	0.2	0.47	0.86	0.1
[d]P-enriched + DFAM	0.65	0.869	0.2	0.67	0.878	0.2

[†] Sterile abiotic media (MM9)
[§] Biotic: *Pseudomonas putida* culture grown in media (MM9)
[a] Media (MM9) with phosphorus
[b] Media (MM9) prepared without phosphorus
[c] Media (MM9) with phosphorus + DFAM added
[d] Media (MM9) prepared without phosphorus + DFAM added
[e] Initial 1st order rate constant expressed as $(\ln[Fe]/[Fe]_0)/t$, calculated from a linear fit of $\ln[Fe]/[Fe]_0$ vs. time within the first 2 days of reactivity.
[f] Values are correlation coefficients for the regression analyses.
[g] MSE (mean square error) from ANOVA regression analysis is the estimate of the variance about the population regression line.

Table 2.3: Al release rates

	[†]Abiotic			[§]Biotic		
Media Treatment	[e]Rate	[f]r^2	[g]MSE	[e]Rate	[f]r^2	[g]MSE
[a]P-depleted	0.05	0.652	0.004	0.03	0.386	0.01
[b]P-depleted + DFAM	0.14	0.633	0.04	0.07	0.623	0.01
[c]P-enriched	---	---	---	0.34	0.808	0.07
[d]P-enriched + DFAM	0.43	0.811	0.12	0.29	0.765	0.07

[†] Sterile abiotic media (MM9)
[§] Biotic: *Pseudomonas putida* culture grown in media (MM9)
[a] Media (MM9) with phosphorus
[b] Media (MM9) prepared without phosphorus
[c] Media (MM9) with phosphorus + DFAM added
[d] Media (MM9) prepared without phosphorus + DFAM added
[e] Initial 1st order rate constant expressed as $(\ln[Al]/[Al]_0)/t$, calculated from a linear fit of $\ln[Al]/[Al]_0$ vs. time within the first 2 days of reactivity.
[f] Values are correlation coefficients for the regression analyses.
[g] MSE (mean square error) from ANOVA regression analysis is the estimate of the variance about the population regression line.

Table 2.4: Si release rates

	[†]Abiotic			[§]Biotic		
Media Treatment	[e]Rate	[f]r^2	[g]MSE	[e]Rate	[f]r^2	[g]MSE
[a]P-depleted	0.53	0.794	0.2	0.43	0.918	0.04
[b]P-depleted + DFAM	0.59	0.742	0.3	0.48	0.915	0.05
[c]P-enriched	0	---	---	0.62	0.88	0.1
[d]P-enriched + DFAM	0.79	0.861	0.3	0.61	0.946	0.05

[†] Sterile abiotic media (MM9)
[§] Biotic: *Pseudomonas putida* culture grown in media (MM9)
[a] Media (MM9) with phosphorus
[b] Media (MM9) prepared without phosphorus
[c] Media (MM9) with phosphorus + DFAM added
[d] Media (MM9) prepared without phosphorus + DFAM added
[e] Initial 1st order rate constant expressed as $(\ln[Si]/[Si]_0)/t$, calculated from a linear fit of $\ln[Si]/[Si]_0$ vs. time within the first 2 days of reactivity.
[f] Values are correlation coefficients for the regression analyses.
[g] MSE (mean square error) from ANOVA regression analysis is the estimate of the variance about the population regression line.

Table 2.5: Saturation indices (SI) with respect to multiple secondary phases after 35 days of reactivity. SI calculated using WEB-PHREEQ: Aqueous Geochemical Modeling[Ω].

Treatment	Saturation Indices						
	pH	$Fe(OH)_{3(a)}$	Gibbsite	Goethite	Hematite	Kaolinite	Quartz
Abiotic P-depleted	4.0	-6.41	0.49	-0.52	0.97	2.47	0.33
Abiotic P-depleted + DFAM	3.9	-6.73	0.13	-0.83	0.34	1.62	0.27
Biotic P-depleted	4.2	-6.21	1.04	-0.32	1.37	3.16	0.12
Biotic P-depleted + DFAM	4.4	-4.83	1.52	1.06	4.12	3.86	0.00
Abiotic P-enriched	7.2	-0.25	1.28	5.64	13.28	-0.85	-2.12
Abiotic P-enriched + DFAM	7.22	-0.22	1.24	5.67	13.34	-0.91	-2.11
Biotic P-enriched	7.3	-0.00	1.24	5.89	13.78	-1.08	-2.2
Biotic P-enriched + DFAM	8.6	0.20	-0.25	6.10	14.20	-5.64	-2.98

[Ω] An online implementation of the aqueous geochemical modeling program PHREEQC by David Parkhurst of the USGS.

Table 2.6. Redox potential, *Eh*

	[†]**Abiotic**		[§]**Biotic**	
Media Treatment	[e]Mean *Eh*	STDEV	[e]Mean *Eh*	STDEV
[a]P-depleted	0.8	0.67	0.86	1.24
[b]P-depleted + DFAM	0.8	0.96	---	---
[c]P-enriched	0.83	0.94	0.79	0.97
[d]P-enriched + DFAM	0.83	1.07	0.82	1.15

[†] Sterile abiotic media (MM9)
[§] Biotic: *Pseudomonas putida* culture grown in media (MM9)
[a] Media (MM9) with phosphorus
[b] Media (MM9) prepared without phosphorus
[c] Media (MM9) with phosphorus + DFAM added
[d] Media (MM9) prepared without phosphorus + DFAM added
[e] Mean *Eh* represents the entire 35-day trial, and was calculated from the ratio between the activity of Fe^{3+} and Fe^{2+}. In some cases the activity of Fe^{2+} was below detection and *Eh* could not be calculated.

Figure 2.1. Composition of the hydroxamate siderophore desferrioxamine B (from Kalinowski et al., 2000)

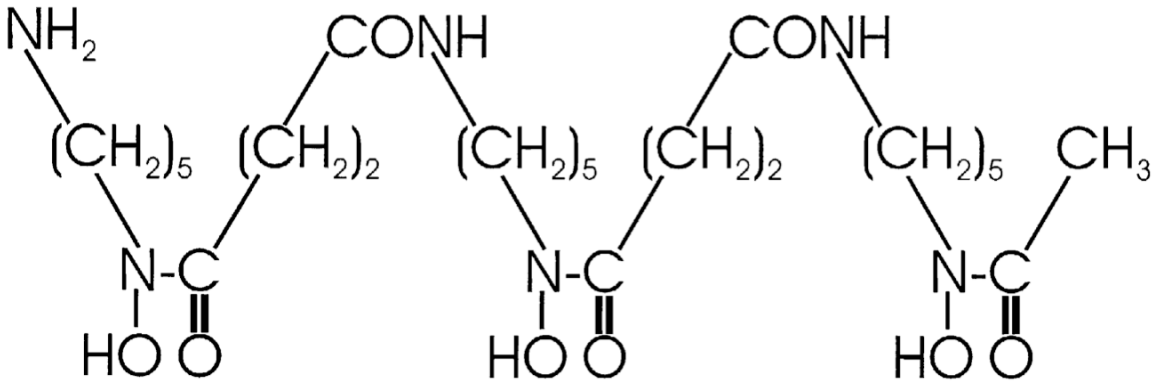

Figure 2.2. a) Hydroxamate b) Catecholate c) Siderophore-Fe cycling from mineral to cell (Kalinowski et al., 2000).

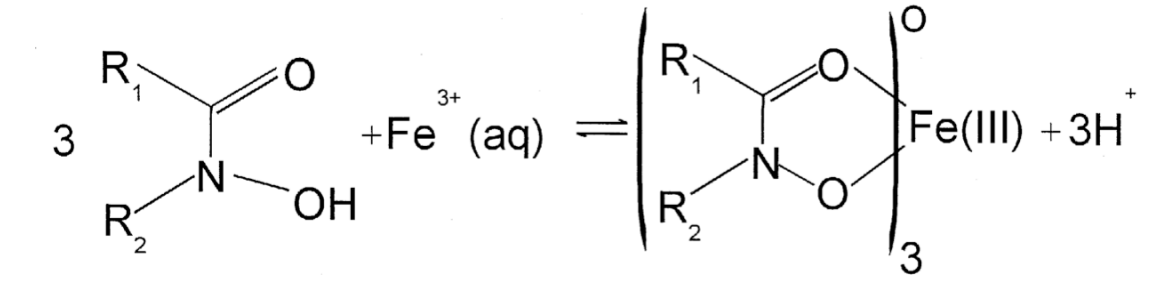

a) Hydroxamate

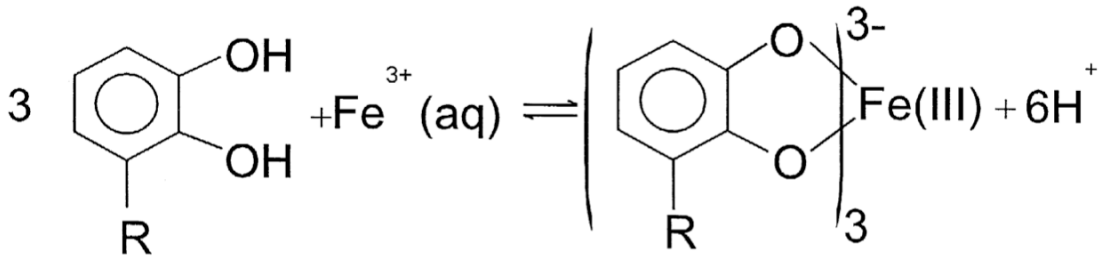

b) Catecholate

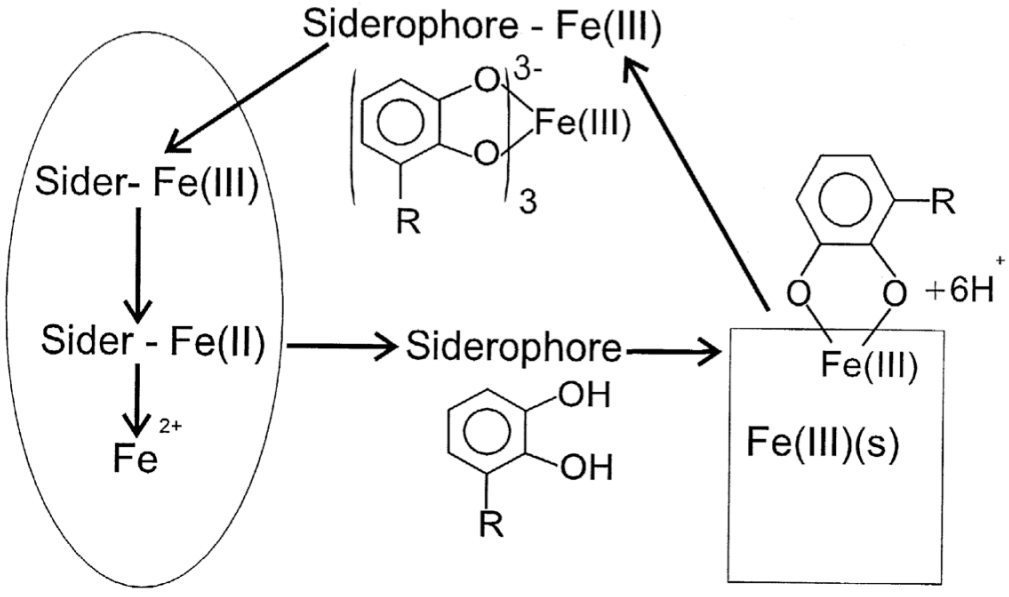

c) Bacterium Hornblende

Figure 2.3: Map of Panama with inset showing Barro Colorado Island. Taken from www.stri.org, 2006.

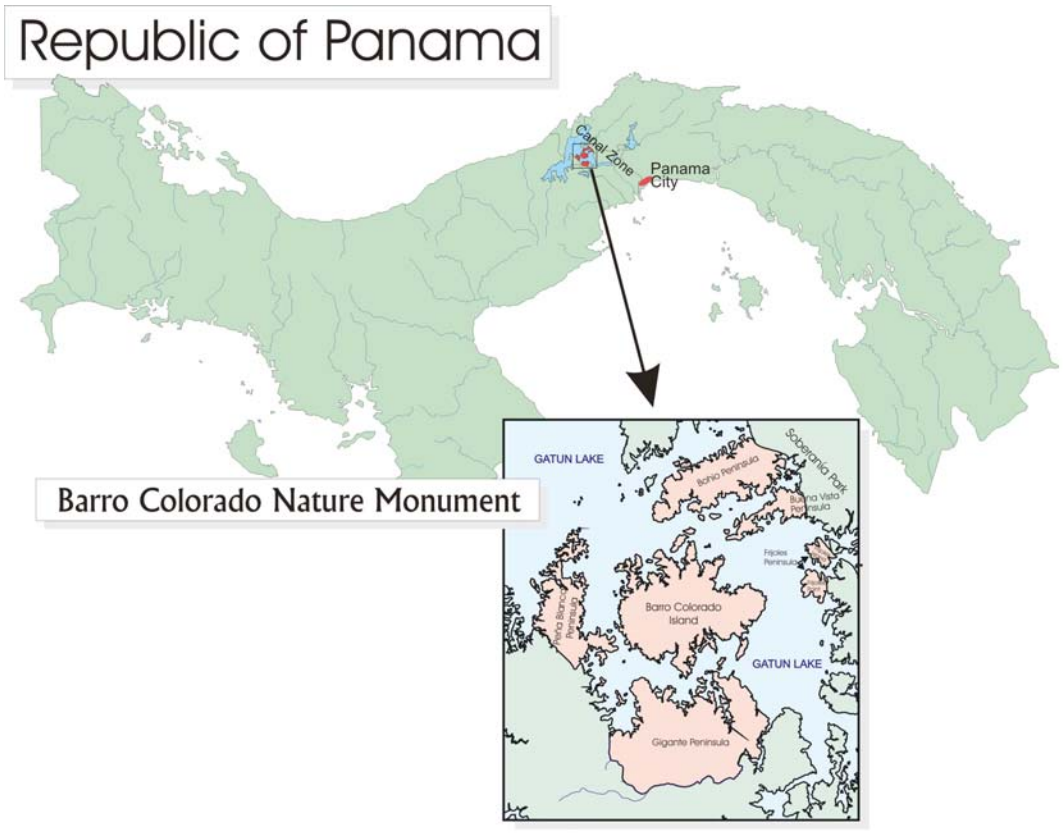

Figure 2.4: BCI soil map (from Baillie et al., 2007).

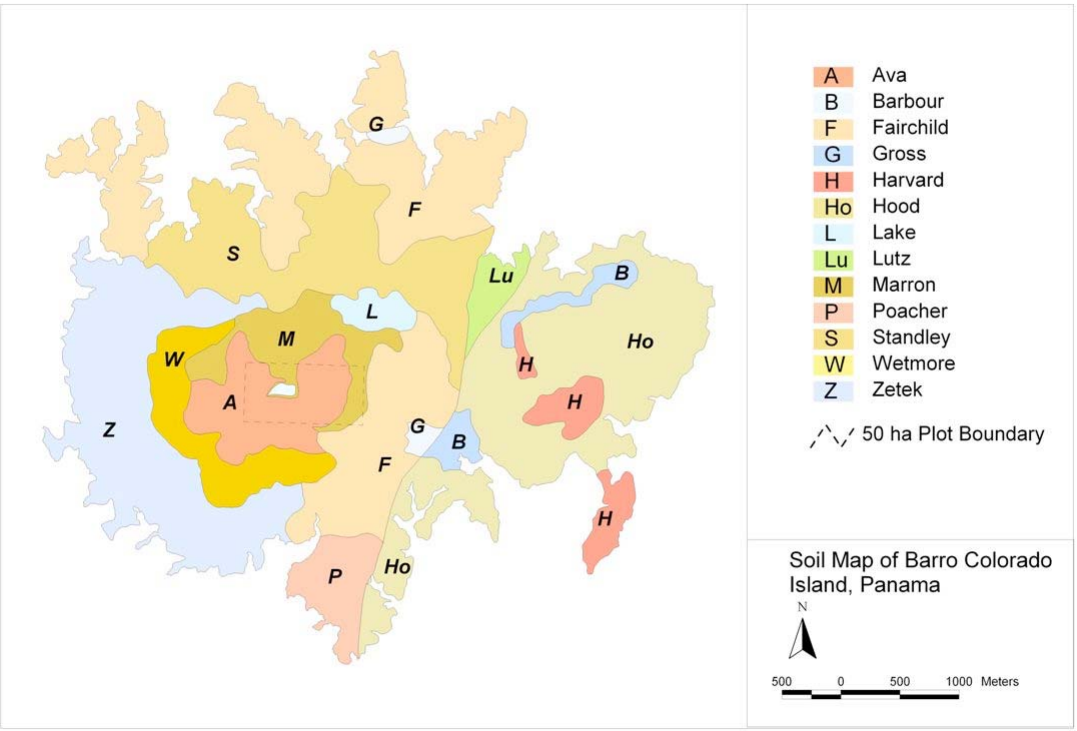

Figure 2.5: Contour map of Barro Colorado Island, Panama with “red star” denoting the location of the soil collection site. *Taken from www.stri.org, 2006.

Figure 2.6: XRD scan of Miller forest soil sample from 65-70 cm.

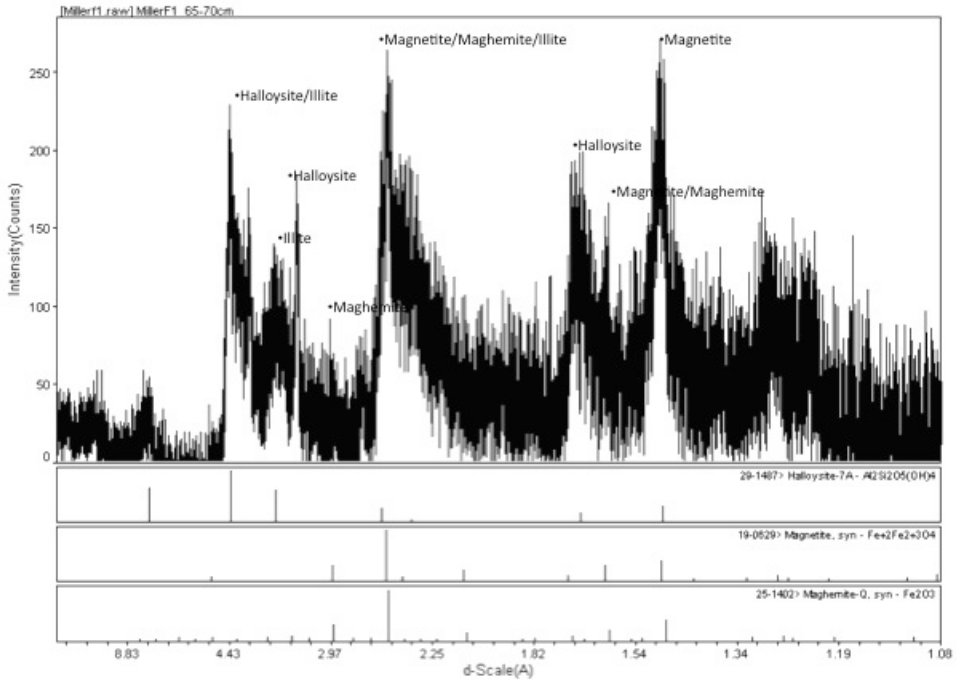

Major mineral components of soil:

–Halloysite ($Al_2Si_2O_5(OH)_4$)
- (D_2-spacing = 4.36Å, D_3-spacing = 3.35Å)

–Magnetite (Fe_3O_4)
- (D_1-spacing = 2.53Å, D_2-spacing = 1.614Å, D_3-spacing = 1.483Å)

–Maghemite (γ-Fe_2O_3)
- (D_1-spacing = 1.61Å, D_2-spacing = 2.52Å, D_3-spacing = 2.95Å)

–Illite ($K_yAl_4(Si_{8-y},Al_y)O_{20}(OH)_4$, usually with $1 < y < 1.5$, but always with $y < 2$)
- (D_1 = 4.43Å, D_2 = 2.56Å, D_3 = 3.66Å)

Figure 2.7: Scanning electron microscopic image of *Pseudomonas putida* cells in soil matrix. Image taken from P-depleted biotic treatment at the end of the first sampling interval (T < 1 hour). Rod shaped *P. putida* cells were often aggregated into filamentous branches (arrows) that were several segments longer than individual rods. Mineral grains range in size from 2-5 μm.

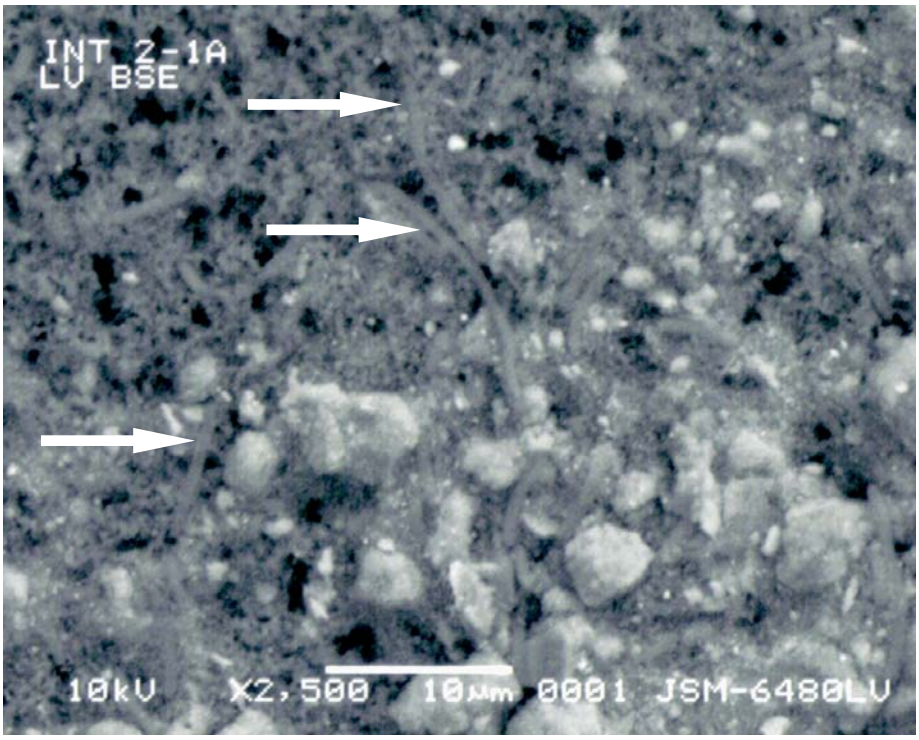

Figure 2.8: Solution pH for each of the media treatments (P-enriched, P-depleted, P-enriched + DFAM, P-depleted + DFAM) under (a) abiotic, and (b) biotic conditions.

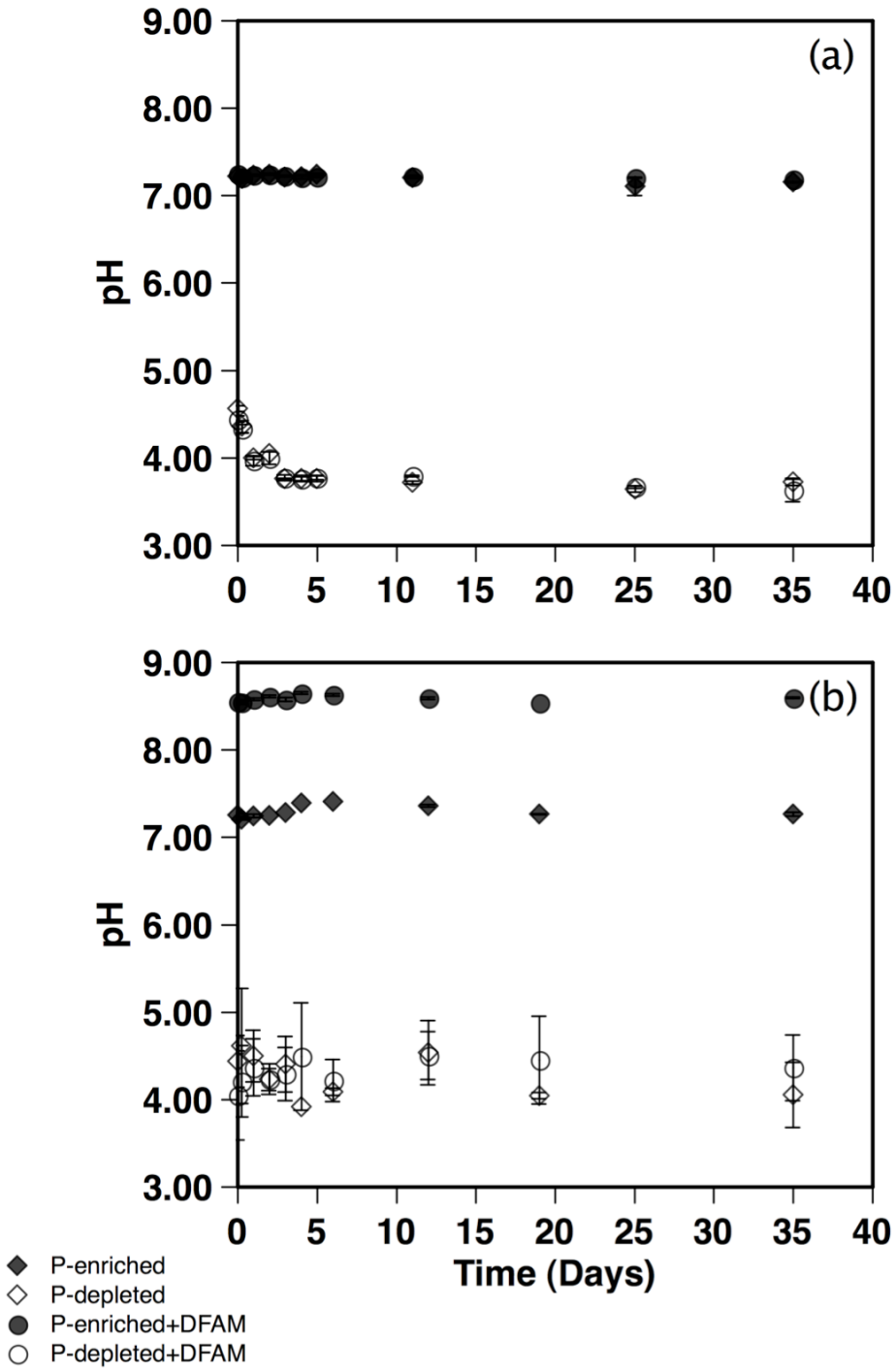

Figure 2.9: Aqueous Fe (μmol L^{-1}) versus time (days) for treatments (*P. putida*, *P. putida* + DFAM, Abiotic, Abiotic + DFAM) in (a) P-depleted and (b) P-enriched media.

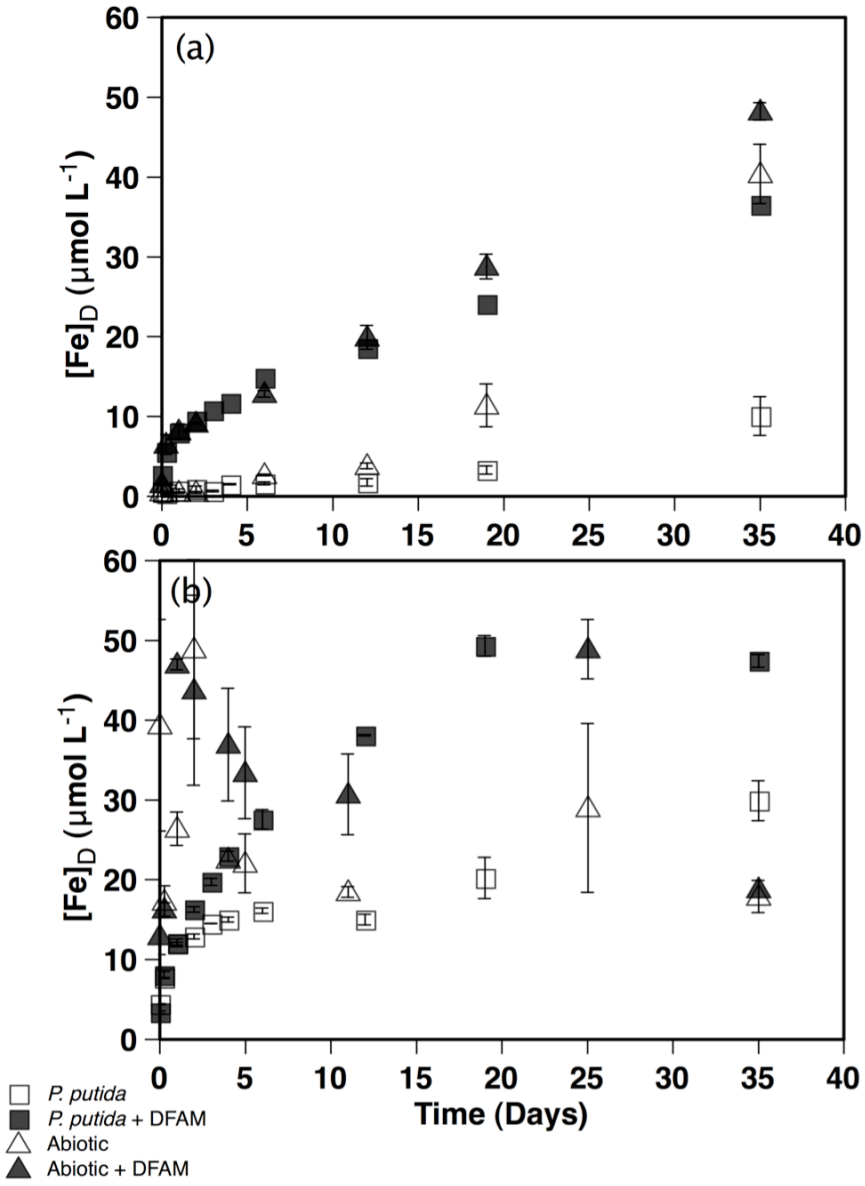

Figure 2.10: Aqueous Fe(II) (μmol L^{-1}) versus time (days) for treatments (*P. putida*, *P. putida* + DFAM, Abiotic, Abiotic + DFAM) in (a) P-depleted and (b) P-enriched media.

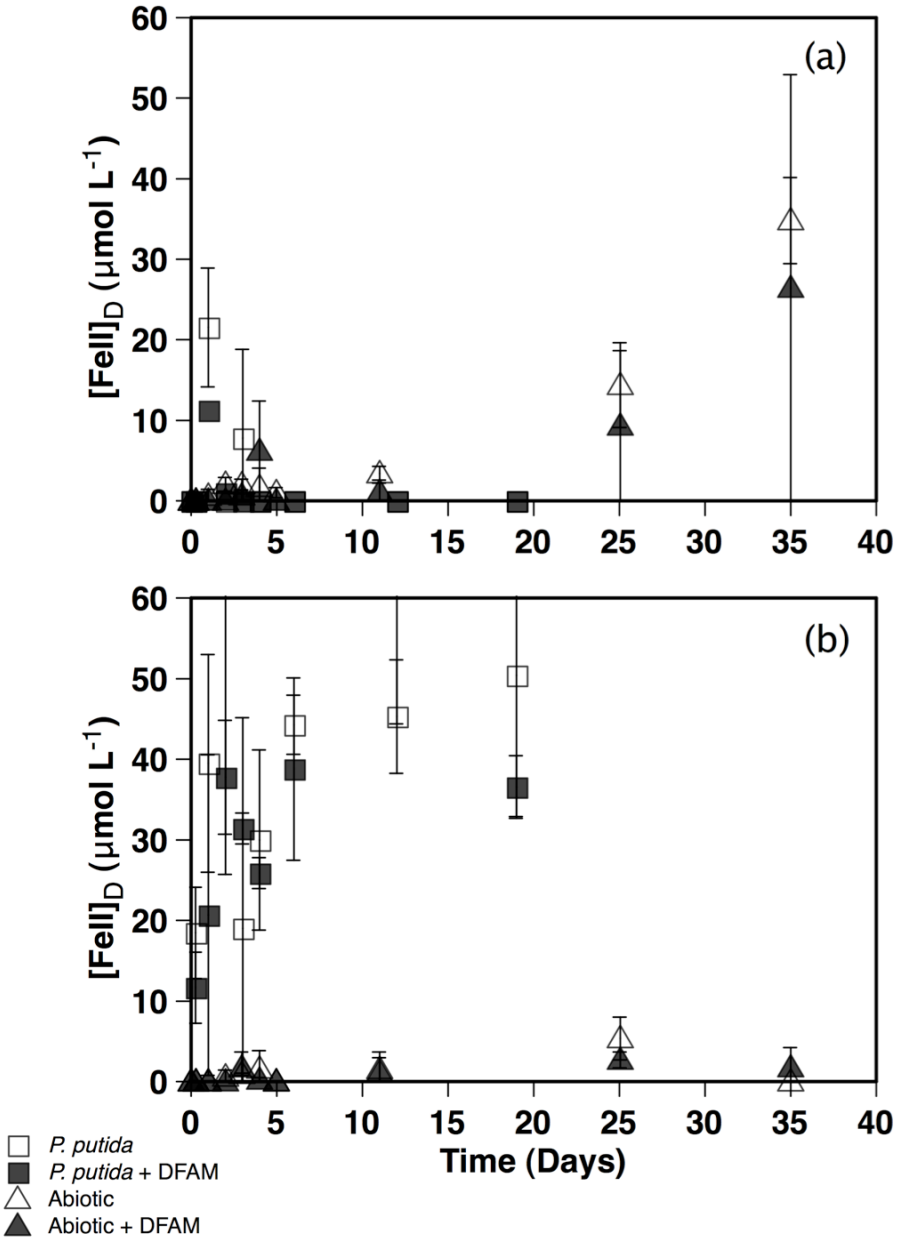

Figure 2.11: Aqueous Fe(III) (μmol L^{-1}) versus time (days) for treatments (*P. putida*, *P. putida* + DFAM, Abiotic, Abiotic + DFAM) in (a) P-depleted and (b) P-enriched media.

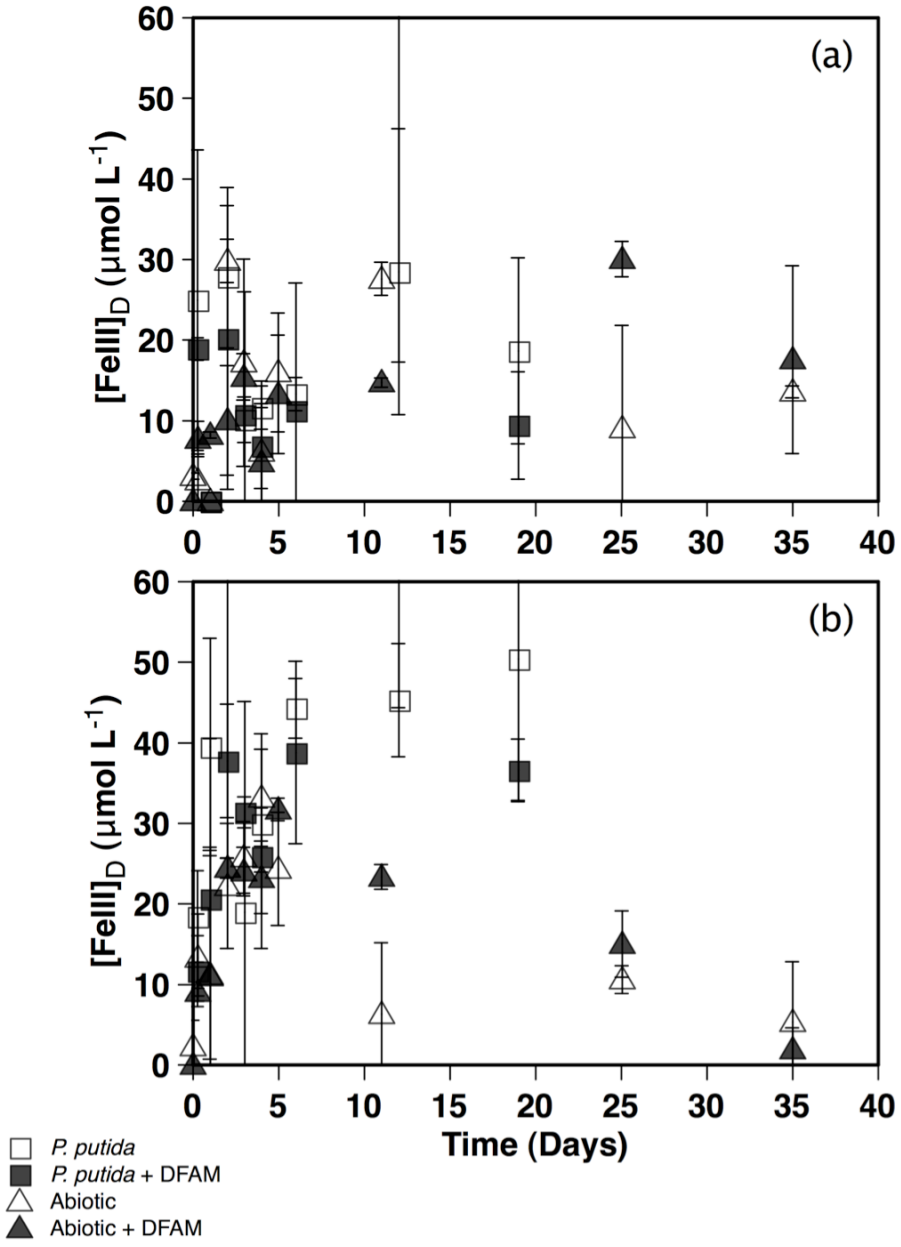

Figure 2.12: Aqueous Al (μmol L^{-1}) versus time (days) for treatments (*P. putida*, *P. putida* + DFAM, Abiotic, Abiotic + DFAM) in (a) P-depleted and (b) P-enriched media.

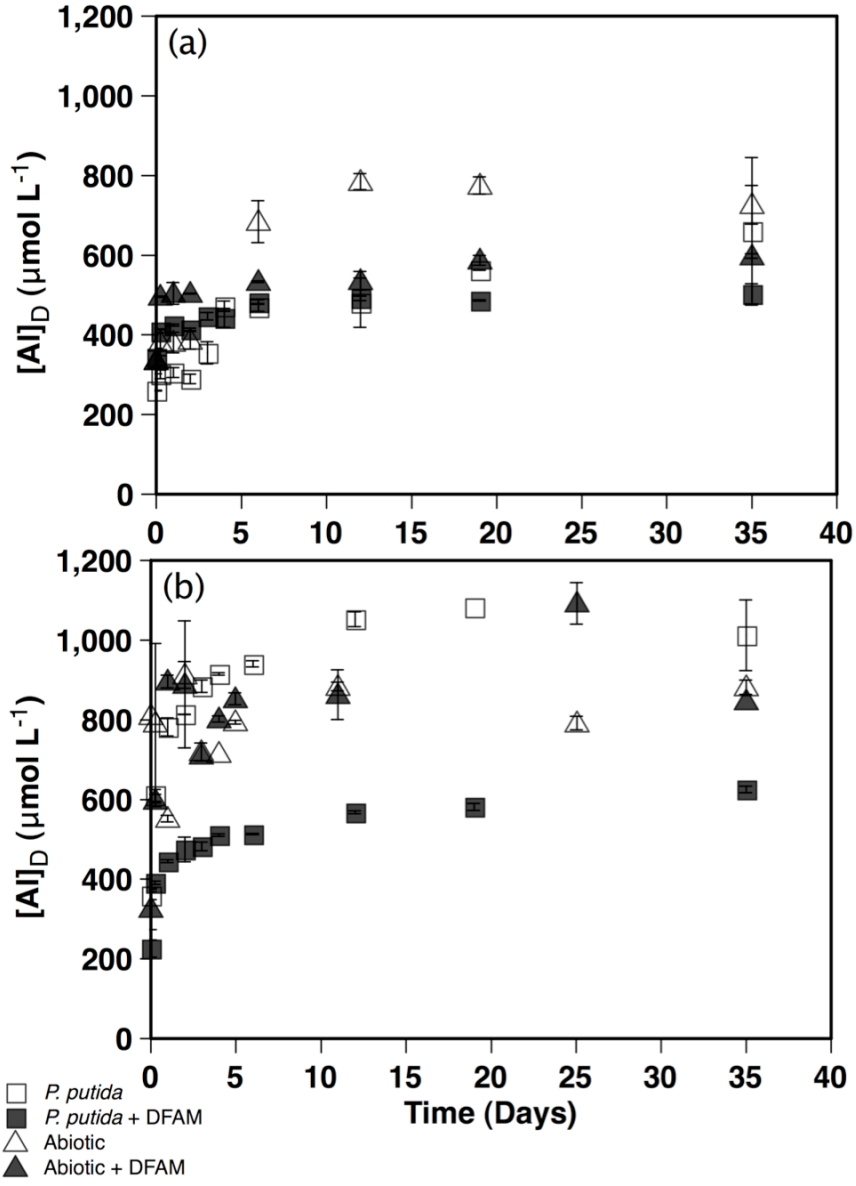

Figure 2.13: Aqueous Si (µmol L^{-1}) versus time (days) for treatments (*P. putida*, *P. putida* + DFAM, Abiotic, Abiotic + DFAM) in (a) P-depleted and (b) P-enriched media.

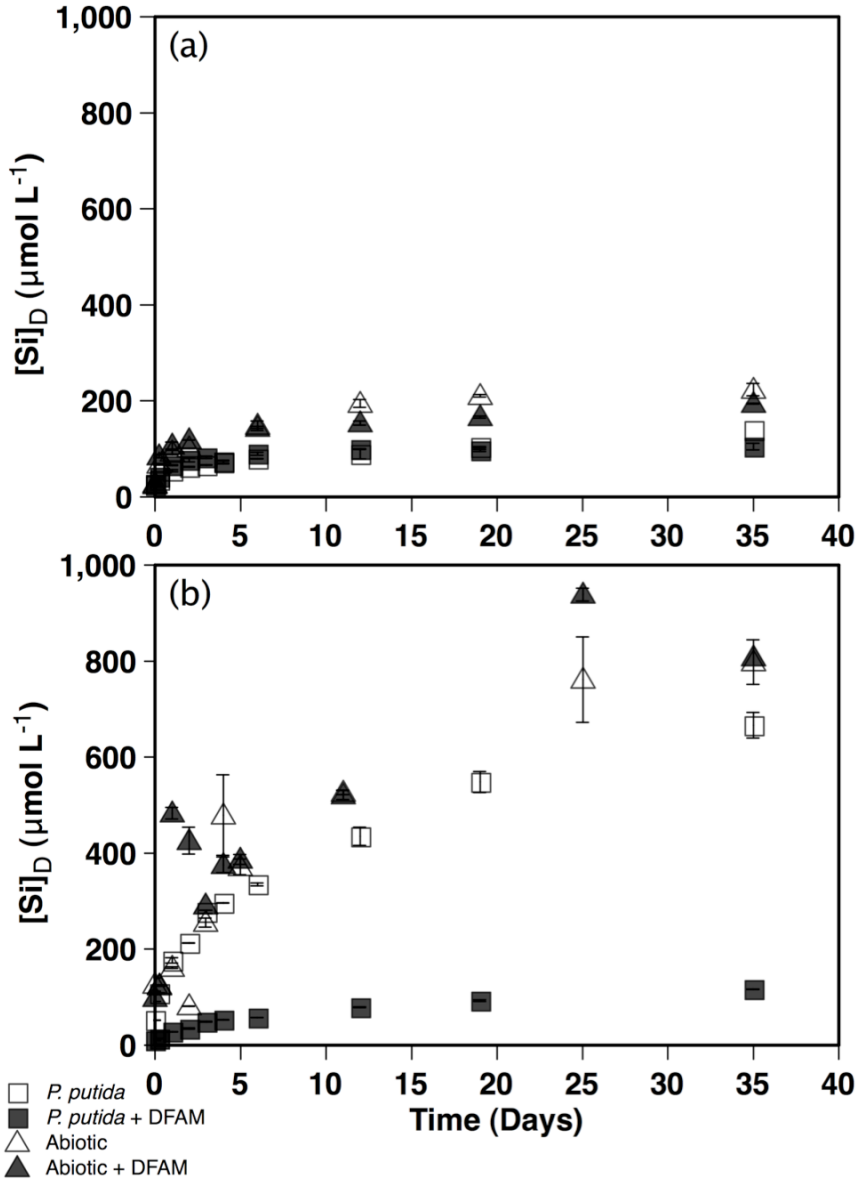

CHAPTER 3

METHANOTROPHS IN PANAMA

INTRODUCTION

In chapter 2 (this volume), soils were collected from Barro Colorado Island (BCI), Panama (figure 3.1) and used in a study investigating the role of siderophores upon mineral weathering. As an Fe(III) chelating compound, siderophores promote mineral weathering by forming surface complexes with Fe(III) and detaching from the mineral matrix (Holmen and Casey, 1996). Numerous microorganisms dependent upon Fe for energy will generate siderophores when Fe is not readily available in solution (Kraemer, 2004). The highly weathered oxisols of BCI tend to be enriched with iron oxide minerals in the residuum. However, Fe is sparingly mobile under these conditions, and bacteria become reliant upon chelating agents such as siderophores to promote Fe solubility and fulfill their nutrient demands. In addition to Fe deficiency, the mobility of metals, such as Cu is also limited, and is of interest because Cu is a key nutrient for methanotrophs.

Methanotrophs are microorganisms that oxidize CH_4 and rely upon it for their sole source of carbon and energy (Hanson and Hanson, 1996). During methanotrophy, CH_4 and O_2 are converted to CO_2 and H_2O. Copper is used by methanotrophs to regulate the enzymes responsible for activating methane oxidation, i.e., the soluble (sMMO) and particulate methane monooxygenase (pMMO) enzymes, see below). This requirement for Cu may in fact result in a number of biological processes that promote enhanced mineral weathering when aqueous Cu is scarce. During periods of Cu stress, several methanotrophs are known to generate a Cu-binding compound called methanobactin (Kim et al., 2004). Similar to the relationship between siderophores and Fe(III)

(Kalinowski et al., 2000), methanobactin is expected to enhance Cu solubility in minerals by the formation and detachment of a surface complex. Bioavailable Cu will benefit methanotrophs with respect to their enzymatic activity. If a direct linkage exists between mineral solubility reactions, Cu availability, and methanotrophy, then these relationships need to be measured in order to improve upon the precision of traditional carbon cycling models (e.g., Berner, 1999).

The presence of methanotrophs on BCI was examined for the purpose of identifying environmental isolates and determining whether these isolates shared common attributes with strains such as *Methylosinus trichosporium* OB3b, a well known, and thoroughly studied methanotroph with the capability of generating methanobactin (Graham et al., 2003; Hakamenian et al., 2005; Kim et al., 2004; Murrell, 2009). In a previous collaboration (Knapp et al., 2007), soil samples collected from BCI were used to evaluate the gene expression of methane monoxygenase (MMO) as mediated by methanobactin in the presence of different mineral copper sources. The soils I collected were from a site on BCI (Miller Forest, figure 2.5) where the soil profile had previously been characterized for Cu and other metals (Wilson, 2005). The soil samples were used to generate evidence for the presence of methanotrophs in Panama (DNA sequencing performed by A.H. O'Neill, 2005), and the published findings indicated that an alternate system to the Fe-siderophore relationship (siderophore-promoted Fe mobilization) exists within soils of Panama (Knapp et al., 2007). The alternate system involves a methanobactin-mediated process of Cu acquisition from mineral sources to fulfuill the metabolic requirement of methanotrophs. In addition to soil collection, my contribution to the article was the synthesis of Cu-substituted borosilicates and iron oxides which were

used in the gene expression experiments. I also provided evidence for the surface colonization of Cu-substituted borosilicate glass by *M. trichosporium* OB3b cells by means of scanning electron microscopy [the cover image for PNAS volume 104 (Appendix VI)].

Methanotrophy

Methanotrophic bacteria, or methanotrophs, are aerobic prokaryotes that use CH_4 as a sole carbon and energy source (Hanson and Hanson, 1996). The habitat for methanotrophs includes any location where air and CH_4 are simultaneously present. Such habitats include soils, sediments, wetlands, lakes, and marine systems where a boundary between oxic and anoxic conditions exists. The practical significance of methanotrophs is the role that they play in the global carbon cycle (Cicerone and Oremland, 1988; Thiesen and Murrell, 2005). Methane, a potent greenhouse gas in terms of how strongly it absorbs long wave radiation (Cicerone and Oremland, 1988; Conrad, 1996; Wuebbles and Hayhoe, 2002), is mineralized by the activity of methanotrophs. The complete pathway for CH_4 oxidation occurs via multiple stages of carbon transformation before CH_4 is converted to CO_2:

$$CH_4 \rightarrow CH_3OH \rightarrow CH_2O \rightarrow HCOO^- \rightarrow CO_2 \qquad (3\text{-}1)$$

In this sequence, methanotrophs will assimilate formaldehyde (CH_2O) as a major source of cellular carbon. The defining characteristic of methanotrophs is the use of enzymes known as methane monooxygenases (MMOs) to catalyze the initial oxidation of CH_4 to methanol (CH_3OH) (Hanson and Hanson, 1996; Madigan and Martinko, 2005).

Methanotroph Ecology

Sufficient CH_4 is required to stimulate methanotrophic activity. While atmospheric concentrations of CH_4 (1.7 ppmv) are adequate to sustain the activity of methanotrophic bacteria, mixing ratios of CH_4 in air must exceed 100 to 1000 ppmv for soils to exhibit increases in microbial CH_4 oxidation activity and the numbers of methanotrophic bacteria (Bender and Conrad, 1995; Dunfield et al., 1999). A number of physicochemical soil parameters will also influence methanotrophic activity and these include soil moisture, pH, temperature, ammonium (NH_4^+) concentration, Cu^{2+} concentration and aggregate size (Hanson and Hanson, 1996). Oxygen content has also been shown to have an influence on methanotrophic activity where soils incubated with 0.2 or 2% oxygen exhibited lower methanotrophic activity compared to soils incubated with ambient air (Schnell and King, 1995). Kightley et al. (1995) showed that CH_4 oxidation potentials were greatest in porous, coarse sand soil where vertical profiles of O_2 and CH_4 overlap. Ammonia/ammonium is used as a source of nitrogen by all methanotrophs (Whittenbury et al., 1970; Bedard and Knowles, 1989; Hanson and Hanson, 1996; Hooper et al., 1997). Many are capable of using NO_3^- (Leak and Dalton, 1986; Roy and Knowles, 1994) and NO_2^- (Bedard and Knowles, 1989; King and Schnell, 1994), whereas some methanotrophs participate in N_2-fixation (Kim and Graham, 2003; Bowman, 2006; Murrell, 2009).

Methanotroph genera have been separated into three major assemblages, Type I, Type II and Type X, based on numerous morphological and physiological differences (Hanson and Hanson, 1996). The predominance of one type over the other can be determined by a given set of environmental conditions. Type II methanotrophs are more

prevalent in environments with abundant CH_4 but low oxygen, Cu and nitrogen, while Type I methanotrophs are more successful under the opposite conditions (Graham et al., 1993; Amaral et al., 1995). Type I methanotrophs typically express pMMO for CH_4 oxidation, while Type II and Type X strains can express both pMMO and sMMO depending upon the copper-to-biomass conditions (Hanson and Hanson, 1996). However, the prevalence of pMMO over sMMO in the soil is regulated by Cu bioavailability (Burrows et al., 1984; Dalton et al., 1984; Hanson and Hanson, 1996), which is expected to control methanotroph selection and consequently CH_4 flux rates.

Methanotrophs are neutrophilic and as such prefer soil aqueous conditions with a pH near 7 (Bender and Conrad, 1992). While reports of growing methantrophs at pH values below 5.0 are scarce, there have been studies showing methanotrophic populations that are partially adapted to acidic environments (Hanson and Hanson, 1996; Dedysh et al., 2001; Dedysh, 2002). While a wide range of pH values have been reported for tropical soils, acidic conditions are more common (Mohr et al., 1972; Brady and Weil, 2002). Key factors that determine soil pH include the type of mineral and organic matter content (Zinke, 1962; Boettcher and Kalisz, 1990; Finzi et al., 1998; Bronick and Lal, 2005; Williard et al., 2005), and hydrologic conditions (Hornung et al., 1986; Brady and Weil, 2002; White et al., 2004). In any case, methanotrophic communities have been confirmed at specific sites within the rainforest soils of Barro Colorado Island, Panama (Knapp et al., 2007).

Most methanotrophs are mesophiles, and, therefore, the optimum temperature for CH_4 oxidation is ~25^{o}C for most peat soils. However, in nature, methanotrophs adapt to changes in temperatures and different soils exhibit varying CH_4 oxidation responses with

respect to temperature. Methane oxidation has been documented at temperatures as low as 0 to 10^{o}C, typical of temperate and subarctic peat bogs (Hanson and Hanson, 1996; Dunfield et al., 1993) boreal forests (Hanson and Hanson, 1996; Whalen et al., 1992) or tundra soils (Hanson and Hanson, 1996; Whalen and Reeburgh, 1990), and as high as 35^{o}C, more representative of tropical wetlands (Hanson and Hanson, 1996; Dedysh et al., 2001).

Wetland soils are generally anoxic due to a relatively high water table compared to uplands. At shallow depths below the water table, within the phreatic zone, the dissolved oxygen content is rapidly depleted by heterotrophic aerobes (Eby, 2004). The soils may even be subjected to extended periods of inundation. However, atmospheric oxygen penetration from the surface creates a thin (1- to 5-mm-deep) oxic soil layer (Conrad, 1996). As much as 90% of the CH_4 produced from wetlands is consumed in the oxic surface layer, although significant variability has been observed (Conrad, 1996; Le Mer and Roger, 2001; Segers, 1998). While wetlands are traditionally considered to be major sources of CH_4, conditions may shift such that the wetland becomes a CH_4 sink. Methane oxidation becomes more dominant during a drying cycle, where the water table drops and the previously anaerobic zones of the depth profile become aerobic (Saarnio et al., 1997). The upward migration of microbially generated CH_4 from the anaerobic zone to the overlying aerobic zone promotes the metabolic oxidation of CH_4 to CO_2 by methanotrophs (Riveros-Iregui and King, 2008). Typically, the “hot spot” for methanotrophy occurs just above the anoxic-oxic boundary, where microaerophilic conditions persist (Conrad, 1996; Dumont and Murrell, 2005; Hanson and Hanson, 1996). In soils, the microaerophilic boundary layer is limited to a narrow band

(Mancinelli, 1995), while in lake water columns the microaerophilic zone has been known to expand and migrate vertically (Carini et al., 2005).

Kinetics of Methane Oxidation in Soils and Sediments

Michaelis-Menten kinetics can be used to describe the kinetics of methane oxidation, where V_{max} is the maximum rate of reaction and K_m is the substrate concentration when the rate of the reaction (V) is equal ½ V_{max}. Two types of kinetic patterns for CH_4 oxidation have been encountered in soils and sediments. The first type is known as low-affinity CH_4 consumption, and is observed in all CH_4 -producing soils, in particular natural wetlands, landfills, and rice paddies. Conventional type I and II methanotrophs are responsible for this kinetic pattern where threshold CH_4 concentrations are less than 1nM and K_m values range from 800 to 66,000 (Conrad, 1996). The second type of kinetic pattern is referred to as high-affinity CH_4 oxidation and only occurs in soils that receive CH_4 from the atmosphere. Low apparent K_m values (20-200) are observed in these soils where threshold CH_4 concentrations range from 0.03 to 0.7 nM (Conrad, 1996; Bodelier and Laaunbroek, 2004; Bender and Conrad, 1992). Recent findings indicate that CH_4 oxidation kinetics are influenced differently by the active enzymes, which are dependent upon both the CH_4 mixing ratio (Banni and Liesack, 2008), and the bioavailable concentration of Cu (Hanson and Hanson, 1996). Reported K_m and V_{max} values for CH_4 oxidation using purified MMO were 3 μM and 56 nmol mg of protein^{-1} min^{-1}, respectively (Fox et al., 1989; Hanson and Hanson, 1996).

Enzymatic oxidation of CH_4 and the role of Cu

Methanotrophs use copper (Cu) to regulate the enzymatic oxidation of CH_4. The two major enzymes involved include soluble methane monooxygenase (sMMO) and particulate methane monooxygenase (pMMO), however, not all methanotrophs are capable of expressing sMMO (Hanson and Hanson, 1996). For the methanotroph species that are capable of expressing sMMO (i.e., *M. trichosporium* OB3b), the activation of sMMO vs. pMMO is determined by the Cu-to-biomass ratio. At a low Cu-to-biomass ratio (< 0.89 μmole of Cu per g [dry weight] of cells) sMMO is expressed, while at a high Cu-to-biomass ratio (> 0.89 μmole of Cu per g [dry weight] of cells) pMMO is expressed (Burrows et al., 1984; Dalton et al., 1984; Hanson and Hanson, 1996). Research efforts have made significant advances in terms of understanding of the function of these enzymes. For instance, we know that sMMO is activated within the cytoplasm of the cell, whereas, pMMO is activated on the cell wall (Lontoh and Semrau, 1998). Considering that low Cu concentrations are required for sMMO expression, internal utilization of Cu is necessary to oxidize CH_4. At higher Cu concentrations, activation of pMMO is necessary to regulate the amount of Cu that enters the cell for CH_4 oxidation and to prevent toxicity (Murrell et al., 2000). The active pMMO enzyme, when expressed, supports higher CH_4 oxidation rates than sMMO (Lontoh and Semrau, 1998; Choi et al., 2003; Zahn and DiSpirito, 1996), which would have a substantial effect on the mass transfer of CH_4 to the atmosphere. Copper concentrations greater than 4.3 mM Cu^{2+} inhibit CH_4 oxidation activity in soils (Bender and Conrad, 1995).

Methanobactin

Methanotrophs often rely on molecular-mediated extracellular Cu acquisition for delivery of Cu to the cell. Methanobactin is a high affinity, Cu-binding compound (a chalkophore) synthesized by some methanotrophs, e.g., *Methylosinus trichosporium* OB3b and *Methylococcus capsulatus* Bath (Balasubramanian and Rosenzweig, 2008; Kim et al., 2004). This non-ribosomal chromopeptide ($C_{45}N_{12}O_{14}H_{62}Cu$, 1216 daltons) is utilized by the methanotrophic bacterium to acquire and shuttle Cu back to the cell during CH_4 oxidation. The primary sequence of methanobactin has been described as N-2-isopropylester-(4-thionyl-5-hydroxy-imidazole)- Gly^1-Ser^2-Cys^3-Tyr^4-pyrrolidine-(4-hydroxy-5-thionyl-imidazole)-Ser^5-Cys^6 -Met^7. A number of moieties of the mb molecule thought to bind Cu using nitrogen and sulfur ligands include the 4-thiocarbonyl-5-hydroxy imidazole (THI), 4-hydroxy-5-thiocarbonyl imidazole (HTI) and possibly tyrosine, methionine, among other residues (Balasubramanian and Rosenzweig, 2008; Kim et al., 2004; 2005) (Figure 3.2b – schematic of methanobactin). The Cu binding affinity of methanobactin produced from *M. trichosporium* OB3b has been estimated to be $>8 \times 10^{16}$ M^{-1}, which suggests a potential role as an extracellular component of Cu acquisition (Choi et al., 2006).

In addition to Cu uptake, methanobactin may function in the regulation of MMO expression, protection against Cu toxicity, and to sustain pMMO activity (Balasubramanian and Rosenzweig, 2008; Knapp et al., 2007). Methanobactin has been shown to accelerate Cu uptake by *M. trichosporium* OB3b and shorten the growth lag that is typically observed upon a sudden elevation of Cu levels from previously Cu-starved conditions (Kim et al., 2005). Copper toxicity to *M. trichosporium* OB3b was

suppressed by the addition of sufficient quantities of mb, where 1:1 ratios of Cu and mb prevented the immediate decrease in 16S-rRNA transcript levels (Knapp et al., 2007). The protective effect is derived from superoxide dismutase activity, which is active in Cu-mb complexes (Choi et al., 2003).

Relevance of methanobactin in soils

In natural soil settings, methanobactin may be responsible for the enhancement of mineral weathering when the Cu supply is limited. The high Cu affinity of methanobactin is analogous to iron siderophores, suggesting a similar mechanism of handling (Balasubramanian and Rosenzweig, 2008; Kim et al., 2004). In addition to binding with Cu, methanobactin is capable of forming complexes with number other metals of similar ionic radii (e.g., Ag(I), Au(III), Cd(II), Co(II), Fe(III), Hg(II), Mn(II), Ni(II), Pb(II), U(IV) and Zn(II); Choi DW et al., 2006), however, the specificity for Cu far exceeds that of other metals (Tellez et al., 1998).

We examined the role of siderophores and siderophore generating microorganisms (i.e., *Pseudomonas putida*) with respect to mineral weathering in chapter 2 of this volume. The structure of methanobactin with respect to how it coordinates Cu is similar to siderophores such as azobactin and pyoverdin in terms of how Fe(III) is coordinated (figure 3.2). In methanobactin, Cu is tetrahedrally coordinated by dual nitrogen- and sulfur-donating systems from the thionyl imidazolate moieties (Kim et al., 2004). The geometric structure of mb:Cu complex permits a limited number of Cu atoms per methanobactin molecule, as such Cu transport to the cell is regulated by the number of methanobactin molecules (Kim et al., 2004). The same can be said for Fe(III)

regulation to the cell by siderophores. While the Fe(III) coordination structure can vary between siderophores (e.g., figure 3.2a and c), the multidentate coordinations, like the mb:Cu complex, or the pyoverdin-Fe(III) complex, are associated with high stability constants (Boukhalfa et al., 2006, Choi et al, 2006). The high affinities promote solubility as the surface of mineral matrix is destabilized by the formation and detachment of ligand-metal complex. Consequently, the solubility of Cu as promoted by methanotrophs via methanobactin production may perhaps represent a novel mechanism for mineral weathering.

The release of Cu from mineral sources is expected to influence rates of CH_4 oxidation by activating the MMO enzymes (sMMO or pMMO) in methanotrophs. Laboratory investigations applying reverse transcript-polymeric chain reactions (RT-PCR) suggest that pMMO transcript levels in *M. trichosporium* OB3b will increase in the presence of methanobactin and Cu from mineral sources (Knapp et al., 2007). The implications of these findings are that Cu is mobilized from the solid phase by biological processes, with a direct influence upon the enzymatic activity of methanotrophs.

Methanotrophs in the Tropical Soils of Panama

Barro Colorado Island was chosen as a key location to investigate methanotrophy in tropical soils due to the multiple biological sources and sinks of CH_4 found throughout the island (figure 2.5 – BCI, Panama). Methane flux from soils on BCI is attributed to changes in soil moisture content where CH_4 consumption is favored during seasonal dry conditions as compared to the wet season, which is responsible for generating long periods of soil inundation and anaerobic conditions. The various swamps on BCI and

Gatun Lake represent the wet environments that emit significant quantities of CH_4. A wetland area of 2500 m^2 is estimated to release as much CH_4 as a square kilometer of forest will consume (Keller and Stallard, 1994; Condit et al., 2001) resulting in a net surplus of CH_4 production when the ratio of wetland-to-forest is in equal proportion.

In March 2005, soil samples were collected from multiple sites on BCI with the objective to characterize the community structure with respect to methanotrophs. One site included multiple soil sample collections from stream sediments at depth along the site of the Armour-Zetec trail junction (shortcut) within the 50-hectare plot (figures 3.3 and 3.4). At this particular site on BCI, the surface soil conditions have been thoroughly characterized for nutrients, metals, and pH. While CH_4 mixing ratios have a significant influence on the metabolic activity of methanotrophs, the soil pH, and Cu and N content are also relevant. Additionally, because these sediments were saturated and qualitatively appeared to be anaerobic at depth (based on observations of sediment color) a source of biogenic methane was assumed. Samples collected were used to isolate methanotrophs native to this tropical soil setting. Sterile mini corers were used to collect soil samples. To prevent cross-contamination and maintain sterility, nitrile gloves were worn by sample-collectors and extraction equipment was cold-sterilized with ethanol prior to collection. Upon collection, the sediment cores were returned to STRI where they were stored at -80^oC until being shipped to the Great Lakes Institute for Environmental Research (GLIER), University of Windsor, for continued storage at -80^oC. Some samples were shipped to the Department of Geology, University of Kansas, for microbial community structure analysis. Descriptions of the colonies grown on NSM-Noble agar medium plates from each section of the Armour-Zetec core are provided (table 3.1). Cream colored, egg-

like features were observed, which is typical of methanotroph colonies such as *M. trichosporium* OB3b (Graham et al., 1992).

Several successful methanotroph isolates were acquired and assayed for their ability to consume methane (C.W. Knapp, unpublished data; figure 3.3). Isolates from samples [AZ3-1, AZ3-2, AZ3-3, AZ5-1, AZ5-2, and AZ5-3 (Amour-Zetec core 3, 1-2 cm depth, 2-3 cm depth, 3-4 cm depth and Amour-Zetec core 5, 1-2 cm, 2-3 cm, and 3-4 cm, respectively)] were grown on separate plates and then inoculated into 30-ml of nitrate minimal salts (NSM) growth media in individual 125-ml serum vials with a headspace mixture of air and CH_4 (50%). The monitoring of CH_4 consumption over a 14-day trial for soils with no Cu and soils spiked with Cu (2.5 μM Cu) was compared using C14/C0 box plots where C14 represents the CH_4 concentration on the 14^{th} day and C0 is the CH_4 concentration at time zero (figure 3.4, Knapp unpublished data, 2005). Rates of CH_4 consumption were determined, which confirmed that methanotrophs were revived from the Armour-Zetec isolates both in the presence and absence of Cu. Genotypic characterization of one of the soil isolates placed it in the Type II cluster near *M. trichosporium* OB3b within the Alphaproteobacterial division of the eubacterial domain and the name *Methylosinus sporium* strain NR3K was applied (Knapp et al., 2007, figure 3.5). This demonstrates that strains similar to *M. trichosporium* OB3b are as common as are the wetland environments that host them, therefore, activity of these methanotrophs on a global scale should have a profound impact upon CH_4 consumption.

In parallel with the isolate characterization, the successfully grown cultures were maintained in separate 2-L bioreactors under the growing conditions used for all methanotrophs (Kim et al., 2005; Stanley et al., 1983; Whittenbury et al., 1970). Upon

reaching a cell density corresponding to an OD_{600} between 0.4 and 0.6, the spent media was harvested for the screening of methanobactin-like molecules. Following the methanobactin isolation protocol by Kim et al. (2005), 1,215.4-Da fragments were detected in both media, which resemble known fragments from *M. trichosporium* OB3b (figure 3.6, Knapp et al., 2007). A recognizable similarity between MALDI-TOF spectra for methanobactin isolated from *M. trichosporium* OB3b and *Methylosinus sporium* strain NR3K can be identified. This not only implies that other methanotrophs are capable of methanobactin production, but that methanobactin production on BCI is possible given the appropriate conditions, e.g., low Cu-to-biomass ratios.

The predominant methanotroph type and concentration of bioavailable Cu in a natural setting will impact local rates of CH_4 oxidation since the active pMMO enzyme yields considerably higher growth rates and a greater affinity to CH_4 compared to sMMO (Hanson and Hanson, 1996). The higher growth efficiency when pMMO is activated has been attributed to a reduced NADH requirement for CH_4 oxidation (Leak and Dalton, 1986). Presumably, increased cell numbers results in greater consumption of CH_4. Therefore, the prevalence of pMMO over sMMO in a natural setting has implications with respect to greenhouse gas suppression and attempts to regulate these enzymes will impact the local gas fluxes. While the linkage between CH_4 flux and methanotroph ecology needs further clarification, the presence of methanobactin and its role in Cu sequestration has been recognized (Kim et al., 2004).

Quantitative gene expression (sMMO and pMMO) correlated with soil Cu content and methanobactin concentrations

Efforts to understand the role of methanobactin in natural systems have been attempted by means of laboratory experiments that address the issue of Cu bioavailability through a number of different quantitative approaches. From batch cultures of *M. trichosporium* OB3b, Knapp et al. (2007) used real-time reverse transcription of mRNA to quantify the expression of pMMO with increasing mb concentration. A variety of Cu sources were compared in separate experiments, which included Cu-bearing silicate glasses, synthetic Cu-substituted iron oxides, and Cu-bearing oxisols from Panama (prepared or collected by Kulczycki, Appendix A and B). The resultant elevated gene expression observed for *M. trichosporium* OB3b suggests that solid phase Cu can influence the enzyme activity of methanotrophs. The enhanced response to heterologous methanobactin suggests that Cu had been liberated from the mineral with immediate benefit to *M. trichosporium* OB3b.

The implication of Knapp's discovery (2007) is that the enzymatic activity of methanotrophs is influenced by solid phase sources of Cu, particularly if methanobactin is involved. Copper is only bioavailable in the aqueous phase. In oxidizing environments, Cu is often restricted to the mineral phase (e.g., clay minerals and Fe oxides). Hence, a biologically mediated Cu dissolution mechanism is suspect, and may be dependent upon methanobactin. Furthermore, the mobilization of Cu in response to methanotroph-mediated processes is expected to directly impact rates of biological CH_4 oxidation. Quantification of these processes may uncover a novel linkage between biologically

mediated mineral weathering and the carbon cycle, which hinges on Cu availability and methanobactin production.

In addition to the significant role that Cu has on determining methane oxidation rates it is not the only variable controlling this process. A number of field studies have shown that CH_4 oxidation in soil sediments is inhibited by the introduction of NH_4^+ or NO_3^- (Adamsen and King, 1993; Chan et al., 2005; Gulledge and Schimel, 1998; Gulledge et al., 2004; King and Schnell, 1994; Schnell and King, 1995). As previously postulated, the formation of NO_2^- from methanotrophic NH_4^+ oxidation is largely responsible for the inhibitory effect upon CH_4 oxidation (Dunfield and Knowles, 1995; King and Schnell, 1994; Schnell and King, 1995).

Methanotrophs and autotrophic nitrifiers both possess MMO enzymes, which makes them both capable of oxidizing CH_4 (Bedard and Knowles, 1989; Conrad, 1996; Gulledge et al., 2004). The ammonia monooxygenase (AMO) enzyme possessed by ammonia-oxidizing bacteria is also capable of activating CH_4 oxidation reactions (Hanson and Hanson, 1996). Several properties are shared between AMO and pMMO, which includes in vitro regulation by Cu, hence, a number of researchers have postulated that Cu is an active site in both enzymes (Ensign et al., 1993; Hanson and Hanson, 1996; Nguyen et al., 1994).

Specific methanotroph species that can oxidize NH_4^+ to NO_2^- in the presence of CH_4 have been identified (Bedard and Knowles, 1989), which includes *Methylobacter albus* BG8 and *Methylosinus trichosporium* OB3b (King and Schnell, 1994). Most methanotrophs assimilate ammonia and NO_3^- by the glutamine synthetase-glutamine 2-oxoglutarate aminotransferase system (Bellion and Bolbot, 1983; Murrell and Dalton,

1983; Toukdariant and Lidstrom, 1984). Methanotrophs also can assimilate nitrogen from amino acids and other complex mixtures such as yeast extract. In addition, many methanotrophs are able to fix atmospheric nitrogen, e.g., all Type II methanotrophs, and a few Type I methanotrophs, which include *Methylomonas* spp., *Methylococcus capsulatus*, and *Methylosphaera hansonii* (Bowman, 2006; Murrell, 2009). In most cases the nitrogenase formed is oxygen-sensitive (Murrell and Dalton, 1983b; Zhivotchenko et al., 1995) except for *Methylosphaera hansonii*, which appears to possess a more oxygen-tolerant enzyme (Bowman et al., 1997).

Tropical rainforests contribute abundant NH_4^+ to soil during the decomposition of detritus (leaf litter and other non-living particulate organic matter), a key process in the soil-plant N cycle (Barraclough, 1997; Yavitt, 2000). On Barro Colorado Island, the atmosphere itself is a major source of ammonia and NO_3^- during the abundant rainfall events (Mitchell, 2000). Ammonium can be consumed by several processes among which include plant uptake, nitrification, immobilization and volatilization. Heterotrophic bacteria that access the inorganic and organic pools of N compete more effectively for NH_4^+ than for NO_3^- during mineralization-immobilization turnover reactions (Jansson, 1958; Jenkinson et al., 1985; Schimel et al., 1989). While NH_4^+ is rapidly converted to NO_2^- and then NO_3^- by the enzymatic activity of NH_4^+ oxidizing microorganisms, a fraction of NH_4^+ is oxidized by methanotrophs as well (Dunfield and Knowles, 1995; King and Schnell, 1994; Schnell and King, 1994; Hanson and Hanson, 1996).

The production of biogenic CH_4 in tropical rainforest wetlands results from the abundant accumulation of soil organic matter during periods of inundation (Neue et al., 1997; Melack et al., 2004; Zhuang et al., 2009). A series of incubation experiments has

shown that optimum CH_4 production occurs at neutral pH and between an *Eh* range of -150 to -160 mV (Wang et al., 1993). With the lowering of the water table in response to a seasonal shift to dryer conditions, CH_4 oxidation is promoted at the soil-water interface (Saarnio et al., 1997; Riveros-Iregui and King, 2008). However, methanotrophy is inhibited if NH_4^+ is present, since MMO will co-oxidize both molecules (Dunfield and Knowles, 1995; Hanson and Hanson, 1996).

The soils of Barro Colorado Island represent a setting where the cycling of C and N, as controlled by Cu-activated MMO activity in methanotrophs, can be examined. In these highly weathered soils (i.e., oxisols) the source of Cu is expected to be restricted to the regolith or recalcitrant soil mineral content, in which case microbial agents of solubility (i.e., methanobactin) are required to make Cu bioavailable. Multiple soil characterization efforts have been performed on Barro Colorado Island that are relevant to the ecology of methanotrophs, which includes nutrient content within the 50-hectare plot (John et al., 2007), and trace metals at the forest and grassland sections of the Miller lighthouse (Wilson, 2005). Of particular relevance to methanotrophs, the mean soil Cu concentration and mineralized nitrogen (N_{min}) rates in the 50-hectare plot were 8.08 ± 2.04 mg kg^{-1}, and 17.84 ± 12.82 mg kg^{-1} per 28 days, respectively, with a soil pH of 5.66 ± 0.34 at the time of sampling (John et al., 2007). The forested site at the Miller lighthouse had a mean whole soil-Cu concentration of 105 ± 2 mg kg^{-1} and a mean pH of 5.22 ± 0.32, while the grassland had a mean whole soil-Cu concentration of 49 ± 11 mg kg^{-1} and a mean pH of 4.77 ± 0.16 (Wilson, 2005). Knowing how much Cu or inorganic-N is in the soil, as well as the pH, can provide an indication of how ecologically suitable the habitat at each site is for methanotrophs. Other variables need to be considered (i.e.,

CH_4 mixing ratios), however, when examining the role of Cu and NH_4^+, in terms of how efficiently the methanotroph enzyme (MMO) activity is performing in the field, these parameters become particularly valuable.

Table 3.1. Descriptions of colonies grown on plates from Armour-Zetec soil samples (modified from Knapp, 2005)

ID#	Core Source	Colony description	16S rDNA Sequencing	Liquid Growth
1	AZ5-1 (-,1)	Cream: egg-like features	**	**
3	AZ5-3 (-,1)	Cream: irregular		
5	AZ3-2 (-,1)	Smear		
9	AZ5-3 (+,1)	Cream: egg-like features		
10	AZ3-1 (+,1)	Light pink: faint		
13	AZ5-1 (-,.02)	Cream: irregular borders	Planned	**
14	AZ5-2 (-,.02)	Cream: egg-like features	Planned	**
15	AZ5-3 (-,.02)	Cream		
19	AZ5-1 (+,.02)	Cream: irregular borders, Pink colonies		
20	AZ5-2 (+,.02)	Cream: egg-like features		
23	AZ3-2 (+,.02)	Cream: egg-like features		

Figure 3.1. Map of Panama with inset showing Canal Zone and Barro Colorado Island (colored red). Taken from www.stri.org, 2006.

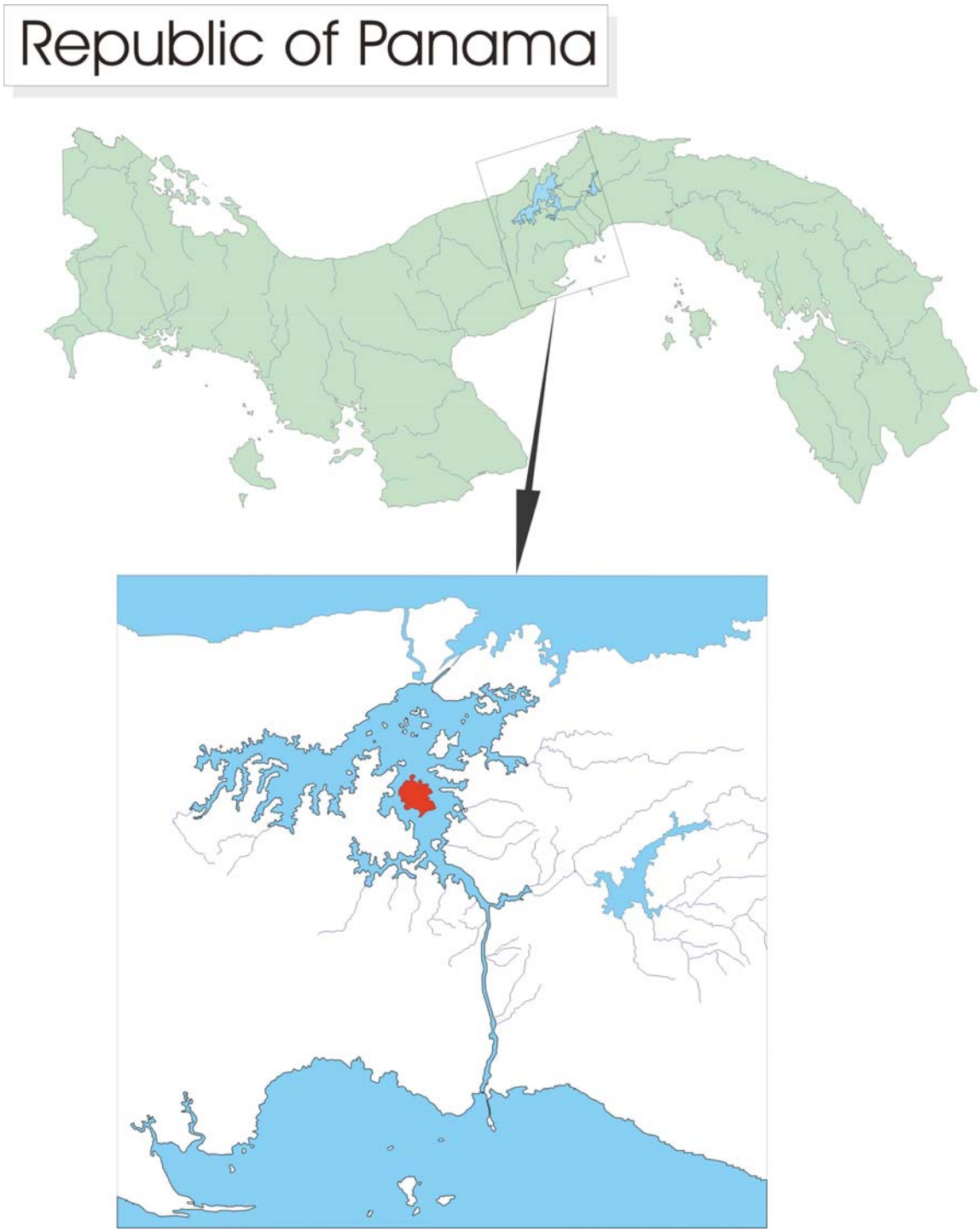

Figure 3.2. Chelate structures: (a) Pyoverdin complexed with Fe^{3+} from *Pseudomonas putida*. From DeMange *et al*. (1990). (b) Schematic of the revised structure of methanobactin From Behling et al., (2008). (c) Structure of azotobactin d from *Azotobacter vinelandii* complexed with Fe^{3+}. From DeMange *et al*. (1988).

(a)

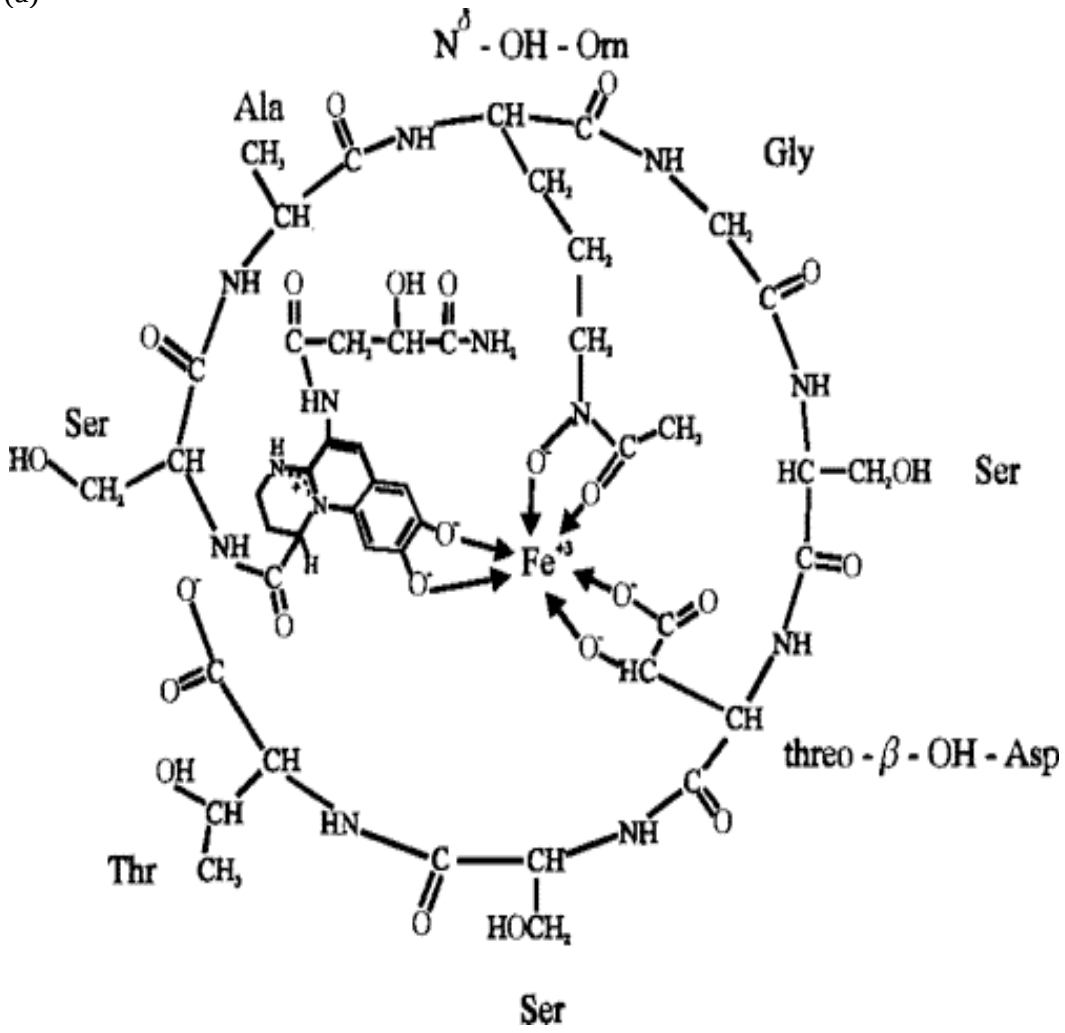

(b)

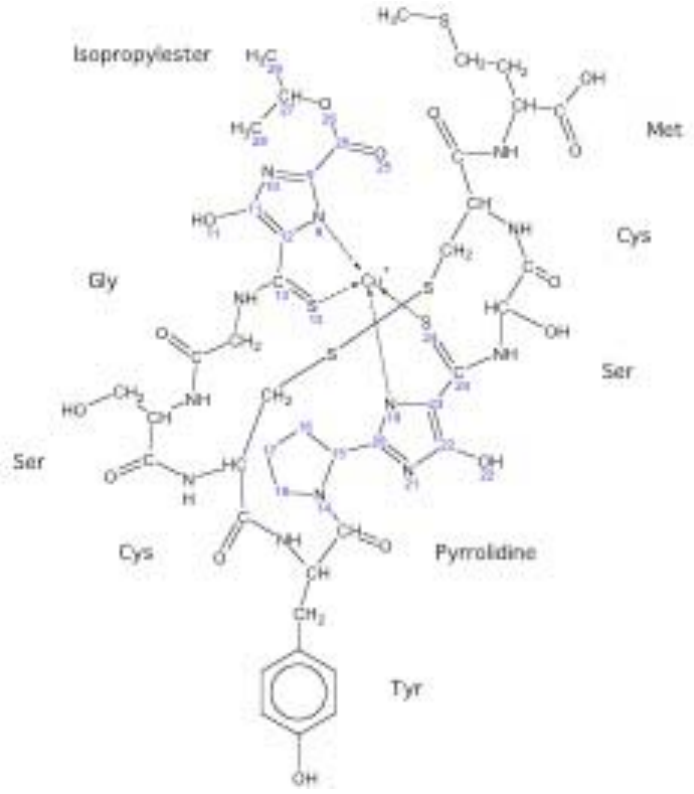

(c)

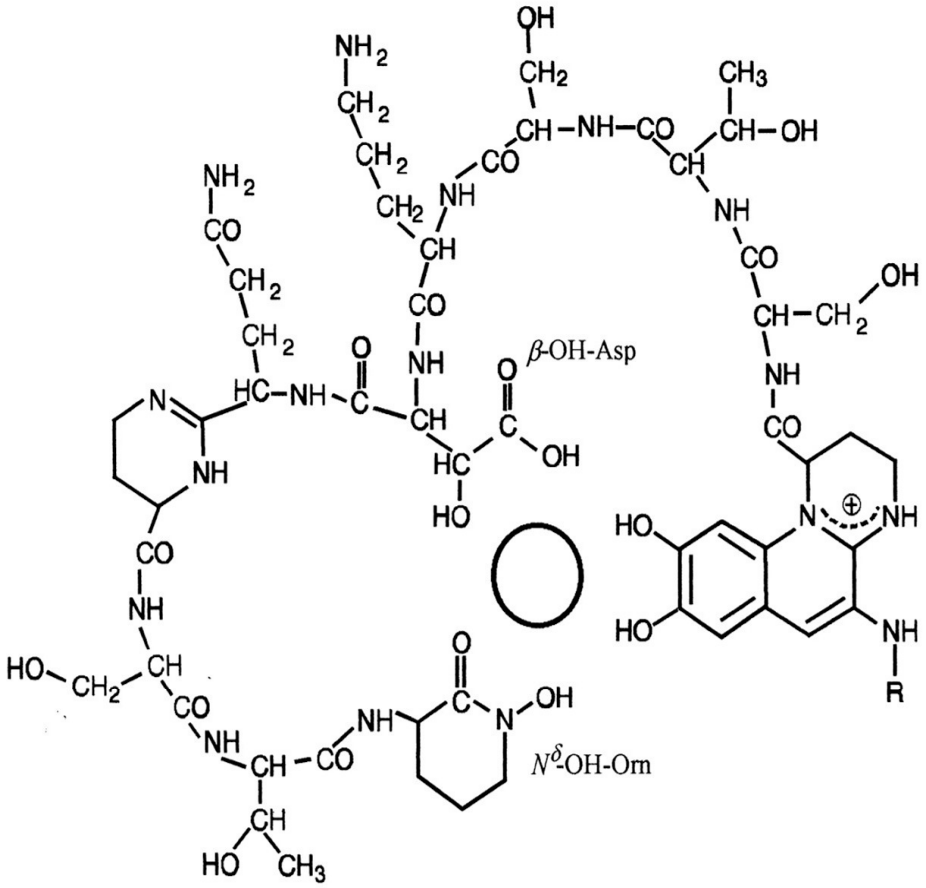

Figure 3.3. 50-hectare plot on Barro Colorado Island, Panama. Taken from www.stri.org, 2006. Soil collection site indicated by black arrow.

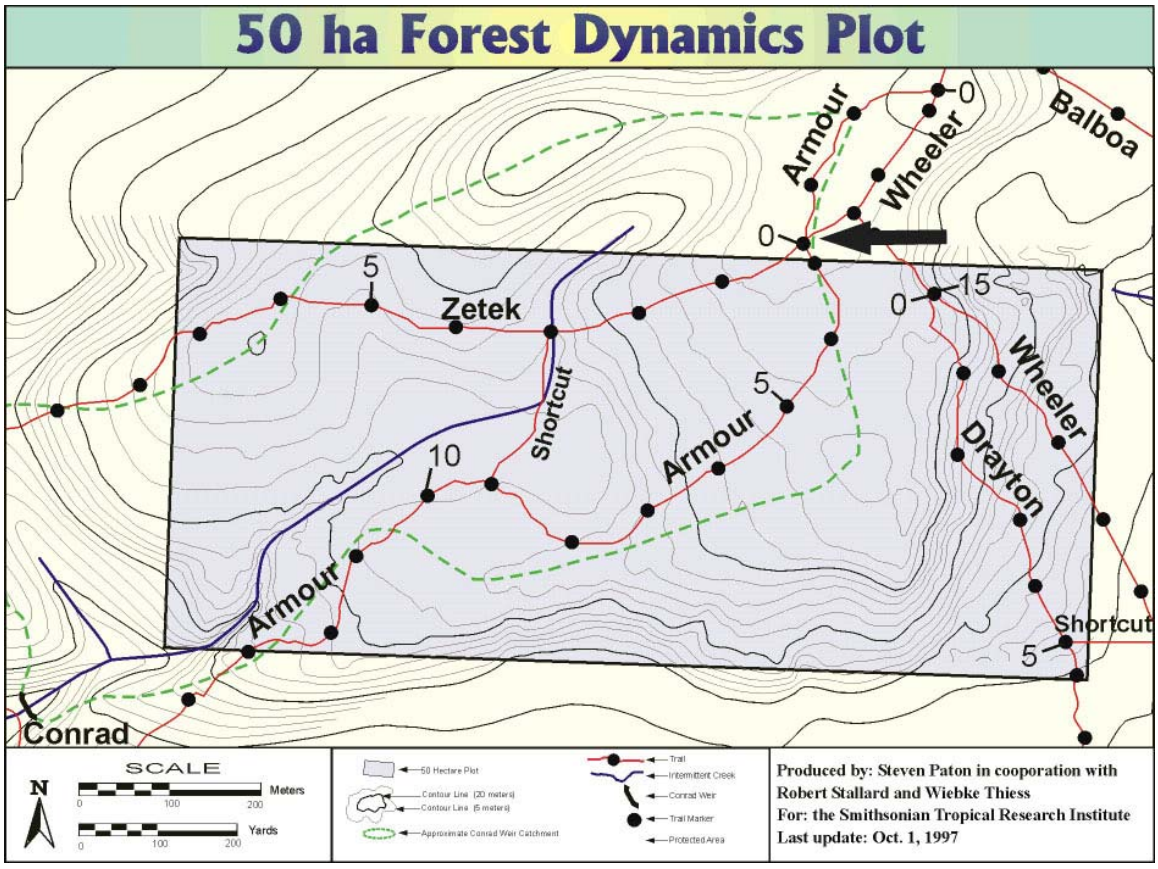

Figure 3.4. Methane consumption rates of soil isolates from the site of Armour-Zetec trail intersection on Barro Colorado Island, Panama. Isolates were used to inoculate 30-ml of growth media in 125-ml serum vials with 50% CH_4 headspace atmosphere. Rates were expressed as box plots for the C14/C0 ratio of CH_4 concentrations on the 14th day and at time zero. One treatment set had no Cu added while the other was spiked with Cu yielding a fluid concentration of 2.5 µM. Data from C.W. Knapp (unpublished data, 2005).

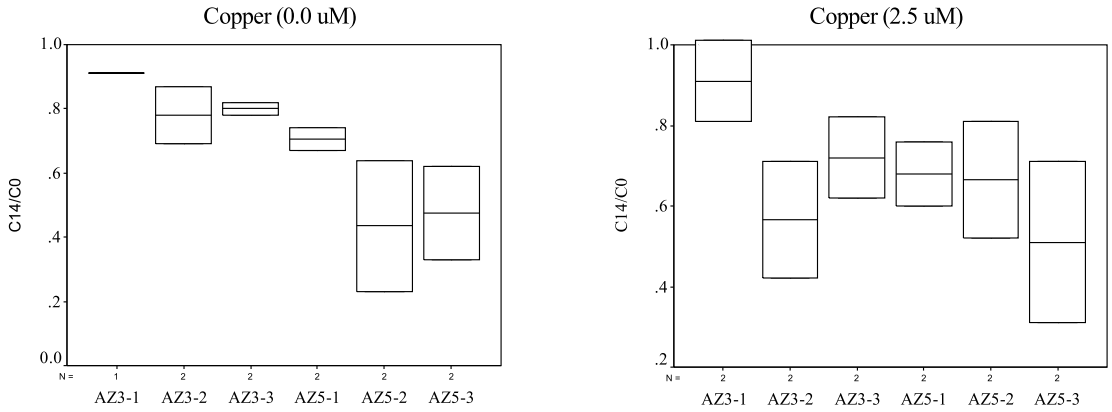

Figure 3.5. Maximum likelihood tree of methanotrophs on BCI, Panama (from Knapp et al., 2007, supplemental information figure 4). *Methylosinus sporium* str. NR3K was isolated from soil collected from the site of the Armor-Zetec trail junction within the 50-hectare plot on BCI. This strain shares similarities with *Methylosinus trichosporium* OB3B, both being Type II methanotrophs belonging to the Alpha subdivision of the Proteobacteria.

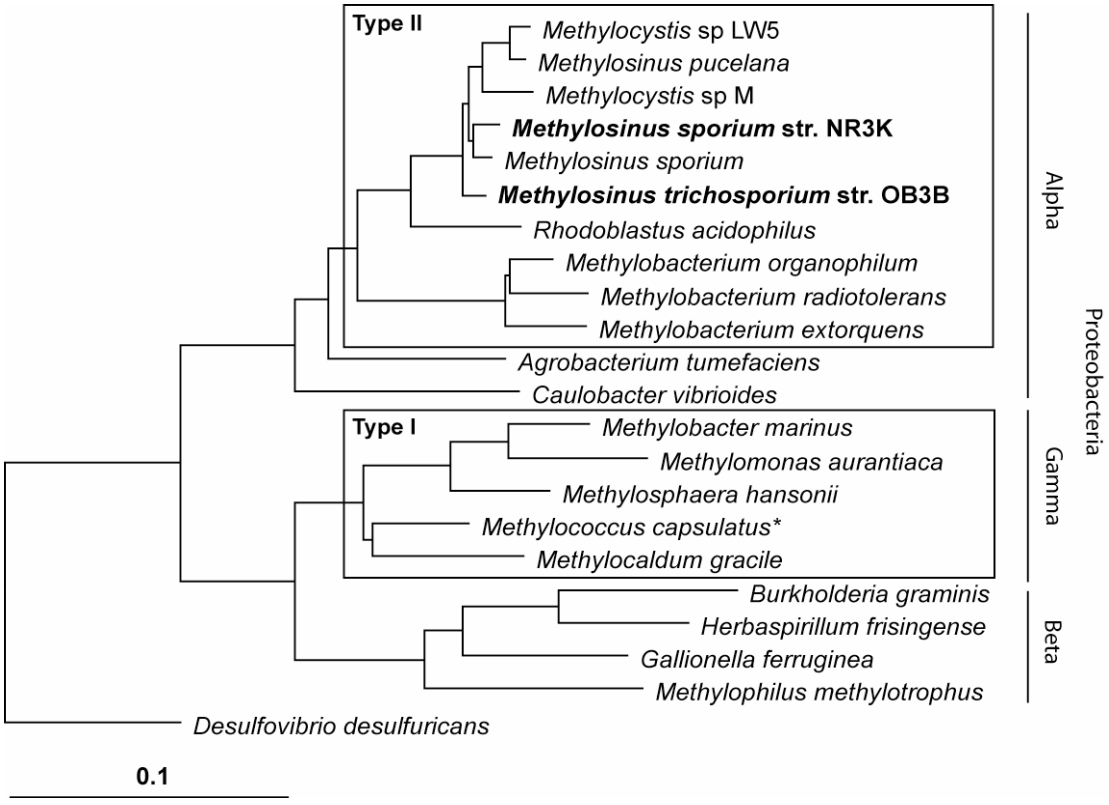

Figure 3.6. MALDI-TOF mass spectra for (A) methanobactin from *M. trichosporium* OB3b (from Knapp et al., 2007, supplemental information figure 3A) and (B) the presumed methanobactin from the Panamanian isolate (from Knapp et al., 2007, supplemental information figure 3B), *M. sporium* NR3K.

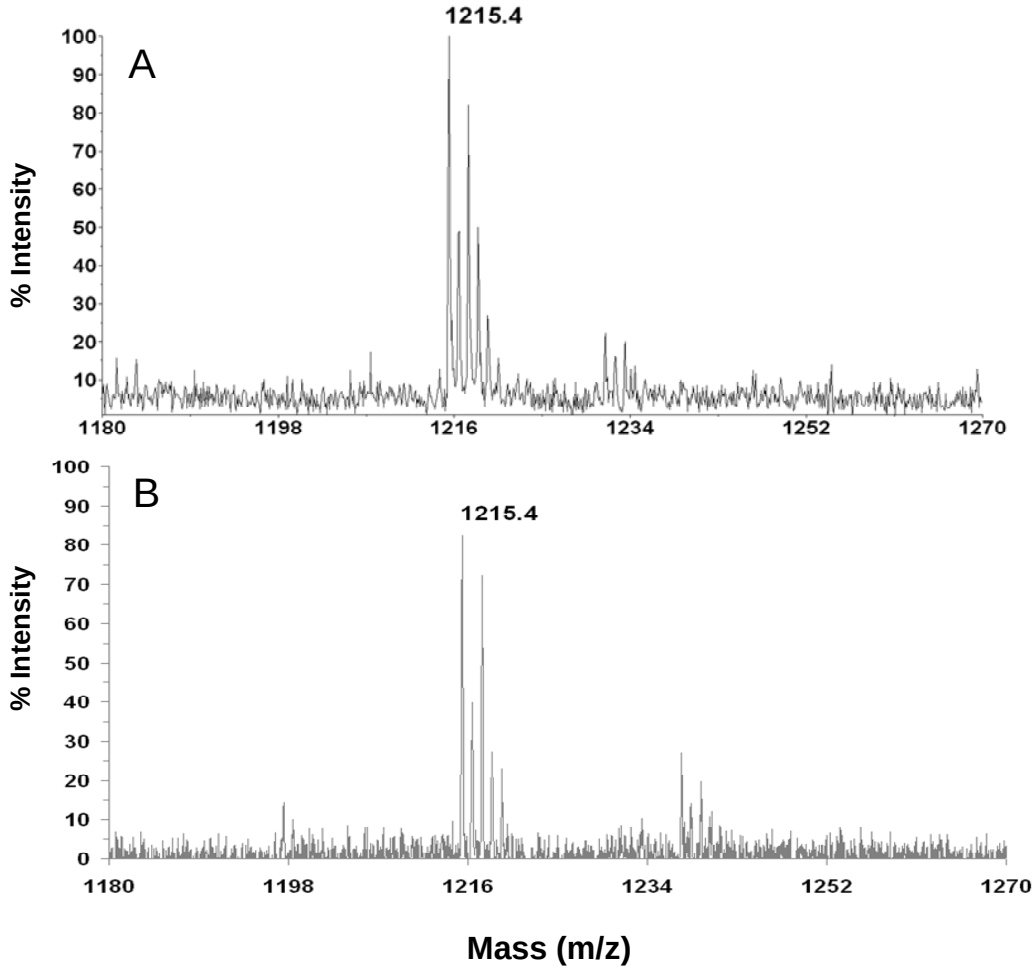

CHAPTER 4

METHANOBACTIN-PROMOTED DISSOLUTION OF CU-SUBSTITUTED BOROSILICATE GLASS

Published as a separate article:
Kulczycki, E., Fowle, D.A., Knapp, C., Graham, D.W. and Roberts, J.A., (2007) Methanobactin-promoted dissolution of Cu-substituted borosilicate glass, Geobiology, 5, 251-263.

ABSTRACT

Mineral weathering plays an important role in the global cycling of carbon and metals and there is an increasing realization that subsurface microbial activity may be a key factor controlling specific biogeochemical reactions and their rates. Methanobactin (mb) is an extracellular copper-binding compound excreted by methanotrophs to acquire copper for the regulation of methane oxidation. Bioavailable Cu regulates the expression and activity of pMMO versus sMMO (particulate versus soluble methane monooxygenase, respectively), key enzymes responsible for bacterial methane oxidation. In this study, we investigate the effect of methanobactin on the dissolution of Cu-substituted borosilicate glass at low temperature and near neutral pH conditions, using batch dissolution experiments. Methanobactin promotes the dissolution of Cu-substituted glasses at rates faster than control experiments. Glasses with lower concentrations of copper (80 p.p.m.) or no copper are dissolved more rapidly by methanobactin than those with more abundant copper (800 p.p.m.). Within the first 2 hours of reaction, methanobactin sorption onto glass surfaces limits mass transfer of Cu into solution, and at higher concentrations (100 μmolal) of the ligand, inhibits dissolution rates of all glass formulations. These results suggest that both the concentration of methanobactin in solution and the solid phase Cu concentration impact silicate weathering rates and related cycling of carbon in near-surface geologic settings.

INTRODUCTION

Mineral weathering reactions are integral to the global cycling of carbon and metals in near-surface geologic settings (Brantley, 2005). Silicate weathering, for example, directly mitigates the "greenhouse" effect through the transformation of atmospheric CO_2 to dissolved bicarbonate, which ultimately, is transported to the oceans (Berner, 1995). As a consequence of carbonic acid-driven silicate dissolution, metals are liberated from the mineral framework thereby linking these two global element cycles (Brady and Weil, 2002). In surficial environments and the shallow subsurface, microbial activity may drive a number of mineral weathering reactions via the metabolic activity of soil and sediment microorganisms (i.e., Barker et al., 1997).

Microbial activity has been linked to increased silicate mineral weathering in a variety of subsurface environments (Banfield et al., 1999; Barker et al., 1997; Bennett et al., 2001; Benzerara et al., 2005; Hutchens et al., 2003; Liermann et al., 2000a; Ullman et al., 1996; Welch and Ullman, 1993). Silicate dissolution is promoted via four primary mechanisms, including: ionic strength, temperature, pH, and the presence of ligands (e.g., Blake and Walter, 1999; Brantley, 2005; Casey and Bunker, 1990; Grandstaff, 1986; Lasaga, 1981; Pokrovsky and Schott, 2000; Welch and Ullman, 1999; Wollast and Chou, 1992). At near neutral solution pH, most silicate minerals respond to increases in ionic strength and temperature with elevated rates of dissolution (Aitken and Woody, 1994; Dove, 1999; Dove and Crerar, 1990; Dove and Elston, 1992; Dove et al., 2005; Dove and Nix, 1997; Icenhower and Dove, 2000; Karlsson et al., 2001; Lasaga et al., 1994; Brady et al., 1999; White and Blum, 1995; White et al., 2002). Microbial metabolic reactions often adjust solution pH dramatically, driving proton-promoted dissolution (Brantley et

al., 2001; Liermann et al., 2000a; Banfield et al., 1999) or by generating more alkaline conditions (i.e., Maurice et al., 2001).

Microbial oxidation and reduction of silicate-bound metals can also affect mineral dissolution. For example, through enzymatic iron oxidation, the metabolic activity of *Acidithiobacillus ferroxidans* was found to inhibit fayalite dissolution within the pH range of 2 to 4 (Santelli et al., 2001). In contrast, Templeton et al. (2005) found that epilithic Mn(II) oxidizing bacteria facilitate weathering of submarine basaltic glass. Alternatively, it has been shown that the dissolution of Fe(III)-bearing clay minerals can result from the enzymatic reduction of Fe(III) by *Shewanella putrefaciens* and this process is enhanced in the presence of organic ligands (Kostka et al., 1999).

At circum-neutral pH, where silicate dissolution rates are at a minimum, the presence of organic ligands can control dissolution rates through complexation of framework metals (Aagaard and Helgeson, 1982; Helgeson et al., 1984). Bacteria and fungi are known to produce a variety of exudates that drive ligand-promoted silicate dissolution (Barker et al., 1997; Brantley, 2005; Kraemer, 2004; Maurice et al., 2000; Welch et al., 1999). A particularly well-studied example is the microbial production of siderophores, strong ferric iron chelating compounds, which promote dissolution of silicate minerals (Liermann et al., 2000b; Rogers and Bennett, 2004).

Microbially mediated silicate weathering may not be an incidental interaction and could be an adaptive strategy to scavenge essential elements from solid phase mineral sources (Brantley et al., 2001; Madigan and Martinko, 2006; Bennett et al., 2001). A variety of rock forming units contain a relatively high abundance of nutrients (C, P, N, Ca, Mg, K, Na, S, and Fe) and trace elements (Mo, Ni, Cu, Co, V) (Brantley et al., 2001),

which are necessary for cell maintenance and metabolic activity (Madigan and Martinko, 2006). When these nutrients are scarce in solution, it has been proposed that some microorganisms have adapted strategies to seek out and access mineral-bound nutrients, including those contained in primary silicates (i.e., Rogers et al., 1998). Under these conditions, microorganisms may secrete organic acids or ligands to promote the dissolution of the nutrient-bearing mineral (Bennett et al., 2001; Vandevivere et al., 1994; Welch et al., 1999; 2002), such that the silicate provides a sole source of essential nutrients stimulating growth and metabolic activity (i.e., Rogers and Bennett, 2004).

Methanotrophic bacteria gain energy from the conversion of methane to carbon dioxide as regulated by oxygen, nitrogen, and bioavailable copper (Cu). Copper concentration, in particular, is key in regulating the enzymatic pathway of methane oxidation for Type II methanotrophs, with the expression of pMMO (particulate methane monooxygenase) at high Cu:cell ratios and sMMO (soluble methane monooxygenase) when Cu is limited (Kim et al., 2004; Morton et al., 2000a; Choi et al., 2003; 2005; Hanson and Hanson, 1996; Lontoh and Semrau, 1998; Murrell et al., 2000; Zahn and DiSpirito, 1996). In most near-surface geologic environments, however, Cu is scarcely bioavailable, as it has been incorporated in mineral phases, sorbed to mineral surfaces or complexed by dissolved organic matter (Flogeac et al., 2004; Karlsson et al., 2006; Lewis 1995). Thus methanotrophs must execute strategies to scavenge sufficient quantities of Cu, such as the production of the Cu-trafficking molecule methanobactin (mb) (log K = 16 –18.8), which appears to play a role in regulating Cu availability in the cell and in turn the synthesis and expression of sMMO and pMMO (Choi et al., 2006; Kim et al., 2004; Morton et al., 2000a). Methanobactin apparently delivers available copper to the cell

while keeping cellular components protected from potential toxic effects (e.g. Kim et al., 2004). A schematic diagram of methanobactin is given in Figure 4.1, where the primary sequence has been described by Kim et al. (2004) as N-2-isopropylester-(4-thionyl-5-hydroxy-imidazole)-Gly^{1}-Ser^{2}-Cys^{3}-Tyr^{4}-pyrrolidine-(4-hydroxy-5-thionyl-imidazole)-Ser^{5}-Cys^{6}-Met^{7}. Morton et al. (2000b) have shown that methanobactin (termed CBC in that study) competed with the surface functional groups of clays to form a Cu:mb complex and ultimately influenced the sMMO activity of the methanotroph. However, the impact of methanobactin on mineral dissolution rate and linkages to metabolic activity has yet to be determined.

The primary focus of this paper was to investigate ligand-promoted silicate dissolution and Cu liberation by methanobactin, a Cu-specific ligand produced by *Methylosinus trichosporium* OB3b (Kim et al., 2004) via a series of batch dissolution experiments. If such a process is ubiquitous in near-surface micro-aerophilic soil regimes, this study will provide the first evidence for a new pathway connecting silicate weathering and the global carbon cycle.

MATERIALS AND METHODS

Under fixed pH, temperature, and ionic strength conditions, a series of batch-weathering experiments was conducted to examine reaction kinetics of copper:methanobactin (Cu:mb) complexation and rates of dissolution for manufactured Cu-substituted borosilicate glasses. Manufactured glasses were chosen for this study because they are compositionally distinct and virtually homogenous allowing investigation of mb-promoted dissolution reactions as a function of solid-phase Cu

concentration. Glasses were manufactured to span and even exceed the range of Cu concentrations found in natural soils and sediments (U.S. soils range from < 1 – 700 ppm, Shacklette and Boerngen, 1984) while accounting for the limits of toxicity for microbial populations. Chander et al. (1995) demonstrated that soil bacteria are tolerant of Cu concentrations as high as 150 ppm, and Rajapaksha et al. (2004) have shown that the metabolic activity of soil bacteria begins to decrease when Cu concentrations exceed 250 ppm and almost all metabolic activity ceases as Cu concentrations approach 8000 ppm.

Glass Synthesis

The composition of the silicate glasses was calculated using shareware formulae from Lawrence Livermore National Laboratory (Bourcier, person comm. 1997). Stock powders were produced by combining crystalline SiO_2, B_2O_3, Na_2O, Al_2O_3 and CuO (Table 4.1). Glasses with copper concentrations of 0 ppm, 80 ppm, and 800 ppm, designated Cu-0, Cu-1, and Cu-3, respectively, were manufactured. Mixed powders were homogenized on a side arm shaker for 20 minutes, and melted in graphite crucibles at 950 ^oC for at least 12 hours. Upon quenching at room temperature, the glass was ground and sieved to a uniform size fraction (125-250 μm). The glass was then rinsed and sonicated for 1 minute with low power sonication in NANOpure water (18 MΩ); the process was repeated 50 times. The specific surface area of the prepared glass was confirmed (0.16 m^2 g^{-1}) by application of the five-point BET method using a Quantachrome Nova Series E with N_2 as the adsorbate gas. Characterization of the glass by light microscopy shows that the glass was one-phase with no precipitates or discernable clusters, suggesting that the Cu was present within the glass structure.

Methanobactin Production

A continuous culture of *Methylosinus trichosporium* OB3b was maintained for methanobactin production using a BIOSTAT B plus laboratory bioreactor system (B. Braun Biotech Inc.). The culture was grown in a Cu-free nitrate minimal salts medium (NSM) containing 40 μM $FeSO_4$ and set at pH 7 with phosphate buffer according to the method presented in Kim et al. (2005) or similarly in Choi et al. (2005). Culture density was monitored daily by reading the optical density (O.D.) at a wavelength of 600 nm. When O.D. readings exceeded 0.8 absorbance units (late exponential phase), the culture was harvested and centrifuged for 30 minutes at 8000 rpm. The supernatant was decanted and vacuum filtered with (0.2 μm pore size) membrane filters. Molecular constituents of the filtrate were separated on a Sep Pak column using a series of elutions with NANOpure H_2O and 60% acetonitrile to separate crude methanobactin from salts. The purified methanobactin product was then lyophilized and stored at 4 ^oC until use.

Batch Dissolution Experiments

Glass dissolution experiments were run in batch reactors by adding 30 mg of prepared glass to 10 mL of electrolyte solution (described below) in capped 16 mL acid-washed polypropylene test tubes. Reactor solutions were composed of an electrolyte buffer (0.1M KCl), a pH buffer (0.1M Tris-HCl; pH 5), and stock methanobactin (mb). Final concentrations of mb were set at [mb] = 10, 20, 50, and 100 μmole L^{-1} (referred to henceforth as mb10, mb20, mb50 and mb100). Typically, 12.3 to 16.4 μmole L^{-1} of mb is isolated from 3-day-old spent medium copper-limited cultures [optical density at 600

nm ($O.D._{600nm}$) ~ 0.7] (Kim et al., 2004). The buffer solution was autoclaved at 121^{o}C before adding the mb product.

Experiments containing each of the 3 silicate glass treatments (Cu-0, Cu-1, and Cu-3) and four mb concentrations (mb = 10, 20, 50, 100 μmole L^{-1}) were prepared in a series of duplicate reactors. Experimental controls consisted of mb-free electrolyte controls for each of the 3 silicate treatments (Cu-0, Cu-1, and Cu-3), and solution matrix blank reactors with no methanobactin and no glass. All solutions had an initial pH of 5.5 for each treatment. Reaction vessels were rotated end over end at 20 rpm in the dark at 20 ^{o}C. Sacrifice sampling at predefined intervals (t = 0, 6, 24, 48, 72, 96, 144, 240, 408, 672 hours) was performed over the course of 28-days. Aqueous Cu and SiO_2 concentrations were determined using sub-samples filtered (0.2 μm) and acidified using 5% ultrapure HNO_3. Solution concentrations of Cu were determined spectrophotometrically by the bathocuproine method (Standard Methods, 1989) at 484 nm. Dissolved SiO_2 was determined using a colorimetric method based on that of Strickland and Parsons (1968) at 810 nm. Final pH of all reactor solutions was measured on the remaining unfiltered solution. All solubility calculations were made using Geochemist's Workbench®, Bethke (2002).

SEM

Glass surfaces were inspected for the character and extent of surface dissolution features and evidence of secondary precipitates using scanning electron microscopy. Glass material from sacrificed reactors was air dried in a laminar-flow hood, stub-mounted and gold-sputter coated for 2 minutes. Glasses were imaged using a field

emission scanning electron microscope (SEM; LEO 1550 operated at an accelerating voltage of 5 kV). Elemental analysis was performed with an energy dispersive system (EDAX). Analysis of unreacted glass demonstrates a homogenous distribution of Cu and other elements (e.g., Si, B, Na, Al).

Methanobactin Sorption to Glass

To determine the extent of mb sorption onto the glass surfaces, a series of batch reactors with the same treatments (Cu-0, Cu-1 and Cu-3) were prepared according to the experimental conditions of the dissolution trials. Over the course of a 2-hour reaction period, sorption was tested in separate batches using initial mb concentrations that ranged between zero and 100 μmole L^{-1} (0, 5, 10, 25, 75, and 100 μmole L^{-1}). After 2 hours of reaction, solutions were filtered with 0.2 μm diameter pore-size membranes, and analyzed spectrophotometrically at an absorbance wavelength of 342 nm (maximum signal response for mb; Kim et al., 2005). Sorbed mb was calculated as the difference between the aqueous mb concentration at the beginning and end of reaction.

RESULTS

Aqueous copper (Cu) was monitored as a measure of the ability of methanobactin (mb) to release Cu from the solid phase silicate glass. Dissolved SiO_2 was monitored as a measure of glass dissolution. A series of mb concentrations (mb = 10, 20, 50, and 100 μmole L^{-1} noted mb 10, mb 20, mb 50, and mb 100, respectively) were reacted with Cu-free and Cu-bearing glasses (Cu-0, Cu-1, Cu-3) over the course of 28-days. Solution pH varied slightly between treatments (no more than 0.3 pH units), and a small, but

measurable increase in pH was observed over the course of the experiment (pH 5.3 to 5.6). The variation in pH, however, lies within an acceptable range that would not impact the rate of dissolution significantly (Welch et al., 1999; Welch and Ullman, 1993).

Cu release

Monitoring of batch dissolution experiments of the Cu-substituted glasses demonstrated that Cu released into solution increases for both experimental and control experiments as a function of time (Data not shown). We report final concentrations of $Cu_{(aq)}$ detected at the end of the experiments (table 4.2). In the Cu-1 experiments, release of $Cu_{(aq)}$ in experimental treatments exceeded controls in all cases except for mb 20 in the Cu-1 treatment and mb 100 in the Cu-3 treatment. The maximum extent of $Cu_{(aq)}$ release at the end of the experiment (T_{final}: 673.5 hours or 28-days) among the treatments examined (10, 20, and 50 μmole L^{-1}) was 9.0 μmole L^{-1} ± 0.5 in a reactor with 50 μmole L^{-1} mb (table 4.2). Maximum release at T_{final} (571 hours or 24-days) in the control experiments was 3.3 μmole L^{-1} ± 0.1, which was in turn lower than the lowest mb-bearing experiments at T_{final} (mb10, 4.19 μmole L^{-1} ± 0.02). The $Cu_{(aq)}$ release in the Cu-3 treatments at T_{final} was, in general, higher than the Cu-1 treatment for each corresponding initial mb concentration. The highest $Cu_{(aq)}$ concentration at T_{final} was 28.12 μmole L^{-1} ± 0.01 (mb10) and ranged as low as 7.1 μmole L^{-1} ± 0.7 in the mb 100 batch reactor. The release of $Cu_{(aq)}$ in experimental reactors was higher than the control in all cases except mb 100 (T_{final}: 571 hours or 24-days, table 4.2).

SiO_2 release

Release of SiO_2 into solution increased with time for all experimental reactors, with aqueous SiO_2 values approaching maxima after 332.5 hours, and persisting throughout the remainder of the trial for all control reactors (figure 4.2a, b, and c). Unlike Cu, $SiO_{2(aq)}$ was well above the method detection limit and replicate error was small. The Cu-0 experiments exhibited the highest $SiO_{2(aq)}$ concentrations compared to Cu-1 and Cu-3 for all experimental and control treatments. The highest maximum concentration of $SiO_{2(aq)}$ (1284± 206 μmole L^{-1}) occurred in the mb 50 reactor at 673.5 hours. The lowest $SiO_{2(aq)}$ concentration for these experiments was found in the control experiment (892 ± 46 μmole L^{-1}; after 571 hours; table 4.3) For the Cu-1 experiments the highest maximum $SiO_{2(aq)}$ concentration (979 μmole L^{-1} ± 40) was in the mb 50 batch reactor (table 4.2, figure 4.2a) at 673.5 hours. The lowest $SiO_{2(aq)}$ concentration in solution (793 μmole L^{-1} ± 24, 571 hours) occurred in the control experiment. Maximum $SiO_{2(aq)}$ concentrations for Cu-3 were measured in the mb 20 treatment (709 μmole L^{-1} ± 26, 673.5 hours), and the lowest concentration in the control (573 μmole L^{-1} ± 10, 571 hours; tigure 4.2b, table 4.3).

Stoichiometry of Cu/Si release

Although both $Cu_{(aq)}$ and $Si_{(aq)}$ concentrations increased with time over the course of the experiments the stoichiometry of release changed as a function of reaction time and Cu concentration in the solid phase. Figure 4.3 depicts the molar ratio of Cu to Si released as a function of time for the range of mb concentrations (0, 10, 20, 50, 100 μmole L^{-1}) and all glass formulations. In Cu-1 experiments, the highest Cu/Si ratios

occurred in the first hour of reaction for all treatments, including the control, ranging from 0.042 ± 0.06 for mb 100 to 0.25 for the control. These ratios dropped rapidly after 8 hours to ~0.01 ± 0.02 and were maintained for the duration of the experiment.

Similar to the Cu-1 Cu/Si ratios, the highest Cu/Si values for the Cu-3 experiments were also detected in the first hour of the trial for the mb 10 (0.26 ± 0.02), mb 20 (0.29 ± 0.08), and mb 50 (0.22 ± 0.03) treatments and a similar rapid decline to ~ 0.02 ± 0.004 was observed (figure 4.4b). The control and the mb 100 treatments showed slightly different trends. The Cu/Si ratio for the control peaked in the first hour (0.24) but then declined gradually over the course of the experiment reaching 0.042 ± 0.007 after 45 hours and was constant to the end of the experiment. For the mb 100 treatment, the Cu/Si value reached a maximum (0.14 ± 0.08) at 8 hours, dropping gradually to 0.018 ± 0.001 after 45 hours and changing little for the duration of the experiment.

Glass surface alteration

At the completion of the experiment (693 hours of reaction time) glass surfaces were inspected for surface alteration using SEM. All surfaces exhibit surface features consistent with the manufacturing process, including air bubbles and compaction features from quenching, and abrasion features from grinding. Minimal surface etching for all glass compositions (Cu-0, Cu-1, and Cu-3) was observed for control treatments, in which no methanobactin was present. Secondary mineral formation, however, was detected in control experiments. SEM-EDAX analysis indicated that the rhombohedral crystals (~ 1 μm in diameter) observed to be in close proximity to the etch pits on the surface of glass containing 80 ppm Cu were mainly composed of Si and O (Cu-1; figure 4.4a). More

prominent dissolution features were observed for all glass compositions in the presence of 50 μmole L^{-1} methanobactin. These surfaces exhibit deeper etching, including clusters of triangular etch pits and secondary grooves that crosscut cooling- and fracture-features (figure 4.4b).

Surface sorption of Methanobactin

After two hours of reaction time mb sorption occurred only on those glasses that contained Cu (Cu-1 and Cu-3). Glass surfaces without Cu (Cu-0) did not exhibit mb sorption (figure 4.5). For both Cu-containing glasses, sorption increased linearly across the range of mb concentrations (0 to 100 μmole L^{-1}) with greater sorption occurring on the glass with the higher Cu concentration (800 ppm Cu) (Cu-1: equation of the line of fit is $y = 2.02x + 1.6$ ($r^2 = 0.901$); Cu-3: equation of the line of fit is $y = 3.28x - 22.2$ ($r^2 = 0.995$)).

DISCUSSION

Rates of Dissolution

Results from batch dissolution experiments of copper (Cu)-doped borosilicate glasses demonstrate that the chalkophore, methanobactin (mb), increases glass dissolution rates (based on SiO_2 release) compared to mb-free electrolyte solutions. In this study, mb promoted the release of Cu from both Cu-1 and Cu-3 glasses. The concentration of mb, however, controlled release and in some cases, the maximum concentration of Cu was equivalent or less than the non-chelating control. Concentrations of $Cu_{(aq)}$ detected at the end of the experiments for mb100 were equal or less than the control for both glasses

(table 4.2). Low $Cu_{(aq)}$ concentrations are likely due to surface sorption of mb and slow desorption of the Cu:mb complex or resorption of Cu to the reactive silica surface, as supported by results from batch sorption experiments (figure 4.5). Monodentate Cu-ligand complexes such as Cu(II) hydroxide have been shown to adsorb to silica and form a monolayer (Xia et al., 1997). This phenomenon is also analogous to the slow desorption of the Fe(III)-hydroxamate complex that occurred in a study conducted by Holmen and Casey (1996) where excess hydroxamate adsorbed to the surface of goethite while attempting to co-ordinate Fe(III). Unlike the Fe system, however, Cu functions as both a critical nutrient/trace element and also a toxic substance for microorganisms (Nies, 1999). There may be a dual role for methanobactin as a chaperone that mobilizes Cu but also shields the cell against toxic effects (e.g., Kim et al., 2005). Therefore, slow desorption of the Cu:mb complex may function to limit release based on methanotroph uptake.

Methanobactin promotes the release of SiO_2 from Cu-substituted glass at rates higher than the non-chelating electrolyte for all mb concentrations and glass formulations (table 4.3). Release rates were calculated from the linear portion of the data from 0 to 167.5 hours. The rate of release is dependent upon both the concentration of Cu in the glass and the concentration of mb in solution (table 4.3, figure 4.2) at pH 5.5. SiO_2 release rates were slowest for Cu-3 increasing for Cu-1 and Cu-0, respectively, for each mb concentration (0, 10, 20, 50, 100 μmole L^{-1}) (table 4.3, figure 4.2).

Consistent trends in SiO_2 release rates occur between the Cu-1 and Cu-3 treatments (figure 4.6). In both treatments, an increasing trend in mb concentrations from 0 to 50 μmole L^{-1} corresponds to higher SiO_2 release rates with global maxima occurring at 50

μmole L^{-1} in the Cu-1 treatment (rate = 1.77 μmole m^{-2} h^{-1}, r^2 = 0.983) and 10 μmole L^{-1} in the Cu-3 treatment (rate = 1.0 μmole m^{-2} h^{-1}, r^2 = 0.996). Surface etching of the glass surfaces, commiserate with dissolution, was observed using SEM (figure 4.4b). Unlike dissolution under non-Cu-chelating conditions where secondary precipitates were detected (figure 4.4a), mb-promoted dissolution produces extensive etching without secondary mineral formation. A decrease in release rate for both treatments is observed when the mb concentration is as high as 100 μmole L^{-1}.

The rates of mb-promoted SiO_2 dissolution of Cu-substituted glass reported here are at least three orders of magnitude higher than results from similar studies of ligand-promoted silicate dissolution, which reported dissolution rates for amorphous silica (table 4.4, Elmer and Nordberg, 1958; Mazer and Walther, 1994; Rimstidt and Barnes, 1980; Seidel et al., 1997), silica glass (table 4.4, Icenhower and Dove, 2000), borosilicate glass (table 4.4, Roberts Rogers and Bennett, 2004), and kaolinite (Table 4.4, Sutheimer et al., 1999). These comparisons would suggest that mb is a ligand that is reactive with Cu but also capable of increasing the rate of dissolution of Cu-bearing silicate phases likely via Al chelation (e.g. Oelkers and Gislason, 2001), potentially increasing Cu availability to subsurface microorganisms (e.g., Roberts Rogers and Bennett, 2004) on timescales relevant to metabolic activity.

While SiO_2 release rates increase in the presence of mb at low concentration, dissolution rates are hindered at mb concentrations of 100 μmole L^{-1}. Methanobactin reacts with the glass surface initially through sorption (figure 4.5) and forms a surface complex. Formation of this surface complex slows the rate of Cu release even at low mb concentrations, however, only higher concentrations of mb inhibit SiO_2 release (table

4.3). Irreversible binding of microbial extracellular polymers to mineral surfaces has been shown to hinder silicate dissolution in previous studies (e.g., Benzerara et al., 2005; Luttge and Conrad, 2004). Welch et al. (1999) demonstrated an overall decrease in the rate of plagioclase dissolution when the polysaccharides pectin and gum xanthan were reacted in excess. Welch and Vandevivere (1994) demonstrated that Si release from feldspar is inhibited by acidic polysaccharides. Ullman and Welch (2002) have proposed that the inhibition of feldspar dissolution occurs when organic polymers irreversibly bind to the mineral surface thus reducing the effective reactive surface. Similarly, in this study, the slower rates of SiO_2 release at 100 μmole L^{-1} mb for all glass formulations, suggests that the surface is approaching saturation with mb, effectively blocking the interaction between mb in solution and potential active surface sites. Inhibition of dissolution can occur if surface groups are blocked by hydrophobic moieties of macromolecules (Stumm and Wollast, 1990), such as the high mb concentration in the 100 μmole L^{-1} reactors, and therefore, contribute to steric blocking of the surface reactive groups. As detachment is the slowest, and therefore rate-determining step in the ligand-promoted dissolution mechanism (Stumm and Morgan, 1996), increasing abundance of mb molecules on the surface of the glass may form multiple layers, which require more time to detach. Sorption data together with solution geochemistry data support a model in which functional group bonding reaches a threshold capacity where increasing mb concentrations will result in a decreasing rate of dissolution at the glass surface compared to the peak dissolution rate.

Observed decreases in glass dissolution rates of the non-mb controls in this study may be attributed to the formation of secondary phases (figure 4.4a; table 4.3, Bourcier et al.,

1989; Casey and Bunker, 1990). No secondary precipitates form in mb reactors, consistent with the higher rates of dissolution for mb concentrations ranging from 10 μmole L^{-1} to 100 μmole L^{-1}. The relative inhibition of SiO_2 dissolution rates occurring at higher mb concentrations (100 μmole L^{-1}) implies that a threshold capacity has been reached. However, it should be noted that these dissolution rates are still higher than controls.

Mechanism of Dissolution

The solubility of silicates is at a minimum in solutions that are at near neutral pH and low temperature (Stumm and Morgan, 1996). Under these conditions the coordination of organic ligands with framework silicate cations at the mineral surface can increase the rate of silicate dissolution (Stumm and Furrer, 1987). In a ligand-promoted dissolution reaction, three elementary steps occur. Initially, a surface complex is formed by ligand exchange between the ligand and surface hydroxyl groups. For dissolution to occur the chelate must be strong enough to weaken the metal-oxygen bonds, accomplished through bond polarization (Zinder et al., 1986). Once the surface complex has formed, the rate-determining step of the dissolution reaction is the slow detachment of the surface metal species. Upon detachment of the metal complex, rapid protonation of the negatively charged surface species follows (Furrer and Stumm, 1986; Stumm and Wollast, 1990; Stumm and Morgan, 1996).

The dissolution of borosilicate glass proceeds with the formation of an alkali-depleted amorphous surface (gel) layer (Bourcier et al., 1989), which is consistent with the preferential leaching of network modifying elements that occurs at the surface of volcanic

glasses during weathering (Casey and Bunker, 1990; Oelkers and Gislason, 2001). As a consequence the leached layer typically becomes enriched with Si and other network forming cations, e.g., Al, or Fe(III) (Oelkers and Gislason, 2001). In amorphous silicate solids, such as the borosilicate glasses used here, dissolution rates are affected by all components concentrated in the surface layer (e.g., Cu, Al, Si), and the overall rate of glass dissolution is limited by formation of the gel layer.

This study demonstrates that mb enhances dissolution in the absence of solid-phase Cu, suggesting that the ligand is forming a stable complex with an alternate metal in the leach layer. Methanobactin has been shown to form complexes with metals other than Cu, such as Ag(I), Au(III), Co(II), Cd(II), Fe(III), Hg(II), Mn(II), Ni(II), Pb(II), U(VI), and Zn(II) (Choi et al., 2006a). In the present study, it is highly probable that mb is chelating Al(III) from the Cu-0 glass (as well as Cu-1 and Cu-3 glasses), since Al(III) is similar to Fe(III) in terms of ionic radii (0.5 – 0.7) and coordination chemistry (IV, V, VI) (Shannon, 1976). It is also likely that dissolution of these aluminum-bearing borosilicate glasses will proceed in a similar fashion to other aluminosilicate minerals (e.g. Oelkers et al., 1994) and glasses (Oelkers and Gislason, 2001; Roberts Rogers and Bennett, 2004), whose dissolution mechanism is dictated by the removal of Al from the surface leach layer (e.g. Oelkers et al., 1994; Gautier et al., 1994; Oelkers and Schott, 1995). This together with increased dissolution of Cu-0 in the presence of mb, suggests that the chalkophore is promoting dissolution of these glasses by removing Al from the leach layer. It appears that the presence of Cu in the glass is not critical to this reaction because of its low abundance, however due to its role as a network forming element, increasing Cu concentration in the glass effectively decreases its overall solubility (see figure 4.2,

controls). It should be emphasized that the ability of mb to mobilize Cu from a silicate source (even when in low abundance in the solid phase) has significant biological implications that extend beyond silicate dissolution kinetics.

Stoichiometry of Cu release

Relatively higher Cu/Si values indicate that rapid release of Cu from the surface of the Cu-substituted glass occurs within the first few hours of reactivity with mb and controls. This non-stoichiometric initial release of Cu indicates that the high solubility of the glass permits rapid removal of surface available Cu within the first few hours of reaction regardless if mb is involved (figure 4.3). It appears that the majority of the weakly bound surface Cu is rapidly removed from the glass, resulting in a subsequent sharp decline in Cu/Si release. Thereafter, the amount of Cu exposed at the glass surface is dependent upon the rate of SiO_2 removal or detachment. As more Cu is removed from the glass, less Cu becomes available to the Cu-free mb. Furthermore, the solid-solution gradient of Cu is reduced over time as more Cu is released into solution, which inevitably slows down the reaction kinetics with time.

In the Cu-1 treatment, the highest Cu/Si values were detected in the first hour of the experiment for all mb concentrations tested and the control. The value for the control in the first hour (0.25) is markedly higher (2.5 to 5 orders of magnitude) than any of the mb treatments. Methanobactin interactions with the glass surface may slightly inhibit desorption rates of the Cu:mb complex (figure 4.5) and be responsible for this observation. Stoichiometric dissolution of the Cu-substituted glass would yield an ideal Cu/Si value of 9.35×10^{-5}. Therefore, it can be concluded that non-stoichiometric

dissolution occurs during the initial stage of the trial. During the remainder of the trial, Cu/Si values for all tested variables approach zero but are not low enough (9.35×10^{-5}) to assume that stoichiometric dissolution is achieved.

Chalkophore-mineral interactions and methanotrophy

Analogous to heterotrophic microorganisms that produce siderophores under conditions of ferric iron limitation (Brantley et al., 2001; Hersman et al., 2000; Kalinowski et al., 2000; Kraemer, 2004; Maurice et al., 2001), methanotrophs produce mb when Cu availability is limited (Kim et al., 2004). As siderophores have been shown to promote dissolution of iron bearing minerals as well as aluminosilicates (Kalinowski et al., 2000), results from this study demonstrate that methanobactin is capable of promoting the dissolution of Cu-bearing silicates. The "vital effect" (Weiner and Dove, 2003) of live methanotrophic organisms was absent from these experiments. Without live cells, there is no mechanism to trigger the trafficking of Cu by mb for methane oxidation and therefore, it is expected that Cu release rates would increase in the presence of live methanotrophic cultures, barring any inhibitory effects by microbially produced polysaccharides (Welch et al., 1999). Like other studies of ligand-promoted glass dissolution, however, we cite the mechanism of dissolution as Al removal from the leach layer, and this process is incidental to Cu complexation in this particular system due to relatively low concentrations of Cu in the solid phase.

The results of this study suggest that mb can promote dissolution of borosilicate glass and likely other silicate phases present in subsurface sedimentary environments. Methanobactin-promoted dissolution of glass in the study system appears incidental to

Cu mobilization but may be accelerated in the presence of metabolizing organisms and deserves further investigation with respect to its impact upon MMO activity rates of methane oxidation. Methane oxidation occurs through the pMMO enzymatic pathway at high Cu-to-biomass ratios (> 0.89 μmole of Cu per g [dry weight] of cells) (Hanson and Hanson, 1996; Morton et al., 2000a) and supports methane oxidation rates that are approximately 60% higher than the low Cu enzymatic pathway, sMMO (Choi et al., 2003; Lontoh and Semrau, 1998; Murrell et al., 2000; Zahn and DiSpirito, 1996). The availability and regulation uptake mechanisms of Cu to methanotrophs therefore has a major impact upon rates of methane oxidation, and results from this study demonstrate that geologic material present in the subsurface microbial habitat may be accessible sources of Cu in the presence of the chalkophore, methanobactin.

SUMMARY

The results of this study show that methanobactin (mb) promotes the dissolution rate of copper (Cu)-substituted borosilicate glasses at rates faster than non-mb controls. However, glasses with no Cu (0 ppm), or lower concentrations of Cu (80 ppm) are dissolved faster than glasses with higher Cu concentrations (800 ppm). Methanobactin sorbs to Cu-bearing glass surfaces, however little to no mb sorption occurs on glasses without Cu. The sorption of mb contributes to slower glass dissolution rates as a threshold capacity for mb on the glass surface is approached in the presence of excess ligand. This has significant implications in terms of the behavior of mb in soils and sediments, because mb will preferentially accumulate on the surfaces of Cu-bearing solid materials. While the impact of mb on mineral weathering needs further investigation, this

study demonstrates that mb can promote the dissolution of Cu-substituted borosilicate glass and in turn paints a compelling picture where soil mineral composition may have a profound impact on hotspots of methanotrophic activity.

ACKNOWLEDGEMENTS

The authors would like to thank Danny Flanagan for formulation of glasses used in this study and Sarah Tsoflias for sampling support. The authors also acknowledge support for this research from NSF Biogeosciences (EAR 0433980 awarded to Roberts and Graham) and KU Geology Associates (Fowle). Furthermore, the authors wish to thank the two anonymous reviewers for their constructive criticism that served to improve the quality of the paper as a final product.

Table 4.1. Composition of manufactured Cu silicate glasses.

Glass	[a]SiO_2	B_2O_3	Na_2O	Al_2O_3	[b]CuO (p.p.m.)
Cu-0	81.5	12.0	4.3	2.2	—
Cu-1	81.49	12.0	4.3	2.2	80
Cu-3	81.4	12.0	4.3	2.2	800

[a]All values are expressed as mole %, except for CuO, which is expressed in p.p.m.
[b]80 and 800 p.p.m. are equivalent to 0.01 and 0.1 mole %, respectively.

Table 4.2. Copper release from borosilicate glass.

[a]System	Cu			
	[b]Cu-1		[b]Cu-3	
	[c]$[Cu]_{T\ final}$	[d]Error	[c]$[Cu]_{T\ final}$	[d]Error
Control	3.3	0.1	15.4	0.3
mb10	4.19	0.02	28.12	0.01
mb20	2.98	0.02	21.3	0.3
mb50	9.0	0.5	21.89	0.01
mb100	3.8	0.6	7.1	0.7

[a]Experimental run time = 673.5 h (28 days). Control is Cu-substituted glass not reacted with mb. mb10, mb 20, mb50, mb100 represent batch systems reacted with mb = 10 μmole L^{-1}, mb = 20 μmole L^{-1}, mb = 50 μmole L^{-1}, mb = 100 μmole L^{-1}, respectively.
[b]Cu-1 and Cu-3 represent Cu-substituted glasses with Cu concentrations 80 and 800 p.p.m., respectively.
[c]Final concentration of Cu (μmole L^{-1}) measured at the end of the experiment, t = 28-days for mb10, mb20, and mb50 or t = 24-days for Control and mb100.
[d]Error is one standard deviation about the mean.

Table 4.3. Net SiO_2 release rates from borosilicate glass.

[a]System	SiO_2											
	[b]Cu-0				[b]Cu-1				[b]Cu-3			
	[c]*r*	[d]r^2	[e]Error	[f]$[SiO_2]_{Tfinal}$	[c]*r*	[d]r^2	[e]Error	[f]$[SiO_2]_{Tfinal}$	[c]*r*	[d]r^2	[e]Error	[f]$[SiO_2]_{Tfinal}$
Control	1.73	0.991	0.26 (n=6)	892 ± 46	1.01	0.979	0.16 (n=8)	793 ± 24	0.59	0.971	0.11 (n=8)	573 ± 10
mb10	2.28	0.989	0.36 (n=6)	1126 ± 112	1.36	0.990	0.17 (n=7)	805 ± 64	1.00	0.996	0.08 (n=7)	696 ± 1
mb20	2.15	0.996	0.20 (n=6)	994 ± 50	1.66	0.990	0.21 (n=7)	932 ± 36	0.91	0.998	0.05 (n=7)	709 ± 26
mb50	2.35	0.966	0.67 (n=6)	1284 ± 206	1.77	0.983	0.29 (n=7)	979 ± 40	0.90	0.997	0.06 (n=7)	644 ± 12
mb100	2.07	0.968	0.58 (n=6)	996 ± 18	1.35	0.998	0.06 (n=8)	844 ± 44	0.79	0.970	0.15 (n=8)	658 ± 60

[a]Experimental run time = 673.5 h. Control is Cu-substituted glass not reacted with mb. mb10, mb 20, mb50, mb100 represent batch systems reacted with mb = 10 μmole L^{-1}, mb = 20 μmole L^{-1}, mb = 50 μmole L^{-1}, mb = 100 μmole L^{-1}, respectively.
[b]Cu-0, Cu-1 and Cu-3 represent Cu-substituted glasses with Cu concentrations of 0, 80, and 800 p.p.m., respectively.
[c]Rate constants for SiO_2 release expressed as μmole SiO_2 m^{-2} h^{-1}, calculated from a linear fit of SiO_2 concentrations vs. time between t = 0 and t = 167.5 h.
[d]r^2, Values are correlation coefficients for the regression analyses.
[e]Error based on Confidence slope * t value (e.g. 95% Confidence interval)
[f]Final concentration of SiO_2 (μmole L^{-1}) measured at the end of the experiment, t = 28-days for mb10, mb20, and mb50 or t = 24-days for Control and mb100.

Table 4.4. Comparison of published rates of amorphous silica dissolution

Study	Glass Composition	T°C	[a]pH	Electrolyte	Log Rate (mol m^{-2} s^{-1})
This Study	Cu glass	20	5.5	0.1 KCl	-3.19 to -3.60
Elmer and Nordberg 1958	Amorphous silica	95		DI	-11.6
Rimstidt and Barnes 1980	Amorphous silica	18		DI	-9.95
Mazer and Walther 1994	Amorphous silica	40		DI	-11.5
Seidel et al. 1997	Amorphous silica	25		DI	-12
Icenhower and Dove 2000	Si glass	60	5.7	0.1 M NaCl	-9.4
Rogers and Bennett 2004	Apatite Goethite glass	25	5	Acetate	-4.22
Rogers and Bennett 2004	Apatite Goethite glass	26	5	3,4 DHBA	-4.18
Sutheimer et al. 1999	Kaolinite	22	3	Oxalate and 0.01 M $NaNO_3$	0.0912

[a]pH was not reported for all studies.

Figure 4.1. Schematic diagram of methanobactin. From Kim HJ, Graham DW, DiSpirito AA, Alterman MA, Galeva N, Larive CK, Asunskis D, Sherwood PMA (2004) Methanobactin, a copper-acquisition compound from methane-oxidizing bacteria. *Science* **305**, 1612-1615. Reprinted with permission from AAAS (www.sciencemag.org).

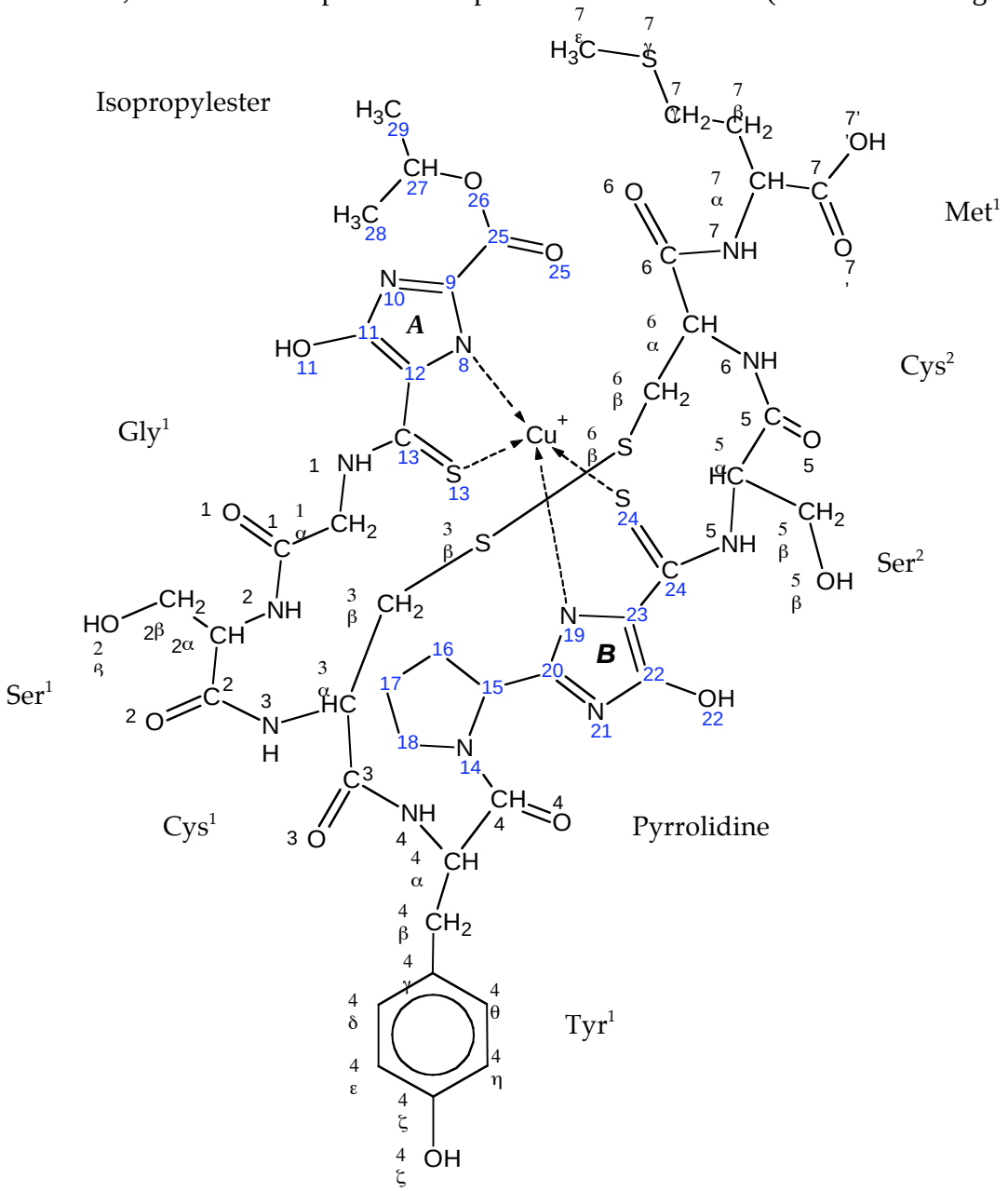

Figure 4.2. SiO_2 release as a function of mb concentration (mb = 0, 10, 20, 50, and 100 μmole L^{-1}) for (a) Cu-0 Treatment (b) Cu-1 Treatment $[Cu]_i$ = 80 ppm, and (c) Cu-3 Treatment $[Cu]_i$ = 800 ppm.

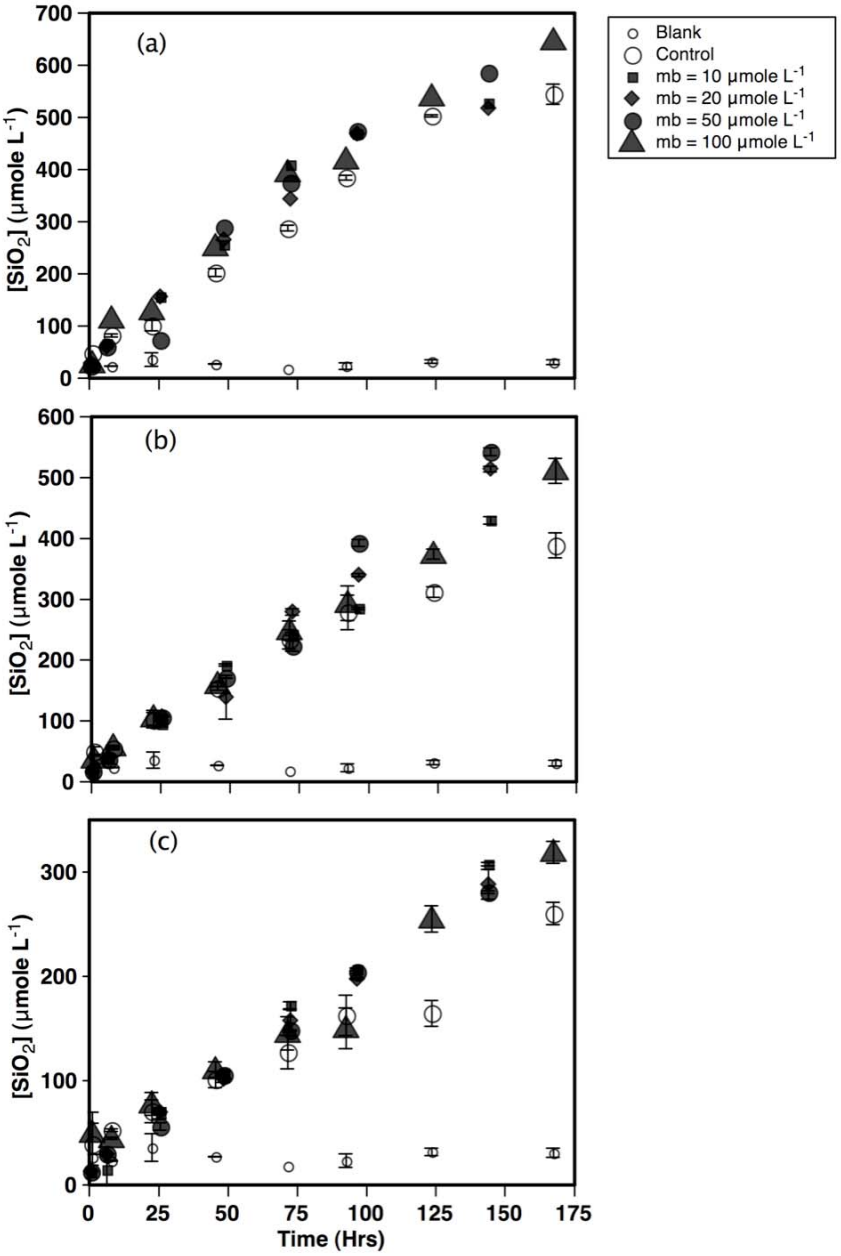

Figure 4.3. Cu/Si release as function of time for (a) Cu-1 Treatment $[Cu]_i$ = 80 ppm, and (b) Cu-3 Treatment $[Cu]_i$ = 800 ppm. The Cu/Si stoichiometric ratio in the bulk glass is 9.35×10^{-5} and 9.35×10^{-4}, for the Cu-1 and Cu-3 treatments, respectively.

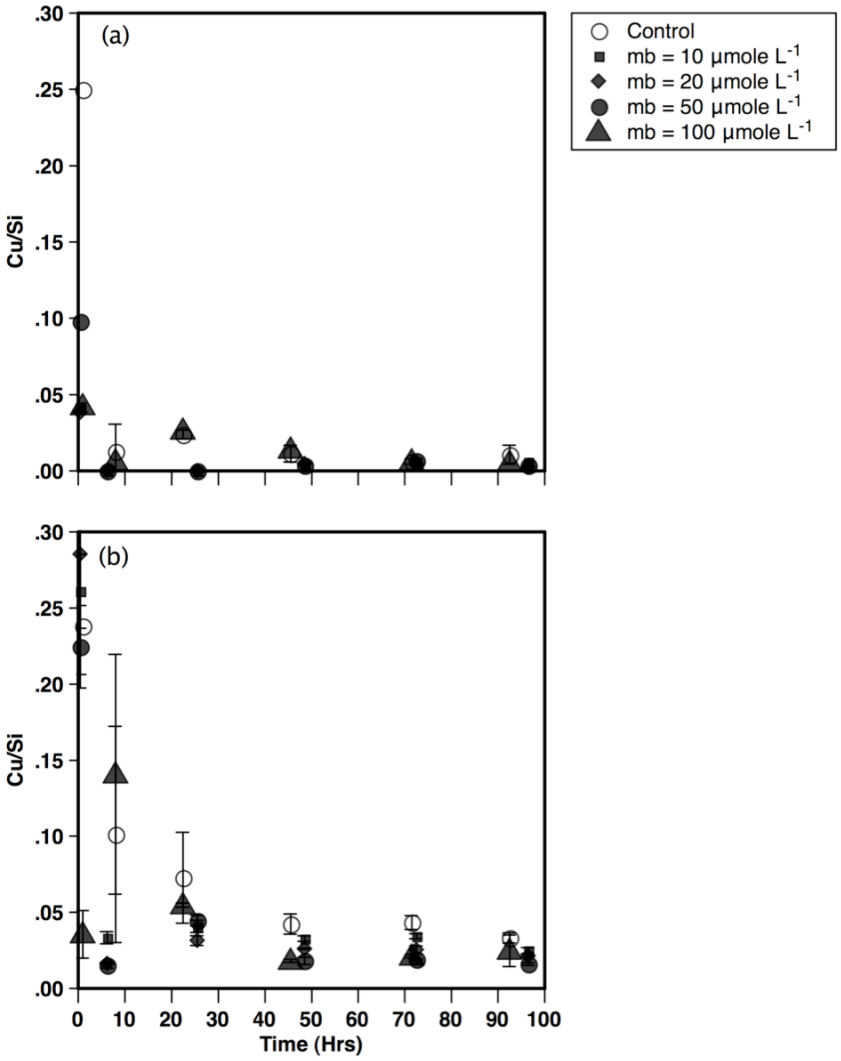

Figure 4.4. Scanning electron micrograph images of glass surfaces. (a) Glass with 80 ppm. Cu and no mb shows the formation of a small etchpit with secondary mineral precipitation in close proximity. EDAX confirmed the secondary precipitates to be composed mainly of Si and O. (b) Glass with 80 ppm Cu and 50 μmole L^{-1} mb shows extensive etching along and across conchoidal fractures. No secondary precipitates were detected. In both cases the glasses were extracted from the experimental reactors at 28-days and filtered with 0.45-μm pore size diameter membranes, followed by air-drying for 48 hours. All specimens were gold-coated for 2 minutes prior to examination.

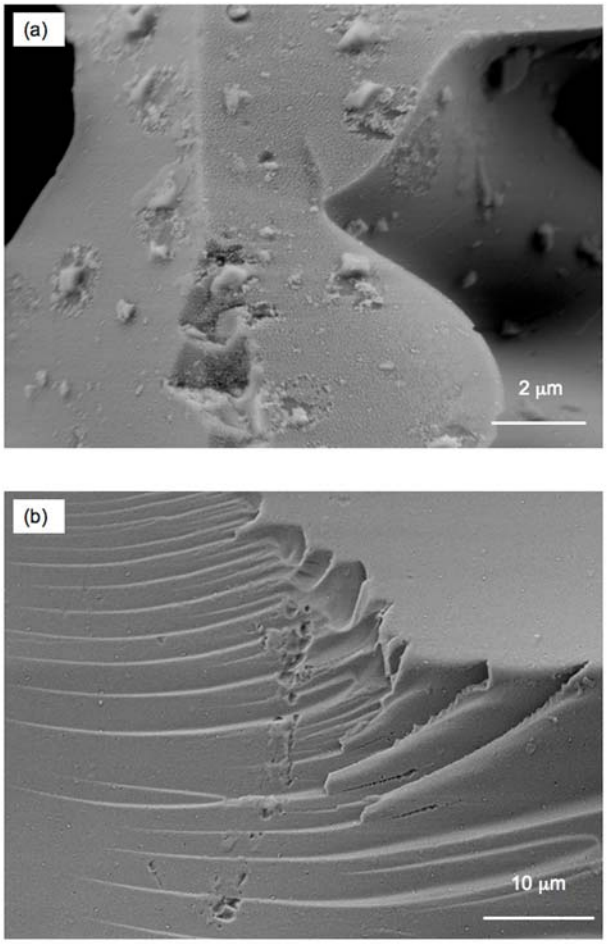

Figure 4.5. Sorption isotherm of mb bound to glass surface (μmoles g^{-1}) for mb sorption onto glass (no Cu, solid circle); mb sorption onto glass (80 ppm Cu, open circle), equation for the line of fit is $y = 2.02x + 1.6$ ($r^2 = 0.901$); mb sorption onto glass (800 ppm Cu,), equation for the line of fit is $y = 3.28x - 22.2$ ($r^2 = 0.995$).

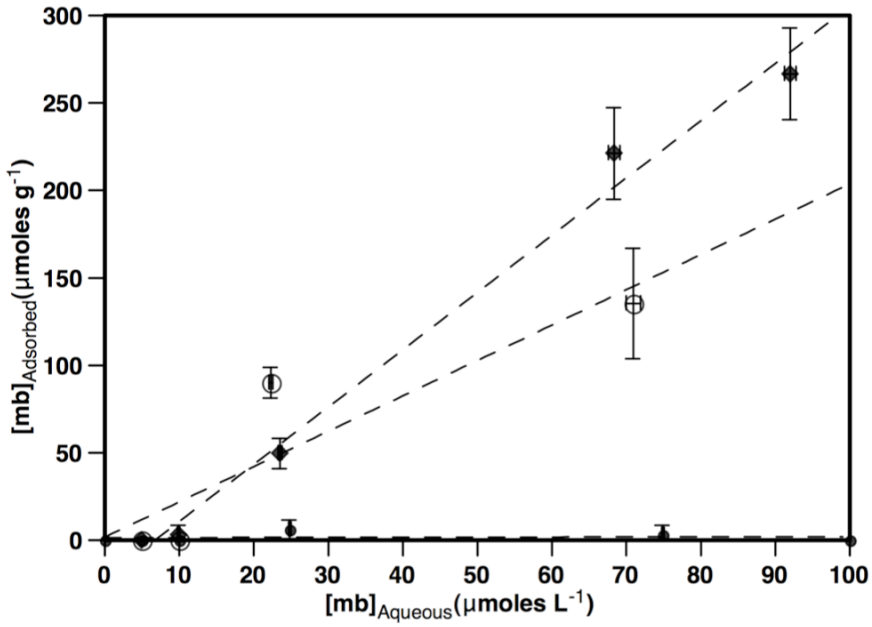

Figure 4.6. SiO_2 dissolution rates (r_{mb}; μmole SiO_2 m^{-2} h^{-1}) as a function of mb (μmole L^{-1}) concentration for Cu-substituted glasses with 80 ppm and 800 ppm Cu.

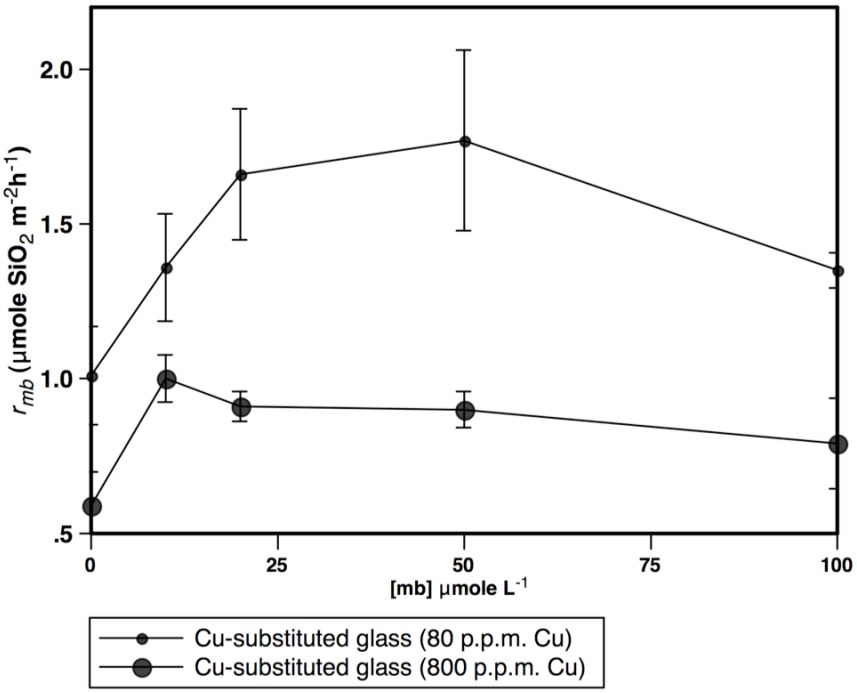

CHAPTER 5:

STIMULATION OF METHANOTROPH ACTIVITY BY CU-SUBSTITUTED BOROSILICATE GLASS

Published as a separate article:
Kulczycki E., Fowle D.A., Kenward P.A., Leslie K., Graham D.W., Roberts J.A. 2010. Stimulation of methanotroph activity by Cu-substituted borosilicate glass. Geomicrobiology Journal, *In Press*.

ABSTRACT

Previous investigations have shown that bacteria can derive benefits from elements within mineral assemblages associated with/or proximal to their point of attachment; however to date, no study has shown a direct connection between mineral dissolution and the biological oxidation of the greenhouse gas methane (CH_4). Here we investigate linkages between the Cu content of silicate glasses (Si-glasses) and CH_4 oxidation rates in *Methylosinus trichosporium* OB3b, a type II methanotroph. A series of batch growth experiments were performed under varying solid phase Cu (0, 80, 200, 400, and 800 ppm Cu) and initial aqueous phase methane concentrations (40, 70, and 130 nM CH_4). Under near equilibrium conditions, the release of Cu from the glasses increased in association with *M. trichosporium* OB3b activity. The acquisition of Cu from the glasses directly influenced CH_4 oxidation rates of *M. trichosporium* OB3b, presumably by promoting the expression and activity of copper-containing particulate methane monooxygenase (pMMO), the most efficient MMO produced by this organism. Highest CH_4 oxidation rates were observed in glasses with 80 ppm Cu. However, rates generally displayed an inverted-U relationship with solid-phase Cu concentration; i.e., rates were lower with solid phase Cu concentrations < 80 ppm or > 200 ppm. We conclude that *in situ* methanotroph activity in soils and sediments is strongly influenced by the ambient solid-phase Cu concentration, which has important implications to interpreting greenhouse gas flux data in geologic settings.

INTRODUCTION

Microorganisms depend upon a variety of elements for their metabolic function and many provisional macro- and micro-nutrients are contained in minerals (Uroz et al., 2009). However, some mineral-bound metals may not be readily available to microorganisms if they are in the solid phase as an interstitial mineral constituent or surface-sorbed species. Under such circumstances, microorganisms can colonize mineral surfaces impacting mineral dissolution (Bennett et al., 2001; Fowle et al., 2004; Hoppert et al., 2004; Liermann et al., 2000; Roberts, 2004; Roberts et al., 2004; 2006), subsequent nutrient release and preferentially acquire required nutrients from the host mineral (Brantley et al., 2001; Rogers et al., 1998; Rogers and Bennett, 2004). For example, soil bacteria have been shown to release trace elements (e.g., Fe, Ni, V, and Mn) from minerals such as hornblende for nutritive benefit (Brantley et al., 2001; Kalinowski et al., 2000). Further, cyanobacteria promote the dissolution of apatite during uptake of phosphorus (Schaperdoth et al., 2007). Finally, N_2-fixing soil bacteria have been implicated in the dissolution of silicates when targeting Mo (Liermann et al., 2005). In summary, if the nutrient supply is limited, microorganisms can promote mineral weathering to satisfy their energetic and nutritional demands through a variety of acquisition strategies (Rogers and Bennett, 2004).

In the soil subsurface environment, microorganisms may also be indirectly responsible for the release of metals from minerals. For instance, Hausrath et al. (2007) showed that Ni-requiring methanogens alter the surrounding solution pH by consuming CO_2, which consequently enhances mineral dissolution rates

compared to abiotic controls. Other microorganisms have been shown to alter solution pH by secreting organic or inorganic acids that subsequently promote the weathering of minerals and nutrient release; e.g., Ca, P, Y, Fe and Cu (Goyne et al., 2006; Neaman et al., 2005a; 2005b; Schaperdoth et al., 2007; Welch et al., 2002). A number of microorganisms generate ligands capable of chelating specific metals through surface reactions that mechanistically promote mineral weathering, such as siderophore production for ferric iron reduction (Hersman et al., 1996; Holmen and Casey, 1996; Kraemer, 2004; Liermann et al., 2000) or "molybdophore" production for Mo (Liermann et al., 2005).

In this study we further demonstrate that that mineral phases can impact enzyme activity in biota by examining the impact of solid phase Cu concentrations on rates of methane oxidation by the methanotroph *M. trichosporium* OB3b. Copper is critical to *M. trichosporium* OB3b because it regulates gene expression and the manufacture of copper-containing particulate versus non-copper soluble methane monooxygenases (pMMO and sMMO, respectively; Balasubramanian and Rosenzweig, 2008) in the cell: enzymes that differ in methane oxidation efficiency. Knapp et al. (2007) showed that *M. trichosporium* OB3b conditionally up-regulates pMMO-related gene expression when Cu is provided as silicate glasses or iron oxides, mediated by a Cu trafficking molecule known as methanobactin (mb) (Kim et al., 2004). Furthermore, Kulczycki et al. (2007) demonstrated that mb enhanced Cu dissolution from Cu-substituted borosilicate glass. However, neither study compared methane oxidation rates with solid-phase Cu concentrations, which is

of greatest importance when predicting *in situ* CH_4 flux in natural soil and sedimentary environments and is addressed in the current study.

METHODS

To quantify the relationship between methanotrophic activity and reactivity of Cu-bearing silicate glasses, parallel batch reactors containing *M. trichosporium* OB3b cultures were grown using manufactured Cu-substituted borosilicate glass chips as the sole Cu source. Different reactors were provided with different mixtures of air and methane in their headspace (in replicate), and individual reactors were sacrificed at regular time intervals to monitor changes in aqueous metals such as Si (a proxy for weathering), Cu, and CH_4 concentrations for up to 100 hours. Slopes of the linear trends were used to calculate rates of glass dissolution and CH_4 oxidation, respectively (Lasaga, 1981).

Manufactured glasses were employed as a means to control the concentrations of copper in the experiments, while providing a similar bulk substratum for dissolution. Glasses were manufactured to span the range of Cu concentrations found in natural soils and sediments (U.S. soils range from < 1 – 700 ppm; Shacklette and Boerngen, 1984) with consideration of the limits of toxicity for microbial populations (e.g., 150 ppm Cu in soil bacteria; Chander et al., 1995).

Glass Synthesis

Glass was synthesized according to the method used by Kulczycki et al.

(2007). In summary, the composition of the silicate glasses was first calculated using shareware formulae from Lawrence Livermore National Laboratory (Bourcier personal comm. 1997). Stock powders were produced by combining crystalline SiO_2, B_2O_3, Na_2O, Al_2O_3 and CuO (Kulczycki et al., 2007), and glasses with Cu concentrations of 0 ppm, 80 ppm, 200 ppm, 400 ppm, and 800 ppm were manufactured (designated Cu (0), Cu(80), Cu (200), Cu (400) and Cu (800), respectively). Mixed powders were homogenized on a side arm shaker for 20 minutes, and melted in graphite crucibles at 950 ^{o}C for 12 hours using a muffle furnace (Isotemp Programmable 800 Series). Upon quenching at room temperature, the glass was ground and sieved to a uniform size fraction (125-250 μm). The glass was rinsed and sonicated for 1 minute with low power sonication in NANOpure water (18 MΩ) 50 times prior to use.

The specific surface area of each prepared glass was confirmed (0.16 m^2 g^{-1}) by application of the five-point BET method using a Quantachrome Nova Series E (Quantachrome Instruments, Boynton Beach, Fl, USA) with N_2 as the adsorbate gas. Characterization of the glass by light microscopy confirmed one-phase glasses with no precipitates or discernible clusters, suggesting that Cu was present within the glass structure; however, these glasses likely possess some spatial heterogeneity in Cu distribution. X-ray powdered diffraction (XRD) analysis (Bruker D8 Discovery powder X-ray diffractometer; University of Notre Dame, Environmental Mineralogy and Crystal Structures Lab) was also performed on each glass to confirm that they were single phase amorphous glasses (devoid of minerals, which may form during the quenching process) and after reaction to

detect any abundant secondary precipitates forming as a result of the weathering process.

Batch Experiments

M. trichosporium OB3b batch cultures (200-ml suspensions) were pre-grown to optical cell densities ca. 0.25 to 0.3 (OD_{600}; equivalent to cell densities that range from $1x10^7$ to $3.5x10^7$ cells ml^{-1}) in nitrate salts medium (NSM at pH 7, see table 5.1; Kim et al. 2005) at 30°C in hermetically sealed 500-ml serum vials shaken in the dark at 200 rpm. The initial headspace gas mixture of air and methane was set at atmospheric pressure (1 bar).

Two sets of batch experiments were performed: a long-term experiment where reactors were sacrificed over ~100 hours, and a shorter experiment that was performed for 24 hours. The long-term experiment was initiated by transferring 10-ml aliquots (using sterile 25G 1½ syringes; Becton Dickinson) from a common pre-grown stock culture (OD_{600} = 0.25 to 0.3) to a series of previously prepared sterile 60-ml crimp-sealed glass serum vials with defined headspace gas (air and CH_4 mixture: "low-methane", 36 mM CH_4; "mid-methane", 60 mM CH_4; "high-methane", 116 mM CH_4) and 30 mg of glass chips with a specific surface area of 0.16 m^2 g^{-1}. For each methane concentration examined, a series of 10 to 12 batch reactors were prepared and sacrificed at chosen time intervals. Each reactor series was sorted according to aqueous CH_4 concentration (40 nM, 70 nM, or 130 nM) and solid-phase Cu concentration (i.e., 0 ppm, 80 ppm, or 800 ppm Cu in glass). The resulting mixtures were agitated at 30°C in the dark at 100 rpm (a reduced

mixing rate was used because preliminary testing showed that it minimized impact dissolution). Two sets of controls without glass chips also were monitored; a control with cells and one without cells. Both controls were monitored in parallel to the experimental treatments.

The short-term experiment was performed to quantify "instantaneous" methane oxidation rates. These experiments were performed as above with the following modifications. Replicate batch reactors were prepared with 150 mg of borosilicate glass chips (formulations with Cu concentrations of: 0, 80, 200, 400, and 800 ppm) in 125-ml glass serum vials containing 50-ml aliquots from a common pre-grown stock culture of *M. trichosporium* OB3b grown to late log phase (OD_{600} = 0.3). Upon crimp-sealing the serum vials, the headspace conditions were set (air and CH_4 mixture) with an initial aqueous CH_4 concentration of ~ 8 μM. Biotic reactors were prepared in triplicate with the following abiotic controls: growth media only (no cells), a culture blank (cells with no glass chips), and a media blank (growth media without cells or glass chips). The resulting reactors were agitated at 30^{o}C in the dark at 100 rpm (similar to the long-term experiments). In each of the short-term experiments, headspace CH_4 and CO_2 concentrations were monitored over time and solution sub-samples were collected at defined intervals over 24 hours.

Prior to sacrificing, reactor headspace gases were quantified in quadruplicate using an Agilent Technologies Network GC System 6890N with Thermal Conductivity Detector (TCD). Specifically, CH_4 and CO_2 phases in the headspace were separated in an isotemperature run on an Alltech Hayesep Q 80/100 Packed

Column with an oven temperature of 90 °C and analytical error of 0.5%. Upon sacrificing, culture samples were sub-divided for aqueous metal, sorbed metal (long-term experiments only), cell enumeration, and pH analysis. Sub-samples for metal analysis, using an ICP-OES (Perkin Elmer Optima 5300 DV), were filtered using 0.2 μm polycarbonate filters (Nucleopore Track-Etch Membrane) and preserved by acidification (5% ultrapure HNO_3, which prevents metal sorption onto polypropylene containers). For cell metal analysis, 1-mL samples were diluted to 2.5-ml with nanopure H_2O, and supplemented with 0.5-ml of 70% trace metal grade HNO_3 (Fisher Scientific) and 1-ml 30% H_2O_2 (Fisher Scientific certified A.C.S., Kulczycki et al., 2002; 2005). Each sample was then heated at 60^{o}C overnight to digest the bacteria and then analyzed using ICP-OES similar to the aqueous samples. Reported extracted and aqueous-phase metal concentrations are designated as Me_{Ext} and $Me_{(aq)}$ (where Me = Cu or Si), respectively. Sub-samples (50-μl) for cell enumeration via direct counts were diluted immediately in 1-ml sterile NANOpure H_2O and vacuum filtered onto 0.2-μm polycarbonate filters (Nucleopore Track-Etch Membrane). The cells were then fixed with 2.5% glutaraldehyde, washed with a DAPI pretreatment solution (4.2 g citric acid, 0.5-ml Tween 80 in 100-ml H_2O), and stained with DAPI (10 mg L^{-1}) before mounting onto slides for examination by fluorescent light microscopy (Yu et al. 1995). The remaining unfiltered sample was used for pH determination.

Scanning Electron Microscopy

Scanning electron microscopy (SEM) was used to examine glass surfaces for

evidence of secondary precipitates, dissolution features, and microbial colonization. In preparation for scanning electron microscopy, glass particles and solution samples were vacuum filtered onto 0.2-μm polycarbonate filter (Nucleopore Track-Etch Membrane), and the filter papers were stored in 2% (v/v) glutaraldehyde to fix the bacteria. The samples were subsequently dehydrated via application of a chemical critical-point drying method (Vandevivere and Bevaye, 1993). The dried filter paper samples were stub-mounted and gold-sputter coated for two minutes. Glasses were imaged using a field emission scanning electron microscope (SEM; LEO 1550 operated at an accelerating voltage of 12 kV) equipped with an electron dispersive system (EDAX).

RESULTS AND DISCUSSION

Initial Cell Densities and Solution Chemistry

DAPI direct counts and OD_{600} were used in the experiments to quantify associated cell densities. The mean initial cell density among long-term experiments was $1.2 \pm 1.0 \times 10^7$ cells ml^{-1} (table 5.2), while the mean initial cell density was $2.4 \pm 0.1 \times 10^7$ cells ml^{-1} for short-term experiments. Cells were always in exponential growth phase prior to use.

Solution pH values for each biotic reactor, regardless of glass composition, were circum-neutral for all experiments (mean pH at $t_0 = 7.2 \pm 0.1$) due to the buffer used in the growth media. Therefore, proton-promoted glass dissolution was unlikely among experiments. Initial solution pH values in the Cu (0), Cu (80), and Cu (800) abiotic controls were 7.5, 7.3, and 7.3, respectively.

Small pH drops were noted over time in each experiment, typically < 0.08 units in abiotic controls and < 0.4 units in biotic systems. The larger shift in pH in the biotic reactors was attributed to CO_2 production during growth (data not shown). However, all observed pH variations were sufficiently small as to not likely influence rates of dissolution (e.g. Welch and Ullman, 1993; Welch et al., 1999). It is important to note that initial solution chemistry includes media constituents (table 5.1) that might influence Al and Cu speciation. In particular, the majority of remaining phosphate could interact with glass surface sites through sorption reactions and potentially lead to incongruent dissolution reactions through the formation of solid phosphate phases; however, this is not supported by XRD or SEM analysis. In short-term experiments, initial pH for all experiments was 7.1 ± 0.1and final pH =6.8 ± 0.1.

Bacterial colonization and surface alteration of glass

Scanning electron microscopy (SEM) examination of the reacted silicate glasses in the presence of growing *M. trichosporium* OB3b showed surface colonization associated with all glass formulations and experimental treatments. SEM examination of the glass chips suggested that X-ray amorphous SiO_2 formed on glass surfaces in both abiotic and biotic systems (data not shown). Clay formation could not be confirmed by XRD analysis because the weathered fraction was relatively minor compared to the bulk glass. As such, we interpret the secondary precipitation observed by SEM to be amorphous to nanocrystalline in character. In addition, SEM observations coupled with energy dispersive X-ray

analysis (EDAX) indicate that surface colonizing cells were coated with an amorphous gel composed of Si, Al, and O (data not shown), which is similar in elemental composition to precipitates found on the surface of the glass. These morphologies are consistent with siliceous gels seen in other studies (Knecht and Wright 2004).

Si release

Aqueous silicon ($Si_{(aq)}$) was monitored as an indicator of net Si release from the borosilicate glass throughout all experiments. In all cases, an increase in $Si_{(aq)}$ was observed with time (figure 5.1). Si saturation levels (amorphous silica; 1913.5 μM, Morey et al., 1964) were never reached within a 100-hour time frame for any of the experiments (long-term or short-term). Figure 5.1 shows that $Si_{(aq)}$ concentrations for long-term experiments increased linearly over the first 60 hours of exposure to glass, but became more parabolic thereafter. Secondary precipitation of Si from the aqueous phase onto the surfaces of the microbial cells and glass chips would explain the nonlinear increase in $Si_{(aq}$. While precipitates of unknown composition were observed with SEM specific quantification of Si bound to cell walls and glass surfaces was not performed.

Overall, Si release rates differed according to glass Cu concentration indicating different solubilities of individual glass formulations. Aqueous Si concentrations never exceeded 2 μM for blanks and culture controls absent of glass within 100 hours. These differences in solubility were expected and therefore, we present Si release merely as a point of reference. Limited Si release

was observed in the short-term experiments (data not shown).

Although the formation of secondary mineral phases limits interpretation, we calculated the first order rates of release ($\mu M\ Si\ h^{-1}$) via linear curve-fitting $Si_{(aq)}$ concentrations vs. time for the first 60 hours (Faure, 1998; Lasaga, 1981). A statistical examination of the trends in Si release between each biotic treatment and the abiotic control of the same glass composition indicates that there were no differences (figure 5.1 and table 5.2), based on overlapping confidence intervals (confidence of slope*T-value). As such, the presence of *M. trichosporium* OB3b does not appear to influence rates of Si release under the conditions investigated in this study.

Cu release

Aqueous Cu ($Cu_{(aq)}$) was monitored in all treatments during both the short-term and long-term experiments. Aqueous Cu was not detectable in any treatment of the short-term experiments, nor was it detected in the Cu(0) and Cu(80) treatments of the long-term experiments (data not shown). To account for Cu release from the borosilicate glass that was taken up by the *M. trichosporium* OB3b cells in suspension, a sample digestion was performed (see methods), and the Cu content of the suspension was described as extractable Cu (Cu_{Ext}). Only in the long-term experiments (treatments with initial $CH_{4(aq)}$ concentrations of 40 nM) was cell extractable Cu monitored, and it was only detectable in the Cu(800) treatment (figure 5.2). A comparison between $Cu_{(aq)}$ and Cu_{Ext} in the biotic Cu(800) treatment (figure 5.2a and b, respectively) shows that cellular uptake of

Cu was happening. The expression used to describe how extractable Cu (Cu_{Ext}) relates to aqueous Cu ($Cu_{(aq)}$) and the amount of Cu directly associated with the cells (Cu_B) is the following:

$$Cu_{Ext} = Cu_{(aq)} + Cu_B$$

Aqueous Cu ($Cu_{(aq)}$) was subtracted from both sides of the expression to solve for Cu_B and the trend is shown in figure 5.2c.

Rates of Cu release were calculated from the slopes of the linear trends according to zero-order rate kinetics (Faure, 1998; Lasaga, 1981). Here we present both abiotic and biotic-promoted rates of Cu release from the Cu(800) glass treatments (table 5.3), where the trend in extractable Cu was used to calculate the biotic rate. A higher rate of Cu release was observed in the biotic treatment (r = 0.15 μmole l^{-1} Cu) compared to the abiotic one (r = 0.05 μmole l^{-1} Cu) indicating that Cu leaching is enhanced by the presence of *M. trichosporium* OB3b.

Overall, these results show that Cu preferentially associates with active methanotroph cells, which is consistent with direct Cu uptake or binding to the outer cell wall membrane (Hakemian and Rosenzweig, 2007; Hanson and Hanson, 1996; Kim et al., 2004). The clear trends in increasing cell associated Cu that were observed in the Cu(800) treatments are evidence of microbially-promoted leaching of Cu from the glass. The presence of bacterial cells is expected to increase the flux of cations (i.e., Cu), as bacterial cell walls are known to sorb mineral-forming cations and subsequently promote enhanced mineral solubilities (Wightman and Fein 2004). Our data do not allow us to distinguish a

metabolically driven flux of Cu from the glass or determine if the gradient was simply caused by cell binding of Cu to the surface functional groups. However, given the metabolic requirements for Cu during methane oxidation (Bedard and Knowles, 1989), preferential leaching of Cu by *M. trichosporium* OB3b is worth considering as a possible explanation for the enhanced rates of Cu release that were observed.

CH_4 depletion, CO_2 production and rates of CH_4 oxidation

The concentration of aqueous CH_4 decreased over time in every biotic treatment in both the long-term and short-term experiments, indicating *M. trichosporium* OB3b was metabolically active through the experiments. Further, no abiotic controls showed decreases in CH_4 concentrations over the course of the experiment (data not shown). Finally, decreases in aqueous CH_4 concentrations were concomitant with increasing aqueous CO_2 concentrations (data not shown), suggesting respiration. Carbon dioxide generation rates were relatively consistent with CH_4 oxidation rates, although mass balances were not 100%, probably due to carbon-assimilation into biomass. *M. trichosporium* OB3b is a pseudo-autotroph and obtains some carbon from CO_2-fixation (Hanson and Hanson, 1996).

A first-order kinetic model was employed to estimate CH_4 oxidation rates and constants from declining slopes in $CH_{4(aq)}$ concentrations in the short-term experiments (figure 5.3). Rates were generally consistent with rates calculated for the long-term experiments, although we will focus on short-term data for simplicity. Statistical analysis of the CH_4 oxidation rate data using ANOVA

comparison at the 90% confidence interval indicates that the Cu(80) and Cu(200) treatments had the highest rates of CH_4 oxidation (though did not significantly differ from each other) and were distinct from the other treatments. Lowest rates were observed for the Cu(0) and Cu(800) treatments, which were statistically the same, but were significantly lower than the other Cu treatments. Overall, the CH_4 oxidation rate pattern followed Cu(80) = Cu(200) > Cu(400) > Cu(0) = Cu(800) and displayed an inverted-U between rate and solid-phase Cu concentration (figure 5.3). Therefore, we suggest that among the five glass treatments examined, the Cu content of the Cu (80) and Cu (200) glasses are at concentrations that promote optimum rates of CH_4 oxidation when made bioavailable to *M. trichosporium* OB3b cells during cell interaction with the glass.

The rates of CH_4 oxidation also were modeled according to the mixed-order Michaelis-Menten kinetic function (table 5.4) using a parameter estimator based on the simplex optimization of a least squares fit with bisquared weighting (Devlin, 1994; Goudar and Devlin, 2001). The maximum rate of reaction, V_{max}, is the rate of reaction when the reactive enzyme (i.e., pMMO or sMMO) is assumed to be saturated with substrate (CH_4). The relationship between the rate of CH_4 oxidation and the initial CH_4 concentration also is a function of the affinity coefficient, K_m, which is the substrate concentration when $V = ½ V_{max}$ (Alexander, 1999; Schnell and Maini, 2003; Stevens and Price,1999). High affinity coefficients are associated with enzymes that have low affinities for the substrate, and relatively high substrate levels are required to achieve V_{max}. Whereas, low K_m values indicate a high affinity between enzyme and substrate, and higher reaction rates occur at low substrate concentrations but then do not vary

dramatically as a function of increasing substrate levels (Alexander, 1999; Schnell and Maini, 2003; Stevens and Price, 1999).

Michaelis-Menten-type modeling of CH_4 oxidation rates and solid-phase Cu concentration for the short-term experiment indicates three different possible relationships involving K_m versus Cu concentration and initial CH_4 concentration (table 5.4). The Cu(0) and Cu(800) treatments had significantly higher K_m values relative to the S_0 (initial aqueous CH_4 concentration in μM) indicating that MMO in these cases had a low affinity for CH_4. In contrast, the Cu(200) and Cu(400) treatments show K_m values near S_0, which indicates moderate affinities and reaction rates approximately one half of V_{max}. Finally, the Cu(80) treatment had a very low K_m relative to S_0, indicating that MMO had a high affinity for CH_4 and observed rates likely approach V_{max} with this Cu supply. In summary, a solid phase Cu concentration of Cu(80) appears to permit MMO to function most efficiently relative to CH_4 oxidation suggesting a moderate Cu supply "optimizes" CH_4 oxidation, which is consistent with pMMO expression and activity and possible Cu toxicity at higher solid-phase Cu concentrations.

Modeled V_{max} and K_m data (table 5.4) correlate well with observed first order CH_4 oxidation rates (figure 5.3). Lower substrate affinities (high K_m values) in the Cu(0) and Cu(800) treatments are consistent with lowest rates of CH_4 oxidation (Cu(0): 8.93 ± 1.9 h^{-1}; Cu(800): 8.59 ± 3.7 h^{-1}). The higher substrate affinities (low K_m values) seen in the Cu(80) treatment correlated to the highest CH_4 oxidation rates (17.41 ± 3.7 h^{-1}). Whereas, K_m and S were similar in both the Cu(200) and Cu(400) treatments, and intermediate CH_4 oxidation rates were observed (Cu(200): 15.61 ± 1.6 h^{-1}; Cu(400): 12.75 ± 1.4 h^{-1}). Previous work has shown that increasing ionic Cu concentrations result (below toxic

levels) in proportionate increases in rates of CH_4 oxidation probably because *M. trichosporium* OB3b utilizes Cu to sustain pMMO (Hanson and Hanson, 1996; Knapp et al., 2007). Our results for solid-phase Cu sources display a similar trend where an optimal solid-phase concentration (i.e., 80 ppm Cu) was identified for CH_4 oxidation. We posit that Cu deficiency in the Cu(0) treatment, and associated sMMO expression and activity resulted in relatively lower CH_4 oxidation rates. In contrast, aqueous Cu concentrations greater than ~ 4.3 mM Cu^{2+} are known to inhibit CH_4 oxidation activity in methanotrophs (Bender and Conrad, 1995), and while aqueous concentrations of Cu in this study never exceeded ~ 8 μM Cu, we speculate that Cu release from the 800 ppm Cu glass likely caused extraneous cell activity to minimize Cu toxicity. Apparently, while the amount of Cu released from the Cu (200) and Cu (400) was less than optimal for MMO activity, reduced rates of CH_4 oxidation were not as severe as the Cu(800) treatment.

It is not uncommon for methanotroph growth medias to contain 5 μM of $CuSO_4$. Presumably the Cu is deliberately added to suppress sMMO activity in *M. trichosporium* OB3b (Phelps et al., 1992). In the short-term experiments of our study, aqueous Cu was below detection, and the amount that was taken up by the cells may have been low enough to activate sMMO (< 0.80 μmoles Cu per gram dry weight of cells, Hanson and Hanson, 1996). Unfortunately, we did not extract Cu from the cells during these experiments, and cannot speculate whether sMMO or pMMO was active during CH_4 oxidation by *M. trichosporium* OB3b. At the dry mass concentration of *M. trichosporium* OB3b used in our study (2.54 g/L), the Cu concentration would have to be less than 2.3 micromoles per liter for sMMO activation to occur, which is not improbable.

The CH_4 oxidation rates ($r_{CH4\ ox}$) reported here are consistent with those

reported by others for *M. trichosporium* OB3b grown in mineral salts medium (Whittenbury et al., 1970) and soils exposed to atmospheric CH_4 (Bender and Conrad, 1994). While rates here are comparable to literature values, it is noteworthy that our rates were obtained using solid-phase Cu as the Cu source, which strongly supports the assertion that soil- and sediment-Cu are likely bioavailable to these organisms and allow *in situ* methanotrophic activity. Furthermore, soils and sediments with Cu concentrations examined in this study can result from the weathering of a number of soil-forming rocks and other natural materials that include ultramafic (2-100 ppm Cu) and basaltic (30-160 ppm Cu) igneous rocks, shales and clays (18-120 ppm Cu), and black shales (20-200 ppm Cu), while weathering ore bodies, polluted sediments or biosolids may yield soil/sediment Cu concentrations in the 400 to 800 ppm range or higher (Adriano, 1986; Tourtelot, 1971). Finally, this report shows that the mineral composition directly impacts the metabolic activity of *M. trichosporium* OB3b, as the amount of bioavailable Cu being released from the silicate determines how efficiently CH_4 is being oxidized.

SUMMARY

Copper in substituted borosilicate glasses clearly supports metabolic activity of *M. trichosporium* OB3b as evidenced by the variation in CH_4 oxidation rates between treatments. We can conclude that rates of CH_4 oxidation are enhanced when an appropriate quantity of Cu is made available to cells, through partitioning of Cu from the glass phase. The direct utilization of Cu for pMMO

activation contributes to more efficient oxidation of CH_4, as observed in the 80 ppm Cu glass treatments, although elevated glass-bound Cu appears to suppress rates of CH_4 oxidation (e.g., 800-ppm Cu glass treatments). Relative to weathering, the flux of Cu from the mineral phase was enhanced by *M. trichosporium* OB3b, probably as surface reactive cell walls bind metals and maintain a gradient between the mineral and solution. While silicate weathering processes are difficult to interpret, it appears that liberation of Cu from Cu-containing glass impacts CH_4 oxidation.

This study provides the first quantitative assessment of how rates of CH_4 oxidation by *M. trichosporium* OB3b are influenced by solid-phase Cu. These early results may now be integrated into models to quantitatively predict the degree of CH_4 consumption that might occur in near-surface geologic settings, provided that the ecology, hydrogeology, mineralogy and trace element geochemistry of the system is constrained.

ACKNOWLEDGEMENTS

The authors would like to thank Charles W. Knapp for instruction and advice on methanotroph culturing, Peter C. Burns for use of the Bruker D8 Discovery powder X-ray diffractometer, David Moore for assistance with the LEO 1550 field emission SEM, and two anonymous reviewers for their insightful comments. The authors also acknowledge support for this research from NSF Biogeosciences (EAR 0433980 awarded to Roberts and Graham), NSF Low Temperature Geochemistry and Geobiology (EAR 0750009 awarded to Fowle,

Roberts and Graham) and KU Geology Associates (Fowle).

Table 5.1. Solution chemistry of media used to grow *Methylosinus trichosporium* OB3b

Chemical Species	**Activity (M)**
$NaNO_3$	0.01
K_2SO_4	0.001
KH_2PO_4	0.0039
Na_2HPO_4	0.006
Chemical Species	**Activity (μM)**
$MgSO_4$	150
$CaCl_2.2H_2O$	47.6
$ZnSO_4.7H_2O$	2
$MnSO_4.H_2O$	1.6
H_3BO_3	6
$CoCl_2.6H_2O$	0.4
KI	1
$FeSO_4$	40

The initial solution chemistry within each glass serum vial before inoculating with *Methylosinus trichosporium* OB3b.
The solution pH = 7.

Table 5.2. Net Si release rates from borosilicate glass

	†Cu(0)					†Cu(80)					†Cu(800)				
*Reactor Variants	‡r	§r^2	¶Error	**Sig. (95%)	ΨB_0 (cells ml^{-1})	‡r	§r^2	¶Error	**Sig. (95%)	ΨB_0 (cells ml^{-1})	‡r	§r^2	¶Error	**Sig. (95%)	ΨB_0 (cells ml^{-1})
Abiotic control	9.7	0.975	1.2 (n=11)	---	---	0.6	0.961	0.1 (n=11)	---	---	2.9	0.985	0.3 (n=11)	---	---
40 nM CH_4	8.4	0.971	1.1 (n=11)	no	$2 \pm 0.5x10^7$	1.0	0.836	0.4 (n=11)	no	$2 \pm 0.3x10^7$	3.0	0.985	0.3 (n=11)	no	$1 \pm 0.2x10^7$
70 nM CH_4	9.5	0.963	3.8 (n=5)	no	$8 \pm 0.1x10^7$	0.7	0.88	0.3 (n=7)	no	$5 \pm 0.6x10^6$	4.1	0.948	1.0 (n=8)	no	$8 \pm 0.2x10^6$
130 nM CH_4	8.3	0.947	3.0 (n=6)	no	$5 \pm 0.7x10^6$	0.7	0.986	0.1 (n=7)	no	$4 \pm 2x10^5$	3.5	0.985	0.7 (n=6)	no	$3 \pm 0.5x10^6$

*Reactor variants are distinguished by initial aqueous CH_4 concentrations. †Cu(0), Cu(80) and Cu(800) represent Cu-substituted glasses with Cu concentrations of 0, 80, and 800 ppm, respectively.

‡ Rate constants expressed as μM Si h^{-1}, calculated from a linear fit of aqueous Si concentrations vs. time within the first 60 hours of the experiment.

§Values are correlation coefficients for the regression analyses.

¶Error based on confidence slope **t-value* (e.g. 95% confidence level)

**Sig. (95%) is the significance that the slopes of two population trends (biotic reactor variant vs. abiotic control) are different based on the *t* distribution for a 95% confidence level.

ΨB_0 is the initial cell density of *Methylosinus trichosporium* OB3b in each respective reactor variant.

Table 5.3. Cu release rates from Cu(800) borosilicate glass

*Treatment	‡r	§r^2	¶Error	**Sig. (95%)
Abiotic	0.05	0.894	0.01 (n=11)	---
Biotic	0.15	0.886	0.04 (n=11)	yes

* Initial CH_4 and Cu concentrations were the same for the abiotic and biotic treatments at 40 nM $CH_{4(aq)}$ and 800 ppm Cu, respectively.
‡ Rate constants expressed as μmole l^{-1} Cu, calculated from a linear fit of aqueous Cu concentrations vs. time within the first 60 hours of reactivity. The biotic rate was calculated from the cell extracted Cu (Cu_{Ext}) data.
§ Values are correlation coefficients for the regression analyses.
¶ Error based on confidence slope **t-value* (e.g. 95% confidence level)
** Sig. (95%) is the significance that the slopes of two population trends (biotic reactor variant vs. abiotic control) are different based on the *t* distribution for a 95% confidence level.

Table 5.4. Michaelis-Menten kinetic modeling

Treatment	S_0 (μM)	V_{max} (μM h^{-1})	K_m (μM)
Cu(0) (n=6)	8.69	4.25 ± 2.5 x 10^6	3.36 ± 2.0 x 10^4
Cu(80) (n=7)	8.63	1210 ± 140	0.96 ± 0.9
Cu(200) (n=7)	9.10	2780 ± 320	9.09 ± 1.8
Cu(400) (n=7)	7.70	1950 ± 270	7.42 ± 2.0
Cu(800) (n=5)	6.74	6.02 ± 2.0 x 10^6	4.33 ± 1.4 x 10^4

S_0 is the initial aqueous substrate (CH_4) concentration in μM.
V_{max} is the maximum rate of reaction (μM h^{-1}) when the enzyme is saturated with substrate (CH_4).
K_m is the Michaelis constant of the enzyme (μM).

Michaelis-Menten equation: $V_0 = \frac{V_{max}[S]}{K_m + [S]}$

where V_0 is the initial reaction rate, and S is the substrate concentration.
* Error on V_{max} and K_m represents the range between the 95% confidence interval.

Figure 5.1. Si release (μM) as a function of time in the long-term experiments comparing biotic reactors with the corresponding abiotic control for each of the glass treatments: Cu(0) reactor $[Cu]_i$ = 0 ppm, Cu(80) reactor $[Cu]_i$ = 80 ppm, and Cu(800) reactor $[Cu]_i$ = 800 ppm. Data points represent a compilation of Si data from each bioreactor variant (40 nM, 70 nM, and 130 nM $CH_{4(aq)}$). Note that biotic and abiotic trends overlap. Error bars reflect the error on analysis of the same solution.

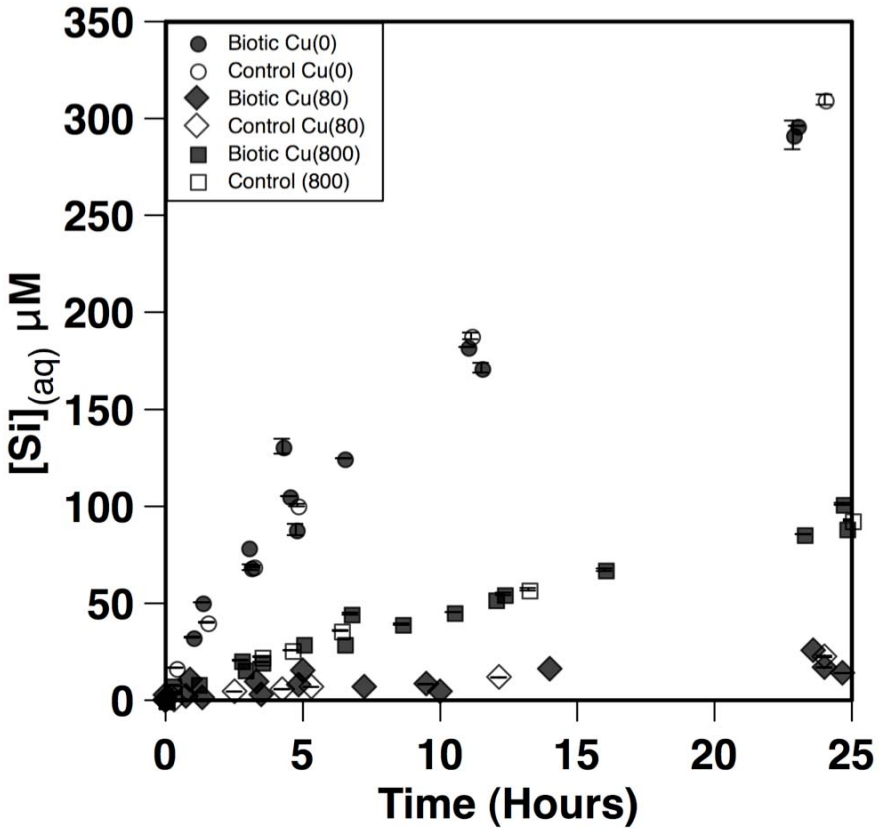

Figure 5.2. Cu release (μM) from the Cu(800) glasses (800 ppm Cu) is examined as a function of time comparing a set of reactors that vary with initial $CH_{4(aq)}$ concentration where (a) and (b) compare the aqueous ($Cu_{(aq)}$) and extractable Cu (Cu_{Ext}), respectively, and (c) is the cell associated Cu (Cu_B) calculated from the difference between Cu_{Ext} and $Cu_{(aq)}$. Biotic reactor variants are distinguished by initial CH_4 concentrations of 40 nM, 70 nM, and 130 nM, respectively. Error bars reflect the error on analysis of the same solution. Cu extracted samples are only available for the biotic reactors with initial $CH_{4(aq)}$ concentrations of 40 nM CH_4. In the Cu(0) (0 ppm Cu) and Cu(80) (80 ppm Cu) glass reactors, Cu release is near the detection limits of the analytical approach used for both the aqueous and extractable Cu and was therefore omitted from this figure.

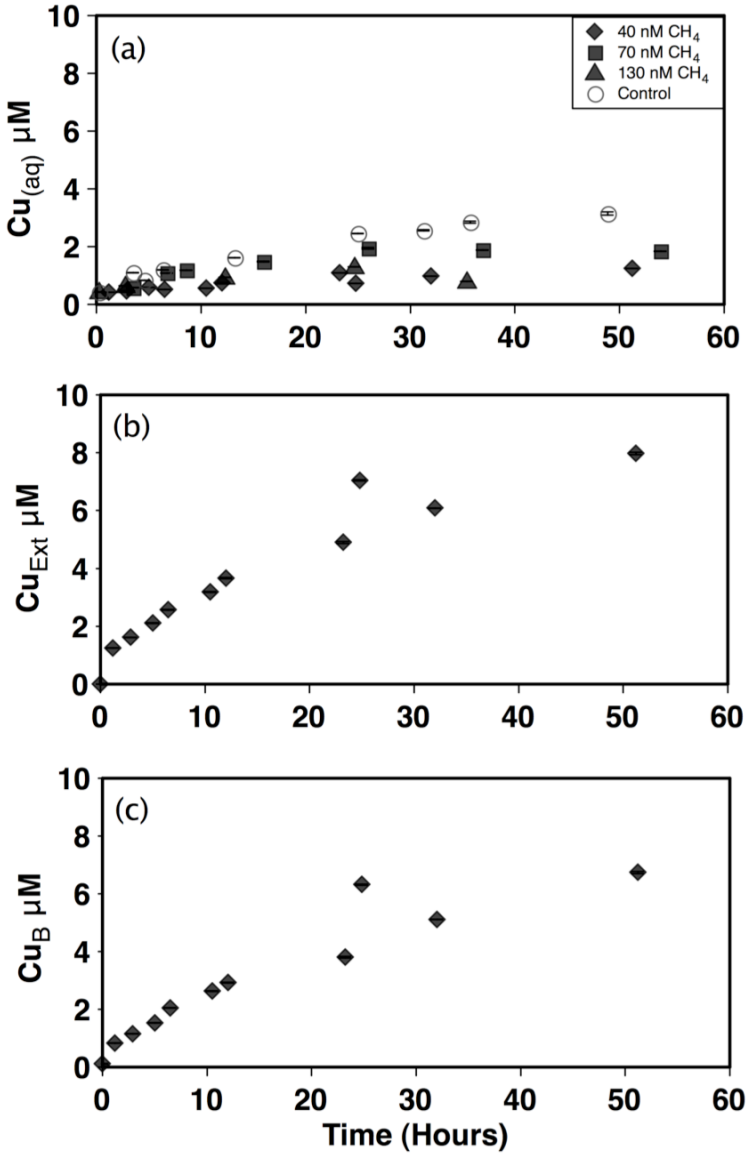

Figure 5.3. Methane depletion by *Methylosinus trichosporium* OB3b in short-term (24 hours) biotic reactor experiments as impacted by Cu concentration of the borosilicate glass. Panel (a) shows first order trends of CH_4 depletion as a function of time and (b) shows first order rates of CH_4 depletion (s^{-1}). Cu concentrations in the glasses had the following variations: 0 ppm, 80 ppm, 200 ppm, 400 ppm, and 800 ppm. Error bars represent the 90% confidence interval.

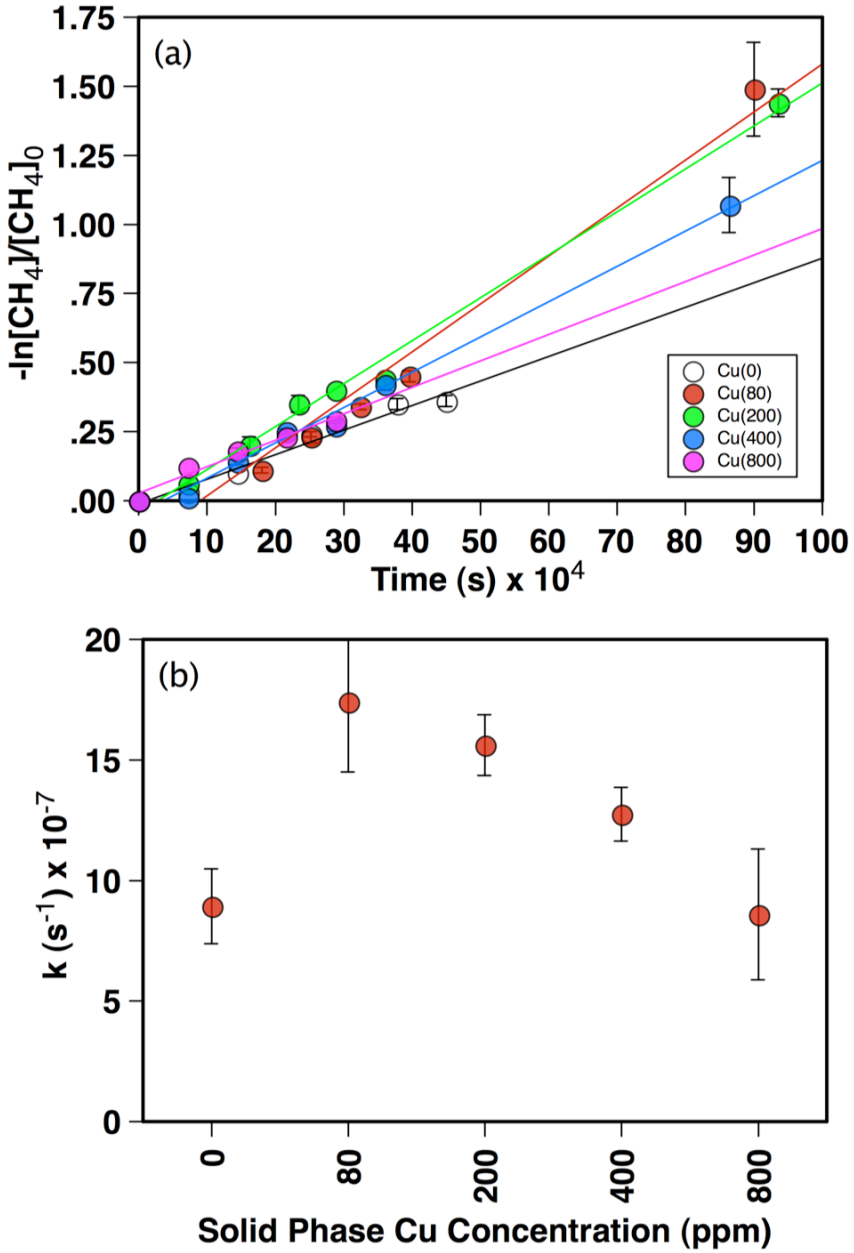

CHAPTER 6

MICROBIALLY PROMOTED MINERAL WEATHERING: A CASE FOR METHANOTROPHS

ABSTRACT

Previous investigations have demonstrated that bacteria derive benefits from the elemental composition of mineral assemblages associated with, or proximal to their point of attachment, however to date, no study has shown direct connections between mineral dissolution and biological oxidation of the greenhouse gas methane (CH_4). In this study, methanotroph-mediated batch reactivity experiments were performed to examine the weathering of silicate glasses as a function of varying Cu concentrations in the mineral phase. *Methylosinus trichosporium* OB3b was used as the model methanotroph with differing initial aqueous CH_4 concentrations in the presence and absence of methanobactin, a microbially generated Cu-chelating compound. Compared with abiotic controls, the release of Cu and Al from the glasses increased in the presence of active *M. trichosporium* OB3b cells, and is attributed to surface reactivity of the cell walls. The microbial presence is responsible for the maintenance of an elevated metal gradient between the mineral phase and the bulk solution, which promotes metal release until equilibrium conditions are met. The presence of methanobactin in solution permits higher Cu saturation levels due to the formation of a soluble Cu-methanobactin complex. Furthermore, Cu acquisition from the glasses is directly influenced by *M. trichosporium* OB3b's metabolic requirement for Cu during CH_4 oxidation. Overall, the metabolic efficiency with respect to rates of CH_4 oxidation by *Methylosinus trichosporium* OB3b

appears to be controlled by Cu flux from the silicate mineral, and can be enhanced by the addition of methanobactin to the system provided that an appropriate Cu concentration is maintained. Here we demonstrate that soil and sediment geochemistry, particularly solid-phase concentrations of Cu, may be an important parameter in regulating methanotroph activity.

INTRODUCTION

The interaction between microorganisms and minerals often results in the release of elements into the environment (Uroz et al., 2009). This is not to say that mineral weathering only occurs in the presence of microorganisms because there are numerous abiotic factors that drive mineral weathering, which include temperature, mineral solubility, reactive surface area, aqueous chemistry, aqueous transport, to name a few. All of which fall under the umbrella of reaction thermodynamics (Berner, 1995; Brantley, 2005; Lasaga et al., 1994; Maher et al., 2009; Oelkers and Schott, 2009). However, the presence of microbes can alter the reaction thermodynamics by either enhancing mineral dissolution or inhibiting it.

The dissolution of minerals by microorganisms can occur in a number of different ways as outlined by Berthelin et al., (2000). The production of acids and bases as products of metabolism may contribute to the dissolution and release of metal ions from minerals, i.e., enhanced weathering of aluminosilicates in response to the microbial production of organic acids (Barker et al., 1998). Microbial generation of organic complexing compounds in response to environmental stress can directly influence mineral solubility, i.e., enhanced dissolution of silicate minerals by organic ligands

(Ullman et al., 1996). Furthermore, oxidation or reduction reactions induced by microorganisms may promote enhanced or suppressed solubility of metals, i.e., reductive dissolution of ferric iron containing minerals by moderately thermophilic iron-oxidizing bacteria (Bridge and Johnson, 1998). A plethora of unique examples exists for each category. While metal-chelating compounds, such as siderophores or methanobactin, have demonstrated the ability to promote mineral dissolution (chapter 2 and 4, respectively, this volume), an assessment of the impact of the actual microorganisms responsible for generating these chelates will more accurately reflect how minerals are dissolved in natural systems. A thorough investigation of methanobactin promoted mineral dissolution is presented in chapter 4 (this volume, Kulczycki et al., 2007), however, the impact of *Methylosinus trichosporium* OB3b upon mineral weathering must also be determined.

In most near-surface geologic environments, Cu is scarcely bioavailable (Morton et al., 2000). Microbiota have evolved unique strategies to scavenge sufficient quantities of Cu to satisfy their metabolic needs. For example, methanotrophic species produce a Cu-trafficking molecule called methanobactin (mb), which appears to play a role in regulating Cu availability in the cell and in turn the synthesis and expression of sMMO and pMMO (Kim et al., 2004). pMMO is activated at high Cu-to-biomass ratios (> 0.89 μmole of Cu per g [dry weight] of cells) compared to sMMO, which is activated at low Cu-to-biomass ratios (< 0.89 μmole of Cu per g [dry weight] of cells) (Hanson and Hanson, 1996). The active pMMO enzyme, when expressed, is suspected to support CH_4 oxidation rates that are ~60% higher than sMMO (Choi et al., 2003; Hanson and Hanson, 1996; Lontoh and Semrau, 1998; Murrell et al., 2000; Zahn and DiSpirito, 1996), which

would have a substantial effect upon the mass transfer of CH_4 to the atmosphere. Considering that the major reservoir of Cu in wetlands and soils are mineral phases (e.g., clay minerals and Fe oxides), methanotrophic bacteria may have evolved to produce mb to access this refractory source of Cu. This role for mb in the ligand-promoted dissolution of Cu-containing minerals is circumstantially supported by mb's high affinity and specificity for binding Cu (log K > 18.8, Choi et al., 2006a). A new and important feedback between the global carbon cycle, climate, and mineral weathering may be realized by demonstrating the linkage of Cu-sequestration with rates of dissolution and rates of CH_4 oxidation.

Kulczycki et al., (2007; Chapter 4, this volume) found that methanobactin promotes the dissolution of Cu-substituted borosilicate glass. Having confirmed that methanobactin actively promotes the enhanced weathering of silicates compared to controls, the mechanism of dissolution was attributed to the formation and detachment of a Cu:mb complex. The degree of enhanced mineral dissolution was determined by the methanobactin concentration, Cu concentration in the borosilicate glass, and the solubility of the glass. A ligand-promoted dissolution mechanism would also explain the impact that methantrophs have upon the weathering of Cu-substituted borosilicates. However, we were not able to substantiate this hypothesis experimentally (Chapter 5 this volume, Kulczycki et al., 2010). The results did show that the enzymatic activity of *Methylosinus trichosporium* OB3b was sensitive to varying Cu concentrations of the dissolving glasses, which resulted in different rates of CH_4 oxidation. Here I will examine whether methanotrophs enhance the solubility of Cu-doped glasses in the presence and absence of methanobactin.

METHODS

To evaluate if methanotrophs weather Cu-bearing silicate glasses, parallel batch reactors containing *M. trichosporium* OB3b cultures in the presence and absence of methanobactin, were grown using manufactured Cu-substituted borosilicate glass chips as the sole Cu source. Different reactors provided different mixtures of air and methane in their headspace (in replicate), and individual reactors were sacrificed at regular time intervals to monitor changes in aqueous metals such as Al and Si (a proxy for silicate weathering), Cu, and CH_4 concentrations for up to 100 hours. Slopes of the linear trends were used to calculate rates of glass dissolution and CH_4 oxidation, respectively (Lasaga, 1981).

Manufactured glasses were employed as a means to control the concentrations of copper in the experiments, while providing a similar bulk substratum for dissolution. Glasses were manufactured to span the range of Cu concentrations found in natural soils and sediments (U.S. soils range from < 1 –700 ppm; Shacklette and Boerngen, 1984) with consideration of the limits of toxicity for microbial populations (e.g., 150 ppm Cu in soil bacteria; Chander et al., 1995).

Glass Synthesis

Glass was synthesized according to the method used by Kulczycki et al. (2007). In summary, the composition of the silicate glasses was first calculated using shareware formulae from Lawrence Livermore National Laboratory (Bourcier, personal comm. 1997). Stock powders were produced by combining crystalline SiO_2, B_2O_3, Na_2O, Al_2O_3 and CuO (Kulczycki et al., 2007), and glasses with Cu concentrations of 0 ppm, 80 ppm,

and 800 ppm were manufactured (designated Cu (0), Cu(80), and Cu (800), respectively). Mixed powders were homogenized on a side arm shaker for 20 minutes, and melted in graphite crucibles at 950 ^{o}C for 12 hours using a muffle furnace (Isotemp Programmable 800 Series). Upon quenching at room temperature, the glass was ground and sieved to a uniform size fraction (125-250 mm). The glass was rinsed and sonicated for 1 minute with low power sonication in NANOpure water (18 MW) 50 times prior to use.

The specific surface area of each prepared glass was confirmed (0.16 m^2 g^{-1}) by application of the five-point BET method using a Quantachrome Nova Series E (Quantachrome Instruments, Boynton Beach, Fl, USA) with N_2 as the adsorbate gas. Characterization of the glass by light microscopy confirmed one-phase glasses with no precipitates or discernible clusters, suggesting that Cu was present within the glass structure, however these glasses likely possess some spatial heterogeneity in Cu distribution. X-ray powdered diffraction (XRD) analysis (Bruker D8 Discovery powder X-ray diffractometer; University of Notre Dame, Environmental Mineralogy and Crystal Structures Lab) was also performed on each glass to confirm that they were single phase amorphous glasses (devoid of minerals, which may form during the quenching process) and after reaction to detect any abundant secondary precipitates forming as a result of the weathering process.

Batch Experiments

M. trichosporium OB3b batch cultures (200-ml suspensions) were pre-grown to optical cell densities ca. 0.25 to 0.3 (OD_{600}) (equivalent to cell densities that range from $1x10^7$ to $3.5x10^7$ cells ml^{-1}) in nitrate salts medium (NSM at pH 7, see table 5.1; Kim et al., 2005) at 30°C in hermetically sealed 500-ml serum vials shaken in the dark at 200 rpm. The initial headspace gas mixture of air and CH_4 was set at atmospheric pressure (1 bar). Methanobactin (mb) was prepared from pre-grown *M. trichosporium* OB3b cultures according to Kulczycki et al. (2007, chapter 4, this volume). The biotic experiments were compared in parallel with abiotic controls.

Batch experiments were performed over a period of ~100 hours. The experiment was initiated by transferring 10-ml aliquots (using sterile 25G 1½ syringes; Becton Dickinson) from a common pre-grown stock culture (OD_{600} = 0.25 to 0.3) to a series of previously prepared sterile 60-ml crimp-sealed glass serum vials with defined headspace gas (air and CH_4 mixture: low-methane, 36 mM CH_4; mid-methane, 60 mM CH_4; high-methane, 116 mM CH_4) and 30 mg of glass chips with a specific surface area of 0.16 m^2 g^{-1}. For each CH_4 concentration examined, a series of 10 to 12 batch reactors were prepared and sacrificed at chosen time intervals. Each reactor series was sorted according to aqueous CH_4 concentration (40 nM, 70 nM, or 130 nM) and solid-phase Cu concentration (i.e., 0 ppm, 80 ppm, or 800 ppm Cu in glass). An additional set of experiments was performed with mb supplemented solutions (20-µmole l^{-1} mb) and the initial aqueous CH_4 concentration set at 40 nM. The resulting mixtures were agitated at 30°C in the dark at 100 rpm; a reduced mixing rate was used because preliminary testing showed that it minimized impact dissolution. Two sets of controls without glass chips

were monitored also; a control with cells and one without cells. Both controls were monitored in parallel to the experimental treatments.

Prior to sacrificing, reactor headspace gases were quantified in quadruplicate using an Agilent Technologies Network GC System 6890N with Thermal Conductivity Detector (TCD). Specifically, CH_4 and CO_2 phases in the headspace were separated in an isotemperature run on an Alltech Hayesep Q 80/100 Packed Column with an oven temperature of 90 °C and analytical error of 0.5%. Upon sacrificing, culture samples were subdivided for aqueous metal, sorbed metal (long-term experiments only), cell enumeration, and pH analysis. Subsamples for metal analysis, using an ICP-OES (Perkin Elmer Optima 5300 DV), were filtered using 0.2 mm polycarbonate filters (Nucleopore Track-Etch Membrane) and preserved by acidification (5% ultrapure HNO_3, which prevents metal sorption onto polypropylene containers). For cell metal analysis, 1 mL samples were diluted to 2.5-ml with nanopure H_2O, and supplemented with 0.5-ml of 70% trace metal grade HNO_3 (Fisher Scientific) and 1-ml 30% H_2O_2 (Fisher Scientific certified A.C.S., Kulczycki et al., 2002; 2005). Each sample was then heated at 60^oC overnight to digest the bacteria and then analyzed using ICP-OES similar to the aqueous samples. Reported extracted and aqueous-phase metal concentrations are designated as Me_{Ext} and $Me_{(aq)}$ (where Me = Cu and Al), respectively. Subsamples (50-ml) for cell enumeration via direct counts, were diluted immediately in 1-ml sterile NANOpure H_2O and vacuum filtered onto 0.2 mm polycarbonate filters (Nucleopore Track-Etch Membrane). The cells were then fixed with 2.5% glutaraldehyde, washed with a DAPI pretreatment solution (4.2 g citric acid, 0.5-ml Tween 80 in 100-ml H_2O), and stained with DAPI (10 mg L^{-1}) before mounting onto a slide for examination by fluorescent light

microscopy (Yu et al., 1995). The remaining unfiltered sample was used for pH determination.

Scanning Electron Microscopy (SEM)

Scanning electron microscopy (SEM) was used to examine glass surfaces for evidence of secondary precipitates, dissolution features, and microbial colonization. In preparation for SEM, glass particles and solution samples were vacuum filtered onto 0.2 mm polycarbonate filter (Nucleopore Track-Etch Membrane), and the filter papers were stored in 2% (v/v) glutaraldehyde to fix the bacteria. The samples were subsequently dehydrated via application of a chemical critical-point drying method (Vandevivere and Bevaye, 1993). The dried filter paper samples were stub-mounted and gold-sputter coated for two minutes. Glasses were imaged using a field emission scanning electron microscope (SEM; LEO 1550 operated at an accelerating voltage of 12 kV) equipped with an electron dispersive system (EDAX).

RESULTS

Initial Cell Densities and Solution Chemistry

In experiments, DAPI direct counts and OD_{600} were used to quantify cell densities for each experiment. The mean initial cell density was $1.2 \pm 0.99 \times 10^7$ cells ml^{-1}. Cells were always in exponential growth phase prior to use in experiments.

Solution pHs for each biotic reactor, regardless of glass composition, were circum-neutral for all experiments (mean pH at $t_0 = 7.2 \pm 0.1$) due to the phosphate buffer used in the growth media (final pH values reported in Table 6.1). Therefore, proton-

promoted glass dissolution was unlikely among experiments. Initial solution pHs in the Cu (0), Cu (80), and Cu (800) abiotic controls were 7.52, 7.3, and 7.3, respectively. Small pH drops were noted over time in each experiment, typically < 0.08 units in abiotic controls and < 0.4 units in biotic systems. The larger shift in pH in the biotic reactors was attributed to CO_2 production during growth (data not shown). However, all observed pH variations were sufficiently small as to not likely influence rates of dissolution (e.g. Welch and Ullman, 1993; Welch et al., 1999). The initial solution chemistry includes media constituents (table 5.1) that might influence Al and Cu speciation. In particular, the majority of remaining phosphate would interact with glass surface sites through sorption reactions and potentially lead to incongruent dissolution reactions through the formation of solid phosphate phases, however, this is not supported by XRD or SEM analysis. The formation of phosphate complexes has the potential of contributing to surface poisoning of mineral dissolution (Eby, 2004).

Bacterial colonization and surface alteration of glass

SEM examination of the reacted silicate glasses in the presence of *M. trichosporium* OB3b showed surface colonization on all glass formulations and experimental treatments (figure 6.1). Rough estimates of colonization indicate that no more than 0.02% of the total biomass fraction can be interpreted as attached and the extent of attachment was not statistically different between glass types.

Similarly colonization and attachment on mineral surfaces by cells has been observed in other microbially promoted mineral weathering systems where mineral dissolution occurs near the site of attachment (Ullman, 1996; Bennett et al., 2001). While

in some cases surface colonization prevented examination of glass etching, a few minor dissolution features were apparent in the SEM photomicrographs of the reacted glass surfaces. Occasional etching features were detected in the vicinity of attached *M. trichosporium* OB3b cells, indicating an immature stage of pit formation (figure 6.1d). Even fewer dissolution features were found on glass surfaces in the abiotic controls (figure 6.1c), suggesting that etch features developed more rapidly when bacteria were present.

SEM examination of the glass chips suggested that X-ray amorphous SiO_2 formed on glass surfaces in both abiotic (figure 6.1c) and biotic systems (figure 6.1d). Clay formation could not be confirmed by XRD analysis because the weathered fraction was relatively minor compared to the bulk glass. As such, the secondary precipitation observed by SEM was interpreted to be amorphous to nanocrystalline in character. In addition, SEM observations coupled with energy dispersive X-ray analysis (EDAX) indicate that surface colonizing cells were coated with an amorphous gel composed of Si, Al, and O (data not shown), which is similar in elemental composition to precipitates found on the surface of the glass. Additional SEM images of *M. trichosporium* OB3b colonized glasses are provided in appendix F. These morphologies are consistent with siliceous gels seen in other studies (Knecht and Wright, 2004).

Si release

Aqueous silicon ($Si_{(aq)}$) was monitored as an indicator of net Si release from the borosilicate glass throughout all experiments. Si saturation levels (amorphous silica; 1913.5 μM, Morey et al., 1964) were never reached within a 100-hour time frame for any

of the experiments. Si release is incongruent from the glasses and in some part, partitioned from the aqueous phase onto the surfaces of the microbial cells and glass chips, as indicated by the SEM observations (figure 6.1). Quantification of Si bound to cell walls and glass surfaces, however, was experimentally challenging and is not reported.

Figure 6.2 demonstrates that $Si_{(aq)}$ concentrations increased linearly over the first 60 hours of exposure to glass (final Si concentrations reported in table 6.1), but became more parabolic thereafter, however, incongruent dissolution precludes in-depth analysis of this trend. Overall, Si release rates differed according to glass Cu concentration indicating different solubilities of individual glass formulations (figure 6.3). Aqueous Si concentrations never exceeded 2 μM for blanks and culture controls absent of glass within 100 hours. These differences in solubility were expected and, therefore, we present Si release merely as a point of reference.

Although the formation of secondary mineral phases limits interpretation, we calculated the zero order rates of release ($\mu M\ Si\ h^{-1}$) via linear curve-fitting $Si_{(aq)}$ concentrations vs. time for the first 60 hours (Faure, 1998; Lasaga, 1981). A statistical examination of the trends in Si release between each biotic treatment and the abiotic control of the same glass composition indicates that there are no differences (figures 6.2 and 6.3), based on overlapping confidence intervals (confidence of slope*T-value). As such, neither the presence of *M. trichosporium* OB3b nor the presence of exogenous methanobactin appears to influence rates of Si release under the conditions investigated in this study. The presence of phosphate in the media may have formed complexes responsible for surface poisoning of glass dissolution.

Al release

The release of Al from the glasses was not detectable in the aqueous phase for any variation in the glass treatments. We suspect this is because precipitates of aluminum oxides (-35 < log K < -5, i.e., Gibbsite, log K_{25} = -34.1, Gardner, 1970, or $Al(OH)_2HPO_4$, log K_{25} = -29, Kardos, 1955) formed rapidly onto the surface of cells suspended in solution (as well as colonizing the glass) (e.g. figure 6.1). Alternatively, Al may simply have been partitioned out of solution by resorbing to the glasses and binding to the surface functional groups on the bacteria cell wall. Elemental analysis of surface precipitates using SEM-EDAX confirmed abundant Al, Si and O (data not shown), although no mineral phases were observed using XRD, suggesting that the precipitates were X-ray amorphous in character.

To gain insight into the mass transfer of Al between solid phases, we conducted solid phase extractions of bacterial cells. Figure 6.4 shows that extracted Al (Al_{Ext}) was detectable in all biotic experiments after 60 hours. With the exception of the Cu(800) glass treatments, the observed trends in Al_{Ext} were relatively negligible between bioreactors that were spiked with mb and those that were not (figure 4a, and b). In the Cu(800) glass treatments (figure 4c) an increasing trend in Al_{Ext} was observed within the first 60-hours for the bioreactor series not spiked with mb (maximum Al_{Ext} = 13.7 ± 0.2 μM) while Al_{Ext} levels remained relatively static at 3.0 ± 0.4 μM for the mb-spiked bioreactor series. Methanobactin may conditionally “swamp” the surface of the glass when the Cu concentration is as high 800 ppm. Kulczycki et al., (2007; Chapter 4) showed that increased methanobactin sorption onto the surface of borosilicate glass occurs with elevated mb levels and increasing solid phase Cu concentration.

For treatments not spiked with mb, it does not seem likely that Al release was controlled by mb generated from the *M. trichosporium* OB3b cells. Given a scenario where the cell densities are on the order of 10^9 cells ml^{-1}, the maximum concentration of mb that could be generated by a culture of *M. trichosporium* OB3b is not expected to exceed 10 nM. Compared to the mb-supplemented experiments, which had a reactor concentration of 20 μM, the concentration of the unsupplemented microcosms is theoretically too low to expect the mb-promoted mechanism to drive Al dissolution. As a Cu-chelating molecule with the capability of binding other metals (Choi et al., 2006b), methanobactin may share similarities with iron-chelating compounds known as siderophores (Kim et al., 2004). Natural concentrations of siderophores in stagnant pore waters can reach concentrations of approximately 240 μM (Hersman et al., 1995), which has been shown promote enhanced dissolution of Al in addition to Fe and Si in hornblende but not at mb concentrations as low as 10 nM (Kalinowski et al., 2000; Liermann et al., 2000). Therefore, a separate mechanism accounting for microbially driven Al solubility must be considered.

Overall, our data do not show that Al is released via a biotic mechanism other than association with the cell wall, however, if the distribution of Al_2O_3 is not uniform throughout the glass, then the amount of Al release will vary from one sample to the next, accounting for some of the variability observed between experiments. The presence of bacterial cells is expected to increase the flux of cations (i.e., Al^{3+}) as bacterial cell walls are known to sorb mineral-forming cations, which subsequently promotes enhanced mineral solubilities (Wightman and Fein, 2004).

Aluminum has a strong affinity to cell walls of common soil bacteria, even at

conditions as low as pH 4 (Daughney et al., 2002, Fein et al., 1997). In low nutrient, neutral pH conditions, elevated release of Al from gibbsite has been shown to occur with viable *Bacillus subtilis* cells compared to nonviable or cell absent systems resulting from interaction of bacterial exudates and the mineral surface (Lee and Fein, 2000). There was no evidence of lysed cells (as detected with SEM examination), suggesting that Al sorption occurs on intact cells. Equilibrium thermodynamic modeling of metal adsorption onto bacterial cell wall surfaces determined the log stability constant for the Al-carboxyl surface complex on *B. subtilis* to be 5.0 (Fein et al., 1997, Daughney et al., 2002), however, studies have shown a universal sorption edge (Borrok et al., 2004; Yee and Fein, 2001). This work demonstrates that a wide range of bacterial species, including those with gram-positive or gram-negative cell wall architecture, exhibit nearly identical metal sorption behavior with respect to pH. We would, therefore, hypothesize that a similar log stability constant for the Al-carboxyl surface complex is expected for *M. trichosporium* OB3b, and our work provides evidence of a bacterial sorption component in glass dissolution.

The release of Al from the borosilicate glasses appears to be unrelated to Si solubility, otherwise parallel changes in Al solubility would have been observed in each Cu treatment (figures 6.2 and 6.4). Silicon solubility was highest in the Cu(0) treatment followed by Cu(800) and Cu(80) exhibiting the lowest Si solubility (figure 6.2). Aluminum solubility, however, was highest for the Cu(800) treatment absent of mb, while the Cu(0) and Cu(80) treatments were lower and relatively equivalent (figure 6.4). The relatively enhanced Al solubility observed in the Cu(800) treatment absent of mb corresponds with enhanced Cu solubility (see below). This would suggest that in glasses

with significantly higher Cu concentrations, the destabilization of Cu sites during microbial leaching may have weakened the overall atomic arrangement of the glass, which permitted the liberation Al atoms.

Cu release

Neither dissolved Cu ($Cu_{(aq)}$) nor cell extracted Cu (Cu_{Ext}) was detectable for the Cu(0) and Cu(80) glass reactors (data not shown), however, data from the Cu(800) glass treatment suggested significant Cu transfer between the glass and cells Cu_{Ext} (figure 6.5). The trends in $Cu_{(aq)}$ concentrations for each biotic treatment were all lower than the abiotic control with the exception of the mb-spiked treatment (mb20 40 nM CH_4) (figure 6.5a). However, in cell extractable Cu analysis (Cu_{Ext}: 40 nM $CH_{4(aq)}$), the cells accumulated abundant Cu and trends in Cu_{Ext} concentrations were overlapping: well above abiotic controls (figure 6.5b). Calculating the differences between $Cu_{(aq)}$ and Cu_{Ext} (Cu_{Ext} - $Cu_{(aq)}$) indicates the amount of Cu that was adsorbed or internalized by the cells (partitioned from the aqueous phase and bound to the cells, Cu) shown in figure 6.5c. Not surprisingly, when mb was present, the stability of Cu in solution increases as a result of the formation of a Cu:mb complex, which has a high binding affinity constant $\approx 10^{16}$ M^{-1} (Tellez et al., 1998; Choi et al., 2006a).

Although data suggest that sorption significantly affects Cu release, for comparative purposes we calculated Cu release rates from the slope of the linear trend within a 60-hour time frame according to zero-order rate kinetics (Cu(800) treatments; Faure, 1998; Lasaga, 1981). Rates of Cu release calculated from trends in aqueous Cu concentrations ($Cu_{(aq)}$) suggest that each of the varying biotic reactor series were not

significantly different from the abiotic control (table 6.2). The sole exception is the lowest CH_4 bioreactor series (40 nM $CH_{4(aq)}$), which shows a lower rate of Cu release ($r_{40\ nM\ CH4} = 0.02 \pm 0.01\ \mu M\ h^{-1}$) compared to the control ($r_{control} = 0.05 \pm 0.01\ \mu M\ h^{-1}$). However, these rates are misleading because a substantial amount of Cu released from the glasses is associated with the cells and would not be detectable when strictly analyzing aqueous Cu concentrations. As such, rates were calculated from the linear trends in Cu_{Ext}, which includes suspended cell-associated Cu in addition to aqueous Cu (table 6.2), demonstrating that the rates were significantly different from the abiotic control (Note: differences between the $Cu_{(aq)}$ and Cu_{Ext} values were calculated ($Cu_{Ext} - Cu_{(aq)}$) to quantify cell-associated Cu (Cu_B), which yielded a linear trend). When examining maximum Cu concentrations within the 60-hour time frame, the quantity of Cu associated with cells is substantially higher than the amount of aqueous Cu for each bioreactor series.

Preferential Cu association with the active methanotroph cells was confirmed in this study. Such findings are consistent with the propensity of these organisms to uptake Cu directly or bind it to the outer cell wall membrane (Hakemian and Rosenzweig, 2007; Hanson and Hanson, 1996; Kim et al., 2004). Microbially promoted leaching of Cu from the glass was evident from the clear trends in increasing cell associated Cu in the Cu(800) treatments. While our data does not allow us to distinguish whether Cu uptake was controlled by (1) a metabolically driven flux of Cu from the glass vs. (2) a stronger diffusion gradient generated by cell binding of Cu to the surface functional groups; given the known metabolic requirement of Cu for CH_4 oxidation (Bedard and Knowles, 1989; Hanson and Hanson, 1996; Murrell, 2009), the preferential leaching of Cu by *M.*

trichosporium OB3b is the most likely explanation for the enhanced rates of Cu release that were observed in this study.

DISCUSSION

Mechanism of Weathering

Our data demonstrate that the primary mode of microbial glass leaching is the partitioning of metals onto the cell walls of *Methylosinus trichosporium* OB3b. The data is equivocal with respect to microbially promoted Si release, however, both Cu and Al are released at significantly higher levels than the control when reacting with Cu(800) glass. Given that pH remained constant at neutral conditions it is unlikely that proton-promoted dissolution played a significant role in the weathering of the glasses. We suggest that leaching of these metals from the glass results from either the specific need for Cu by the methanotroph, which destabilizes the matrix through Cu utilization releasing other metals, or possibly, by maintaining a metal gradient between the glass and solution by direct sequestration of aqueous metals onto the reactive surface of the microbial cell wall.

In the bioreactors supplemented with methanobactin, Al_{Ext} levels were inhibited, while Cu_{Ext} levels were not. Copper is metabolically utilized by *M. trichosporium* OB3b cells, hence, the flux of Cu from the glass to the cells should occur more readily than for Al (e.g. figures 6.4 and 6.5). Methanobactin preferentially associates with Cu, but overall has very little discernible impact on Cu release, perhaps because the vital effect of the active microbial culture overwhelms its contribution.

The non-stoichiometric release of elements is an indication of incongruent dissolution due to the formation of secondary precipitates (i.e., amorphous SiO_2) or the formation of a protective leach layer on the surface of the glass (Oelkers, 2001; Wollast, 1967; Wollast and Chou, 1988). Parabolic trends in elemental release (as observed for Si release in these experiments between 60 and 1500 hours; data not shown) are consistent with diffusion-controlled mechanisms of dissolution due to the formation of a leach layer. However, much of the observed secondary mineralization in the biotic experiments occurs on the cell surfaces, which may indirectly promote further glass dissolution by minimizing passivation layer formation on the glass surface.

Methane Oxidation

The impact of Cu leaching by *M. trichosporium* OB3b is reflected in the CH_4 oxidation data. The concentration of aqueous CH_4 decreased in every biotic treatment (figure 6.6, not normalized to cell density), indicating that the *M. trichosporium* OB3b was metabolically active throughout the experiments, while abiotic controls showed no decrease in CH_4 concentration over the course of the experiment (data not shown). In addition, a corresponding increase in cell density was observed in each biotic treatment over the 100-hour time frame (table 6.3) with colonization on the surface of the glasses and no detected cell lysis (e.g., figure 6.1a, b, and d).

With application of the zero order kinetic model, rates of CH_4 oxidation by *M. trichosporium* OB3b were calculated from the slopes of the decreasing linear trend in cell normalized $CH_{4(aq)}$ concentrations (table 6.3). For all glass treatments (Cu(0), Cu(80), and Cu(800)), rates of CH_4 oxidation increased with higher initial CH_4 concentrations,

indicating that rates are dependent upon supply. Rates of CH_4 oxidation in the Cu(80) glass treatments were consistently higher than those observed in the Cu(0) and Cu(800) glass treatments for bioreactors with corresponding initial $CH_{4(aq)}$ concentration. This report shows that the mineral composition directly impacts the metabolic activity of *M. trichosporium* OB3b, as the amount of bioavailable Cu being released from the silicate determines how efficiently CH_4 is being oxidized. The amount of Cu that was released from the Cu(800) glass appears to have exceeded the amount that would generate optimum rates of CH_4 oxidation, i.e., Cu(80). A degree of toxicity is reflected in the suppressed rates of CH_4 oxidation due to the excess amount of Cu delivered to the cells.

The presence of mb does not appear to significantly impact rates of CH_4 oxidation (table 6.3). The consistency between rates of CH_4 oxidation for both Cu(800) treatments (with and without mb) at an initial aqueous CH_4 concentration of 40 nM loosely correlates with overlapping trends in Cu_{Ext} (figure 6.5b) and equivalent rates of Cu release as determined from cell extractable Cu (table 6.2). While some studies report a chaperone role for mb under toxic concentrations of Cu, our data do not directly support this role.

SUMMARY

The weathering of silicate glasses as mediated by *M. trichosporium* OB3b results in enhanced Cu and Al solubility compared to abiotic controls at neutral pH conditions. Net Si release on the other hand, is not enhanced by *M. trichosporium* OB3b, or is not quantifiable in terms of the amount that was partitioned by cells according to the experimental approach used in this study. Enhanced mineral weathering by *M.*

trichosporium OB3b is attributed to the partitioning of metals from solution by the anionic surface functional groups positioned along the outer cell wall membrane. The binding of metals by bacterial cells not only lowers the saturation levels in solution but also maintains a gradient between the mineral and solution. Continued weathering is possible provided that equilibrium conditions have yet to be established. In addition, the metabolic requirement for Cu by *M. trichosporium* OB3b during CH_4 oxidation promotes continued Cu leaching from the silicate glass. The delivery of Cu to the cell regulates which methane monooxygenase enzyme (sMMO or pMMO) is active during CH_4 oxidation. Hence, metabolically driven methanotroph mediated-mineral weathering is depdendent upon both Cu demand and CH_4 supply since Cu demand will cease with the expiration of CH_4 supply. Otherwise, mineral weathering is strictly controlled by the biophysical properties of the cell wall membrane in terms of how metal partitioning will influence the kinetics of the thermodynamic equilibrium reactions.

Table 6.1. Final aqueous Si concentrations and pH

$[CH_4]_{(aq)}$ nM	Treatment	$[Si]_{(aq)}$ $_{Final}$ (μM)	t (h)	pH_{Final}
40	OB3b Cu(0)	505±0	58	6.85
	OB3b Cu(80)	52±0	50	6.79
	OB3b Cu(800)	153±0	51	6.89
70	OB3b Cu(0)	481±15	48	6.78
	OB3b Cu(80)	32.4±0	51	6.76
	OB3b Cu(800)	218±7	54	6.99
130	OB3b Cu(0)	394±13	46	6.81
	OB3b Cu(80)	36.1±0.2	50	6.90
	OB3b Cu(800)	124±2	36	6.94
	OB3b Cu(0)	454±0	54	6.89
40 (mb20)	OB3b Cu(80)	36.8±0	51	6.98
	OB3b Cu(800)	156±0	58	6.93
Abiotic	Cu(0)	570±5	59	7.25
Controls	Cu(80)	37.7±1	60	7.18
	Cu(800)	178±11	61	7.21

Note that final values represent the last sampling interval within a 60-hour time frame.

Table 6.2. Aqueous Cu ($Cu_{(aq)}$) and Cu_{Ext} (cell digested supernatant) release rates from Cu(800) borosilicate glass.

»$Cu_{(aq)}$			†Cu(800)	
*Reactor Variants	‡r	§r^2	¶Error	**Sig. (95%)
Abiotic control	0.05	0.894	0.01 (n=11)	---
40 nM CH_4	0.02	0.769	0.01 (n=11)	yes
70 nM CH_4	0.03	0.649	0.02 (n=8)	no
130 nM CH_4	0.02	0.458	0.03 (n=6)	no
mb20 40 nM CH_4	0.04	0.699	0.02 (n=11)	no
ζCu_{Ext}			†Cu(800)	
*Reactor Variants	‡r	§r^2	¶Error	**Sig. (95%)
Abiotic control	0.05	0.894	0.01 (n=11)	---
40 nM CH_4	0.15	0.886	0.04 (n=11)	yes
mb20 40 nM CH_4	0.14	0.946	0.03 (n=11)	yes

» $Cu_{(aq)}$ is an abbreviation for aqueous Cu.
ζ Cu_{Ext} is an abbreviation for cell extracted Cu. Data taken from table 5.3 of Kulczycki et al., (2010, chapter 5, this volume), mb20 reactor variant excepted.
*Reactor variants are distinguished by initial aqueous CH_4 concentrations. The last reactor variant (bottom row, mb20 40 nM CH_4) was spiked with 20 µM mb.
†Cu(800) represents Cu-substituted glass with Cu 800 ppm. No rates were calculated for the reactor variants containing the Cu(0) and Cu(80) glass reactors as aqueous Cu was approaching detection limits.
‡ Rate constants expressed as µmole l^{-1} Cu, calculated from a linear fit of aqueous Cu concentrations vs. time within the first 60 hours of reactivity.
§ Values are correlation coefficients for the regression analyses.
¶ Error based on confidence slope **t-value* (e.g. 95% confidence level)
** Sig. (95%) is the significance that the slopes of two population trends (biotic reactor variant vs. abiotic control) are different based on the *t* distribution for a 95% confidence level.

Table 6.3. Rates of CH_4 oxidation and changes in cell density

	†Cu-0				†Cu-1				†Cu-3			
*Reactor Variants	‡r	§r^2	¶Error	δCell Density	‡r	§r^2	¶Error	δCell Density	‡r	§r^2	¶Error	δCell Density
40 nM CH_4	0.04	0.894	0.01 (n=10)	2.8±0.7 x 10^7 (61%)	0.06	0.933	0.02 (n=9)	3.6±0.6 x 10^7 (67%)	0.03	0.761	0.01 (n=12)	4.0±0.6 x 10^7 (75%)
70 nM CH_4	0.2	0.903	0.1 (n=6)	4.7±0.7 x 10^7 (86%)	0.81	0.989	0.17 (n=5)	6.4±1.2 x 10^6 (58%)	0.09	0.825	0.04 (n=9)	1.6±0.5 x 10^7 (67%)
130 nM CH_4	0.54	0.779	0.44 (n=6)	3.1±0.4 x 10^7 (87%)	4.03	0.743	2.5 (n=8)	1.1±0.6 x 10^6 (73%)	0.32	0.769	0.22 (n=7)	3.3±0.6 x 10^6 (50%)
mb20 40 nM CH_4	0.02	0.793	0.01 (n=11)	4.3±0.6 x 10^7 (67%)	0.11	0.786	0.06 (n=8)	4.2±1.1 x 10^7 (84%)	0.02	0.908	0.004 (n=11)	2.2±0.3 x 10^7 (38%)

*Reactor variants are distinguished by initial aqueous CH_4 concentrations. The last reactor variant (bottom row, mb20 40 nM CH_4) was spiked with 20 μM mb.
†Cu(0), Cu(80) and Cu(800) represent Cu-substituted glasses with Cu concentrations of 0, 80, and 800 ppm, respectively.
‡ Rate constants expressed as amole CH_4 $cell^{-1}$ h^{-1}, calculated from a linear fit of aqueous CH_4 concentrations vs. time within the first 100 hours of reactivity.
§Values are correlation coefficients for the regression analyses.
¶Error based on confidence slope **t-value* (e.g. 95% confidence level).
δ Relative change in cell density (cells ml^{-1}) within a 100-hour time frame. Percentage change is given in parentheses.

Figure 6.1. Scanning electron micrograph images of glass surfaces. (a) *Methylosinus trichosporium* OB3b cells colonizing the surface of Cu(0) borosilicate glass after 38.5 hours. (b) Cu(80) borosilicate glass (80 ppm Cu) abundantly colonized with *M. trichosporium* OB3b cells after 19 hours. (c) Abiotically reacted Cu(800) glass (800 ppm Cu) after 33 hours. Minimal etching observed. However, extensive secondary precipitation is evident and EDAX confirmed these precipitates to be composed mainly of Si and O (data not shown). (d) Biotically reacted Cu(800) glass (800 ppm Cu) after 17 hours. Early formation of dissolution features such as etch pits are observed. Extensive secondary precipitation is evident and EDAX confirmed these precipitates to be composed mainly of Si and O (data not shown). Abundant glass colonization is also evident. The *M. trichosporium* OB3b cells are coated by an amorphous, silica gel (EDAX, data not shown).

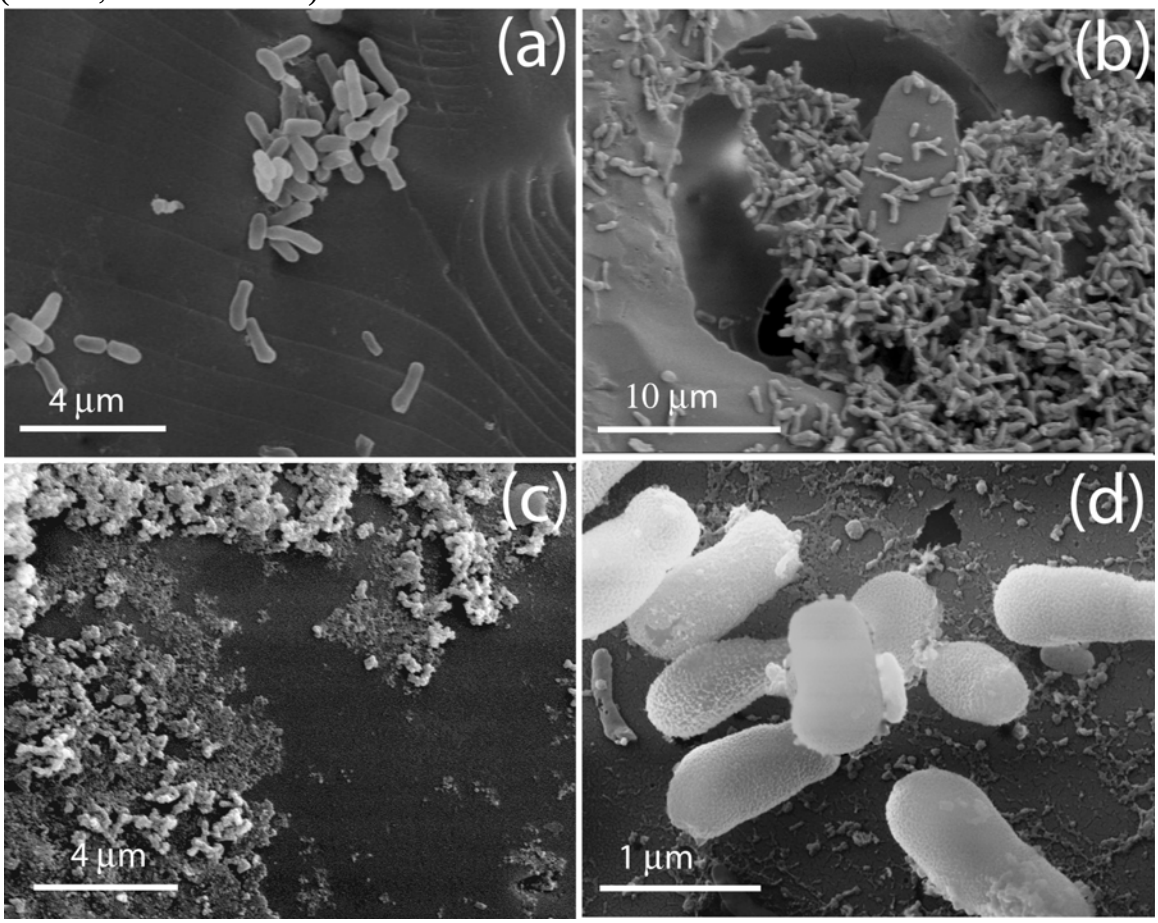

Figure 6.2. Si release (μM) as a function of time comparing a set of reactors that vary with initial $CH_{4(aq)}$ concentration and glass reactors (a) Cu(0) reactor, (b) Cu(80) reactor $[Cu]_i$ = 80 ppm, and (c) Cu(800) reactor $[Cu]_i$ = 800 ppm. Biotic reactor variants are distinguished by initial CH_4 concentrations of 40 nM, 70 nM, 130 nM, and 40 nM spiked with 20 μM mb (mb20 40 nM), respectively. Error bars reflect the error on analysis of the same solution. Data retrieved from figure 5.1 of Kulczycki et al. (2010, chapter 5, this volume) however the presentation of the data has been modified, mb20 reactor variant excepted.

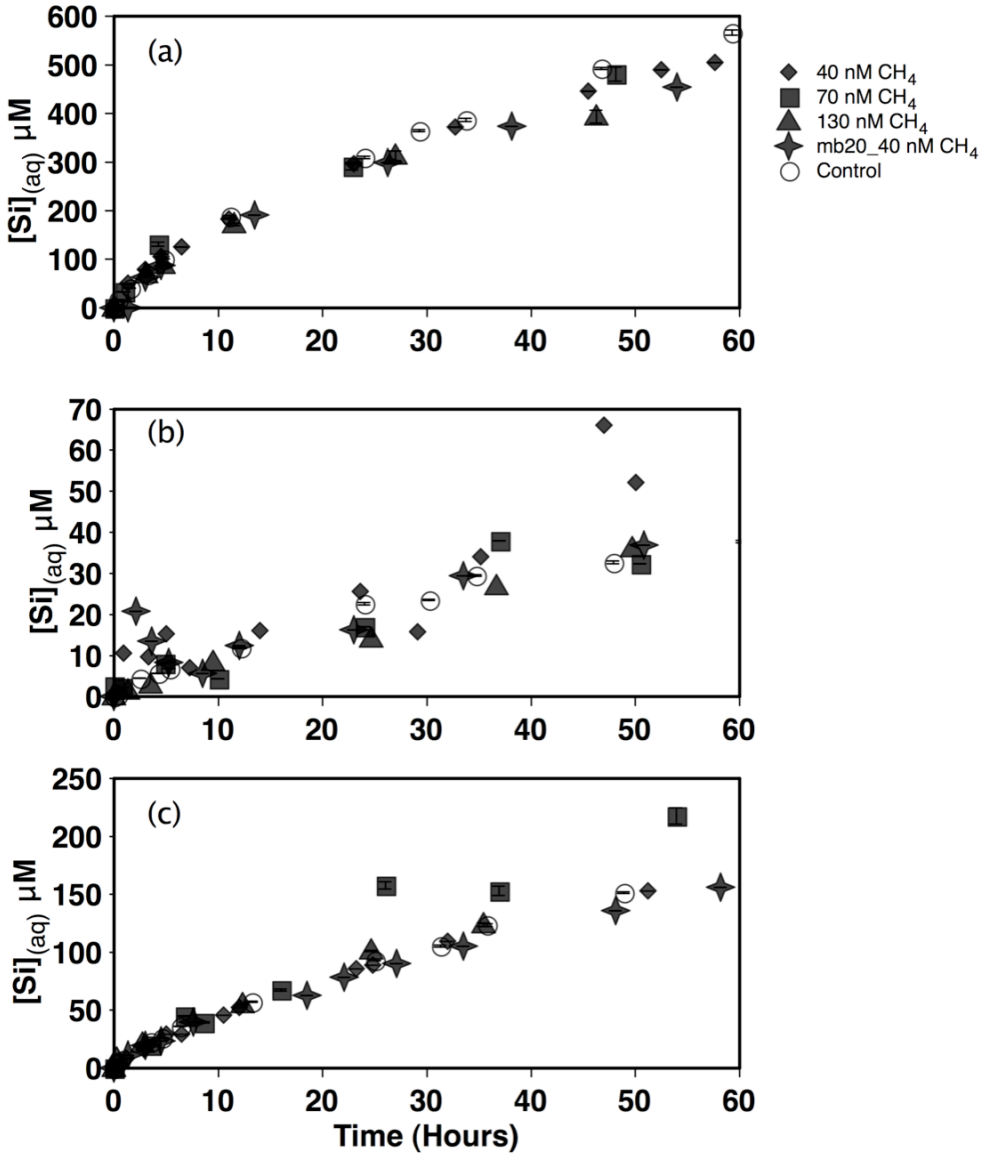

Figure 6.3. Rates of Si release (μM h^{-1}) comparing the abiotic control with each of the biotic reactor variants: 40 nM, 70 nM, 130 nM, and 40 nM spiked with 20 μM mb (mb20 40 nM) in each Cu treatment (a) Cu(0), (b), Cu(80), and (c) Cu(300). T-test statistics confirm that in no case is the Si release significantly different from the corresponding abiotic control. Error bars are based on confidence slope *t-$value$ (e.g. 95% confidence level).

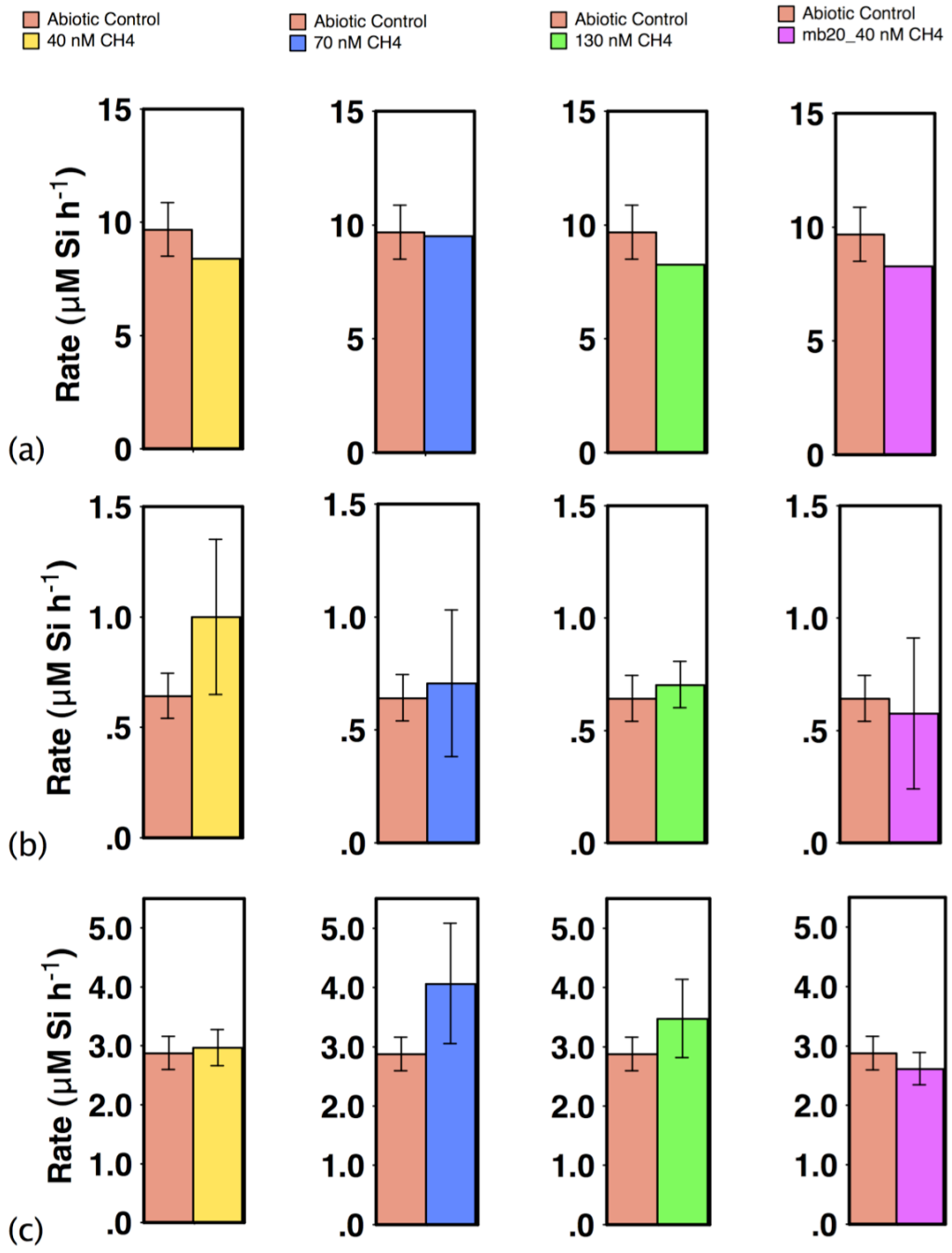

Figure 6.4. Al release (μM) as a function of initial $CH_{4(aq)}$ concentration in the biotic reactors compared to the abiotic control for each of the glass reactors (a) Cu(0) reactor, (b) Cu(80) reactor $[Cu]_i$ = 80 ppm, and (c) Cu(800) reactor $[Cu]_i$ = 800 ppm. Since no dissolved Al was detected, Al release could only be shown for extracted Al ($Al_{Ext.}$) samples, the "low-range" CH_4 (40 nM CH_4) and mb spiked (mb 20 40 nM CH_4) reactor variants. Error bars reflect the error on analysis of the same solution.

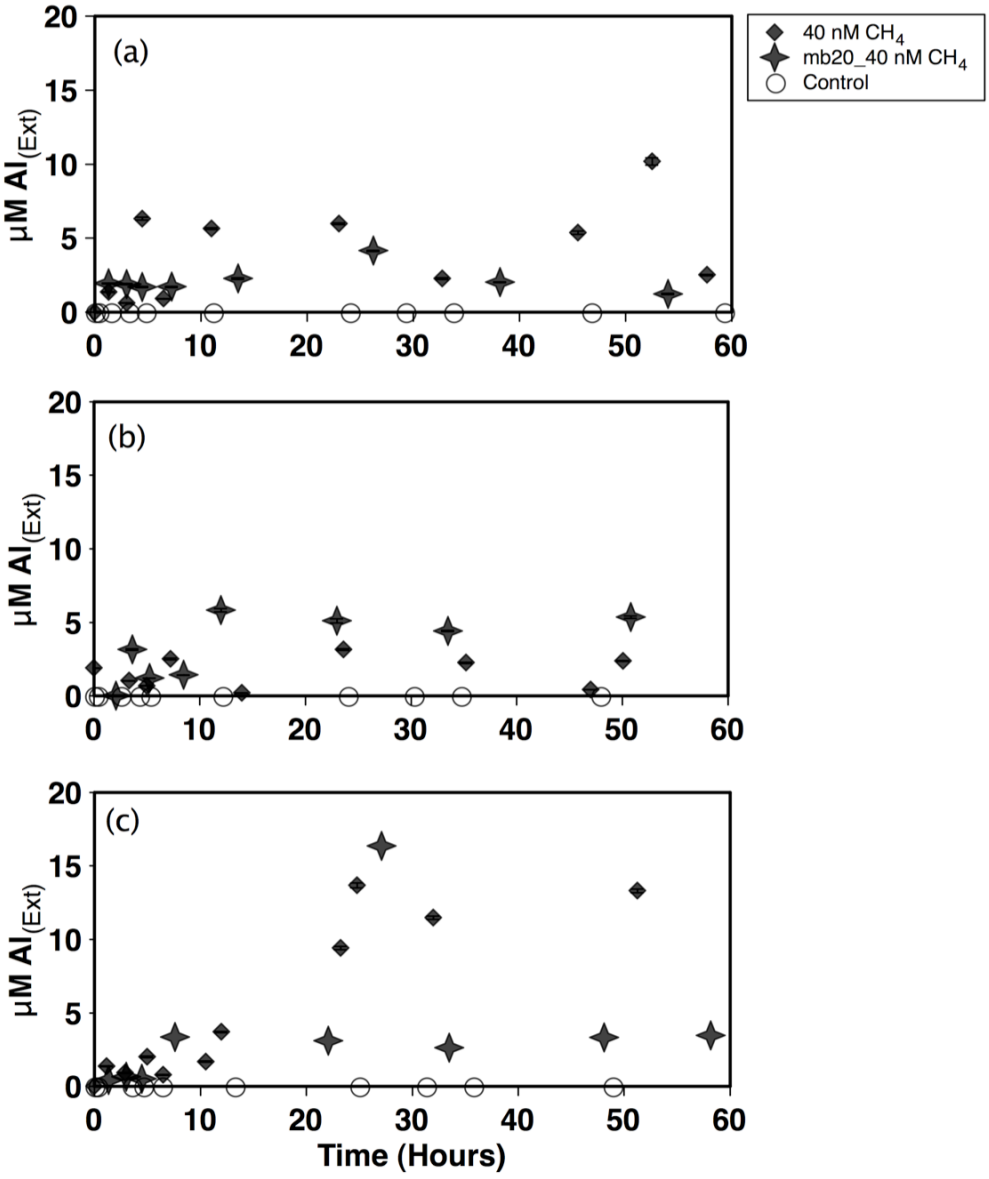

Figure 6.5. Cu release (μM) from the Cu(800) glasses (800 ppm Cu) is examined as a function of time comparing a set of reactors that vary with initial $CH_{4(aq)}$ concentration where (a) and (b) compare the aqueous ($Cu_{(aq)}$) and extractable Cu (Cu_{Ext}), respectively, and (c) is the cell associated Cu (Cu_B) calculated from the difference between Cu_{Ext} and $Cu_{(aq)}$. Biotic reactor variants are distinguished by initial CH_4 concentrations of 40 nM, 70 nM, 130 nM, and 40 nM spiked with 20 μM mb (mb20 40 nM), respectively. Error bars reflect the error on analysis of the same solution. Cu extracted samples are only available for the bioreactors with initial $CH_{4(aq)}$ concentrations of 40 nM CH_4, including ones that were spiked with mb (mb20 40 nM CH_4). In the Cu(0) and Cu(80) (80 ppm Cu) glass reactors, Cu release is near the detection limits of the analytical approach used for both the aqueous and extractable Cu and was therefore omitted from this figure. Data retrieved from figure 5.2 of Kulczycki et al. (2010, chapter 5, this volume) however the presentation of the data has been modified, mb20 reactor variant excepted.

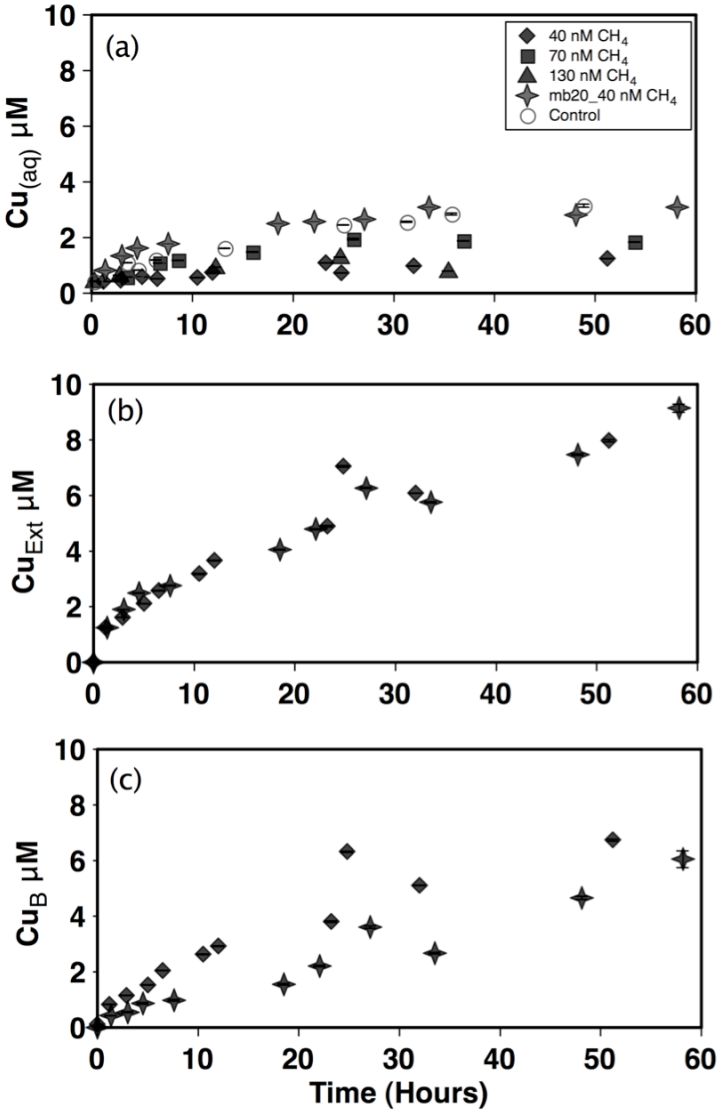

Figure 6.6. Aqueous CH_4 depletion with time (nmole l^{-1} vs. hours) for each glass treatment (Cu(0), Cu(80), and Cu(800)), where (a), (b), and (c) represent biotic reactor series with initial $CH_{4(aq)}$ concentrations of 130 nM, 70 nM, 40 nM, respectively, and (d) has an initial $CH_{4(aq)}$ concentration of 40 nM and a mb concentration of 20 μM (mb20 40 nM CH_4). Error bars reflect the error on analysis of the same solution. The abiotic reactor series showed no CH_4 depletion (data not shown).

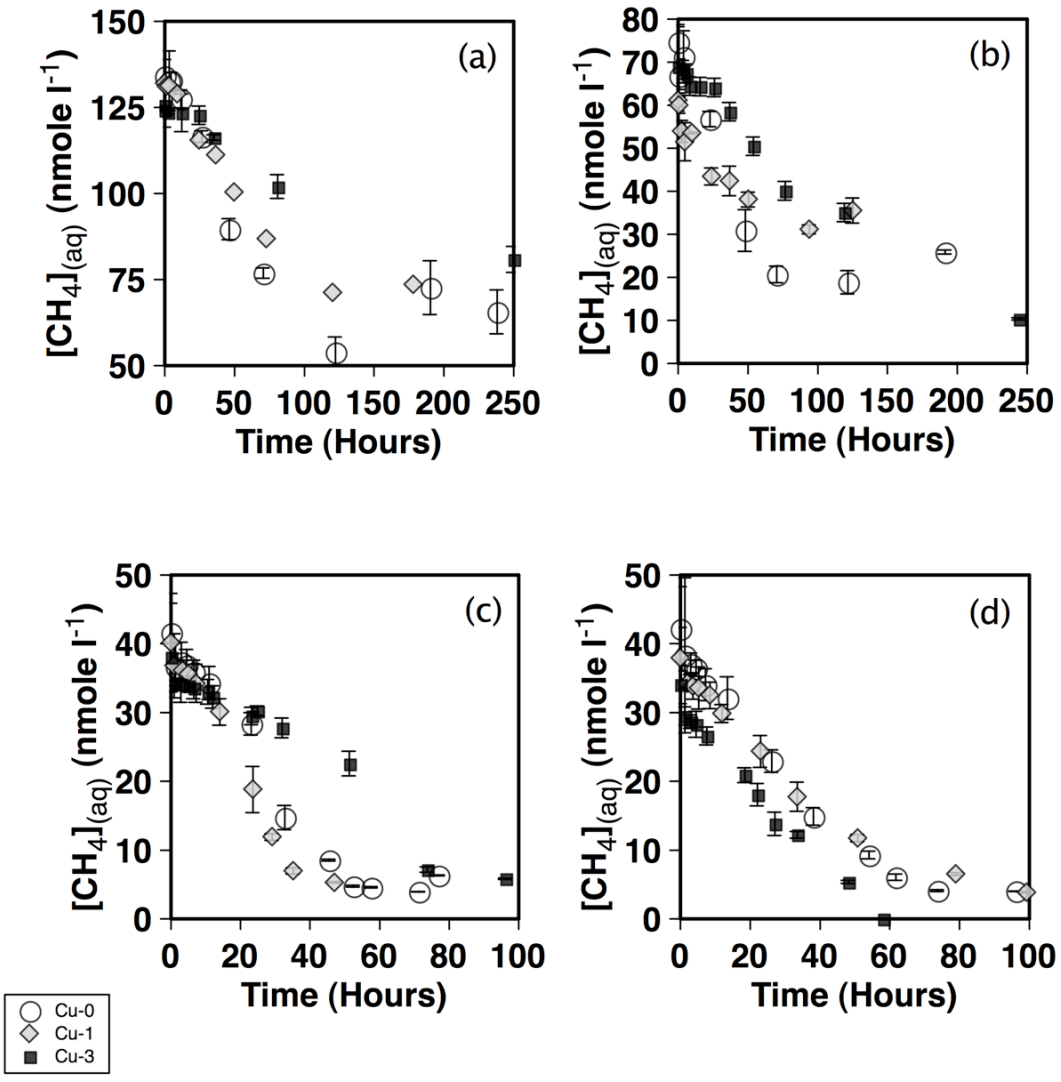

CHAPTER 7

IMPACT OF NUTRIENT FLUX UPON METHANOTROPHY

ABSTRACT

Rates of methane (CH_4) oxidation by *Methylosinus trichosporium* OB3b are influenced by nutrients such as copper (Cu) and ammonium (NH_4^+). The soluble and particulate methane monooxygenase (sMMO and pMMO) enzymes responsible for activating methane oxidation are regulated by Cu concentration, and Cu in excess will impose a toxic effect. Ammonium oxidation can be activated by pMMO, therefore, the presence of NH_4^+ poses a competitive effect that hinders CH_4 oxidation. Soils containing smectite clays such as montmorillonite provide high cation exchange capacity with the capability of influencing of the enzymatic activity of methanotrophs as nutrients such as Cu and NH_4^+ are adsorbed and then desorb back into solution. This investigation examines the impact of desorbing Cu and NH_4^+ upon rates of CH_4 oxidation by *Methylosinus trichosporium* OB3b. In the absence of Cu, desorbing NH_4^+ inhibits the rate of CH_4 oxidation with initial batch concentrations as low as 100 μM. Rates are not further inhibited even when initial batch NH_4^+ concentrations are as high as 2000 μM. At an initial batch Cu concentration of 50 μM, a relatively lower rate of CH_4 oxidation is observed compared to zero Cu systems. With initial batch Cu concentrations fixed at 50 μM, an optimum rate of CH_4 oxidation occurs at an initial batch NH_4^+ concentration of 200 μM, and declines with increasing NH_4^+ concentration. Therefore, Cu evokes a toxic response from *Methylosinus trichosporium* OB3b at this concentration. Nitrification was not confirmed in this study however complex redox cycling associated with inorganic

nitrogen is implicated with the inhibition of CH_4 oxidation by *Methylosinus trichosporium* OB3b.

INTRODUCTION

Methane is a greenhouse gas that absorbs long wave radiation at a factor that is approximately 25 times more powerful than carbon dioxide (Hanson and Hanson, 1996; Wuebbles and Hayhoe, 2002). The biogenic sources of CH_4 include wetlands, rice agriculture, biomass burning and ruminant animals while typical industrial sources include fossil fuel mining and distribution (Forster et al., 2007). Global contributions have caused atmospheric CH_4 mole fractions to rise to present day levels of 1.7 ppm (Cicerone and Oremland, 1988). Evidence from ice cores indicates that the value has more than doubled over the past 200 years (Craig and Chou, 1988; Khalil and Rasmussen, 1987; Pearman et al., 1986). The rapid increase of CH_4 in the atmosphere during this period has been attributed to human activities related to agriculture, natural gas distribution and landfill utilization (Ehhalt et al., 2001). While anthropogenic activity is recognized for significant contributions, the greatest global source of atmospheric CH_4 is from natural wetlands (92-225 Tg CH_4 $year^{-1}$, or 15-37% of total atmospheric CH_4 budget, Ehhalt et al., 2001; Houweling et al., 1999, Hanson and Hanson, 1996). Tropical wetlands account for approximately 60% of the total wetland emission (66 Tg CH_4 $year^{-1}$) while northern wetlands release 38 Tg CH_4 $year^{-1}$ (34% of the total). Subtropical and temperate wetlands release only 5 Tg CH_4 $year^{-1}$ (Hanson and Hanson, 1996). Contributions from wetlands will vary according to soil organic matter content and the length of time that anaerobic conditions prevail.

Characteristically, wetlands are environments with standing water for all or parts of the year and represent a transition between upland soils and deep aquatic systems (Hanson and Hanson, 1996; Mitsch and Gosselink, 2000). The major factors that affect CH_4 production and oxidation in wetlands are water depth, soil water content, type of vegetation and temperature (Hanson and Hanson, 1996; Le Mer and Roger, 2001; Segers, 1998). Wetland development in the tropics is promoted by high rates of precipitation and high primary productivity (Bartlett and Harriss, 1993; Hanson and Hanson, 1996). The geomorphologic setting must have a shallow sloping gradient and the soils should be poorly draining to promote conditions for standing water and the accumulation of abundant soil organic matter (SOM) (Mitsch and Gosselink, 2000). Biogenic CH_4 generation is promoted by anoxic/reducing conditions in waterlogged soils where the methanogenic nutrient requirements may be met from the partially degraded organic matter. Furthermore, the optimum temperature range for methanogenesis is between 30 and 40^{o}C (Hanson and Hanson, 1996; Le Mer and Roger, 2001), which is consistent in the tropics.

Wetland soils are generally anoxic due to being submerged in water. However, atmospheric oxygen penetration from the surface creates a thin (1- to 5-mm-deep) oxic soil layer (Conrad, 1996). It has been estimated that as much as 90% of the CH_4 produced from wetlands is consumed in the oxic surface layer of wetlands, although significant variability has been observed (Conrad, 1996; Le Mer and Roger, 2001; Segers, 1998). While wetlands are traditionally considered to be major sources of CH_4, conditions may shift such that the wetland becomes a CH_4 sink. Methane oxidation becomes more dominant during a drying cycle, where the water table drops and the previously anaerobic

zones of a depth profile become aerobic. The upward migration of microbially generated CH_4 from the anaerobic zone to the overlying aerobic zone promotes the metabolic oxidation of CH_4 to CO_2 by methanotrophs. Typically, the "hot spot" for methanotrophy occurs just above the anoxic/oxic boundary, where microaerophilic conditions persist (Conrad, 1996; Dumont and Murrell, 2005; Hanson and Hanson, 1996).

Fluctuations in the height of the water table due to precipitation cycles can promote a change in the groundwater chemistry. Following an inundation event, ionic exchange between the newly flooded soil/sediment particles and ground water will occur. The degree of exchange will vary depending upon the cation exchange capacity (CEC) of the clay components in the soil. The dominant clays in mollisols are the 2:1 silicate type silicate, which have high cation exchange capacities, while oxisols, with kaolinite and Fe-, Al-oxides being dominant, tend to have low cation exchange capacities. Soils abundant with organic matter, such as histosols, generally have the highest CEC, and are commonly found in wetland environments (Brady and Weil, 2002). The speciation of metal ions and inorganic nutrients in low temperature aqueous geochemical environments is often controlled by sorption processes (Davis and Kent, 1990; Hayes and Katz, 1995), which control the mobility, toxicity and bioavailability of these cations (McBride, 1994; Hayes and Traina, 1998). The microbial ecology of the subsurface or aquatic habitat is impacted by exchangeable cations (Allison et al., 2007; Bennett et al., 2001; Essa and Farragallah, 2006; Hendricks, 1993; Roberts Rogers and Bennett, 2004), particularly during periods of soil inundation. Methanotrophs in particular will respond to the release of Cu^{2+} and NH_4^+, which are made available either by mineral dissolution or desorption processes.

Methanotrophs use Cu to regulate the enzymatic oxidation of CH_4. The two major enzymes, soluble methane monooxygenase (sMMO) and particulate methane monooxygenase (pMMO) are activated at different Cu-to-biomass ratios. At low Cu-to-biomass ratios (< 0.89 μmole of Cu per g [dry weight] of cells) sMMO is expressed, and at high Cu-to-biomass ratios (> 0.89 μmole of Cu per g [dry weight] of cells) pMMO is expressed (Hanson and Hanson, 1996). Research efforts have made significant advances in terms of understanding the function of these enzymes. For instance, we know that sMMO is activated within the cytoplasm of the cell, whereas, pMMO is activated on the cell wall (Lontoh and Semrau, 1998). Considering that low Cu concentrations are required for sMMO expression, internal utilization of Cu is necessary to oxidize CH_4. At higher Cu concentrations, activation of pMMO is necessary to regulate the amount of Cu that enters the cell for CH_4 oxidation and to prevent toxicity (Murrell et al., 2000). The active pMMO enzyme, when expressed, supports higher growth rates than sMMO (Lontoh and Semrau, 1998; Choi et al., 2003; Zahn and DiSpirito, 1996), a factor that impacts CH_4 oxidation rates and the mass transfer of CH_4 to the atmosphere. Copper concentrations greater than 4.3 mM Cu^{2+} inhibit the induction of CH_4 oxidation activity in soils (Bender and Conrad, 1995). The source of Cu in natural settings is often limited to the solid phase, or local minerals, and is not bioavailable unless released from the mineral by dissolution or desorption processes.

The efficiency of CH_4 oxidation by methanotrophs is hindered by inorganic nitrogen exposure, e.g., NH_4^+, NO_3^-, and NO_2^-. A number of field studies have shown that CH_4 oxidation in soil sediments from varying climate zones and varying depths is inhibited by the introduction of NH_4^+ or NO_3^- (Adamsen and King, 1993; Chan et al.,

2005; Gulledge and Schimel, 1998; Gulledge et al., 2004; King and Schnell, 1994; Schnell and King, 1994). These findings have been reinforced with experimental microcosms, which also detected decreases in CH_4 oxidation in the presence of specific inorganic nitrogen compounds, NO_2^-, NO_3^-, NH_4^+, as well as urea (Bender and Conrad, 1994; Dunfield and Knowles, 1995; King and Schnell, 1994). It has been documented that NH_4^+ fertilization of varying soils for agriculture purposes has diminished the rate of atmospheric CH_4 oxidation by 50 to 85% according to several studies carried out over the past 17 years (Chan et al., 2005; Gulledge et al., 2004; Kightley et al., 1995; Steudler et al., 1989). It has been proposed by a number of authors that the formation of NO_2^- from methanotrophic NH_4^+ oxidation is largely responsible for the inhibitory effect upon CH_4 oxidation (Dunfield and Knowles, 1995; King and Schnell, 1994; Schnell and King, 1994).

Methanotrophs and autotrophic nitrifiers both possess MMO enzymes capable of oxidizing CH_4 (Bedard and Knowles, 1991; Conrad, 1996; Gulledge et al., 2004; Hooper et al., 1997). The ammonia monooxygenase (AMO) possessed by ammonia-oxidizing bacteria is capable of oxidizing CH_4 (Hanson and Hanson, 1996). Several properties are shared between AMO and pMMO. It has been proposed that Cu is an active site in both enzymes and the regulation of these enzymes by Cu occurs in vitro (Ensign et al., 1993; Hanson and Hanson, 1996; Nguyen et al., 1994). Specific methanotroph species that can oxidize NH_4^+ to NO_2^- in the presence of CH_4 have been identified and include *Methylobacter albus* BG8 and *Methylosinus trichosporium* OB3b (Bedard and Knowles, 1991; King and Schnell, 1994).

The delivery of inorganic N compounds from plant derived organic matter (via ammonification, and subsequent nitrification) is expected to diminish rates of CH_4 oxidation by soil methanotrophs. However, the extent that inorganic N compounds are available to methanotrophs in tropical soils is not well understood. The amount of NH_4^+ ions that are adsorbed and fixed by 2:1 clay minerals needs to be quantified.

In this study, we investigate whether the release of adsorbed Cu and NH_4^+ from smectite (montmorillinite) clay will influence rates of CH_4 oxidation by a common type II methanotroph (*Methylosinus trichosporium* OB3b). We expect that the release of appropriate concentrations of Cu from the smectite clay will have a positive influence upon rates of CH_4 oxidation and the release of NH_4^+ from the smectite clay will hinder rates of CH_4 oxidation by *M. trichosporium* OB3b. We identify threshold concentrations of these species in combination and find their predominance over the other is dependent upon the proportional concentrations of each compound that is released during desorption or dissolution processes.

METHODS

Clay

Texas Montmorillonite (STx-1) from the Manning formation, Jackson Group (Eocene), county of Gonzales, Tx, was obtained from the Source Clays Repository of the Clay Minerals Society. The sample was pre-characterized for chemical composition (%): (SiO_2: 70.1, Al_2O_3: 16.0, TiO_2: 0.22, Fe_2O_3: 0.65, FeO: 0.15, MnO: 0.009, MgO: 3.69, CaO: 1.59, Na_2O: 0.27, K_2O: 0.078, F: 0.084, P_2O_5: 0.026, S: 0.04), cation exchange capacity (CEC): (84.4 meq/100g, major exchange cation Ca), surface area (N_2 area: 83.79

± 0.22 m^2/g), and structure ($Ca_{0.27}$, $Na_{0.04}$, $K_{0.01}$)[$Al_{2\ 0.41}$, Fe(III) $_{0.09}$, $Mn_{tr.}$, $Mg_{0.71}$, Ti $_{0.03}$][$Si_{8.00}$]$O_{2\ 0}$ $(OH)_4$, Octahedral charge: -0.68, Tetrahedral charge: 0.00, Interlayer charge: -0.68, Unbalanced charge: -0.08, Extra Si: 0.59) (The Clay Minerals Society).

Size separation

The <2 μm fraction was separated by suspension in pH 10 Na_2CO_3 solution followed by centrifugation in 50-ml centrifuge tubes at 500 rpm for 10 minutes. The supernatant was decanted into a separate centrifuge tube for additional separation step. To separate the <0.2 μm fraction of montmorillonite, the < 2μm fraction was centrifuged at 2500 rpm for 10 minutes, and the supernatant was discarded. The remaining fraction (<0.2 μm) was saturated with KCl by a series of five 24-hour washings in 1M KCl. After saturation, the montmorillonite was washed free of excess salt with NANOpure deionized water (18 MΩ). Wet pellet to dry mass correlations were performed to determine the density of the clay (2 g wet clay = 0.5 g dry clay). Wet samples were dried in an oven set at 60^oC for as many days required for the mass remain stable after all water had evaporated (> 5 days).

Adsorption-desorption isotherms at constant pH

Freshly prepared montmorillonite (see above) was suspended in a 0.03 M KCl solution buffered to pH 6.8 with 5 mM PIPES Buffer so that clay concentration was 0.5 g L^{-1}. As such, the ionic strength of the electrolyte solution used in the adsorption-desorption isotherms would be the same as the growth media used in the methane oxidation efficiency experiments. Three different sets of isotherm experiments were

pursued: (1) Cu isotherms (2) NH_4^+ isotherms and (3) mixed Cu and NH_4^+ isotherms. The range of initial Cu concentrations in the Cu sorption/desorption isotherms was from 0 to 150 μM (0, 25, 50, 75, 100, 125, and 150 μM). In the NH_4^+ sorption/desorption isotherms, the range of initial NH_4^+ concentrations was from 0 to 1500 μM (0, 250, 500, 750, 1000, 1250, and 1500 μM). In the mixed Cu and NH_4^+ sorption/desorption isotherms, the initial Cu concentration was fixed at 50 μM in all samples while the range of initial NH_4^+ concentrations was varied according to the NH_4^+ isotherms.

Depending upon the experiment, the montmorillonite slurry (0.5 g L^{-1}) was spiked with Cu, or NH_4^+, or both, to achieve the desired concentration. From the spiked slurry, triplicate 5-ml portions were rotated end-over-end in 15-ml BD Falcon Conical Centrifuge Tubes at 50 rpm for 24 hours under room temperature conditions. In previous studies examining montmorillonite sorption of Cu the 24-hour reaction period was confirmed as a sufficient length of time for equilibrium conditions to be reached (Morton et al., 2001). Control solutions absent of montmorillonite were prepared in triplicate and included in the 24-hour mixing period. At the end of the 24-hour adsorption phase, the pH of the slurry was measured prior to separating the clay from solution by centrifugation at 4000 rpm for 40 minutes. From the supernatant, 2.5-ml of solution was filtered using 0.2 μm polycarbonate filters (Millipore Isopore), 2-ml of which was preserved by acidification (5% ultrapure HNO_3, to prevent metal sorption onto polypropylene containers) for metals analysis by ICP-OES. The remaining 0.5-ml of filtrate was stored at -20^oC for determination of NH_4^+/NH_3 content by flow-injection analysis (described below). The amount of Cu or NH_4^+ adsorbed was calculated as the difference between the initial concentration of the spiked slurry and the concentration of the aqueous solution

after filtration. The control solutions without montmorillonite were used to quantify the amount of Cu or NH_4^+ that had sorbed to the polypropylene tubes.

To quantify Cu and NH_4^+ desorption, the montmorillonite was resuspended in the 2.5-ml of unfiltered solution and the volume was raised back to 5-ml with fresh electrolyte solution absent of clay, Cu or NH_4^+. In other words, a portion of the total Cu or total NH_4^+ in the system was removed when quantifying sorption onto the clay. The "new" slurry was equilibrated as before for another 24-hour period (desorption phase). For the purposes of the study, Cu or NH_4^+ adsorption was considered reversible if the Cu or NH_4^+ desorbed and reached the same equilibrium as was observed for adsorption during the equivalent reaction period. Hence, desorption isotherm data was as critical as the adsorption isotherm data for determining reversibility. Once the 24-hour desorption phase was complete, the pH of the slurry was measured before running another 40-minute centrifuge cycle at 4000 rpm and the equilibrium distribution between solution and montmorillonite was determined as described earlier. Any desorbed Cu or NH_4^+ would be detected as an aqueous species in the filtrate. Comparison of the adsorption and desorption isotherms would indicate whether a reversible reaction could be delineated from reactions that were either kinetically or thermodynamically limited in the desorption step under the abiotic conditions used in this component of the study. Reversibility can be concluded if the desorption isotherms coincide with the adsorption isotherms. Irreversibility can be concluded if the desorption step exhibits a steeper slope than the adsorption step. Given the 2:1 structure and high cation exchange capacity of montmorillonite, it is not unlikely for interlayer binding sites to be stingy with respect to

the release of Cu^{2+} or NH_4^+ under the short time frame examined within this study. Irreversibility was calculated using the same method applied by Morton et al., (2001).

Determination of NH_4^+ concentration by flow-injection analysis

The solution NH_4^+ content was determined using the rapid, flow-injection analysis (FIA) system where a gas-permeable membrane was used to remove NH_3 from basic (NH_4^+) reagent streams into a mildly acidic receiving stream and conductivity detector (Hall and Aller, 1992). The carrier solution consisted of 10 mM NaOH and 0.2 M Na-citrate, while the receiving solution was composed of 50 μM HCl. In the basic reagent stream, the stable form of the NH_4^+/NH_3 solute was in the gas phase (NH_3). Upon passing the carrier stream over a gas-permeable hydrophobic membrane and into the mildly acidic receiving stream, the stable form of the NH_4^+/NH_3 solute was no longer in the gas phase. The quantity of NH_4^+/NH_3 solute was determined by transferring the receiving stream to the e-corder 821 equipped with an eDAQ Conductivity Pod, since the conductivity of the solution was used as a sensitive measure of the NH_4^+ concentration (Hall and Aller, 1992). The flow rate (1.4 ml min^{-1}) of the stream was controlled by use of a Masterflex L/S Computerized Drive combined with a Masterflex L/S Cartridge Pump.

Culturing

Methylosinus trichosporium OB3b cultures were grown in a 2.5 L bioreactor controlled by B. Braun Biotech computer console at 30^{o}C with a rotating propeller set at 200 rpm. Cultures were supplied with a Cu-deficient nitrate minimal salts (NSM)

medium, buffered to pH 7 with phosphate, and supplemented with trace metals and $FeSO_4$ according to Cornish et al., (1984)(table 5.1). The reactor was steadily sparged with instrument grade CH_4 and a supply of regulated air such that the partial pressure of O_2 in the reactor atmosphere was confined between ~0.01 to 0.16. Increasing cell density caused O_2 partial pressures to decrease. Cultures were grown between mid to late exponential phase prior to harvesting as determined by optical density monitoring at 600 nm ($0.6 < OD_{600} < 0.8$). Upon harvesting, culture suspensions were centrifuged in 50-ml Fisherbrand polypropylene falcon tubes at 4000 rpm for 10 minutes. The supernatant was discarded and the pellet was resuspended in growth media, centrifuged for 10 minutes and the cycle was repeated three times.

Dry mass analysis of *M. trichosporium* OB3b was performed to draw a correlation between optical density of cells in suspension and grams of dry cell mass per liter of fluid suspension. Quadruplicate 10-ml cell suspensions with OD_{600} of 0.3 were dried in an oven at 60^oC for 5 days before determining the dry mass. The 5-day period was confirmed to be a sufficient amount of time for no further change in mass associated with desiccation to occur.

Methane oxidation efficiency experiments

Mixed suspensions of montmorillonite and *Methylosinus trichosporium* OB3b were prepared in batch with conditions that varied according to initial Cu and NH_4^+ concentrations. Prior to combining clay with bacteria, 0.5 g L^{-1} batch suspensions of montmorillonite in 0.03 M KCl were prepared in 50-ml Fisherbrand polypropylene falcon tubes. The batch suspensions were spiked with Cu and NH_4^+, and rotated end-over-end at

50 rpm for a 24-hour sorption period. Essentially, two groups of experiments were performed: 1) zero Cu added to clay, with varying initial NH_4^+ concentrations (0, 100, 200, 500, 1000, and 2000 μM), and 2) 50 μM Cu added to clay, with varying initial NH_4^+ concentrations (0, 100, 200, 500, 1000, and 2000 μM). Upon completion of the 24-hour sorption period, the suspensions were centrifuged for 40 minutes at 4000 rpm, and the supernatant was decanted. The conditioned montmorillonite was resuspended in 50-ml of fresh growth media with *M. trichosporium* OB3b set at a cell density of 2.54 g L^{-1} corresponding to an OD_{600} of 0.3 (as determined from dry mass analysis). The new slurry was added to 125-ml glass serum vials and hermetically sealed. The headspace atmosphere of the reactors was a mixture of ambient air spiked with CH_4 (~140 ± 20 ppmv). Biotic reactors were prepared in triplicate with a corresponding abiotic control, which was prepared with fresh growth media and no bacteria. The resulting reactors were agitated at 30°C in the dark at 100 rpm. In each experiment, headspace CH_4 and CO_2 concentrations were monitored over time and solution sub-samples were collected at defined intervals over 24 hours.

Prior to sacrificing, reactor headspace gases were quantified in quadruplicate using an Agilent Technologies Network GC System 6890N with Thermal Conductivity Detector (TCD). Specifically, CH_4 and CO_2 phases in the headspace were separated in an isotemperature run on an Alltech Hayesep Q 80/100 Packed Column with an oven temperature of 90 °C and analytical error of 0.5%. Upon sacrificing, culture/montmorillonite slurry samples were sub-divided for aqueous metal, inorganic N (NH_4^+/NH_3, NO_2^-, NO_3^-), and pH analysis. Sub-samples for metal analysis, using an ICP-OES (Perkin Elmer Optima 5300 DV), were filtered using 0.2 μm polycarbonate filters

(Millipore Isopore) and preserved by acidification (5% ultrapure HNO_3). Prior to acidification, an additional 0.5-ml sub-sample of the filtered solution was stored at -20^{o}C until the series of inorganic N analyses could be performed. Once ready, 100-µl aliquots were diluted to 1-ml to generate sufficient sample volume to perform the analysis. The solution NH_4^+ content was determined using the rapid, flow-injection analysis (FIA) system (Hall and Aller, 1992). Nitrite and nitrate production was monitored using an Ion Chromatograph (Dionex Corporation) equipped with an AS18 analytical column (4 x 250 mm), AG18 guard column (4 x 50 mm), ASRS 300 suppressor (4 mm), and CD25 conductivity detector. Samples were eluted with 45 mM KOH and isocratic anion separation was performed at a flow rate of 1.0 ml min^{-1}, with the current set at 130 mA.

RESULTS

Adsorption-desorption isotherms at constant pH

In each of the three sets of adsorption-desorption experiments, the pH remained relatively stable at 6.8 throughout each 24-hour equilibration period (adsorption and desorption). Standard deviations did not exceed 0.28 pH units in any of the sets of experiments. The adsorbent behavior of Cu with montmorillonite is displayed in figure 7.1, while that of NH_4^+ is shown in figure 7.2. In the set of experiments examining Cu adsorption to montmorillonite in the absence of NH_4^+, the adsorbed Cu concentration increased from 34.4 to 107 µmoles g^{-1} for initial batch Cu concentrations between 25 µM and 150 µM, respectively. A characteristic L-shaped (Langmuir) isotherm was observed where the slope decreased with increasing Cu concentration, indicating that the number of vacant adsorption sites decreases with increasing coverage of the monolayer (figure

7.1a). A Langmuir plot (K_d vs. q) was used to calculate the equilibrium constant (K = 0.04, initial slope (-) of isotherm) and maximum sorption capacity (b = 134 μmol g^{-1}, x-intercept) to describe the Cu sorption isotherm according to the Langmuir equation:

$$q = \frac{bKc}{1 + Kc}$$

Where q is the amount adsorbed in μmol g^{-1}, c is the molarity (μmol L^{-1}), and $K_d = q/c$ (Sposito, 1984). This type of adsorption behavior would suggest that montmorillonite has a high affinity for Cu at low concentrations however the affinity decreases with increasing Cu concentration. A much steeper slope was observed for the Cu desorption trend, which indicates that a large proportion of the Cu was irreversibly adsorbed within the examined time frame. The range in aqueous Cu concentration associated with desorption after 24 hours was 3.2 to 11.4 μM, which corresponds to initial batch Cu concentrations in the clay slurry that range between 25 μM and 150 μM, respectively. The irreversibly adsorbed Cu increases linearly with increasing Cu adsorption onto montmorillonite (figure 7.1c). The adsorption/desorption behavior of Cu with respect to the Ca-montmorillonite from Gonzales County Texas in this study was similar to a previous study performed by Morton et al. (2001) with a Ca-montmorillonite from Apache Co. Arizona. The X-ray absorption spectroscopy (XAS) analysis performed by Morton et al. (2001) indicated that outer-sphere monomer and dimer Cu surface complexes had formed when adsorbed on the permanent charge sites of montmorillonite, which would permit sorption reversibility.

In the set of experiments examining Cu adsorption to montmorillonite in the presence of NH_4^+ ("Mixed Cu and NH_4^+"), none of the classical isotherm patterns was observed, nor were they expected since the initial Cu concentration (50 μM) was the

same in each experiment. The initial NH_4^+ concentration, however, was tested across a range between zero and 1500 μM. In these experiments, the adsorbed Cu decreased linearly with increasing NH_4^+ concentration (from 60.1 to 42.7 μmoles g^{-1}; figure 7.1b) suggesting that a competition for sorption sites on the surface of clay was occurring between Cu and NH_4^+. The Cu desorption trend displayed a steep slope with a relatively small proportion of aqueous Cu (range: 2.24 to 4.63 μM). While the amount of Cu desorption appears to decrease with increasing NH_4^+ content, an anomaly from the trend was observed, i.e., the lowest aqueous Cu concentration was associated with an initial NH_4^+ concentration of 1000 μM. The decreasing trend in aqueous Cu was also inversely correlated to increasing adsorbed Cu, however, the same anomaly was repeated in this comparison, i.e., the lowest aqueous Cu concentration was associated with a mid-range adsorbed Cu concentration (46.0 μmoles g^{-1}). The irreversibly adsorbed Cu increases linearly with increasing Cu adsorption onto montmorillonite (figure 7.1d) with a single anomaly from the trend sharing association with the anomalous data point observed in the desorption trend (figure 7.1b).

In a set of experiments designed to examine NH_4^+ adsorption to montmorillonite in the absence of Cu, the adsorbed NH_4^+ concentration increased from 203 to 849 μmoles g^{-1}. A characteristic L-shaped (Langmuir) isotherm was observed where the slope decreased with increasing NH_4^+ concentration (figure 7.2a). A Langmuir plot (K_d vs. q) was used to calculate the equilibrium constant (K = 0.0009) and maximum sorption capacity (b = 1910 μmol g^{-1}) to describe the NH_4^+ sorption isotherm according to the Langmuir equation provided above. As with Cu, montmorillonite has a high affinity for NH_4^+ at low concentrations and the affinity decreases with increasing NH_4^+

concentration. A much steeper slope was observed for the NH_4^+ desorption trend, which indicates that a large proportion of the NH_4^+ was irreversibly adsorbed within the examined time frame. The range in aqueous NH_4^+ concentration associated with desorption after 24 hours was 29.5 to 170 μM, which corresponds to initial batch NH_4^+ concentrations in the clay slurry that range between 250 μM and 1500 μM, respectively. The irreversibly adsorbed NH_4^+ increases linearly with increasing NH_4^+ adsorption onto montmorillonite (figure 7.2c).

In the "Mixed Cu and NH_4^+" experiments, NH_4^+ adsorption to montmorillonite did not reach a maximum adsorption capacity for the examined time frame and spectrum of NH_4^+ concentrations (figure 7.2b). The adsorbed NH_4^+ concentration increased from 0 to 662 μmoles g^{-1} for initial batch NH_4^+ concentrations ranging between 250 μM and 1500 μM, respectively. The presence of Cu in the system generates a competition for binding sites on the montmorillonite monolayer, hence limiting the kinetics of NH_4^+ adsorption. Desorption of NH_4^+ was only observed in experiments where the batch initial NH_4^+ concentration was 1250 μM or higher. For initial batch concentrations of NH_4^+ below 1250 μM, continued adsorption onto surface sites of montmorillonite was occurring during the intended desorption period (the 2nd 24-hour equilibration period, negative desorption not shown on plot). A plot of the calculated irreversibly adsorbed NH_4^+ is shown in figure 7.2d. An increasing quantity of irreversibly adsorbed NH_4^+ occurs with increasing total concentration. The sorption/desorption behavior of montmorillonite with respect to Cu and NH_4^+ allows us to predict the concentrations that will be released under abiotic conditions. However, in the presence of a metabolically

active methanotroph culture Cu and NH_4^+ desorption from montmorillonite is expected to be more complex since multiple oxidation pathways become possible.

Methane oxidation efficiency

Montmorillonite pretreated with Cu, or NH_4^+, or both, was reacted in batch microcosms containing *Methylosinus trichosporium* OB3b with a headspace mixture of CH_4 and air over a 24-hour time period (see experimental procedures). Since *Methylosinus trichosporium* OB3b is sensitive to both Cu (Hanson and Hanson, 1996) and NH_4^+ (King and Schnell, 1994), the release of these species from the clay was expected to impact rates of CH_4 oxidation. Trends in CH_4 depletion for each of the varying NH_4^+ treatments (0, 100, 200, 500, 1000, and 2000 μM) were plotted according first order kinetics for both zero Cu (figure 7.3a) and 50 μM Cu (figure 7.3b) treated montmorillonite suspensions. In all cases, CH_4 depletion increased with time, however, some treatments had comparatively steeper slopes. First order rates of CH_4 oxidation were calculated from the slopes of the trends and plotted in figure 7.3c, and d, for zero Cu and 50 μM Cu treated montmorillonite suspensions, respectively.

In the zero Cu batches (figure 7.3a and c), only the zero NH_4^+ treatment is distinguished from the others by showing a comparatively higher rate of CH_4 oxidation (8.83 ± 0.5 (s^{-1}) x 10^{-7}, $p = 0.1$). Each of the varying NH_4^+ treatments (100, 200, 500, 1000, and 2000 μM) yielded a rate of CH_4 oxidation (6.5 ± 0.3 (s^{-1}) x 10^{-7}, $p_{two\text{-}tails} = 0.2$) that was not significantly different from the others at the 80% confidence level (CL) or higher. In the 50 μM Cu treated montmorillonite suspensions (figure 7.3b and d), the optimum rate of CH_4 oxidation was demonstrated by the 200-μM NH_4^+ treatment ($6.92 \pm$

1.0 (s^{-1}) x 10^{-7}, $p_{two\text{-}tails}$ = 0.2). However, this data point may represent an outlier from the rest of the set. If removed, the rates appear to decrease with increasing NH_4^+ content per treatment. The statistical T-test indicates that rates for the zero- and 100-μM NH_4^+ treatments (5.32 ± 0.4 (s^{-1}) x 10^{-7} and 5.49 ± 0.6 (s^{-1}) x 10^{-7}, respectively) are not significantly different from one another at the 80% CL ($p_{two\text{-}tails}$ = 0.2), however, each is significantly different from the rest of the group (200-, 500-, 1000-, and 2000-μM NH_4^+ treatments, figure 7.3d). Both rates observed for the zero- and 100-μM NH_4^+ treatments are lower than the 200- μM NH_4^+ treatment and higher than the 500-, 1000-, and 2000-μM NH_4^+ treatments. Rates for the 1000- and 2000- μM NH_4^+ treatments (2.69 ± 0.7 (s^{-1}) x 10^{-7} and 2.35 ± 0.7 (s^{-1}) x 10^{-7}, respectively) are not significantly different from one another at the 80% CL ($p_{two\text{-}tails}$ = 0.2), however, both are significantly different (lower) than the rest of the group (0-, 100-, 200-, and 500-μM NH_4^+ treatments, figure 7.3d).

A comparison between the zero Cu and 50 μM Cu treated montmorillonite experiments indicates how the presence of Cu can influence rates of CH_4 oxidation (figure 7.3). In the absence of NH_4^+, the presence of Cu at an initial batch concentration of 50 μM causes a relative decline in the rate of CH_4 oxidation. Rates of CH_4 oxidation were only significantly different at the 60% CL ($p_{two\text{-}tails}$ = 0.4) when making direct comparisons between zero Cu and 50 μM Cu montmorillonite treatments with lower initial NH_4^+ concentrations (100 μM and 200 μM). In experiments with initial batch NH_4^+ concentrations of 500 μM or higher, relatively lower rates of CH_4 oxidation were observed for microcosms containing Cu compared to those without Cu.

In each experiment the solutions were analyzed for aqueous Cu, NH_4^+, NO_2^-, and NO_3^- to account for the variation in observed rates of CH_4 oxidation. Depending upon the

concentration, Cu has the ability to enhance or inhibit rates of CH_4 oxidation. At Cu concentrations below 0.89 μmol of Cu per gram (dry mass) of cells, sMMO is activated while concentrations above this value result in the activation of pMMO (Dalton, 1992; Hanson and Hanson, 1996). As expected, no Cu was detected in the zero Cu treated montmorillonite suspensions for any experimental time interval (data not shown). However, detection of aqueous Cu in the 50 μM Cu treated montmorillonite suspensions permitted the monitoring of desorption with time (figure 7.4).

Generally speaking the controls for each experimental system (initial Cu concentration fixed at 50 μM and NH_4^+ concentration ranging between 0 and 2000 μM) exhibited aqueous Cu concentrations of ~10 μM throughout the length of the experiment (24-hours). Only in two experiments was there a relatively negligible difference in aqueous Cu concentration between the control and the biotic samples (figure 7.4b and c, which represents experimental systems that vary according to initial NH_4^+ concentration: 100 μM and 200 μM, respectively). Otherwise, the aqueous Cu concentration was typically lower in the biotic samples compared to the control (figure 7.4a, d, e, and f). In the controls, the detectable concentration of Cu reflects the amount that had desorbed from the montmorillonite. In the biotic treatments, a quantifiable amount of Cu may have been partitioned by the anionic surface functional groups that make up components of the cell wall of *M. trichosporium* OB3b or alternatively had been internalized by *M. trichosporium* OB3b for cellular function, or both.

The presence of NH_4^+ was expected to inhibit methanotrophy by providing a competing substrate capable of being oxidized by methane monooxygenase (Hooper et al., 1997; King and Schnell, 1994; Schnell and King, 1994). To account for this effect

imposed by desorption of NH_4^+ from the clay, the aqueous NH_4^+ concentration was monitored with time in each experiment (figures 7.5 and 7.6, for initial Cu concentrations of zero and 50 μM, respectively). In the zero Cu experimental system, the concentration of aqueous NH_4^+ in the controls approached the detection limit of analysis for initial NH_4^+ concentrations of zero, 100 and 200 μM (figures 7.5a, b and c, respectively), while exhibiting consistently higher concentrations with increasing initial concentrations above 500 μM (figures 7.5d, e, and f). Little change in aqueous NH_4^+ concentration was observed between time zero and the 24th hour. The biotic samples on the other hand exhibited increasing aqueous NH_4^+ concentrations with time, provided that NH_4^+ had been added to the batch (figures 7.5b, c, d, e and f). In experiments with initial batch NH_4^+ concentrations of 200 μM or higher, maximum aqueous NH_4^+ concentrations were 265 μM or higher (figures 7.5c, d, e and f). In the 0-100 experiment (initial batch concentration of 100 μM NH_4^+), a maximum aqueous NH_4^+ concentration of 160 ± 12 μM was observed (figure 7.5b), while no NH_4^+ was detected in the 0-0 experiment (initial batch concentration of zero μM NH_4^+).

In the 50 μM Cu experimental system, the concentration of aqueous NH_4^+ in the controls approached the detection limit of analysis for batch initial NH_4^+ concentrations of zero and 100 μM (figures 7.6a and b, respectively). In control experiments with batch initial concentrations above 500 μM, at least 5 hours was required for the aqueous NH_4^+ concentration to equilibrate (figures 7.6d, e, and f), while immediate equilibration was observed in the 0-200 experiment (initial batch concentration of 200 μM NH_4^+, figure 7.6c). A significantly higher maximum aqueous NH_4^+ concentration (212 ± 15 μM) was observed in the 0-2000 experiment (initial batch concentration of 2000 μM NH_4^+)

compared to the others. In most cases, the patterns of aqueous NH_4^+ concentration in the biotic experiments mimicked the controls. The sole exception was in the 0-2000 experiment where the aqueous NH_4^+ concentration increased with time for the biotic samples rather than declining before equilibrating (figure 7.6f).

Since rates of CH_4 oxidation were observed to decline in the presence of NH_4^+ (figure 7.3 and c), the production of NO_2^- via nitrification was expected for these experiments. However, NO_2^- was below detection in each of the experiments (data not shown). While NO_3^- production would also indicate active nitrification, the background NO_3^- levels in the growth media (10 mM) were too high for minor increases to be detected outside the range of analytical error.

DISCUSSION

The presence of both Cu and NH_4^+ in the clay has directly impacted rates of CH_4 oxidation by *M. trichosporium* OB3b (figure 7.3). In the zero Cu experiments, regardless of the initial NH_4^+ concentration (100 to 2000 μM), rates of CH_4 oxidation were inhibited by the presence of NH_4^+ (figure 7.3a and c). Increasing initial NH_4^+ concentration did not result in an increase in the degree of inhibition. The fact that relatively similar aqueous NH_4^+ concentrations were observed in each experiment (figures 7.5b, c, d, e and f) would lead one to conclude that the NH_4^+ desorption trends were the same for each. This observation was reinforced by the "adsorption-desorption" experiments that were performed with NH_4^+ and clay in the absence of *M. trichosporium* OB3b where the range of desorption was between 29.5 to 170 μM for initial batch NH_4^+ concentrations of zero to 1500 μM (figure 7.2a). Detection of NH_4^+ in the microcosms that NH_4^+ had not been

provided exogenously may perhaps be evidence of NO_2^- reduction following its production during assimilatory reduction of NO_3^- from the growth media (Knowles, 2005).

It does appear that an over-amplification of NH_4^+ concentration may have occurred by the method of analysis for NH_4^+ detection (FIA) in some experiments (zero Cu with initial batch NH_4^+ concentrations of 100 and 200 μM, figure 7.5b and c, respectively). Over-amplifications may occur when NH_4^+ concentrations are approaching the limit of detection, particularly if residual NH_4^+ from previous analyses has not been successfully removed from the flow through lines, or reactive membrane. However, the determination of NH_4^+ by FIA was always performed at concentrations within the recommended range of linear detection (0.1 to 100 μM NH_4^+, Hall and Aller, 1992). Therefore, the exceptionally high NH_4^+ concentrations that were observed may be further evidence of NO_2^- reduction (Higgins et al., 1981).

The primary mechanism of inhibition is attributed to co-oxidation of NH_4^+ with CH_4 by methane monooxygenase (MMO), as has been reported in other studies (Dunfield and Knowles, 1995; King and Schnell, 1994; Schnell and King, 1994). The lack of detectable NO_2^- may either have been caused by sorption of NO_2^- onto the clay (Nese and Ennil, 2007), or inhibition of nitrification by a high concentration of potassium salts inducing NH_4^+ fixation (Chappell and Evangelou, 2000). Assimilation of nitrogen by methanotrophs is also known to occur after NO_2^- has been reduced to NH_3 (Higgins et al., 1981). Alternatively, the rapid oxidation of NO_2^- to NO_3^- may have limited its detection. As previously stated, the background NO_3^- concentration in the growth media was too high for NO_3^- production to be detected since changes in NO_3^- concentration were no

greater than the error of analysis (± 5 to 455 μM, data not shown). Nitrate production may also have been masked by NO_3^- sorption to clay (Xi et al., 2009).

In an earlier study, increased inhibition of CH_4 oxidation by *M. trichosporium* OB3b was shown to correspond with increasing NH_4Cl concentration and a decrease in NO_2^- production down to trace levels (Whittenbury et al., 1970). No clay was involved in this study therefore the adsorption explanation does not apply. At high NH_4^+ concentrations (> 18.7 mM), the rate of NO_2^- oxidation may have been at pace with the rate of NH_4^+ oxidation, which would account for the lack of NO_2^- detection. However, the highest initial batch NH_4^+ concentration examined in our study was ~9 orders of magnitude lower than for the study performed by Whittenbury et al. (1970). Hence some NO_2^- detection was expected, provided that no adsorption or reduction had occurred.

In the 50 μM Cu experiments, *M. trichosporium* OB3b was more sensitive to variations in initial NH_4^+ concentration, as reflected by the observed changes in CH_4 oxidation rates (figure 7.3b and d). While an optimum rate of CH_4 oxidation was observed when the initial NH_4^+ concentration was 200 μM, the progressive decline in rate that was observed with increasing initial NH_4^+ concentration may be a consequence of Cu. As the initial NH_4^+ concentration increases from 500 μM to 2000 μM, the aqueous Cu concentration declines in the biotic experiments but not in the controls. The presence of *M. trichosporium* OB3b cells in the biotic samples is responsible for the observed decline, either because of a physical sorption effect caused by the anionic surface functional groups of the cell wall outer membrane (Beveridge, 1989; Beveridge and Koval, 1981; Beveridge and Murray, 1976; 1980; Ferris, 1989; Yee and Fein, 2001) or by direct uptake and internalization for cellular function related to enzyme activity (i.e.,

methanotrophy; Balasubramanian and Rosenzweig, 2008; Berson and Lidstrom, 1996; Kim et al., 2004; Lieberman and Rosenzweig, 2004; Morton et al., 2000), or both. The fact that an equal decline in aqueous Cu concentration was not observed in the controls places emphasis upon the presence of *M. trichosporium* OB3b. The coincidence of declining rates of CH_4 oxidation and a decline in aqueous Cu concentration suggests that the cell partitioning of Cu from the aqueous phase has an inhibiting effect upon methanotrophy. Boiesen et al. (1993) observed Cu toxicity (inhibition of methane degradation) at a concentration of 4.72 μM, which is lower than the some of the aqueous Cu concentrations observed in this study. The coincidence of increasing NH_4^+ concentration and a decline in the rate of CH_4 oxidation remains a puzzle since this response was not observed in the zero Cu experiments. It would seem that Cu is playing a more significant role with respect to inhibiting the rate of methane oxidation than NH_4^+ concentration. However, increasing aqueous NH_4^+ concentration in the biotic experiments correlates with decreasing aqueous Cu concentration, particularly with a higher initial batch NH_4^+ concentration (figure 7.6f). This is likely to be evidence for enhanced cation exchange between sites on the surface of montmorillonite and the bulk solution in the presence of *M. trichosporium* OB3b. On the other hand, direct partitioning of Cu from the clay to the cell may have permitted the release of more NH_4^+ molecules that would otherwise be blocked within the 2:1 layers of the montmorillonite due to steric hindrance of Cu atoms positioned along the edge sites (Morton et al., 2001).

In general, sites available for the formation of surface complexes on smectite clays exist within the siloxane ditrigonal cavities of the permanent charge interlayer or on the hydroxyl edge sites of the interrupted crystal structure (Morton et al., 2001; Sposito,

1984). Spectroscopic investigations have indicated that Cu adsorbs in the interlayer of 2:1 clays as an outer-sphere complex (Brown and Kevan, 1988; McBride, 1982) and on edge, step or kink sites as an inner-sphere monomer or multinuclear complex (Farquhar et al., 1996; Hyun et al., 2000). At circum-neutral pH conditions, Cu binding on montmorillonite has been shown to be edge site dominated in solutions with Na concentrations of 0.1 M, and interlayer dominated in solutions with Na concentrations approaching 0 M (Morton et al., 2001). The Na concentration of the growth media amounts to 0.016 M (table 1), suggesting that Cu adsorption onto montmorillonite would have been distributed as a mixture between edge and interlayer sites. The presence of other cations in the media drives up the ionic strength of the solution to 0.02 M, which would result in an increase in the number of edge sites for Cu binding onto montmorillonite, however, multiple interlayer binding sites would have remained (Morton et al., 2001).

In the "adsorption-desorption" experiments that were performed with NH_4^+ and Cu in the absence of *M. trichosporium* OB3b, NH_4^+ desorption was observed for initial batch NH_4^+ concentrations of 1250 μM or higher (figure 7.2b). The final aqueous NH_4^+ concentrations in the biotic experiments reflected this desorption behavior (figure 7.6). Copper desorption was observed across the entire range of initial batch NH_4^+ concentrations (figure 7.1b) and the values were consistent with the final aqueous Cu concentrations observed in the biotic experiments (figure 7.4).

Due to the absence of Cu in montmorillonite for the "zero Cu" CH_4 oxidation experiments, the aqueous Cu concentration for all samples in each treatment were below detection, and it is presumed that sMMO was expressed by *M. trichosporium* OB3b

during CH_4 consumption since low Cu-to-biomass ratios (< 0.89 μmole of Cu per g [dry weight] of cells) are required for this to happen (Hanson and Hanson, 1996). With a minimum *M. trichosporium* OB3b cell density of 2.54 g L^{-1} at beginning of each time course experiment, the Cu-to-biomass ratio for the 50 μM Cu treated montmorillonite suspensions were estimated to be approximately 4 μmole of Cu per g [dry weight] of cells. This estimate was based upon the aqueous Cu concentration of 10 μM, which was approximated from the results each of the control treatments in figure 4. It should be acknowledged that any increase in cell density during the 24-hour experiment would result in a decrease in Cu-to-biomass ratio. However, based on previous research (Kulczycki et al., 2010), population increases for *M. trichosporium* OB3b were not substantial within this time frame if a cell density corresponding to an OD_{600} of 0.3 had already been established. At Cu-to-biomass ratios above 0.89 μmole of Cu per g [dry weight] of cells, pMMO is expressed by *M. trichosporium* OB3b (Hanson and Hanson, 1996), and as such, is expected to be active in the 50 μM Cu treated montmorillonite suspensions. The concentration of Cu appears to have been high enough to elicit a toxic response from *M. trichosporium* OB3b (Boiesen et al., 1993), as is evident with the decline in CH_4 oxidation rates compared to the corresponding "zero Cu" experiments (figure 7.3). The sole exception from this trend was observed in the treatments with an initial NH_4^+ concentration of 200 μM.

The lack of aqueous NO_2^- data prevents the co-oxidation hypothesis (a decline in the rate of CH_4 oxidation being caused by the competitive utilization of MMO toward nitrification) from being confirmed, however, it does not necessarily permit its dismissal. The data from each experimental set (zero Cu and 50 μM Cu) shows that the presence of

NH_4^+ results in a decline in CH_4 oxidation rate (figure 7.3). Only at the lower initial NH_4^+ concentrations (0 to 200 μM) in the 50 μM Cu experiments was a decline in CH_4 oxidation rate not observed. In these experiments the aqueous NH_4^+ concentration did not exceed 50 μM for either the biotic samples or the controls. In the zero Cu experiments however, the aqueous NH_4^+ concentration was observed to exceed 50 μM in every biotic experiment that involved NH_4^+ (figure 5). At the very least it can be concluded that a threshold aqueous NH_4^+ concentration of 50 μM needs to be overcome before CH_4 oxidation rates are inhibited.

The amount NH_4^+ desorption is in part controlled by the quantity of bound NH_4^+ to the clay prior to introducing *M. trichosporium* OB3b. Copper would have competed with NH_4^+ for binding sites along the surface of the clay, thus lowering the batch NH_4^+ concentration relative to the zero Cu experiments. Recall that after nutrient sorption onto the clay, the suspensions were centrifuged and the supernatant was replaced with Cu and NH_4^+ "free" growth media prior to initiating the CH_4 oxidation efficiency experiments. The relatively lower concentration of bound NH_4^+ in the 50 μM experiments is reflected by the lower aqueous NH_4^+ concentrations observed in the CH_4 oxidation efficiency experiments when compared with the zero Cu experiments (figures 7.6 and 7.5, respectively). Evidently the combined release of Cu and NH_4^+ from the clay, particularly at higher initial NH_4^+ concentrations, has had a greater impact in terms of inhibiting rates of CH_4 oxidation, compared to when Cu was absent from the equation. Since pMMO activation is dependent upon sufficient Cu supply (Bedard and Knowles, 1989) the impact upon NH_4^+ oxidation by methanotrophs is expected to demonstrate a response that is similar to pMMO dependent CH_4 oxidation. As was mentioned earlier, in vitro studies

of pMMO and AMO suggest similarities between both enzymes with respect to being regulated by Cu (Ensign et al. 1993, Hanson and Hanson 1996, Hooper et al., 1997; Nguyen et al. 1994). The requirement of CH_4 for a source of carbon and energy in methanotrophs promotes the oxidation of CH_4 over NH_4^+ by pMMO (Bedard and Knowles, 1989), however, the proportionately small contribution of pMMO used toward NH_4^+ oxidation may have been enough to inhibit rates of CH_4 oxidation. While competition for MMO by NH_4^+ has been proposed as a mechanism that inhibits CH_4 oxidation, the production of compounds with toxic effects, e.g., hydroxylamine (NH_2OH) and NO_2^-, should also be considered (Schnell and King, 1994). Methane monooxygenase activity of *M. trichosporium* OB3b is inhibited by the NH_2OH intermediate (Hubley et al., 1975), which consequently limits CH_4 consumption. Formate dehydrogenase (a key source of NADH plus H^+) activity is specifically affected by NO_2^- (Schnell and King, 1994). The role of NADH plus H^+ as a reductant is critical to the CH_4 oxidation pathway (Hanson and Hanson, 1996) but also facilitates NH_4^+ oxidation by MMO (Schnell and King, 1994). Biological NO_2^- removal however, can occur during the functioning assimilatory NO_3^- pathway (Payne, 1973) with resultant production of nitrous oxide in the atmosphere (O'Neill and Wilkinson, 1977).

Lastly, NO_2^- and NO_3^- production may have been masked during NH_4^+ oxidation coupled with CH_4 oxidation if denitrification was occurring. Few reports of denitrification coupled with microbial CH_4 oxidation exist and evidence of the process has been constrained to anaerobic conditions (Raghoebarsing et al., 2006). Previous to these findings, the lack of experimental evidence for anaerobic oxidation of CH_4 coupled to denitrification was attributed to the narrow boundary conditions that limit the location

of this process in nature. Methane and nitrogen cycling of this kind is expected to occur at the oxic/anoxic interface in sediments that are generally characterized by steep gradients, within a few millimeters, and as such require a very high degree of precision when attempting to detect the process geochemically (Raghoebarsing et al., 2006). In our study, the conditions were not anaerobic. However, the atmospheric oxygen supply was not replenished during its consumption by *M. trichosporium* OB3b during CH_4 oxidation. Consequently, the conditions may have become more thermodynamically and geochemically favorable for the type of reverse methanogenesis reactions that involve NO_2^- or NO_3^- to occur (Hallam et al., 2004; Knowles, 2005; Kruger et al., 2003; Mason, 1977; Raghoebarsing et al., 2006; Strous and Jetten, 2004; Valentine, 2002). To confirm that these reactions were active in our study would have required the monitoring of NO, N_2O, and N_2 gases in the headspace and dissolved oxygen in the microbial clay slurry. In a study by Lee et al., (2009), pure methanotroph cultures were shown to produce abundant N_2O when expressing pMMO during CH_4 consumption in the presence of NH_4^+, lending credence to the speculation of this process occurring in our study. Regardless, *M. trichosporium* OB3b's response to the presence of NH_4^+ in the clay was a suppressed rate of CH_4 oxidation. The lack of detectable aqueous inorganic N products (e.g., NO_2^-, and NO_3^-) suggests that a complex N cycle may have been activated in the process of microbial CH_4 oxidation provided that NH_4^+ was desorbing from the clay.

SUMMARY

The results of this study show that methanotrophy is sensitive to desorbing Cu and NH_4^+ from montmorillonite and reflects a complex set of processes that occur during

conditions of soil inundation in natural wetlands. In the absence of Cu, a minimum threshold NH_4^+ concentration will suppress rates of CH_4 oxidation by *M. trichosporium* OB3b, and increasing NH_4^+ concentration does not appear to alter the degree that the rate of CH_4 oxidation is inhibited. When Cu is present however, the degree of suppression increases with increasing NH_4^+ concentration. The resultant inhibition of CH_4 oxidation rates during co-oxidation of methane and NH_4^+ in pure cultures of *M. trichosporium* OB3b is most likely caused by a competition for MMO. The lack of detectable NO_2^- or NO_3^- production implies that a complex N cycle may have been activated during the NH_4^+ oxidation as coupled with a decline in O_2 during CH_4 oxidation. While adsorption onto montmorillonite may account for some losses, assimilatory NO_2^- reduction inducing NH_4^+ fixation, and methanotroph driven denitrification should also be considered. Future studies directed at constraining the cycling of inorganic N during co-oxidation of CH_4 and NH_4^+ may reveal some interesting findings regarding processes that are theoretically possible under the appropriate conditions.

Figure 7.1. Adsorption (dark symbols) and desorption (white symbols) of Cu on montmorillonite (0.5 g L^{-1}) in a 0.03 M KCl solution at pH 6.8 (a) for a range of initial Cu concentrations between 0 and 150 µM, and (b) for a fixed initial Cu concentration of 50 µM in the presence of NH_4^+ across a range of initial concentrations between 0 and 1500 µM. Irreversibly adsorbed Cu on montmorillonite calculated from the adsorption-desorption isotherms (c) for a range of initial Cu concentrations between 0 and 150 µM, and (d) for a fixed initial Cu concentration of 50 µM in the presence of NH_4^+ across a range of initial concentrations between 0 and 1500 µM.

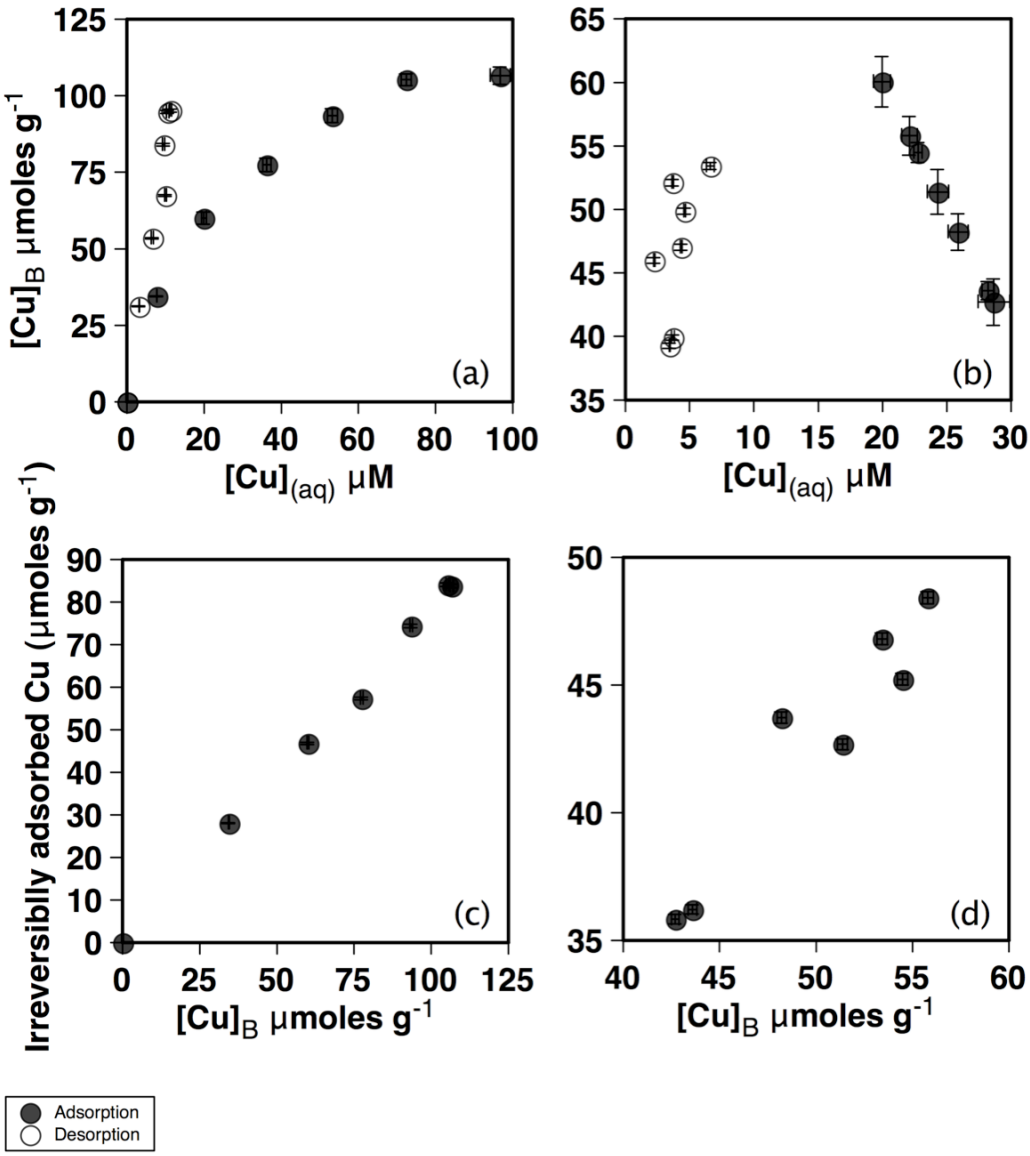

Figure 7.2. Adsorption (dark symbols) and desorption (white symbols) of NH_4^+ on montmorillonite (0.5 g L^{-1}) in a 0.03 M KCl solution at pH 6.8 for a range of initial NH_4^+ concentrations between 0 and 1500 µM, (a) in the absence of Cu, and (b) with an initial Cu concentration of 50 µM. Irreversibly adsorbed NH_4^+ on montmorillonite calculated from the adsorption-desorption isotherms for a range of initial NH_4^+ concentrations between 0 and 1500 µM, (c) in the absence of Cu, and (d) and with an initial Cu concentration of 50 µM.

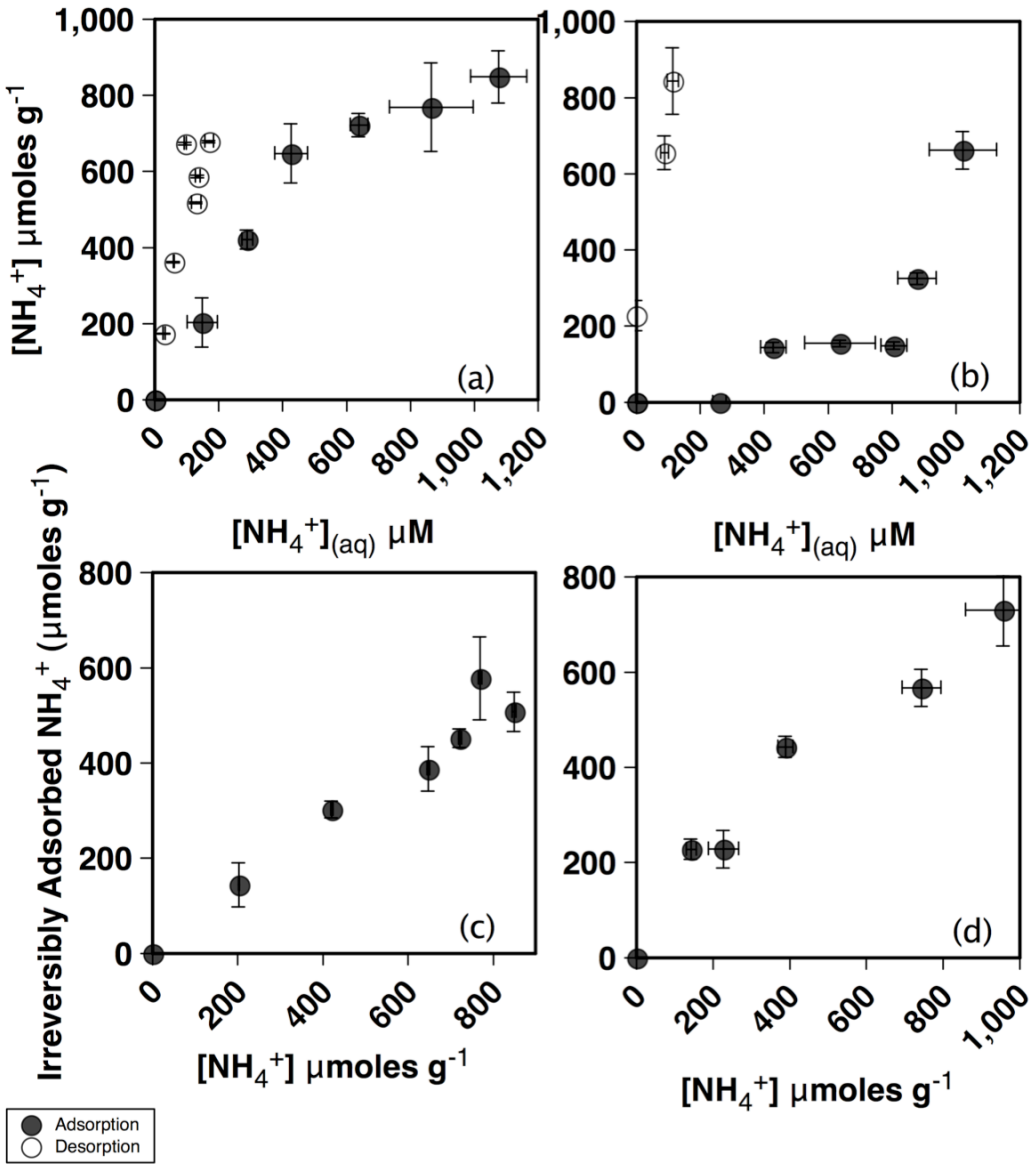

Figure 7.3. Methane consumption by pure culture of *Methylosinus trichosporium* OB3b as impacted by NH_4^+ concentration of the montmorillonite slurry. Panel (a) and (b) show first order trends of CH_4 consumption as a function of time for slurries not spiked with Cu and slurries with an initial Cu concentration of 50 µM prior to adsorption and separation, respectively. First order rates of CH_4 consumption (s^{-1}) are shown in panels (c) and (d), for slurries not spiked with Cu and slurries with an initial Cu concentration of 50 µM prior to adsorption and separation, respectively. Error bars represent the 80% confidence interval.

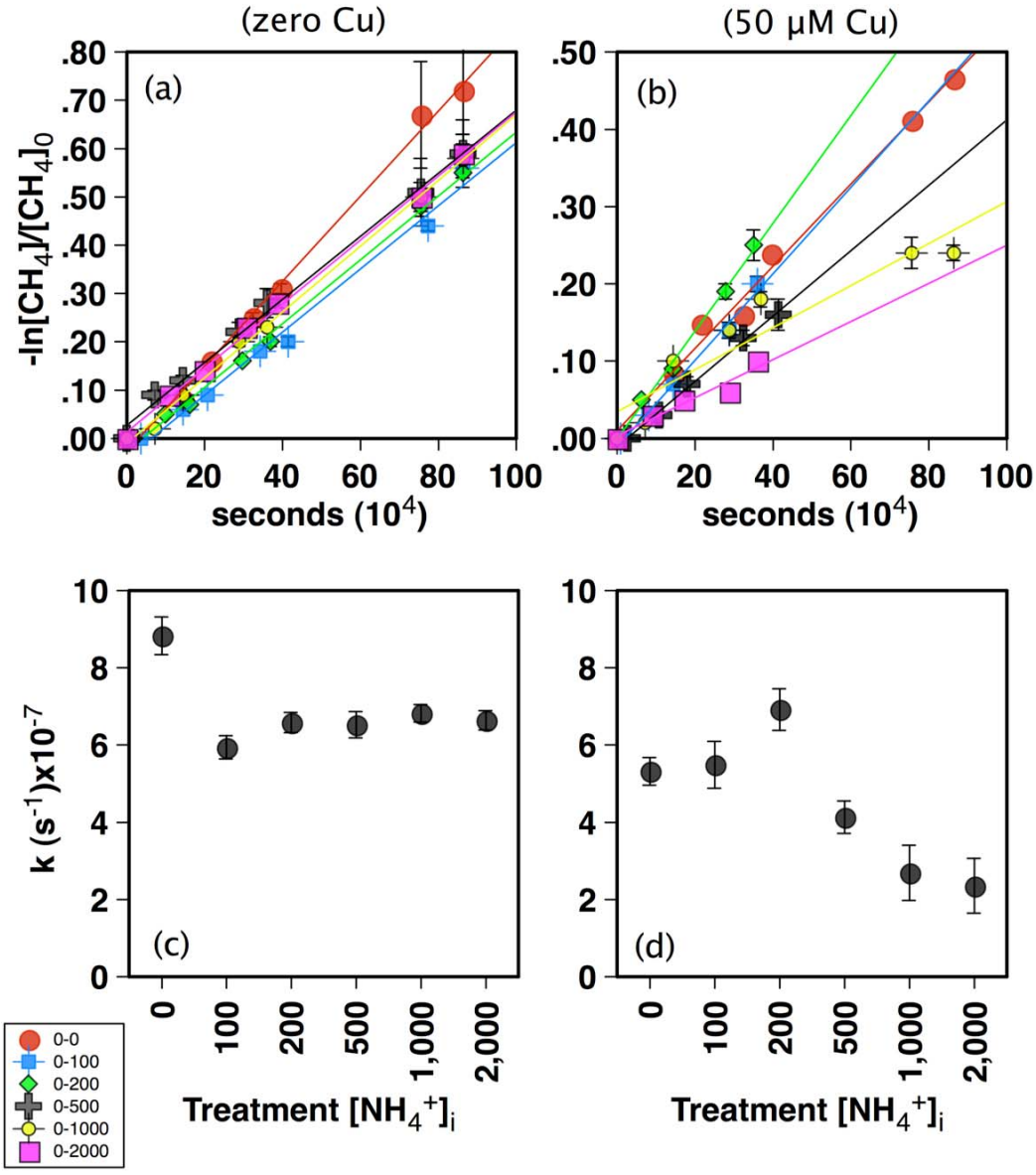

Figure 7.4. Aqueous Cu concentrations in filtered growth media as a consequence of 24 hours of Cu desorption from montmorillonite with an initial Cu concentration of 50 μM prior to adsorption and separation. Aqueous Cu concentrations in the presence of *M. trichosporium* OB3b (dark symbols) and no bacteria abiotic controls (white symbols) for initial NH_4^+ concentrations of (a) 0 μM, (b) 100 μM, (c) 200 μM, (d) 500 μM, (e) 1000 μM, and (f) 2000 μM.

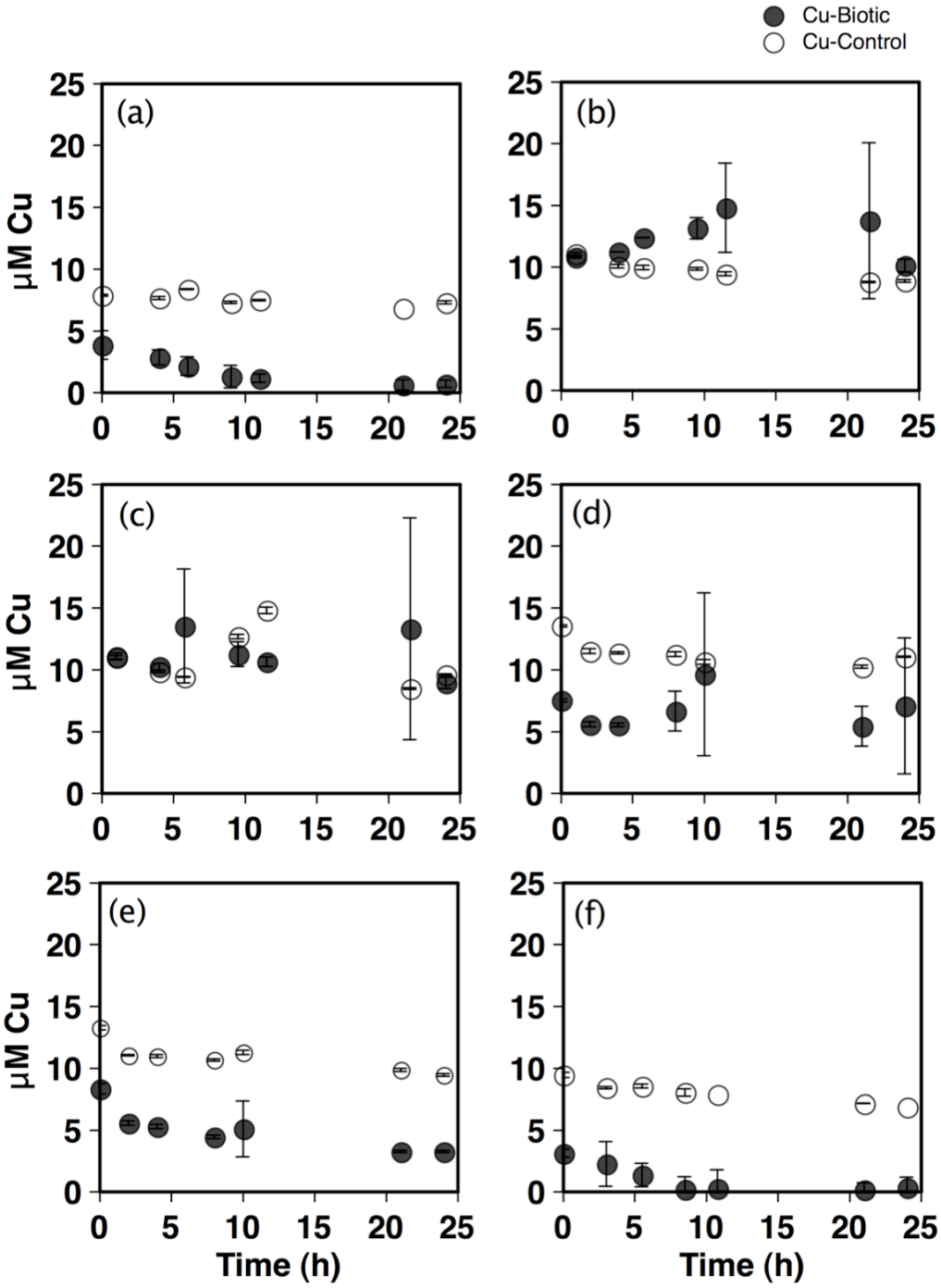

Figure 7.5. Ammonia (NH_3) detection as determined by FIA reflecting NH_4^+ concentrations in filtered growth media as a consequence of 24 hours of NH_4^+ desorption from montmorillonite in the absence of Cu. Aqueous NH_4^+ concentrations in the presence of *M. trichosporium* OB3b (dark symbols) and no bacteria abiotic controls (white symbols) for initial NH_4^+ concentrations of (a) 0 μM, (b) 100 μM, (c) 200 μM, (d) 500 μM, (e) 1000 μM, and (f) 2000 μM.

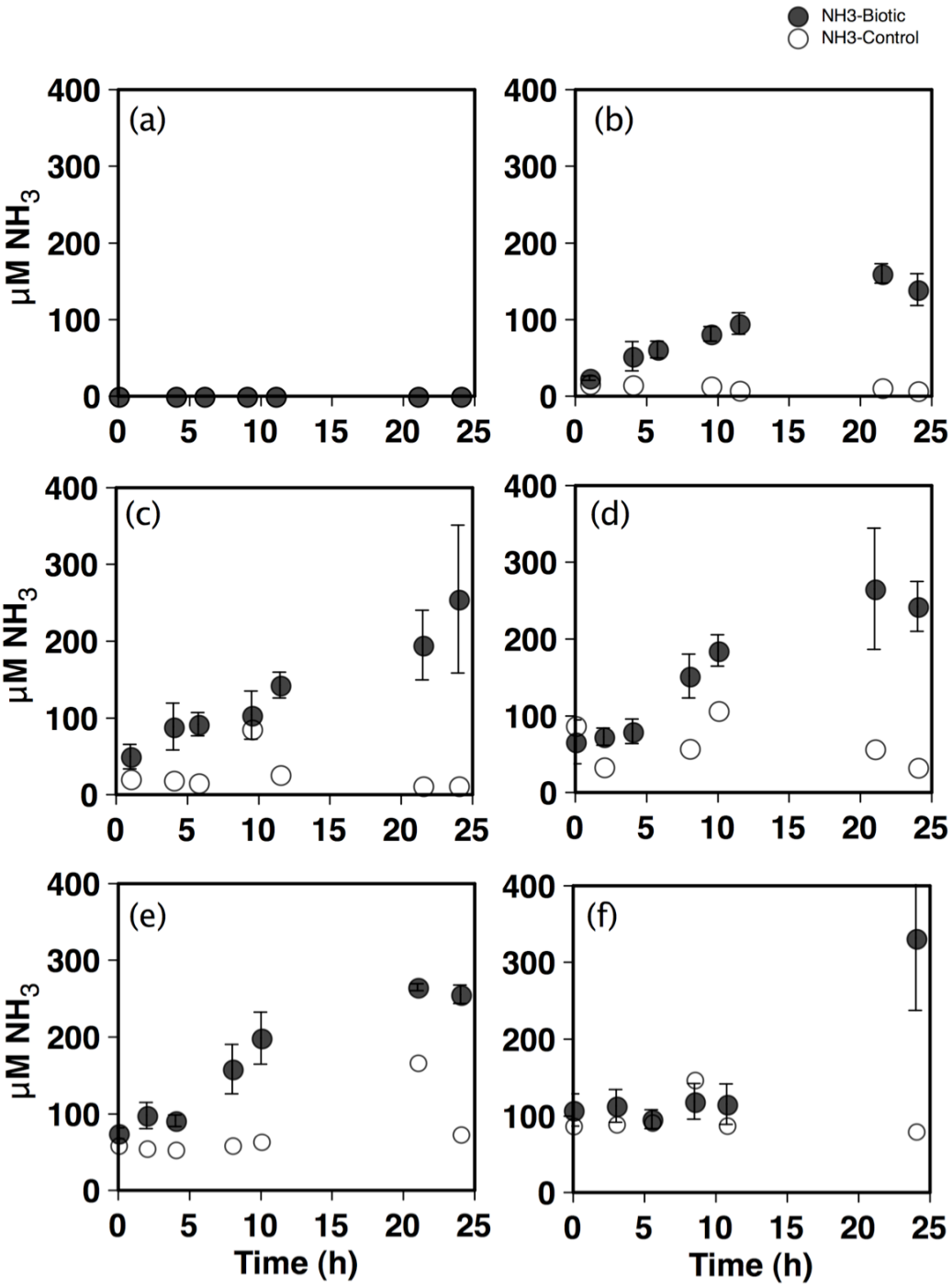

Figure 7.6. Ammonia (NH_3) detection as determined by FIA reflecting NH_4^+ concentrations in filtered growth media as a consequence of 24 hours of NH_4^+ desorption from montmorillonite with an initial Cu concentration of 50 μM prior to adsorption and separation. Aqueous NH_4^+ concentrations in the presence of *M. trichosporium* OB3b (dark symbols) and no bacteria abiotic controls (white symbols) for initial NH_4^+ concentrations of (a) 0 μM, (b) 100 μM, (c) 200 μM, (d) 500 μM, (e) 1000 μM, and (f) 2000 μM.

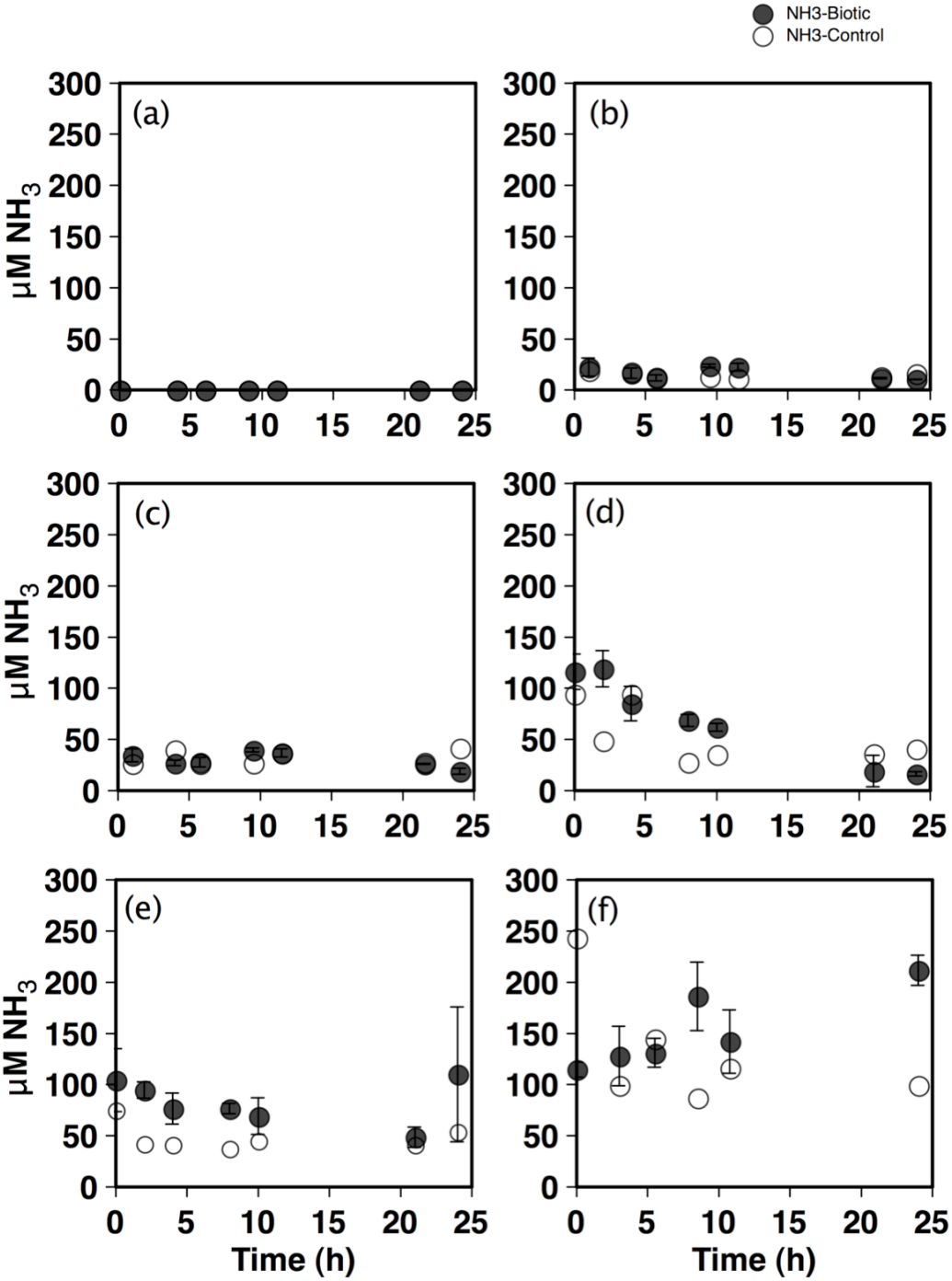

CHAPTER 9

CONCLUSIONS AND IMPLICATIONS

In this dissertation a number of geochemical processes were shown to have a direct impact upon microbial activity. Specifically, mineral weathering and nutrient desorption from clays was examined for the impact upon biological CH_4 oxidation rates. However, biological processes were also shown to influence geochemical systems. This was demonstrated by enhanced mineral solubility in the presence of microorganisms or microbially generated organic compounds. Some microorganisms rely upon extracellular-ligands to promote metal solubility, such as the siderophore and chalkophore studied here. In these circumstances, the formation of an aqueous-metal complex ensures the bioavailability of the target metal, in this case Fe or Cu, that of which the organism is dependent upon to sustain metabolic activity. Since both siderophores and methanobactin are capable of solubilizing metals from mineral sources, the microorganism involved acts as both a contributor and perhaps a beneficiary of mineral weathering. Interestingly, these processes are also linked with carbon cycling, and have implications with respect to the global climate.

Methane is a potent greenhouse gas with a high global warming potential (Forster et al., 2007). While being less abundant than carbon dioxide (CO_2), on a per molecule basis CH_4 is approximately 25 to 43 times more powerful in terms of absorbing long wave or infrared radiation (Hanson and Hanson, 1996; Wuebbles and Hayhoe, 2002). The abundance of CH_4 in the atmosphere has increased as a result of human activities related to agriculture, natural gas distribution and landfill utilization by a factor of about 2.5 since the pre-industrial era (Ehhalt et al., 2001). However, significant contributions of

CH_4 to the atmosphere are also released from natural processes, such as biogenic CH_4 production in wetlands.

The drying of wetlands is expected to result in a decrease in CH_4 production and an increase in its mitigation by methanotrophy. An understanding of the key parameters (i.e., concentrations of dissolved oxygen, CH_4, Cu, and NH_3, etc.) that influence CH_4 oxidation efficiency permits us to model the persistence of CH_4 in the atmosphere. The isolation of point sources of CH_4, i.e., a natural wetland, and the associated processes that regulate the release of CH_4 from its source can be projected into a compilation of localized datasets from which a complete picture can be drawn.

The relationship between mineral weathering and carbon cycling has been mapped out, and several models have emerged to explain these interactions (Berner, 1991; 1994; Berner and Kothavala, 2001; Berner et al., 1983; Veizer et al., 2000; Walker et al., 1981). However, the connection between mineral weathering and CH_4 oxidation is a relatively new concept. The acquisition of Cu from mineral sources and the transport of Cu to methane monooxygenase enzymes (sMMO and pMMO) in methanotrophs are linked to methanobactin. Indeed, more research will be in order to properly elucidate all of the nuances associated with methanobactin, Cu, and the methane monooxygenase enzymes, as a myriad of changing conditions can impact the result of their interplay with direct consequences upon rates of CH_4 oxidation. For instance the abundance of CH_4, the abundance of molecular oxygen (O_2), the ratio of CH_4 to O_2 each represent dynamic parameters that influence rates of CH_4 oxidation. Combining these influences with Cu concentration, methanobactin concentration, and activated methane monooxygenase enzymes add complexity to matrix. This can be further complicated by the addition of

competing nutrients such as NH_4^+ or NO_2^-, and the reactivity of mineralogical substrates. Establishing a set of controlled conditions is critical to isolating the function of each parameter, and must be performed prior to examining the function of two or more parameters in combination. The accumulation of this type of data permits the development of predictive models, which can used to determine how a specific geological setting will impact rates of CH_4 oxidation.

REFERENCES CITED

Aagaard P, Helgeson HC. 1982. Thermodynamic and kinetic constraints on reaction rates among minerals and aqueous solutions. I. Theoretical considerations. American Journal of Science 282: 237-285.

Adamsen APS, King GM. 1993. Methane consumption in temperate and subarctic forest soils: Rates, vertical zonation, and responses to water and nitrogen. Applied and Environmental Microbiology 59: 485-490.

Adriano DC. 1986. Trace elements in the terrestrial environment. New York: Spring-Verlag.

Agbenin JO. 2003. Extractable Iron and Aluminum Effects on Phosphate Sorption in a Savanna Alfisol. Soil Sci Soc Am J 67: 589-595.

Aide M, Pavich Z, Lilly ME, Thorton R, Kingery W. 2004. Plinthite formation in the coastal plain region of Mississippi. Soil Science 169: 613-623.

Aitken RL, Woody PW. 1994. The effect of valence and ionic-strength on the measurement of pH buffer capacity. Australian Journal of Soil Research 32: 975-984.

Alexander M. 1999. Biodegradation and Bioremediation. New York: Academic Press.
Allison VJ, Yermakov Z, Miller RM, Jastrow JD, Matamala R. 2007. Using landscape and depth gradients to decouple the impact of correlated environmental variables on soil microbial community composition. Soil Biology and Biochemistry 39: 505-516.

Amaral JA, Archambault C, Richards SR, Knowles R. 1995. Denitrification associated with Groups I and II methanotrophs in a gradient enrichment system. FEMS Microbiology Ecology 18: 289-298.

Bååth E. 1989. Effects of heavy metals in soil on microbial processes and populations (a review). Water, Air, & Soil Pollution 47: 335-379.

Bagg A, Neilands JB. 1987. Molecular mechanism of regulation of siderophore-mediated iron assimilation. Microbiol. Mol. Biol. Rev. 51: 509-518.

Baillie I, Elsenbeer H, Barthold F, Grimm R, Stallard R. 2007. Semi-detailed soil survery of Barro Coloradio Island, Panama. Report no.

Bala Krishna Prasad M, Ramanathan AL. 2009. Characterization of phosphorus fractions in the sediments of a tropical intertidal mangrove ecosystem. Wetlands Ecology and Management.

Balasubramanian R, Rosenzweig AC. 2008. Copper methanobactin: a molecule whose time has come. Current Opinion in Chemical Biology 12: 245-249.

Banfield JF, Barker WW, Welch SA, Taunton A. 1999. Biological impact on mineral dissolution: Application of the lichen model to understanding mineral weathering in the rhizosphere. Proceedings of the National Academy of Sciences 96: 3404-3411.

Banni M, Liesack W. 2008. Two isozymes of particulate methane monooxygenase with different methane oxidation kinetics are found in *Methylosinus* sp. strain SC2. Proceedings of the National Academy of Sciences 105: 10203-10208.

Barker WW, Welch SA, Banfield JF. 1997. Biogeochemical weathering of silicate minerals. Pages 391-428 in Banfield JF, Nealson KH, eds. Geomicrobiology: Interactions Between Microbes and Minerals. Washington, D.C.

Barker WW, Welch SA, Chu S, Banfield JF. 1998. Experimental observations of the effects of bacteria on aluminosilicate weathering. American Mineralogist 83: 1551-1563.

Barraclough D. 1997. The direct or MIT route for nitrogen immobilization: a 15N mirror image study with leucine and glycine. Soil Biology and Biochemistry 29: 101-108.

Bartlett KB, Harriss RC. 1993. Review and assessment of methane emissions from wetlands. Chemosphere 26: 261-320.

Bedard C, Knowles R. 1989. Physiology, biochemistry, and specific inhibitors of CH4, NH_4^+, and CO oxidation by methanotrophs and nitrifiers. Microbiological Reviews 53: 68-84.

Behling LA, Hartsel SC, Lewis DE, DiSpirito AA, Choi DW, Masterson LR, Veglia G, Gallagher WH. 2008. NMR, mass spectrometry and chemical evidence reveal a different chemical structure for methanobactin that contains oxazolone rings. Journal of the American Chemical Society 130: 12604-12605.

Bellion E, Bolbot JA. 1983. Nitrogen assimilation in facultative methylotrophic bacteria. Current Microbiology 9: 37-44.

Bender M, Conrad R. 1992. Kinetics of CH_4 oxidation in oxic soils exposed to ambient air or high CH_4 mixing ratios. FEMS Microbiology and Ecology 101: 261-270.

Bender M, Conrad R. 1994. Methane oxidation activity in various soils and freshwater sediments: occurrence, characteristics, vertical profiles and distribution on grain size fractions. Journal of Geophysical Research 99: 16531-16540.

Bender M, Conrad R. 1995. Effect of CH_4 concentrations and soil conditions on the induction of CH_4 oxidation activity. Soil Biology & Biochemistry 27: 1517-1527.

Bennett PC, Hiebert FK, Choi WJ. 1996. Microbial colonization and weathering of silicates in a petroleum-contaminated groundwater. Chemical Geology 132: 45-53.

Bennett PC, Hiebert FK, Roberts Rogers J. 2000. Microbial control of mineral-groundwater equilibria: Macroscale to microscale. Hydrogeology Journal 8: 47-62.

Bennett PC, Rogers JR, Choi WJ, Hiebert FK. 2001. Silicates, silicate weathering, and microbial ecology. Geomicrobiology Journal 18: 3-19.

Benzerara K, Menguy N, Guyot F, Vanni C, Gillet P. 2005. TEM study of a silicate-carbonate-microbe interface prepared by focused ion beam milling. Geochimica et Cosmochimica Acta 69: 1413-1422.

Berner RA. 1994. GEOCARB II: A revised model of atmospheric CO_2 over Phanerozoic time. American Journal of Science 294: 56-91.

Berner RA. 1995. Chemical weathering and its effect on atmospheric CO_2 and climate. Reviews in Mineralogy and Geochemistry 31: 565-583.

Berner RA. 1999. A new look at the long-term carbon cycle. GSA Today 9: 1-6.
Berner RA, Kothavala Z. 2001. GEOCARB III: A revised model of atmospheric CO_2 over phanerozoic time. American Journal of Science 301: 182-204.

Berner RA, Lasaga AC, Garrels RM. 1983. The carbonate-silicate geochemical cycle and its effect on atmospheric carbon dioxide over the past 100 million years. American Journal of Science 283: 641-683.

Berson O, Lidstrom ME. 1996. Study of Copper Accumulation by the Type I Methanotroph Methylomicrobium albus BG8. Environmental Science & Technology 30: 802-809.

Berthelin J, Leyval C, Mustin C. 2000. Illustrations of the occurrence and diversity of mineral-microbe interactions involved in weathering of minerals. Pages 7-25 in Cotter-Howells JD, Campbell LS, Valsami-Jones E, Batchelder M, eds. Environmental Mineralogy: Microbial Interactions, Anthropogenic Influences, Contaminated Land and Waste Management. London: The Mineralogical Society of Great Britain and Ireland.

Bethke CM. 2002. The Geochemist's Workbench. Release 4.0. A User's Guide to Rxn, Act2, Tact, React, and Gtplot. Urbana-Champaign, Illinois: University of Illinois.
Beveridge TJ. 1989. Role of Cellular Design in Bacterial Metal Accumulation and Mineralization. Annual Review of Microbiology 43: 147-171.

Beveridge TJ. 1999. Structures of Gram-Negative Cell Walls and Their Derived Membrane Vesicles. J. Bacteriol. 181: 4725-4733.

Beveridge TJ, Murray RG. 1976. Uptake and retention of metals by cell walls of Bacillus subtilis. Journal of Bacteriology 127: 1502-1518.

Beveridge TJ, Murray RG. 1980. Sites of metal deposition in the cell wall of Bacillus subtilis. Journal of Bacteriology 141: 876-887.

Beveridge TJ, Koval SF. 1981. Binding of metals to cell envelopes of Escherichia coli K-12. Applied and Environmental Microbiology 42: 325-335.

Beveridge TJ, Graham LL. 1991. Surface layers of bacteria. Microbiol. Mol. Biol. Rev. 55: 684-705.

Beveridge TJ, Makin SA, Kadurugamuwa JL, Li Z. 1997. Interactions between biofilms and the environment. FEMS Microbiology Reviews 20: 291-303.

Birkeland PW. 1999. Soils and geomorphology. New York: Oxford University Press.
Blake D, Rowland F. 1988. Continuing worldwide increase in tropospheric methane, 1978 to 1987. Science 239: 1129-1131.

Blake RE, Walter LM. 1999. Kinetics of feldspar and quartz dissolution at 70-80^{o}C and near-neutral pH: Effects of organic acids and NaCl. Geochimica et Cosmochimica Acta 63: 2043-2059.

Bland W, Rolls D. 2005. Weathering: An Introduction to the Scientific Principles. New York: Oxford University Press Inc.

Bodelier PLE, Frenzel P. 1999. Contribution of methanotrophic and nitrifying bacteria to CH_4 and NH_4^+ oxidation in the rhizosphere of rice plants as determined by new methods of discrimination. Applied and Environmental Microbiology 65: 1826-1833.

Bodelier PLE, Laaunbroek HJ. 2004. Nitrogen as a regulatory factor of methane oxidation in soils and sediments. FEMS Microbiology and Ecology 47: 265-277.

Bodelier PLE, Roslev P, Henckel T, Frenzel P. 2000. Stimulation by ammonium-based fertilizers of methane oxidation in soil around rice roots. Nature 403: 421-424.

Bodelier PLE, Frenzel P, Drake HL, Hurek T, Kusel K, Lovell C, Megonigal P, Reinhold-Hurek B, Sorrell B. 2006. Ecological aspects of microbes and microbial communities inhabiting the rhizosphere of wetland plants. Ecological Studies 190: 205-238.

Boettcher SE, Kalisz PJ. 1990. Single-Tree Influence on Soil Properties in the Mountains of Eastern Kentucky. Ecology 71: 1365-1372.

Boiesen A, Arvin E, Broholm K. 1993. Effect of mineral nutrients on the kinetics of methane utilization by methanotrophs. Biodegradation 4: 163-170.

Bondietti G, Sinniger J, Stumm W. 1993. The reactivity of Fe(III) (hydr)oxides - Effects of ligands in inhibiting the dissolution. Colloids and Surfaces A 79: 157-167.

Borgias B, Hugi AD, Raymond KN. 1989. Isomerization and solution structures of desferrioxamine B complexe of Al^{3+} and Ga^{3+}. Inorganic Chemistry 28: 3538-3545.

Borrok D, Fein JB, Kulpa CF. 2004. Proton and Cd adsorption onto natural bacterial consortia: Testing universal adsorption behavior. Geochimica et Cosmochimica Acta 68: 3231-3238.

Borrok D, Turner BF, Fein JB. 2005. A universal surface complexation framework for modeling proton binding onto bacterial surfaces in geologic settings. American Journal of Science 305: 826-853.

Boukhalfa H, Reilly SD, Michalczyk R, Iyer S, Neu MP. 2006. Iron(III) Coordination Properties of a Pyoverdin Siderophore Produced by Pseudomonas putida ATCC 33015. Inorganic Chemistry 45: 5607-5616.

Bourcier WL. 1997. Personal Communication.

Bourcier WL, Peiffer DW, Knauss KG, McKeegan KD, Smith DK. 1989. A kinetic model for borosilicate glass dissolution based on the dissolution affinity of a surface alteration layer. Paper presented at Materials Research Society Fall Meeting, Boston, Massachusetts.

Bowman J. 2006. The Methanotrophs — The Families Methylococcaceae and Methylocystaceae. Pages 266-289 in Dworkin M, Falkow S, Rosenberg E, Schleifer K-H, Stackebrandt E, eds. The Prokaryotes. A Handbook on the Biology of Bacteria: Proteobacteria; Alpha and Beta Subclasses, vol. 5. New York: Springer.

Bowman JP, McCammon SA, Skerrat JH. 1997. Methylosphaera hansonii gen. nov., sp. nov., a psychrophilic, group I methanotroph from Antarctic marine-salinity, meromictic lakes. Microbiology 143: 1451-1459.

Brady NC, Weil RR. 2002. The nature and properties of soils. Upper Saddle River, New Jersey: Prentice Hall.

Brady PV. 1991. The effect of silicate weathering on global temperature and atmospheric CO2. Journal of Geophysical Research 96: 101-118.

Brady PV, Dorn RI, Brazel AJ, Clark J, Moore RB, Glidewell T. 1999. Direct measurement of the combined effects of lichen, rainfall, and temperature onsilicate weathering. Geochimica et Cosmochimica Acta 63: 3293-3300.

Brantley SL. 2005. Reaction kinetics of primary rock-forming minerals under ambient conditions in Drever JI, ed. Surface and Ground Water, Weathering, and Soils, vol. 5 Elsevier.

Brantley SL, Liermann L, Bau M, Wu S. 2001. Uptake of Trace Metals and Rare Earth Elements from Hornblende by a Soil Bacterium. Geomicrobiology Journal 18: 37 - 61.

Bridge TAM, Johnson DB. 1998. Reduction of soluble iron and reductive dissolution of ferric iron-containing minerals by moderately thermophilic iron-oxidizing bacteria. Applied and Environmental Microbiology 64: 2181-2186.

Bronick CJ, Lal R. 2005. Soil structure and management: a review. Geoderma 124: 3-22.

Brown DA, Kamineni DC, Sawicki JA, Beveridge TJ. 1994. Minerals Associated with Biofilms Occurring on Exposed Rock in a Granitic Underground Research Laboratory. Appl. environ. Microbiol. 60: 3182-3191.

Brown DR, Kevan L. 1988. Aqueous coordination and location of exchangeable copper(2+) cations in montmorillonite clay studied by electron spin resonance and electron spin echo modulation. Journal of the American Chemical Society 110: 2743-2748.

Burrows KJ, Cornish A, Scott D, Higgins IJ. 1984. Substrate Specificities of the Soluble and Particulate Methane Mono-oxygenases of Methylosinus trichosporium OB3b. J Gen Microbiol 130: 3327-3333.

Carini S, Bano N, LeCleir G, Joye SB. 2005. Aerobic methane oxidation and methanotroph community composition during seasonal stratification in Mono Lake, California (USA). Environmental Microbiology 7: 1127-1138.

Casey WH, Bunker B. 1990. Leaching of mineral and glass surfaces during dissolution. Reviews in Mineralogy and Geochemistry 23: 397-426.
Certini G, Campbell CD, Edwards AC. 2004. Rock fragments in soil support a different microbial community from the fine earth. Soil Biology and Biochemistry 36: 1119-1128.

Chan ASK, Steudler PA, Bowden RD, Gulledge J, Cavanaugh CM. 2005. Consequences of nitrogen fertilization on soil methane consumption in a productive temperate deciduous forest. Biology and Fertility of Soils 41: 182-189.

Chander K, Brookes PC, Harding SA. 1995. Microbial biomass dynamics following addition of metal-enriched sewage sludges to a sandy loam. Soil Biology and Biochemistry 27: 1409-1421.

Chappell MA, Evangelou VP. 2000. Influence of Added K+ on Inducing Ammonium Fixation and Inhibiting Nitrification. Soil Science 165: 420-426.

Choi D, et al. 2006a. Spectral, kinetic, and thermodynamic properties of Cu(I) and Cu(II) binding by methanobactin from *Methylosinus trichosporium* OB3b. Biochemistry 45: 1142-1453.

Choi D, et al. 2006b. Spectral and thermodynamic properties of Ag(I), Au(III), Cd(II), Co(II), Fe(III), Hg(II), Mn(II), Ni(II), Pb(II), U(IV), and Zn(II) binding by methanobactin from Methylosinus trichosporium OB3b. Journal of Inorganic Biochemistry 100: 2150-2161.

Choi DW, Kunz RC, Boyd ES, Semrau JD, Antholine WE, Han J-I, Zahn JA, Boyd JM, de la Mora AM, DiSpirito AA. 2003. The membrane-associated methane monooxygenase (pMMO) and pMMO-NADH:Quinone oxidoreductase complex from *Methylococcus capsulatus* Bath. Journal of Bacteriology 185: 5755-5764.

Choi DW, Antholine WE, Do YS, Semrau JD, Kisting CJ, Kunz RC, Campbell D, Rao V, Hartsel SC, DiSpirito AA. 2005. Effect of methanobactin on the activity and electron paramagnetic resonance spectra of the membrane-associated methane monooxygenase in *Methylococcus capsulatus* Bath. Microbiology 151: 3417-3426.

Chou L, Wollast R. 1985. Steady-state kinetics and dissolution mechanisms of albite. American Journal of Science 285: 963-993.

Cicerone RJ, Oremland RS. 1988. Biogeochemical aspects of atmospheric methane. Global Biogeochemical Cycles 2: 299-327.

Clesceri LS, Greenberg AE, Trussell RR. 1989. Standard Methods: For the Examination of Water and Wastewater. Washington, D.C.: American Public Health Association.

Coates AG, Jackson JBC, Collins LS, Cronin TM, Dowsett HJ, Bybell LM, Jung P, Obando JA. 1992. Closure of the isthmus of Panama-The near-shore marine record of Costa Rica and western Panama. Geological Society of America Bulletin 104: 814-828.

Cocozza C, Tsao CCG, Cheah S-F, Kraemer SM, Raymond KN, Miano TM, Sposito G. 2002. Temperature dependence of goethite dissolution promoted by trihydroxamate siderophores. Geochimica et Cosmochimica Acta 66: 431-438.

Condit R, et al. 2001. The Status of the Panama Canal Watershed and Its Biodiversity at the Beginning of the 21st Century. BioScience 51: 389-398.

Conrad R. 1996. Soil microorganisms as controllers of atmospheric trace gases (H_2, CO, CH_4, OCS, N_2O, and NO). Microbiological Reviews 60: 609-640.

Cornell RM, Schwertmann U. 2003. The Iron Oxides: Structure, Properties, Reactions, Occurences and Uses: John Wiley & Sons.

Cornish A, Nicholls KM, Scott D, Hunter BK, Aston WJ, Higgins IJ, Sanders JKM. 1984. In vivo 13C NMR Investigations of Methanol Oxidation by the Obligate Methanotroph Methylosinus trichosporium OB3b. J Gen Microbiol 130: 2565-2575.

Craig H, Chou CC, Welhan JA, Stevens CM, Engelkemeir A. 1988. The Isotopic Composition of Methane in Polar Ice Cores. Science 242: 1535-1539.

Dalton H. 1992. Methane oxidation by methanotrophs: physiological and mechanistic implications. Pages 85-114 in Murrell JC, Dalton H, eds. Methane and methanol utilizers. New York: Plenum Press.

Dalton H, Prior SD, Leak DJ, Stanley SH. 1984. Regulation and control of methane monooxygenase. Pages 75-82 in Crawford RL, Hanson RS, eds. Microbial growth on C1 compounds. Washington, D.C.: American Society for Microbiology.

Daughney CJ, Fortin D. 2002. Mineral adsorption and absorption by biological cells. Pages 3430-3446 in Hubbard A, ed. Encyclopedia of Surface and Colloid Science. New York: Marcel Dekker.

Davies BE. 1997. Deficiencies and toxicities of trace elements and micronutrients in tropical soils: Limitations of knowledge and future research needs. Environmental Toxicology and Chemistry 16: 75-83.

Davis JA, Kent DB. 1990. Surface complexation modeling in aqueous geochemistry. Reviews in Mineralogy and Geochemistry 23: 177-260.

Dedysh SN. 2002. Methanotrophic bacteria of acidic *Sphagnum* peat bogs. Microbiology 71: 638-650.

Dedysh SN, Derakshani M, Liesack W. 2001. Detection and enumeration of methanotrophs in acidic Sphagnum peat by 16S rRNA fluorescence in situ hybridization, including the use of newly developed oligonucleotide probes for *Methylocella palustris*. Applied and Environmental Microbiology 67: 4850-4857.

Demange P, Bateman A, Dell A, Abdallah MA. 1988. Structure of azotobactin D, a siderophore of Azotobacter vinelandii strain D (CCM 289). Biochemistry 27: 2745-2752.

Demange P, Wendenbaum S, Linget C, Mertz C, Cung MT, Dell A, Abdallah MA. 1990. Bacterial siderophores : structure and NMR assignment of pyoverdins Pa, siderophores of Pseudomonas aeruginosa ATCC 15692. BioMetals 3: 155-170.

Devlin JF. 1994. A simple and powerful method of parameter estimation using simplex optimization. Ground Water 32: 323-327.

Dietrich WE, Windsor DM, Dunne T. 1982. Geology, climate, and hydrology of Barro Colorado Island. Pages 21-46 in Leigh EG, Windsor DM, eds. The ecology of a tropical forest: Seasonal rhythms and long-term changes. Washington, D.C.: Smithsonian Institution Press.

Dietrich WE, Windsor DM, Dunne T. 1996. Geology, climate, and hydrology of Barro Colorado Island. Pages 19-46 in Leigh EG, Rand AS, Windsor DM, eds. The ecology of a tropical forest, seasonal rhythms and long term changes. Washington D.C.: Smithsonian Institution Press.

Dove PM. 1999. The dissolution kinetics of quartz in aqueous mixed cation solutions. Geochimica et Cosmochimica Acta 63: 3715-3727.

Dove PM, Crerar DA. 1990. Kinetics of quartz dissolution in electrolyte solutions using a hydrothermal mixed flow reactor. Geochimica et Cosmochimica Acta 54: 955-969.

Dove PM, Elston SF. 1992. Dissolution kinetics of quartz in sodium chloride solutions: Analysis of existing data and a rate model for 25∞C. Geochimica et Cosmochimica Acta 56: 4147-4156.

Dove PM, Nix CJ. 1997. The influence of the alkaline earth cations, magnesium, calcium, and barium on the dissolution kinetics of quartz. Geochimica et Cosmochimica Acta 61: 3329-3340.

Dove PM, Han N, De Yoreo JJ. 2005. Mechanisms of classical crystal growth theory explain quartz and silicate dissolution behavior. Proceedings of the National Academy of Sciences 102: 15357-15362.

Drever JI. 1994. The effect of land plants on weathering rates of silicate minerals. Geochimica et Cosmochimica Acta 58: 2325-2332.

Drever JI. 1997. The Geochemistry of Natural Waters: Surface and Groundwater Environments. Upper Saddle River, NJ: Prentice Hall.

Dumont MG, Murrell JC. 2005. Community-level analysis: Key genes of aerobic methane oxidation. Methods in Enzymology 397: 413-427.

Dunfield P, Knowles R. 1995. Kinetics of Inhibition of Methane Oxidation by Nitrate, Nitrite, and Ammonium in a Humisol. Applied and Environmental Microbiology 61: 3129-3135.

Dunfield P, Knowles R, Dumont R, Moore TR. 1993. Methane production and consumption in temperate and subarctic peat soils – response to temperate and pH. Soil Biology & Biochemistry 25: 321-326.

Dunfield PF, Liesack W, Henckel T, Knowles R, Conrad R. 1999. High-affinity methane oxidation by a soil enrichment culture containing a type II methanotroph. Applied and Environmental Microbiology 65: 1009-1014.

Eby GN. 2004. Principles of Environmental Geochemistry. Belmont, CA: Brooks/Cole.

Edwards KJ, Bach W, McCollom TM, Rogers DR. 2004. Neutrophilic iron-oxidizing bacteria in the ocean: Their habitats, diversity, and roles in mineral deposition, rock alteration, and biomass production in the deep-sea. Geomicrobiology Journal 21: 393-404.

Ehhalt D, et al. 2001. Atmospheric chemistry and greenhouse gases. Pages 239-288 in Joos F, McFarland M, eds. Climate Change 2001: The Scientific Basis. New York: Cambridge University Press.

Ehrlich HL. 1996. How microbes influence mineral growth and dissolution. Chemical Geology 132: 5-9.

Ehrlich HL. 1998. Geomicrobiology: its significance for geology. Earth-Science Reviews 45: 45-60.

Ehrlich HL. 2006. Geomicrobiology: relative role of bacteria and fungi as geomicrobial agents in Gadd GM, ed. Fungi in Biogeochemical Cycles, Cambridge University Press.

Elmer TH, Nordberg ME. 1958. Solubility of Silica in Nitric Acid Solutions. Journal of the American Ceramic Society 41: 517-520.

Emerson D, Moyer C. 1997. Isolation and characterization of novel iron-oxidizing bacteria that grow at circumneutral pH. Appl. environ. Microbiol. 63: 4784-4792.

Ensign SA, Hyman MR, Arp DJ. 1993. In vitro activation of ammonia monooxygenase from Nitrosomonas europaea by copper. Journal of Bacteriology 175: 1971-1980.

Essa MA, Farragallah MEA. 2006. Clay minerals and their interactions with heavy metals and microbes of soils irrigated by various water resources at Assiut, Egypt. Ass. Univ. Bull. Environ. Res. 9: 73-90.

Farquhar ML, Charnock JM, England KER, Vaughan DJ. 1996. Adsorption of Cu(II) on the (0001) Plane of Mica: A REFLEXAFS and XPS Study. Journal of Colloid and Interface Science 177: 561-567.

Faure G. 1998. Principles and Applications of Geochemistry. Upper Saddle River, New Jersey: Prentice Hall.

Fein JB, Daughney CJ, Yee N, Davis TA. 1997. A chemical equilibrium model for metal adsorption onto bacterial surfaces. Geochimica et Cosmochimica Acta 61: 3319-3328.
Ferris FG. 1989. Metallic ion interactions with the outer membrane of gram-negative bacteria. Pages 295-323 in Beveridge TJ, Doyle RJ, eds. Metal Ions and Bacteria. New York: Wiley.

Ferris FG. 2005. Biogeochemical properties of bacteriogenic iron oxides. Geomicrobiology Journal 22: 79-85.

Ferris FG, Konhauser KO, Lyven B, Pedersen K. 1999. Accumulation of metals by bacteriogenic iron oxides in a subterranean environment. Geomicrobiology Journal 16: 181-192.
Ferris FG, Hallberg RO, LyvÈn B, Pedersen K. 2000. Retention of strontium, cesium, lead and uranium by bacterial iron oxides from a subterranean environment. Applied Geochemistry 15: 1035-1042.

Finzi AC, Canham CD, Van Breemen N. 1998. Canopy tree-soil interactions within temperate forests: Species effects on pH and cations. Ecological Applications 8: 447-454.

Flogeac K, Guillon E, Aplincourt M. 2004. Surface Complexation of Copper(II) on Soil Particles: EPR and XAFS Studies. Environmental Science & Technology 38: 3098-3103.

Forster P, et al. 2007. Changes in atmospheric constituents and in radiative forcing in Solomon S, Qin D, Manning M, Chen Z, Marquis M, Averyt KB, Tignor M, Miller HL, eds. Climate Change 2007: The Physical Science Basis. New York: Cambridge University Press.

Foster RB, Brokaw NVL. 1996. Structure and history of the vegetation of Barro Colorado Island. Pages 67-81 in Leigh EG, Rand AS, Windsor DM, eds. The ecology of a tropical forest, seasonal rhythms and long-term changes. Washington D.C.: Smithsonian Institution Press.

Fowle DA, Kulczycki E, Roberts JA. 2004. Linking bacteria-metal interactions to mineral attachment: A role for outer sphere complexation of cations? Paper presented at International Symposium on Water-Rock Interaction WRI-11, Saratoga Springs, NY, USA.

Fox BG, Froland WA, Dege JE, Lipscomb JD. 1989. Methane monooxygenase from *Methylosinus trichosporium* OB3b. Purification and properties of a three-component system with high specific activity from a type II methanotroph. The Journal of Biological Chemistry 264: 10023-10033.

Furrer G, Stumm W. 1986. The coordination chemistry of weathering: I. Dissolution kinetics of alpha-Al_2O_3 and BeO. Geochimica et Cosmochimica Acta 50: 1847-1860.

Gardner LR. 1970. A chemical model for the origin of gibbsite from kaolinite. The American Mineralogist 55: 1380-1389.

Garrels RM, Christ CL. 1965. Solutions, Minerals and Equilibria. New York: Harper & Row.

Garrison JM, Crumbliss AL. 1987. Kinetics and mechanism of aluminum(III)/siderophore ligand exchange: mono(deferriferrioxamine B) aluminum(III)

formation and dissociation in aqueous acid solution. Inorganica Chimica Acta 138: 61-65.

Gautier J-M, Oelkers EH, Schott J. 1994. Experimental study of K-feldspar dissolution rates as a function of chemical affinity at 150^{o}C and pH 9. Geochimica et Cosmochimica Acta 58: 4549-4560.

Gleeson DB, Kennedy NM, Clipson N, Melville K, Gadd GM, McDermott FP. 2006. Characterization of Bacterial Community Structure on a Weathered Pegmatitic Granite. Microbial Ecology 51: 526-534.

Godsy S, Elsenbeer H, Stallard R. 2004. Overland flow generation in two lithologically distinct rainforest catchments. Journal of Hydrology 295: 276-290.

Gorby Y, et al. 2006. Electrically conductive bacterial nanowires produced by Shewanella oneidensis strain MR-1 and other microorganisms. Proceedings of the National Academy of Sciences 103: 11358-11363.

Goudar CT, Devlin JF. 2001. Nonlinear estimation of microbial and enzyme kinetic parameters from progress curve data. Water Environment Research 73: 260-265.

Goyne KW, Brantley SL, Chorover J. 2006. Effects of organic acids and dissolved oxygen on apatite and chalcopyrite dissolution: Implications for using elements as organomarkers and oxymarkers. Chemical Geology 234: 28-45.

Graham DW, Lindner AS, Kim HJ. 2003. Methanotrophic Bacteria in Bitton G, ed. Encyclopedia of Environmental Microbiology. New York: Wiley Publishing.

Graham DW, Chaudhary JA, Hanson RS, Arnold RG. 1993. Factors affecting competition between Type I and Type II methanotrophs intwo-organism, continuous-flow reactors. Microbiol Ecology 25: 1-17.

Graham DW, Korich DG, LeBlanc RP, Sinclair NA, Arnold RG. 1992. Applications of a colorimetric plate assay for soluble methane monooxygenase activity. Appl. environ. Microbiol. 58: 2231-2236.

Grandstaff DE. 1986. The dissolution rate of forsteritic olivine from Hawaiian beach sand. Pages 41-60 in Colman SM, Dethier DP, eds. Rates of Chemical Weathering of Rocks and Minerals. New York: Academic Press.

Gulledge J, Schimel JP. 1998. Low-Concentration Kinetics of Atmospheric CH4 Oxidation in Soil and Mechanism of NH_4^+ Inhibition. Applied and Environmental Microbiology 64: 4291-4298.

Gulledge J, Hrywna Y, Cavanaugh C, Steudler PA. 2004. Effects of long-term nitrogen fertilization on the uptake kinetics of atmospheric methane in temperate forest soils. FEMS Microbiology Ecology 49: 389-400.

Hakemian AS, Rosenzweig AC. 2007. The biochemistry of methane oxidation. Annual Review of Biochemistry 76: 223-241.

Hakemian AS, Tinberg CE, Kondapalli KC, Telser J, Hoffman BM, Stemmler TL, Rosenzweig AC. 2005. The copper chelator methanobactin from *Methylosinus trichosporium* OB3b binds copper(I). Journal of the American Chemical Society 127: 17142-17143.

Hall POJ, Aller RC. 1992. Rapid, small-volume, flow injection analysis for $\sum CO_2$ and NH_4^+ in marine and freshwaters. Limnology and Oceanography 37: 1113-1119.

Hallam SJ, Putnam N, Preston CM, Detter JC, Rokhsar D, Richardson PM, DeLong EF. 2004. Reverse Methanogenesis: Testing the Hypothesis with Environmental Genomics. Science 305: 1457-1462.

Hanson RS, Hanson TE. 1996. Methanotrophic bacteria. Microbiological Reviews 60: 439-471.

Hausrath EM, Liermann LJ, House CH, Ferry JG, Brantley S. 2007. The effect of methanogen growth on mineral substrates: will Ni markers of methanogen-based communities be detectable in the rock record? Geobiology 5: 49-61.

Hayes KF, Katz LE. 1995. Application of X-ray absorption spectroscopy for surface complexation modeling of metal ion sorption. Pages 147-224 in Brady PV, ed. Physics and Chemistry of Mineral Surfaces. New York: CRC Press.

Hayes KF, Traina SJ. 1998. Metal ion speciation and its significance in ecosystem health. Pages 45-84 in Huang PM, ed. Soil Chemistry and Ecosystem Health, vol. 52. Madison, WI: Soil Science Society of America.

Helgeson HC, Murphy WM, Aagaard P. 1984. Thermodynamic and kinetic constraints on reaction rates among minerals and aqueous solutions. II. Rate constants, effective surface area, and the hydrolysis of feldspar. Geochimica et Cosmochimica Acta 48: 2405-2432.

Hendricks SP. 1993. Microbial Ecology of the Hyporheic Zone: A Perspective Integrating Hydrology and Biology. Journal of the North American Benthological Society 12: 70-78.

Hersman L, Lloyd T, Sposito G. 1995. Siderophore-promoted dissolution of hematite. Geochimica et Cosmochimica Acta 59: 3327-3330.

Hersman L, Maurice P, Sposito G. 1996. Iron acquisition from hydrous Fe(III)-oxides by an aerobic Pseudomonas sp. Chemical Geology 132: 25-31.

Hersman LE, Huang A, Maurice PA, Forsythe JH. 2000. Siderophore production and iron reduction by Pseudomonas mendocina in response to iron deprivation. Geomicrobiology Journal 17: 261-273.

Hider R. 1984. Siderophore mediated absorption of iron. Structure and Bonding 58: 25-87.

Higgins IJ, Best DJ, Hammond RC, Scott D. 1981. Methane-oxidizing microorganisms. Microbiol. Mol. Biol. Rev. 45: 556-590.

Hiroki M. 1992. Effects of Heavy Metal Contamination on Soil Microbial Population. Soil science and plant nutrition 38: 141-147.

Holmen BA, Casey WH. 1996. Hydroxamate ligands, surface chemistry, and the mechanism of ligand-promoted dissolution of goethite [alpha-FeOOH(s)]. Geochimica et Cosmochimica Acta 60: 4403-4416.

Hooper AB, Vannelli T, Bergmann DJ, Arciero DM. 1997. Enzymology of the oxidation of ammonia to nitrite by bacteria. Antonie van Leeuwenhoek 71: 59-67.

Hoppert M, Flies C, Pohl W, Gunzl B, Scheider J. 2004. Colonization strategies of lithobiontic microorganisms on carbonate rocks. Environmental Geology 46: 421-428.

Houweling S, Kaminski T, Dentener F, Lelieveld J, Heimann M. 1999. Inverse modeling of methane sources and sinks using the adjoint of a global transport model. Journal of Geophysical Research 104: 26137-26160.

Hu X, Boyer GL. 1996. Siderophore-Mediated Aluminum Uptake by Bacillus megaterium ATCC 19213. Appl. environ. Microbiol. 62: 4044-4048.

Hubley JH, Thomson AW, Wilkinson JF. 1975. Specific inhibitors of methane oxidation in Methylosinus trichosporium. Archives of Microbiology 102: 199-202.

Hughes MN, Poole RK. 1989. Metals and Microorganisms: Chapman & Hall.

Hutchens E, Valsami-Jones E, McEldowney S, Gaze W, McLean J. 2003. The role of heterotrophic bacteria in feldspar dissolution -- an experimental approach. Mineral Mag 67: 1157-1170.

Hyun SP, Cho YH, Kim SJ, Hahn PS. 2000. Cu(II) Sorption Mechanism on Montmorillonite: An Electron Paramagnetic Resonance Study. Journal of Colloid and Interface Science 222: 254-261.

Icenhower JP, Dove PM. 2000. The dissolution kinetics of amorphous silica into sodium chloride solutions: Effects of temperature and ionic strength. Geochimica et Cosmochimica Acta 64: 4193-4203.

Jansson SL. 1958. Tracer studies on nitrogen transformations in soil with special attention to mineralization-immobilization relationships. Annals of the Royal Agricultural College of Sweden 24: 101-361.

Jenkinson DS, Fox RH, Rayner JH. 1985. Interactions between fertilizer nitrogen and soil nitrogen; the so-called 'priming' effect. European Journal of Soil Science 36: 425-444.

John R, et al. 2007. Soil nutrients influence spatial distributions of tropical tree species. Proceedings of the National Academy of Sciences 104: 864-869.

Johnson MJ, Stallard RF. 1989. Physiography controls on sediments derived from volcanic and sedimentary terrains on Barro Colorado Island Panama. Journal of Sedimentary Petrology 59: 768-781.

Kalinowski BE, Liermann LJ, Givens S, Brantley SL. 2000. Rates of bacteria-promoted solubilization of Fe from minerals: review of problems and approaches. Chemical Geology 169: 357-370.

Kardos LT. 1955. Soil fixation of plant nutrients. Pages 177-199 in Bear FE, ed. Chemistry of the Soil. New York: Reinhold Publishing Corporation.

Karlsson M, Craven C, Dove PM, Casey WH. 2001. Surface charge concentrations on silica in different 1.0 M metal-chloride background electrolytes and implications for dissolution rates. Aquatic Geochemistry 7: 13-32.

Karlsson Tr, Persson P, Skyllberg U. 2006. Complexation of Copper(II) in Organic Soils and in Dissolved Organic Matter ,àí EXAFS Evidence for Chelate Ring Structures. Environmental Science & Technology 40: 2623-2628.

Keller M, Stallard RF. 1994. Methane emission by bubbling from Gatun Lake, Panama. J. Geophys. Res. 99.

Khalil MAK, Rasmussen RA. 1987. Atmospheric methane: Trends over the last 10,000 years. Atmospheric Environment 21: 2445-2452.

Kightley D, Nedwell DB, Cooper M. 1995. Capacity for methane oxidation in landfill cover soils measured in laboratory-scale soil microcosms. Environmental Microbiology 61: 592-601.

Kim D, Duckworth OW, Strathmann TJ. 2010. Reactions of aqueous iron-DFOB (desferrioxamine B) complexes with flavin mononucleotide in the absence of strong iron(II) chelators. Geochimica et Cosmochimica Acta 74: 1513-1529.

Kim HJ, Galeva N, Larive CK, Alterman M, Graham DW. 2005. Purification and physical-chemical properties of methanobactin: A chalkophore from *Methylosinus trichosporium* OB3b. Biochemistry 44: 5140-5148.

Kim HJ, Graham DW. 2003. Effects of oxygen and nitrogen conditions on the transformation kinetics of 1,2-dichloroethenes by *Methylosinus trichosporium* OB3b and its sMMOC mutant. Biodegradation 14: 407-414.

Kim HJ, Graham DW, DiSpirito AA, Alterman M, Galeva N, Larive CK, Asunskis D, Sherwood PMA. 2004. Methanobactin, a copper-acquisition compound from methane-oxidizing bacteria. Science 305: 1612-1615.

King GM. 1990. Regulation by light of methane emissions from a wetland. Nature 345: 513-515.

King GM, Schnell S. 1994. Ammonium and nitrite inhibition of methane oxidation by *Methylobacter albus* BG8 and *Methylosinus trichosporium* OB3b at low methane concentrations. Applied and Environmental Microbiology 60: 3508-3513.

Kjoller A, Andersson M, Miller M, Struwe S. 2001. Selected methods in soil microbiology. Copenhagen, Denmark: Department of General Microbiology, Institute of Molecular Biology, University of Copenhagen.

Knapp CW. 2005. Unpublished data.

Knapp CW, Fowle DA, Kulczycki E, Roberts JA, Graham DW. 2007. Methane monooxygenase gene expression mediated by methanobactin in the presence of mineral copper sources. Proceedings of the National Academy of Sciences 104: 12040-12045.

Knecht MR, Wright DW. 2004. Amine-Terminated Dendrimers as Biomimetic Templates for Silica Nanosphere Formation. Langmuir 20: 4728-4732.

Knowles R. 2005. Denitrifiers associated with methanotrophs and their potential impact on the nitrogen cycle. Ecological Engineering 24: 441-446.

Konhauser KO. 2007. Introduction to Geomicrobiology. Malden, MA: Blackwell Publishing Company.

Kostka JE, Haefele E, Viehweger R, Stucki JW. 1999. Respiration and Dissolution of Iron(III)-Containing Clay Minerals by Bacteria. Environmental Science & Technology 33: 3127-3133.

Kraemer SM. 2004. Iron oxide dissolution and solubility in the presence of siderophores. Aquatic Sciences 66: 3-18.

Kruger M, et al. 2003. A conspicuous nickel protein in microbial mats that oxidize methane anaerobically. Nature 426: 878-881.

Kulczycki E, Ferris FG, Fortin D. 2002. Impact of cell wall structure on the behavior of bacterial cells as sorbents of cadmium and lead. Geomicrobiology Journal 19: 553-565.

Kulczycki E, Fowle DA, Fortin D, Ferris FG. 2005. Sorption of cadmium and lead by bacteria-ferrihydrite composites. Geomicrobiology Journal 22: 299-310.

Kulczycki E, Fowle DA, Knapp CW, Graham DW, Roberts JA. 2007. Methanobactin-promoted dissolution of Cu-substituted borosilicate glass. Geobiology 5: 251-263.

Kulczycki E, Fowle DA, Kenward PA, Leslie K, Graham DW, Roberts JA. 2010. Stimulation of methanotroph activity by Cu-substituted borosilicate glass. Geomicrobiology Journal. *In Press*.

Langley S, Beveridge TJ. 1999. Effect of O-Side-Chain-Lipopolysaccharide Chemistry on Metal Binding. Appl. environ. Microbiol. 65: 489-498.

Lankford CE. 1973. Bacterial assimilation of iron. Critical Reviews in Microbiology 2: 273-331.

Lasaga AC. 1981. Rate laws of chemical reactions. Pages 1-67 in Lasaga AC, Kirkpatrick RJ, eds. Kinetics of Geochemical Processes, vol. 8. Washington, D.C.

Lasaga AC, Soler JM, Ganor J, Burch TE, Nagy KL. 1994. Chemical weathering rate laws and global geochemical cycles. Geochimica et Cosmochimica Acta 58: 2361-2386.

Le Bas MJ. 2000. IUGS reclassification of the high-Mg and picritic volcanic rocks. Journal of Petrology 41: 1467-1470.

Le Mer J, Roger P. 2001. Production, oxidation, emission and consumption of methane by soils: A review. European Journal of Soil Biology 37: 25-50.

Leak DJ, Dalton H. 1986. Growth yields of methanotrophs. Applied Microbiology and Biotechnology 23: 470-476.

Ledyard KM, Butler A. 1997. Structure of putrebactin, a new dihydroxamate siderophore produced by Shewanella putrefaciens. Journal of Biological Inorganic Chemistry 2: 93-97.

Lee J-U, Fein JB. 2000. Experimental study of the effects of Bacillus subtilis on gibbsite dissolution rates under near-neutral pH and nutrient-poor conditions. Chemical Geology 166: 193-202.

Lee S-W, Im J, DiSpirito A, Bodrossy L, Barcelona M, Semrau J. 2009. Effect of nutrient and selective inhibitor amendments on methane oxidation, nitrous oxide production, and key gene presence and expression in landfill cover soils: characterization of the role of methanotrophs, nitrifiers, and denitrifiers. Applied Microbiology and Biotechnology 85: 389-403.

Leigh EG. 1996. Introduction in Leigh EG, Rand AS, Windsor DM, eds. The ecology of a tropical forest, seasonal rhythms and long-term changes. Washington D.C.: Smithsonian Institute.

Leigh EG. 1999. Tropical forest ecology: a view from Barro Colorado Island. New York: Oxford University Press.

Leong J, Neilands JB. 1976. Mechanisms of siderophore iron transport in enteric bacteria. J. Bacteriol. 126: 823-830.

Lewis AG. 1995. Copper in Water and Aquatic Environments. New York: International Copper Association.

Lieberman R, Rosenzweig A. 2004. Biological Methane Oxidation: Regulation, Biochemistry, and Active Site Structure of Particulate Methane Monooxygenase. Critical Reviews in Biochemistry and Molecular Biology 39: 147-164.

Liermann LJ, Kalinowski BE, Brantley SL, Ferry JG. 2000a. Role of bacterial siderophores in dissolution of hornblende. Geochimica et Cosmochimica Acta 64: 587-602.

Liermann LJ, Guynn RL, Anbar A, Brantley SL. 2005. Production of a molybdophore during metal-targeted dissolution of silicates by soil bacteria. Chemical Geology 220: 285-302.

Liermann LJ, Barnes AS, Kalinowski BE, Zhou X, Brantley SL. 2000b. Microenvironments of pH in biofilms grown on dissolving silicate surfaces. Chemical Geology 171: 1-16.

Lontoh S, Semrau JD. 1998. Methane and trichloroethylene degradation by *Methylosinus trichosporium* OB3b expressing particulate methane monooxygenase. Applied and Environmental Microbiology 64: 1106-1114.

Loper JE, Henkels MD. 1999. Utilization of Heterologous Siderophores Enhances Levels of Iron Available to Pseudomonas putida in the Rhizosphere. Appl. environ. Microbiol. 65: 5357-5363.

Luttge A, Conrad PG. 2004. Direct Observation of Microbial Inhibition of Calcite Dissolution. Appl. environ. Microbiol. 70: 1627-1632.

Madigan M, Martinko J. 2005. Brock Biology of Microorganisms. Upper Saddle River, NJ: Prentice Hall, Inc.

Maher K, Steefel CI, White AF, Stonestrom DA. 2009. The role of reaction affinity and secondary minerals in regulating chemical weathering rates at the Santa Cruz Soil Chronosequence, California. Geochimica et Cosmochimica Acta 73: 2804-2831.

Mancinelli RL. 1995. The regulation of methane oxidation in soil. Annual Reviews in Microbiology 49: 581-605.

Margerum DW, Cayley GR, Weatherburn DC, Pagenkopf GK. 1978. Kinetics and mechanisms of complex formation and ligand exchange in Martell AE, ed. Coordination Chemistry, vol. 2. Washington: ACS.

Markwiese JT, Colberg PJS. 2000. Bacterial reduction of copper-contaminated ferric oxide: Copper toxicity and the interaction between fermentative and iron-reducing bacteria. Archives of Environmental Contamination and Toxicology 38: 139-146.

Martinez RE, Smith DS, Kulczycki E, Ferris FG. 2002. Determination of intrinsic bacterial surface acidity constants using a Donnan Shell Model and a continuous pK_a distribution method. Journal of Colloid and Interface Science 253: 130-139.

Mason I. 1977. Methane as a carbon source in biological denitrification. Water Pollution Control Federation 49: 855-857.

Maurice P, Forsythe J, Hersman L, Sposito G. 1996. Application of atomic-force microscopy to studies of microbial interactions with hydrous Fe(III)-oxides. Chemical Geology 132: 33-43.

Maurice PA, Lee YJ, Hersman LE. 2000. Dissolution of Al-substituted goethites by an aerobic Pseudomonas mendocina var. bacteria. Geochimica et Cosmochimica Acta 64: 1363-1374.

Maurice PA, Vierkorn MA, Hersman LE, Fulghum JE, Ferryman A. 2001. Enhancement of kaolinite dissolution by an aerobic *Pseudomonas mendocina* bacterium. Geomicrobiology Journal 18: 21-35.

Mazer JJ, Walther JV. 1994. Dissolution kinetics of silica glass as a function of pH between 40 and 85∞C. Journal of Non-Crystalline Solids 170: 32-45.

McBride MB. 1982. Hydrolysis and dehydration reactions of exchangeable Cu2+ on hectorite. Clays and Clay Minerals 30: 200-206.

McBride MB. 1994. Environmental Soil Chemistry. New York: Oxford University Press.

Melack JM, Hess LL, Gastil M, Forsberg BR, Hamilton SK, Lima IBT, Novo EMLM. 2004. Regionalization of methane emissions in the Amazon Basin with microwave remote sensing. Global Change Biology 10: 530-544.

Mera MU, Beveridge TJ. 1993. Mechanism of silicate binding to the bacterial cell wall in Bacillus subtilis. J. Bacteriol. 175: 1936-1945.

Milonjić S, Kopečni M, Ilić Z. 1983. The point of zero charge and adsorption properties of natural magnetite. Journal of Radioanalytical and Nuclear Chemistry 78: 15-24.

Mitchell MS. 2000. Panama cascading systems in the tropical rain forest. Erosion Control 7.

Mitsch WJ, Gosselink JG. 2000. Wetlands. New York: John Wiley & Sons, Inc.

Mohr ECJ, Van Baren FA, Van Schuylenborgh J. 1972. Tropical Soils —A Comprehensive Study of Their Genesis. The Hague: Mouton lchtiarbaru – Van Hoeve.

Morel FMM, Hering JG. 1993. Principles and Applications of Aquatic Chemistry. New York: Wiley-Interscience.

Morey GW, Fournier RO, Rowe JJ. 1964. The solubility of amorphous silica at 25^{o}C. Journal of Geophysical Research 69: 1995-2002.

Morton JD, Hayes KF, Semrau JD. 2000a. Effect of copper speciation on whole-cell soluble methane monooxygenase activity in *Methylosinus trichosporium* OB3b. Applied and Environmental Microbiology 66: 1730-1733.

Morton JD, Hayes KF, Semrau JD. 2000b. Bioavailability of chelated and soil-adsorbed copper to *Methylosinus trichosporium* OB3b. Environmental Science and Technology 34: 4917-4922.

Muller G, Raymond KN. 1984. Specificity and mechanism of ferrioxamine-mediated iron transport in Streptomyces pilosus. J. Bacteriol. 160: 304-312.

Munsell Color. 1994. Munsell Soil Color Charts, Revised Edition: Macbeth Division of Kollmorgen Instruments Corporation.

Murrell JC. 2009. The Aerobic Methane Oxidizing Bacteria (Methanotrophs). Pages 1953-1966 in Timmis KN, ed. Handbook of Hydrocarbons and Lipid Microbiology. Berlin: Springer.

Murrell JC, Dalton H. 1983. Ammonia Assimilation in Methylococcus capsulatus (Bath) and other Obligate Methanotrophs. J Gen Microbiol 129: 1197-1206.

Murrell JC, Gilbert B, McDonald IR. 2000. Molecular biology and regulation of methane monooxygenase. Archives of Microbiology 173: 325-332.

Nair A, Juwarkar A, Singh S. 2007. Production and Characterization of Siderophores and its Application in Arsenic Removal from Contaminated Soil. Water, Air, & Soil Pollution 180: 199-212.

Neaman A, Chorover J, Brantley SL. 2005. Implications of the evolution of organic acid moieties for basalt weathering over geologic time. American Journal of Science 305: 147-185.

Neilands JB. 1982. Microbial Envelope Proteins Related to Iron. Annual Review of Microbiology 36: 285-309.

Neilands JB. 1995. Siderophores: Structure and Function of Microbial Iron Transport Compounds. Journal of Biological Chemistry 270: 26723-26726.

Neilands JB, Nakamura K. 1991. Detection, determination, isolation, characterization and regulation of microbial iron chelates in Winkelmann G, ed. Handbook of microbial iron chelates. Boca Raton, FL: CRC Press.

Nese O, Ennil KT. 2007. A kinetic study of nitrite adsorption onto sepiolite and powdered activated carbon. Desalination 223: 174-179.

Nguyen H-HT, Shiemke AK, Jacobs SJ, Hales BJ, Lidstrom ME, Chan SI. 1994. The nature of the copper ions in the membranes containing the particulate methane monooxygenase from *Methylococcus capsulatus* (Bath)*. The Journal of Biological Chemistry 269: 14995-15005.

Nies DH. 1999. Microbial heavy-metal resistance. Applied Microbiology and Biotechnology 51: 730-750.

Nordstrom DK, Plummer LN, Langmuir E, Busenberg E, May HM. 1990. Revised chemical equilibrium data for major water-mineral reactions and their limitations. Pages 398-413 in Melchior DC, Bassett RL, eds. Chemical Modeling in Aqueous Systems II. Washington, D.C.: American Chemical Society.

Nuria R, Montserrat S, Alicia F, Jose GL. 1995. Buffering capacity and H+ membrane conductance of Gram-negative bacteria. FEMS Microbiology Letters 130: 103-110.
O'Neill JG, Wilkinson JF. 1977. Oxidation of ammonia by methane-oxidizing bacteria and the effects of ammonia on methane oxidation. Journal of General Microbiology 100: 407-412.

Oelkers EH, Schott J. 1995. Experimental study of anorthite dissolution and the relative mechanism of feldspar hydrolysis. Geochimica et Cosmochimica Acta 59: 5039-5053.

Oelkers EH, Gislason SR. 2001. The mechanism, rates and consequences of basaltic glass disolution: I. An experimental study of the dissolution rates of basaltic glass as a function of aqueous Al, Si and oxalic acid concentration at 25^{o}C and pH = 3 and 11. Geochimica et Cosmochimica Acta: 21.

Oelkers EH, Schott J. 2009. Thermodynamics and kinetics of water-rock interaction: Mineralogical Society of America: Geochemical Society.

Oelkers EH, Schott J, Devidal J-L. 1994. The effect of aluminum, pH, and chemical affinity on the rates of aluminosilicate dissolution reactions. Geochimica et Cosmochimica Acta 58: 2011-2024.

Ojeda JJ, Romero-Gonzalez ME, Pouran HM, Banwart SA. 2008. In situ monitoring of the biofilm formation of Pseudomonas putida on hematite using flow-cell ATR-FTIR spectroscopy to investigate the formation of inner-sphere bonds between the bacteria and the mineral. Mineral Mag 72: 101-106.

Oliveira A, Pampulha ME. 2006. Effects of Long-Term Heavy Metal Contamination on Soil Microbial Characteristics. The Society for Biotechnology, Japan 102: 157-161.
Osei BA, Singh B. 1999. Electrophoretic mobility of some tropical soil clays: effect of iron oxides and organic matter. Geoderma 93: 325-334.

Page WJ. 1993. Growth conditions for the demonstration of siderophores and iron-repressible outer membrane proteins in soil bacteria, with an emphasis on free-living diazotrophs. in Barton LL, Hemming BC, eds. Iron Chelation in Plants and Soil Microorganisms, Academic Press, Inc.

Parkhurst DL. 1995. User's guide to PHREEQC-A computer program for speciation, reaction-path, advective-transport, and inverse geochemical calculations. Lakewood, CO: U.S. Geological Survey. Report no.

Paton S. 2005. 2005 Meteorological and Hydrological Summary for Barro Colorado Island. Panama: Smithsonian Tropical Research Institution. Report no.
Payne WJ. 1973. Reduction of nitrogenous oxides by microorganisms. Bacteriological Reviews 37: 409-452.

Pearman GI, Etheridge D, de Silva F, Fraser PJ. 1986. Evidence of changing concentrations of atmospheric CO_2, N_2O and CH_4 from air bubbles in Antarctic ice. Nature 320: 248-250.

Phelps PA, Agarwal SK, Speitel Jr. GE, Georgiou G. 1992. *Methylosinus trichosporium* OB3b mutants having constitutive expression of soluble methane monooxygenase in the presence of high levels of copper. Applied and Environmental Microbiology 58: 3701-3708.

Pokrovsky OS, Schott J. 2000. Kinetics and mechanism of forsterite dissolution at 25^{o}C and pH from 1 to 12. Geochimica et Cosmochimica Acta 64: 3313-3325.

Raghoebarsing AA, et al. 2006. A microbial consortium couples anaerobic methane oxidation to denitrification. Nature 440: 918-921.

Rajapaksha RMCP, Tobor-Kaplon MA, Baath E. 2004. Metal Toxicity Affects Fungal and Bacterial Activities in Soil Differently. Applied and Environmental Microbiology 70: 2966-2973.

Rimstidt JD, Barnes HL. 1980. The kinetics of silica-water reactions. Geochimica et Cosmochimica Acta 44: 1683-1699.

Riveros-Iregui DA, King JY. 2008. Isotopic Evidence Of Methane Oxidation Across The Surface Water-Ground Water Interface. Wetlands 28: 928-937.

Roberts JA. 2004. Inhibition and enhancement of microbial surface colonization: the role of silicate composition Chemical Geology 212: 313-327.

Roberts JA, Fowle DA, Hughes BT, Kulczycki E. 2006. Attachment behavior of *Shewanella putrefaciens* onto magnetite under aerobic and anaerobic conditions. Geomicrobiology Journal 23: 631-640.

Roberts JA, Bennett PC, Gonzalez LA, Macpherson GL, Milliken KL. 2004. Microbial precipitation of dolomite in methanogenic groundwater. Geology 32: 277-280.

Roberts Rogers J, Bennett PC. 2004. Mineral stimulation of subsurface microorganisms: release of limiting nutrients from silicates. Chemical Geology 203: 91-108.

Roberts Rogers J, Bennett P, Choi WJ. 2001. Enhanced weathering of silicates by subsurface microorganisms: a strategy to release limiting inorganic nutrients? Paper presented at Proceedings of the tenth international symposium on water-rock interaction WRI-10, 1461-1464.

Rogers JR, Bennett PC, Choi WJ. 1998. Feldspars as a source of nutrients for microorganisms. American Mineralogist 83: 1532-1540.

Roy R, Knowles R. 1994. Effects of Methane Metabolism on Nitrification and Nitrous Oxide Production in Polluted Freshwater Sediment. Appl. environ. Microbiol. 60: 3307-3314.

Russell JD, Parfitt RL, Fraser AR, Farmer VC. 1974. Surface structures of gibbsite goethite and phosphated goethite. Nature 248: 220-221.

Saarnio S, Alm J, Silvola J, Lohila A, Nykanen H, Martikainen PJ. 1997. Seasonal variation in CH_4 emissions and production and oxidation potentials at microsites on an oligotrophic pine fen. Oecologia 110: 414-422.

Santelli CM, Welch SA, Westrich HR, Banfield JF. 2001. The effect of Fe-oxidizing bacteria on Fe-silicate mineral dissolution. Chemical Geology 180: 99-115.

Schaider LA, Senn DB, Brabander DJ, McCarthy KD, Shine JP. 2007. Characterization of Zinc, Lead, and Cadmium in Mine Waste: Implications for Transport, Exposure, and Bioavailability. Environmental Science & Technology 41: 4164-4171.

Schaperdoth I, Liermann LJ, Brantley SL. 2007. The Effect of Polymeric Substances on Apatite Reactivity in the Presence of a Freshwater Cyanobacterium. Geomicrobiology Journal 24: 79 - 91.

Schimel JP, Jackson LE, Firestone MK. 1989. Spatial and temporal effects on plant-microbial competition for inorganic nitrogen in a California annual grassland. Soil Biology & Biochemistry 21: 1059-1066.

Schlesinger WH. 1997. Biogeochemistry: An Analysis of Global Change. San Diego: Academic Press.

Schnell S, King GM. 1994. Mechanistic Analysis of Ammonium Inhibition of Atmospheric Methane Consumption in Forest Soils. Applied and Environmental Microbiology 60: 3514-3521.

Schnell S, King GM. 1995. Stability of methane oxidation capacity to variations in methane and nutrient concentrations. FEMS Microbiology and Ecology 17: 285-294.

Schnell S, Maini PK. 2003. A century of enzyme kinetics: Reliability of the K_m and V_{max} estimates. Comments on Theoretical Biology 8: 169-187.

Schott J, Berner RA. 1983. X-ray photoelectron studies of the mechanism of iron silicate dissolution during weathering. Geochimica et Cosmochimica Acta 47: 2233-2240.

Schott J, Berner RA. 1985. Dissolution mechanisms of pyroxenes and olivines during weathering. Pages 35-53 in Drever JI, ed. The chemistry of weathering. Dordrecht, The Netherlands: Reidel.

Schwertmann U, Cornell RM. 1991. Iron Oxides in the Laboratory.

Schwertmann U, Herbillon AJ. 1992. Some aspects of fertility associated with the mineralogy of highly weathered tropical soils. Pages 47-59 in Lal R, Sanchez PA, eds. Myths and Science of Soils of the Tropics, vol. 29.

Segers R. 1998. Methane production and methane consumption: a review of processes underlying wetland methane fluxes. Biogeochemistry 41: 23-51.

Seidel A, Lobbus M, Vogelsberger W, Sonnefeld J. 1997. The kinetics of dissolution of silica 'Monospher' into water at different concentrations of background electrolyte. Solid State Ionics 101-103: 713-719.

Shacklette HT, Boerngen JG. 1984. Element concentrations in soils and other surficial materials of the conterminous United States. Washington: U.S. Geological Survey. Report no.

Shannon R. 1976. Revised effective ionic radii and systematic studies of interatomic distances in halides and chalcogenides. Acta Crystallographica Section A 32: 751-767.

Sher FM, Baker R. 1982. Effect of Pseudomonas putida and a synthetic iron chelator on induction of soil suppressiveness to Fusarium wilt pathogens. Ecology and Epidemiology 72: 1567-1573.

Shockman GD, Barrett JF. 1983. Structure, function, and assembly of cell walls of gram-positive bacteria. Annual Reviews in Microbiology 37: 501-527.

Small TD, Warren LA, Ferris FG. 2001. Influence of ionic strength on strontium sorption to bacteria, Fe(III) oxide, and composite bacteria-Fe(III) oxide surfaces. Applied Geochemistry 16: 939-946.

Sposito G. 1984. The surface chemistry of soils. New York: Oxford University Press.

Stallard R. 1985. River chemistry, geology, geomorphology, and soils in the Amazon and Orinoco basins. Pages 293-316 in Drever JI, ed. The chemistry of weathering. Dordrecht, Netherlands: D. Reidel Publishing Company.

Stanley SH, Prior SD, Leak DJ, Dalton H. 1983. Copper stress underlies the fundamental change in intracellular location of methane monooxygenase in methane-oxidizing organisms: Studies in batch and continuous cultures. Biotechnology Letters 5: 487-492.

Steudler PA, Bowden RD, Melillo JM, Aber JD. 1989. Influence of nitrogen fertilization on methane uptake in temperate forest soils. Nature 341: 314-316.

Stevens L, Price NC. 1999. Fundamentals of enzymology: the cell and molecular biology of catalytic proteins. Oxford: Oxford University Press.

Stone AT. 1997. Reactions of extracellular organic ligands with dissolved metal ions and mineral surfaces. Reviews in Mineralogy and Geochemistry 35: 309-344.

Stookey LL. 1970. Ferrozine: a new spectrophotometric reagent for iron. Analytical Chemistry 42: 779-781.

Strickland JDH, Parsons TR. 1968. A Practical Handbook of Seawater Analysis. Ottawa: Fisheries Board of Canada Bulletin.

Strous M, Jetten MSM. 2004. Anaerobic oxidation of methane. Annual Reviews in Microbiology 58: 99-117.

Stumm W, Furrer G. 1987. The dissolution of oxides and aluminum silicates; examples of surface coordination-controlled kinetics in Stumm W, ed. Aquatic Surface Chemistry. New York: Wiley-Interscience.

Stumm W, Wollast R. 1990. Coordination chemistry of weathering: Kinetics of the surface-controlled dissolution of oxide minerals. Reviews in Geophysics 28: 53-69.
Stumm W, Morgan JJ. 1996. Aquatic Chemistry. New York: John Wiley.

Sutheimer SH, Maurice PA, Zhou Q. 1999. Dissolution of well and poorly crystallized kaolinites: Al speciation and effects of surface characteristics. American Mineralogist 84: 620-628.

Tate KR, Salcedo I. 1988. Phosphorus Control of Soil Organic Matter Accumulation and Cycling. Biogeochemistry 5: 99-107.

Tellez CM, Gaus KP, Graham DW, Arnold RG, Guzman RZ. 1998. Isolation of copper biochelates from *Methylosinus trichosporium* OB3b and soluble methane monooxygenase mutants. Applied and Environmental Microbiology 64: 1115-1122.

Templeton AS, Staudigel H, Tebo BM. 2005. Diverse Mn(II)-Oxidizing Bacteria Isolated from Submarine Basalts at Loihi Seamount. Geomicrobiology Journal 22: 127 - 139.

Theisen AR, Murrell JC. 2005. Facultative methanotrophs revisited. Journal of Bacteriology 187: 4303-4305.

Theng BKG, Wells N. 1995. The flow characteristics of halloysite suspensions. Clay Minerals 30: 99-106.

Toukdariant AE, Lidstrom ME. 1984. Nitrogen Metabolism in a New Obligate Methanotroph, 'Methylosinus' Strain 6. J Gen Microbiol 130: 1827-1837.

Tourtelot HA. 1971. Chemical compositions of rock types as factors in our environment. Pages 13-29 in Cannon HL, Hopps HC, eds. Environmental Geochemistry in Health and Disease, vol. 123. Boulder, CO: Geological Society of America.

Ullman WJ, Welch SA. 2002. Organic ligands and feldspar dissolution. Pages 3-35 in Hellman R, Wood SA, eds. Water-Rock Interactions, Ore Deposits, and Environmental Geochemistry: A Tribute to David A. Crerar, vol. 7. St. Louis, Missouri: The Geochemical Society.

Ullman WJ, Kirchman DL, Welch SA, Vandevivere P. 1996. Laboratory evidence for microbially mediated silicate mineral dissolution in nature. Chemical Geology 132: 11-17.

Uroz S, Calvaruso C, Turpault M-P, Frey-Klett P. 2009. Mineral weathering by bacteria: ecology, actors and mechanisms. Trends in Microbiology 17: 378-387.

Valentine D. 2002. Biogeochemistry and microbial ecology of methane oxidation in anoxic environments: a review. Antonie van Leeuwenhoek 81: 271-282.

Vandevivere P, Bevaye P. 1993. Improved preservation of bacterial exopolymers for scanning electron microscopy. Journal of Microscopy 167: 323-330.

Vandevivere P, Welch SA, Ullman WJ, Kirchman DL. 1994. Enhanced dissolution of silicate minerals by bacteria at near-neutral pH. Microbiol Ecology 27: 241-251.

Vayssieres L. 2009. On the Effect of Nanoparticle Size on Water-Oxide Interfacial Chemistry. The Journal of Physical Chemistry C 113: 4733-4736.

Veizer J, Godderis Y, Francois LM. 2000. Evidence for decoupling of atmospheric CO_2 and global climate during the Phanerozoic eon. Nature 408: 698-701.

Viollier E, Inglett PW, Hunter K, Roychoudhury AN, Van Cappellen P. 2000. The ferrozine method revisited: Fe(II)/Fe(III) determination in natural waters. Applied Geochemistry 15: 785-790.

Vorhies JS, Gaines RR. 2009. Microbial dissolution of clay minerals as a source of iron and silica in marine sediments. Nature Geosci 2: 221-225.

Walker JCG, Hays PB, Kasting JF. 1981. A negative feedback mechanism for the long-term stabilization of the earth's surface temperature. Journal of Geophysical Research 86: 9776-9782.

Wang L, Chua H, Zhou Q, Wong PK, Sin SN, Lo WL, Yu PH. 2003. Role of cell surface components on Cu2+ adsorption by Pseudomonas putida 5-x isolated from electroplating effluent. Water Research 37: 561-568.

Wang ZP, DeLaune RD, Patrick WH, Jr., Masscheleyn PH. 1993. Soil Redox and pH Effects on Methane Production in a Flooded Rice Soil. Soil Sci Soc Am J 57: 382-385.

Weiner S, Dove PM. 2003. An overview of biomineralization processes and the problem of the vital effect. Reviews in Mineralogy and Geochemistry 54: 1-29.

Welch SA, Ullman WJ. 1993. The effect of organic acids on plagioclase dissolution rates and stoichiometry. Geochimica et Cosmochimica Acta 57: 2725-2736.

Welch SA, Vandevivere P. 1994. Effect of microbial and other naturally occurring polymers on mineral dissolution. Geomicrobiology Journal 12: 227 - 238.

Welch SA, Ullman WJ. 1999. The effect of microbial glucose metabolism on bytownite feldspar dissolution rates between 5^{o} and 35^{o}C. Geochimica et Cosmochimica Acta 63: 3247-3259.

Welch SA, McPhail DC. 2003. Mobility of major and trace elements during biologically mediated weathering of granite. Pages 437-440 in Roach IC, ed. Advances in Regolith, CRC LEME.

Welch SA, Barker WW, Banfield JF. 1999. Microbial extracellular polysaccharides and plagioclase dissolution. Geochimica et Cosmochimica Acta 63: 1405-1419.

Welch SA, Taunton AE, Banfield JF. 2002. Effect of microorganisms and microbial metabolites on apatite dissolution. Geomicrobiology Journal 19: 343-367.

Whalen SC, Reeburgh WS. 1990. Consumption of atmospheric methane by tundra soils. Nature 346: 160-162.

Whalen SC, Reeburgh WS, Barber VA. 1992. Oxidation of methane in boreal forest soils: a comparison of seven measures. Biogeochemistry 16: 181-211.

White AF, Blum AE. 1995. Effects of climate on chemical weathering in watersheds. Geochimica et Cosmochimica Acta 59: 1729-1747.

White AF, Blum AE, Schulz MS, Huntington TG, Peters NE, Stonestrom DA. 2002. Chemical weathering of the Panola Granite: Solute and regolith elemental fluxes and the weathering rate of biotite. Paper presented at Water-Rock Interactions, Ore Deposits, and Environmental Geochemistry: A Tribute to David A. Crerar.

White AF, Blum AE, Schulz MS, Vivit DV, Stonestrom SA, Larsen MC, Murphy SF, Eberl DD. 1998. Chemical weathering in a tropical watershed, Luquillo Mountains, Puerto Rico; I: Long-term versus short-term weathering fluxes. Geochimica et Cosmochimica Acta 62: 209-226.

White JR, Reddy KR, Moustafa MZ. 2004. Influence of hydrologic regime and vegetation on phosphorus retention in Everglades stormwater treatment area wetlands. Hydrological Processes 18: 343-355.

Whittenbury R, Phillips KC, Wilkinson JF. 1970. Enrichment, isolation and some properties of methane-utilizing bacteria. Journal of General Microbiology 61: 205-218.

Wichard T, Bellenger J-P, Morel FoMM, Kraepiel AML. 2009. Role of the Siderophore Azotobactin in the Bacterial Acquisition of Nitrogenase Metal Cofactors. Environmental Science & Technology 0.

Widdel F, Schnell S, Heising S, Ehrenreich A, Assmus B, Schink B. 1993. Ferrous iron oxidation by anoxygenic phototrophic bacteria. Nature 362: 834-836.

Wightman PG, Fein JB. 2004. The effect of bacterial cell wall adsorption on mineral solubilities. Chemical Geology 212: 247-254.

Williard KWJ, Dewalle DR, Edwards PJ. 2005. Influence of bedrock geology and tree species composition on stream nitrate concentrations in mid-appalachian forested watersheds. Water, Air, & Soil Pollution 160: 55-76.

Wilson A. 2005. Trace Metal Mobility in Tropical Rainforest and Adjacent Grassland Soils, Central PanamaThe University of Kansas, Lawrence, KS.

Winkelmann G. 1991. Specificity of iron transport in bacteria and fungi. CRC Handbook of Microbial Iron Chelates. Boca Raton, FL: CRC Press.

Wollast R, Chou L. 1992. Surface reactions during the early stages of weathering of albite. Geochimica et Cosmochimica Acta 56: 3113-3121.

Woodring WP. 1958. Geology of the Barro Colorado Island, Canal Zone. Washington D.C. Report no.

Wuebbles DJ, Hayhoe K. 2002. Atmospheric methane: Trends and impacts. Earth Science Reviews 57: 177-210.

Xi Y, Mallavarapu M, Naidu R. 2009. Preparation, characterization of surfactants modified clay minerals and nitrate adsorption. Applied Clay Science In Press.

Xia K, Mehadi A, Taylor RW, Bleam WF. 1997. X-Ray Absorption and Electron Paramagnetic Resonance Studies of Cu(II) Sorbed to Silica: Surface-Induced Precipitation at Low Surface Coverages. Journal of Colloid and Interface Science 185: 252-257.

Yavitt JB. 2000. Nutrient dynamics of soil derived from different parent material on Barro Colorado Island, Panama. Biotropica 32: 198-207.

Yee N, Fein JB. 2001. Cd adsorption onto bacterial surfaces: A universal adsorption edge? Geochimica et Cosmochimica Acta 65: 2037-2042.

Yokel RA. 2002. Aluminum chelation principles and recent advances. Coordination Chemistry Reviews 228: 97-113.

Yu W, Dodds WK, Banks K, Skalsky J, Strauss EA. 1995. Optimal staining and sample storage time for direct microscopic enumeration of total and active bacteria in soil with two fluorescent dyes. Applied and Environmental Microbiology 61: 3367-3372.

Zahn JA, DiSpirito AA. 1996. Membrane-associated methane monooxygenase from *Methylococcus capsulatus* (Bath). Journal of Bacteriology 178: 1018-1029.

Zhivotchenko AG, Nikonova ES, Jørgensen MH. 1995. Effect of fermentation conditions on N2 fixation by Methylococcus capsulatus. Bioprocess and Biosystems Engineering 14: 9-15.

Zhuang Q, Melack JM, Zimov S, Walter KM, Butenhoff CL, Khalil MAK. 2009. Global methane emissions from wetlands, rice paddies, and lakes. EOS, Transactions, American Geophysical Union 90: 37-44.

Zinder B, Furrer G, Stumm W. 1986. The coordination chemistry of weathering: II. Dissolution of Fe(III) oxides. Geochimica et Cosmochimica Acta 50: 1861-1869.

Zinke PJ. 1962. The Pattern of Influence of Individual Forest Trees on Soil Properties. Ecology 43: 130-133.

APPENDICES

Appendix A: Soil Profile Variability on the Barro Colorado Island

Appendix B: Cu-substituted Iron Oxide Synthesis & Methanobactin-promoted weathering of Cu-doped Ferrihydrite

Appendix C: Methanobactin-promoted dissolution of Gibbsite

Appendix D: Analysis of Copper-Methanobactin Complex

i. Chromophore Response to Cu-methanobactin complex formation
ii. Cu to methanobactin ratios
iii. KOH Titration of Cu:mb

Appendix E: Cover illustration of PNAS, volume 104, 2007.

Appendix F: Scanning electron microscopic images

Appendix A: Soil Profile Variability on Barro Colorado Island

ABSTRACT

The characteristics of two soil profiles on Barro Colorado Island (central Panama) are compared to assess the factors that contribute to variations in soil development. Characteristically, humid tropical soils are highly oxidized and intensely weathered. Site AVA2 represents a deeply weathered soil on the summit of a flat terrain that overlies a basaltic parent material. The site at Miller Forest is also highly weathered but is situated on more steeply sloping topography that overlies a parent material composed of basaltic clast conglomerates in a sandy volcaniclastic matrix. While major soil formation processes such as climate and vegetation remain constants for both sites, it is the differences in underlying parent material and topography that influence the variation in weathering and soil development at these two sites. The physical property differences of each soil profile are confirmed by multiple analyses that include determination of soil color, soil moisture, particle size, soil organic matter, and soil pH.

INTRODUCTION

The biochemical process of weathering promotes both the destruction of minerals with synthesis of new minerals, and plays a significant role in soil development (Turner et al. 2003). The five major factors that control soil development include climate, time, living organisms, parent material composition and topography (Jenny 1941). On Barro Colorado Island, climate and vegetation can be considered constants from one site to another. High annual temperatures and precipitation typical of humid tropical climates

promote intense leaching and rapid weathering of soil minerals (Turner et al. 2003; White and Blum 1995).

Semideciduous forests predominate BCI, and very little change in the flora of Panama has occurred over the last 35000 years (Foster and Brokaw 1982). Any minor variations in vegetation that might occur from one site to another (e.g., primary vs. secondary forests) are not expected to have a major impact upon the quantity of organic matter that is introduced into the soil. Forests on BCI have been protected since the island was declared a reserve in 1923 (Foster and Brokaw 1982), therefore anthropogenic disturbance is not an issue at these study sites.

The relative age of a soil may vary in terms of the degree of weathering and profile development, but such influences are dependent upon interaction with the parent material and the local topography. Residual parent materials are subject to greater lengths of soil-forming processes compared to transported parent material (Brady and Weil, 2002). Weathering and soil development will occur more rapidly on a level site compared to a sloping topographical setting, which is more prone to erosion. The type of parent material is particularly relevant to chemical weathering as some rock types are more resistant to weathering, e.g. quartzite (Schulz and White 1999), or are capable of buffering acidity, e.g., limestone (Appelo and Postma 1996). The amount of time that a mineral has been exposed to weathering conditions can also impact the rate at which it will dissolve. For instance, fine-grained micas and magnesium-rich chlorites represent earlier weathering stages of the silicates. Kaolinite and iron and aluminum oxides represent the most advanced stages of weathering. Intermediate stages are represented by smectites (e.g., montmorillonite) (Goldich 1938). More and more silicon tends to be

removed as weathering progresses, leaving a lower Si:Al ratio in the more highly weathered soil horizons (Brady and Weil, 2002).

SITE DESCRIPTION

Barro Colorado Island (BCI)

BCI is an inland island located in central Panama ($9^{o}10'$N, $70^{o}51'$W) that was isolated from the surrounding mainland in 1914 when the Chagras River was dammed and the Gatun Lake was formed (Figure 2.3). The island is a 1500-ha hill that protrudes 137 m above Gatun Lake, with a broad, flat top underlain by dense basalt, from which steep ridges and valleys radiate and cut into sedimentary rocks where volcanic debris has been deposited (Dietrich et al. 1982). Geographically situated in a humid tropical climate zone, BCI predominantly has soils that are classified as Oxisols, and are primarily composed of Fe, Al oxides and silicate clays with low Si/Al ratios. A distinct yellow or red hue is characteristic of these soils, e.g., laterites (Mohr et al. 1972).

AVA2 (Armour Trail)

AVA2 is a marker name for a site located along the Armour Trail ($9^{o}16'$N, $79^{o}85'$W) within the 50-hectare plot in the vicinity of the Conrad Trail Stream (Figure 2.5 and 3.3). This site location is on the broad, flat top of the island with an altitude of 170 m. The underlying parent material is dense basalt composed of extrusive and intrusive andesite (Dietrich et al. 1982, Woodring 1958). On the summit, erosion rates are low, root exposure is minimal and soils are over a meter deep. Cracking red clays are

found at depth while a brown, organically enriched horizon less than 5 cm thick typically occurs at the top of the soil profile (Dietrich et al. 1982).

Miller Forest

Sampling from the Miller Forest was in the location of the lighthouse at the NW coast of BCI ($9^{o}17'$N, $79^{o}85'$W) (Figure 2.5). Topography at this site has narrow, gently sloping (9^{o}) ridges (Dietrich et al. 1982) with an altitude of 81 m. The underlying parent material represents an exposed portion of the Bohio Formation, which contains basaltic clast conglomerates in a sandy volcaniclastic matrix (Woodring 1958). The clast size ranges from 5 to 50 cm in diameter and consist of basaltic andesite (52-57 SiO_2 wt%) (Le Bas 2000) with phenocrysts composed of plagioclase, hornblende or clinopyroxene (Wilson 2005). The poorly sorted sandy matrix is made up of a mixture of rounded, altered volcanic lithic fragments, angular plagioclase, and minor amphibole and magnetite (Wilson 2005). The soils of the Miller Forest are yellow-brown in color, less than 50 cm thick, and overly a layer of saprolite composed of boulder-sized chunks of fresh bedrock and thin weathering rinds. While the soils contain the occasional fresh gravel-sized rock, they are also rich in clay (Dietrich et al. 1982).

EXPERIMENTAL PROCEDURES

Field Sampling

Soil samples were collected from the surface down to one-meter depths from two different sites on BCI:

(1) AVA2 (Armour Trail)

(2) Miller Forest

In each location a soil pit was dug with dimensions 0.5 m wide x 1 m long x 1 m deep. Depth subsections of soil were collected at five cm intervals throughout the profile for a total of 20 samples in each pit. To prevent cross-contamination, gloves were worn by sample-collectors and extraction equipment was cleaned with ethanol before each sample was collected.

In the field, soils were examined using Munsell soil color charts (Munsell Color, 1994), hand texturing, and visual examination for root depth and structure characterization. Post collection, samples were stored in sterile sample bags at 4^{o}C for approximately 3 days before being transported in a cooler to the laboratory for long term storage at -80^{o}C.

LABORATORY METHODS AND TECHNIQUES

Four sets of analyses were performed comparatively between the samples collected from each site from surface to 1-m depth:

- Soil moisture
- Particle size
- Organic matter
- Soil pH

Soil Moisture was determined by the gravimetric method (Brady and Weil, 2002) at 5-cm intervals from surface to 1-m depth. Approximately 20-30 grams of wet soil per depth sampling interval was dried at 100^{o}C for at least 24 hours before weighing the mass of the dry soil. Soil moisture was calculated by the following equation:

100 x (Moisture weight)/(Dry soil weight) = % H_2O

Particle size distribution in the <2-mm fraction of soil was determined by the hydrometer method (Day 1965). Using approximately 50-gram samples at chosen depth intervals (AVA2: 10-cm, 30-cm, 50-cm, 70-cm and 100-cm; Miller Forest: 20-cm, 40-cm, 60-cm, 80-cm and 100-cm), samples were prepared by crushing with a mortar and pestle and plucking out solid organic matter in the form of roots or leaves. Samples were dispersed in a mixture of 5% Calgon solution (sodium hexametaphosphate) overnight (12-24 hours) before being mixed with an electronic mixer. Mixed samples were diluted to 1000 mL with D1 H_2O in a graduated cylinder and disturbed with a plunger before taking the initial hydrometer reading. A minimum of 2 hours elapsed before taking the second hydrometer reading, and both readings were calibrated with a blank solution of D1 H_2O mixed with the same proportion of 5% Calgon solution, while accounting for room temperature. The following calculations determined the percent of soil separates:

% Clay = (corrected hydrometer at 2 hours) x (100/sample weight)

% Silt = (corrected hydrometer reading at 40 seconds) x (100/sample weight) – (% clay)

% Sand = 100 – (% silt + % clay)

Organic matter content was determined by a modified dry combustion loss on ignition (LOI) procedure. Samples from random depth intervals were pre-dried at 100^{o}C for at least 24 hours before loading into muffle furnace. In the muffle furnace the temperature was ramped up to 450^{o}C and held steady at that temperature for 2 hours before cooling. The percentage of organic matter by weight was calculated by the following formula:

% Organic matter = [(C2-C3) / (C2-C1)] x 100

Where C1 = Crucible weight, C2 = Weight of crucible and sample (with organic matter), and C3 = Weight of crucible and sample (without organic matter).

Soil pH measurements were conducted at 5-cm intervals from surface to depth. Approximately 20-grams of sample was mixed with an equal proportion of distilled water, stirred at regular intervals within an hour and the pH was measured with a pre-calibrated glass electrode.

RESULTS

Field Results

Soil samples are collected from two different locations on BCI, which have different underlying parent material, and topography. Classification of soil colors with application of Munsell soil color charts (Munsell 1994) indicates that both soils are highly oxidized due to the reddish brown (site AVA2) and red-yellow brown (Miller Forest) colors that are prevalent throughout each respective profile (see Table A.1). The Munsell soil color chart encodes hue with a letter abbreviation, e.g., YR – yellow red, and value with a number and chroma being the last number (e.g., 7.5YR 3/4 is 7.5hue (yellow red) value/chroma). A value of 0 represents absolute black while a 10 represents absolute white. The soils at both sites are sesquioxide clays (Munsell 1994).

At both sites, the soils have little structure except for some spheroidal ped development where soil organic matter is present. The remainder of the soil is continuous and massive. Large roots extend no further than 25-30 cm into the profile, while smaller roots appear to penetrate the soil at various depths.

At site AVA2, the A horizon of the soil profile extends from the surface down to 15-cm. A Bt horizon represents the majority of the profile from 15-cm down to 100-cm. The reddening of the soil increases with depth. The color indicates that site AVA2 is a highly oxidized and weathered soil.

The Miller Forest has an A horizon extending down to 20-cm. A Bt horizon is evident between 20-cm and 35-cm, at which point whitish yellowish sand sized nodules first appear. The lower in depth the more abundant and larger the nodules become. This saprolitic layer is representative of a transition horizon between B and C to a depth of 60-cm. The sandier texture that predominates from 60-cm down to 100-cm is indicative of the C horizon as it contains a greater mixture of weathered regolith material. The yellowish hue to the brown soil increases with depth. The yellow nodules represent redoximorphic features found typically in environments that experience repeated wetting and drying conditions. These nodules may in fact be plinthites, which are composed of a mixture of iron-rich oxides, clay, and fine quartz (Davies 1997; Aide et al. 2004).

Laboratory Results

Comparative analyses of soil moisture shows that a higher proportion of water is held in the Miller Forest soil from surface to depth compared to soil profile at site AVA2 (Figure A.1). For both sites, a rapid decrease in soil moisture is evident from the upper profile to 15-cm for Miller Forest and 25-cm for AVA2. The moisture content remains stable from these depths down to 100-cm. A minor fluctuation depression occurs at 80-

cm for Miller Forest, while for AVA2, a depression occurs at 85-cm and spike in moisture at 95-cm.

Particle size analysis of site AVA2, indicates a high proportion of clay throughout the 1-m profile (Figure A.2). In the upper horizon of the sampled profile (10-cm), clay percentage drops from 47% down to 64% at 30-cm, and gently increases with depth. Silt percentage at 10-cm is 29%, and gently decreases to 19% at 50-cm, where it's value remains relatively stable down to 100-cm. The sand percentage is approximately 24% at 10-cm, and rapidly drops to 11% at 30-cm. The value remains relatively stable down to 70-cm, at which point it gently decreases down to 8% at 100-cm.

Particle size analysis of the Miller Forest site shows more variability throughout the depth profile (Figure A.3). Clay predominates the profile from 20-cm (50%) down to 60-cm (50%) (Note: at 40-cm, clay percentage increases to 60%), but sand predominates the lower profile from 80-cm (44%) to 100-cm (40%). Sand has the lowest percentage of soil separates at 20-cm (11%) but increases sharply from 40-cm (15%) to 80-cm (44%). The silt percentage value is relatively intermediate to clay and sand at 20-cm (39%) and decreases to 25% at 40-cm, where the value remains stable throughout the remainder of the depth profile. From 60-cm (22%) down to 100-cm (26%) the silt percentage is lower than both clay and sand at each respective interval.

Soil organic matter content for both site AVA2 and Miller Forest is higher than expected for typical tropical soils (Figure A.4) and the organic matter content of the soil at site AVA2 is relatively higher than the values measured for the Miller Forest. At site AVA2, the highest organic matter content (~13%) occurs in the upper profile (15-cm). At 35-cm the value drops to 11% and remains relatively stable throughout the remainder of

the depth profile down to 100-cm. At the Miller Forest site, the highest organic matter content (~10%) also occurs in the upper profile (20-cm). There is a gentle decrease in organic matter content throughout the remainder of the depth profile with approximately 5% organic matter content for 100-cm.

Soil pH measurements indicate that site AVA2 has a higher soil pH than Miller Forest throughout the majority of the profile (Figure A.5), especially from 20-cm down to 100-cm. For both sites, the highest pH values (~5-5.5) occur at the top of the profile (5-cm) and a sharp drop in pH occurs from 5 to 20-cm (~4.5). At site AVA2, the pH trend remains relatively stable from 20-cm down to 55-cm (pH 4.5), and fluctuated between pH 4.3 and 4.2 from 60-cm to 100-cm with a mild increase to pH 4.7 at 80-cm. At the Miller Forest, a gentle decrease in the pH trend is apparent between 20-cm (pH 4.3) and 100-cm (pH 3.6) with stable trends occurring between 40-cm and 60-cm (pH 3.9) and between 65-cm and 80-cm (pH 3.7).

DISCUSSION

Soil moisture differences between site AVA2 and Miller Forest provide a reflection of the strong rainfall seasonality on the Barro Colorado Island. The dry season typically ranges from December to April (Yavitt 2000) or January to May (Godsey et al. 2004). In dry seasons, the hydrology of the soil zone is unsaturated, thus increases in precipitation, moisture, and solvent throughput that occur in wet seasons will increase the wetted reactive surface areas of minerals making them more susceptible to weathering. The heightened moisture content in the soil will also improve the hydrological connectivity where increases in pore water residence times typically provide for more

active weathering sites and higher rates of chemical weathering (Rademacher et al. 2001, White and Blum 1995). Soil samples used in this study were collected from site AVA2 in March 2002, and from the Miller Forest in August 2003 (Wilson, 2005). Therefore, AVA2 samples reflect dry season soil moisture values vs. the wet season soil moisture values for the Miller Forest. It only stands to reason that dry season soil moisture values will be lower than those measured in the wet season at any given site on the island, since previous gravimetric soil moisture monitoring of multiple sites on BCI has consistently yielded values at or near saturation for most of the wet season (Godsey et al. 2004, Terrestrial Ecosystems Study Program (TESP) website, April 2003). It would have been more useful to compare soil moisture values from the same season.

Based on the variations in topography between the two sites it is possible to speculate how soil moisture would compare in the same season. The relatively gentle terrain at site AVA2 (Godsey et al. 2004) would allow for higher water infiltration rates compared to the steeper sloping topography of the Miller Forest (Dietrich et al. 1982), since steep slopes are prone to runoff at a larger scale (Brady and Weil, 2002). Furthermore, the influence of texture (Brady and Weil, 2002) is important since the clay rich soil at site AVA2 is expected to have a greater water holding capacity throughout the profile compared to the sandier soil found in the lower profile of the Miller Forest site. In either case, the high soil moisture contents tend to encourage weathering and soil development (Mohr et al. 1972; White and Blum 1995). However, increased erosion is likely to occur at the Miller Forest due to the higher slope topography, which reduces the thickness of a soil profile (Brady and Weil, 2002).

Particle size analysis indicates that site AVA2 has relatively higher clay content throughout the profile compared to the Miller Forest site, which becomes sandy at depth. Clay rich soils reflect higher rates of weathering and profile development compared to sandy soils (Brady and Weil, 2002; Mohr et al. 1972). Therefore, the variation in particle size is not surprising when considering the gentle terrain of the clay rich site at AVA2 compared to the steeper sloping topographical setting at the Miller Forest, which as mentioned above would be more prone to erosion. Evidence for erosion is provided by the thinner soil profile at the Miller Forest site. Based on changes in percentage of soil separates, a saprolitic transitional horizon, e.g., BC, is evident as the proportion of sand increases relative to decreasing clay content (40-cm to 80-cm). The C horizon must begin at 80-cm as the relative proportion of sand, silt and clay remains stable down the remainder of the profile to 100-cm. In contrast, at site AVA2, the C horizon does not appear within the 100-cm depth profile. Other than a shallow A horizon, that is unlikely to be deeper than 30-cm, the bulk of the profile is a clay rich Bt horizon. Note that performing particle size analysis at more depth intervals would reveal more accurate horizon transitions/boundaries.

Soil organic matter analyses by dry combustion LOI produced anomalously high numbers for tropical soils. The inputs of organic matter into the soil from the accumulation of above ground leaf litter at the soil surface and decomposition of root material should be comparable between both sites since they belong to the same climate zone. The vegetation at the two sites does differ in that the forest at the AVA2 site is a primary forest whereas the Miller Forest represents secondary growth that is nearly 100 years in age (Dietrich et al. 1982).

The relative difference in organic matter between the two sites is difficult to compare since the timing of the sampling events occurred in markedly different seasons (wet vs. dry season). A higher organic matter content was determined for the AVA2 profile, which was sampled in the dry season compared to the Miller Forest profile, which was sampled in the wet season. Typically, decomposition of organic matter resulting from the microbial enzymatic oxidation is exceedingly rapid in aerobic soils compared to anaerobic soils (Brady and Weil, 2002; Conrad 1996). Moisture supersaturation in a soil profile will promote anoxic or low oxygen conditions (Conrad 1996). Therefore, one would expect soils to have higher organic matter contents in the wet season compared to the dry season. However, in this particular scenario, the soil textures are different between both sites, and the higher clay content of the AVA2 soil profile may be correlated with higher organic matter content. Residues of organic matter are often protected from microbial decay when lodged into tiny pores of clay particles that are physically too small (< 0.2 μm in diameter) for microbial access. The highly reactive surface properties of clays may also limit desorption of organic matter that is tightly bound within the pores (Brady and Weil, 2002). Furthermore, the variation in topography between both sites can influence the residence time of organic matter in the upper O and A horizons of the soil profile. Due to the relatively steeper slope at the Miller Forest site erosive forces may have removed a lot more of the degradation resistant organic material from the upper horizon compared with the AVA2 site.

There is an interesting seasonal dynamic in the humid tropics that draws together a relationship between the processes of water infiltration with dissolved organic carbon

(DOC) flux (Moore and Dalva 2001). With the accumulation of leaf litter at the soil surface in the dry season, the onset of the rainy season triggers rapid consumption of leaf litter into the soil (Yavitt 2000). This phenomenon translates into a punctuated flux of DOC entering the soil system, which is expected to be highest at the transition from dry to wet season. At this transitional moment the conditions are not likely to be anaerobic and rapid decomposition of the soil organic matter is promoted. Organic matter becomes more mobile in colloidal form compared to plant tissue in the form of cellulose or lignins (Kogel-Knabner 2002).

Fine textured soils have high capillarity relative to coarse textured soils. Capillarity is dependent upon the pore connectivity (Brady and Weil, 2002). Perched water tables tend to occur when clay layers overly a layer composed of sand, as is the case with the site at the Miller Forest. At high potential levels (high moisture contents), hydraulic conductivity is greater in sands than with clays (Brady and Weil, 2002). A perched water table in the wet season is likely to encourage supersaturated lateral flow (Godsey et al. 2004), which will remove quantities of organic colloids from the system. Therefore, significant proportions of soil organic matter may have been removed before anoxic conditions have set in where decomposition rates decline.

Organic matter contents for both soil profiles should be lower considering the humid tropical climate of Panama. Oxisols, which are typically found in the humid tropics, characteristically are highly weathered, low organic, low pH, low cation exchange capacity soils, which promote the formation of low silica oxide clays. Organic matter contents for Oxisols rarely exceed 5% and are typically much lower (Brady and Weil, 2002; Mohr et al., 1972). However, topographical influences can alter the

prevailing conditions of the soil system and produce atypical soils for the climate zone. The soils in the Miller Forest have been classified as Alfisols (Leigh 1999), while the representative soils found at site AVA2 within the Conrad Trail Stream catchment have been classified as Oxisols (Yavitt 2000). In the upper 100-cm of a profile, Alfisols tend have a slightly lower organic matter content compared to Oxisols (Brady and Weil, 2002).

A last consideration in trying to interpret the anomalously high soil organic matter content for the two tropical soil profiles is the how they were stored over the course of a year. As described in the methods, the soils were stored in a -80^{o}C freezer at varying extended lengths of time, site AVA2 spending several months longer in the freezer. The growth of mold could not have occurred at such low temperatures. Different dry combustion LOI routines were applied, e.g., 950^{o}C for 2 hours, 1000^{o}C for 15 minutes, and finally 450^{o}C for 2 hours, for which the lowest soil organic matter content values were demonstrated.

Soil pH values measured in each profile were typical of what occurs in soils of the humid tropics (pH 4 to 5.5) (Motavalli et al. 1995). The breakdown of organic matter on the surface provides a natural acidifier to a soil, which subsequently drives down the pH of the system (Ugolini and Dahlgren 2002). The soil pH was comparatively lower for the Miller Forest site than at site AVA2, which corroborates with soil organic matter contents. The greater proportion of solid organic matter was converted to DOC through decomposition at the time of sampling for the Miller Forest compared to site AVA2. The highly weathered soils that exist at both sites have long since removed buffering

compounds that might have been introduced from the parent material, which further promotes the lower pH values that prevail in humid tropical soil settings.

To properly assess the influence of parent material upon weathering constituents and soil profile mineral compositions, other analyses need to be performed, which include X-ray diffraction (XRD) to determine the mineralogy and pore water chemistry for solute flux data. An assessment of the microbial ecology to determine the community structure of the soil habitat would also be useful to account for the weathering influences of microorganisms.

SUMMARY

Comparative analysis of two neighboring soil sites on BCI indicate that variations in weathering and soil profile development occur despite belonging to the same climate zone with similar vegetation. Site AVA2 is a relatively deep clay rich soil profile that has developed on the flat terrain summit of the island, overlying basaltic bedrock. The soil profile examined at the Miller Forest is shallower and sandier at depth in comparison with a parent material composed of basaltic conglomerates in a sandy volcaniclastic matrix. The sloping topography has contributed to relatively lower weathering conditions and higher erosion rates, which has resulted in a thinner soil profile. Variability between the two soil profile units is primarily influenced by the different parent material compositions and differences in topography. Further analysis of the mineralogy of the soil at each of the horizons will shed more light on the influence of the parent material with respect to weathering products.

REFERENCES

Aide M, Pavich Z, Lilly ME, Thornton R, Kingery W. 2004. Plinthite formation in the coastal plain region of Mississippi. Soil Science, 169(9): 613:623.

Appelo CAJ, Postma D. 1996. Geochemistry, groundwater and pollution. A.A. Balkema, Rotterdam, the Netherlands.

Brady NC, Weil RR. 2002. The nature and properties of soils. 13th Edition. Prentice Hall. Upper Saddle River, New Jersey.

Conrad R.1996. Soil microorganisms as controllers of atmospheric trace gases (H_2, CO, CH_4, OCS, N_2O, and NO), Microbiological Reviews, 60: 609-640.

Davies BE. 1997. Deficiencies and toxicities of trace elements and micronutrients in tropical soils: Limitations of knowledge and future research needs. Environmental Toxicology and Chemistry, 16(1): 75-83.

Day PR. 1965. Particle fractionation and particle size analysis. In Black A. (Editor). Methods of soil analysis, Part 1. Agronomy Society of America, Madison, Wisconsin, pp. 545-567.

Dietrich WE, Windsor DM, Dunne T. 1982. Geology, climate, and hydrology of Barro Colorado Island. *In*: Leigh EG, Rand AS, Windsor DM (Editors), The ecology of a tropical forest: Seasonal rhythms and long-term changes. Smithsonian Institution Press, Washington, D.C. pp. 21-46.

Foster RB, Brokaw NVL. 1982. Structure and history of the vegetation of Barro Colorado Island. *In*: Leigh EG, Rand AS, Windsor DM (Editors), The ecology of a tropical forest: Seasonal rhythms and long-term changes. Smithsonian Institution Press, Washington, D.C. pp. 67-81.

Godsey S, Elsenbeer H, Stallard R. 2004. Overland flow generation in two lithologically distinct rainforest catchments. Journal of Hydrology, 295: 276-290.

Goldich SS. 1938. A study in rock-weathering. Journal of Geology, 46: 17-58.

Jenny H. 1941. Factors of soil formation: A system of quantitative pedology. McGraw-Hill, New York. 281 p.

Kogel-Knabner I. 2002. The macromolecular organic composition of plant and microbial residues as inputs to soil organic matter. Soil Biology & Biochemistry, 34: 139-162.

Le Bas MJ. 2000. IUGS reclassification of the high-Mg and picritic volcanic rocks. Journal of Petrology, 41: 1467-1470.

Leigh EG. 1999. Tropical forest ecology: A view from Barro Colorado Island. Oxford University Press, New York. 245 p.

Mohr ECJ, Van Baren FA, Van Schuylenborgh. 1972. Tropical soils: A comprehensive study of their genesis. Mouton, Ichtiar Baru, Van Hoeve, The Hague, the Netherlands.

Moore TR, Dalva M. 2001. Some controls on the release of dissolved organic carbon by plant tissues and soils. Soil Science, 166 (1): 38-47.

Motavalli PP, Palm CA, Parton WJ, Elliott ET, Frey SD. 1995. Soil pH and organic C dynamics in tropical soils: evidence from laboratory and simulation studies. Soil Biology & Biochemistry, 27(12): 1589-1599.

Munsell Color, 1994. Munsell Soil Color Charts, Revised Edition. Macbeth Division of Kollmorgen Instruments Corporation.

Rademacher LK, Clark JF, Hudson GBH, Erman DC, Erman NA. 2001. Chemical evolution of shallow groundwater as recorded by springs, Sagehan basin; Nevada County, California. Chemical Geology, 179: 37-51.

Schulz MS, White AF. 1999. Chemical weathering in a tropical watershed, Luquillo Mountains, Puerto Rico III: Quartz dissolution rates. Geochimica et Cosmochimica Acta, 63 (3/4): 337-350.

Turner BF, Stallard RF, Brantley SL. 2003. Investigation of in situ weathering of quartz diorite bedrock in the Rio Icacos basin, Luquillo Experimental Forest, Puerto Rico. Chemical Geology, 202: 313-341.

Ugolini FC, Dahlgren RA. 2002. Soil development in volcanic ash. Global. Environmental Research 6(2): 69-81.

White AF, Blum AE. 1995. Effects of climate on chemical weathering rates in watersheds. Geochimica Cosmochimica Acta, 59, 1729-1747.

Wilson AD. 2005. Trace metal mobility in tropical rainforest and adjacent grassland soils, Central Panama. Master of Science Thesis Dissertation. The University of Kansas.

Woodring WP. 1958. Geology of the Barro Colorado Island, Canal Zone. Smithsonian Institution Miscellaneous Collections, 135 (3), Pub. No. 4304. Washington, D.C.: Smithsonian Institution.

Yavitt JB. 2000. Nutrient dynamics of soil derived from different parent material on Barro Colorado Island, Panama. Biotropica, 32(2): 1989-207.

Table A.1. Color Indices

Sample #	Depth Interval (cm)	Color Index	
		AVA2	Miller Forest
1	5	7.5YR 3/3	7.5YR 3/4
2	10	7.5YR 3/4	ND
3	15	7.5YR 3/4	7.5YR 3/4
4	20	5YR 3/4	7.5YR 3/4
5	25	5YR 3/4	5YR 3/4
6	30	5YR 3/4	ND
7	35	5YR 3/4	5YR 4/6
8	40	5YR 3/4	5YR 4/6
9	45	5YR 3/4	5YR 4/6
10	50	5YR 3/4	ND
11	55	5YR 3/4	5YR 4/6
12	60	5YR 3/4	5YR 3/4
13	65	5YR 3/4	7.5YR 4/6
14	70	5YR 3/4	ND
15	75	5YR 3/4	7.5YR 4/6
16	80	5YR 3/4	7.5YR 4/6
17	85	2.5YR 2.5/4	7.5YR 4/6
18	90	2.5YR 2.5/4	ND
19	95	2.5YR 2.5/4	7.5YR 4/6
20	100	2.5YR 2.5/4	7.5YR 4/6

ND – No Data

The Munsell soil color chart encodes a hue with a letter abbreviation, e.g., YR – yellow red, and value with a number and chroma being the last number (i.e., for the sample collected at 65-70 cm depth, 7.5YR 4/6 is 7.5 hue (yellow red) value/chroma). A value of 0 represents absolute black while a 10 represents absolute white.

Figure A.1. Soil Moisture

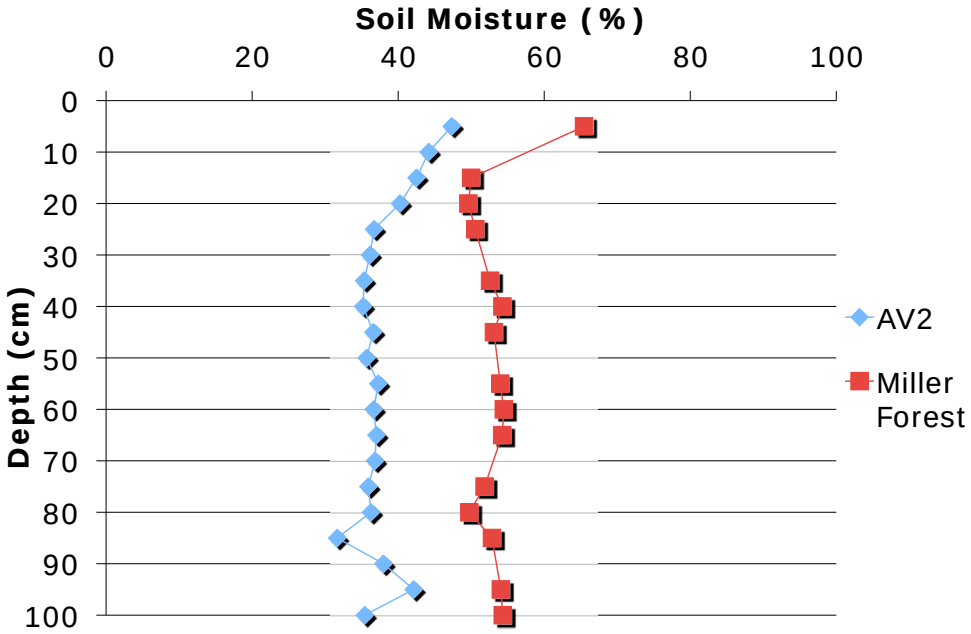

Figure A.2. AVA2 Particle Size Analysis: Hydrometer Method

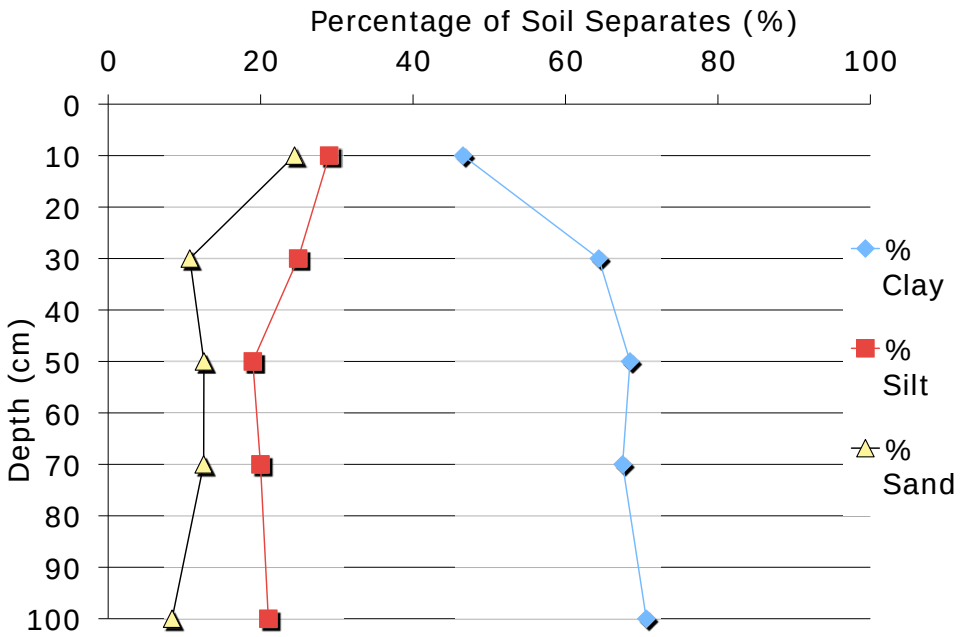

Figure A.3. Miller Forest Particle Size Analysis: Hydrometer Method

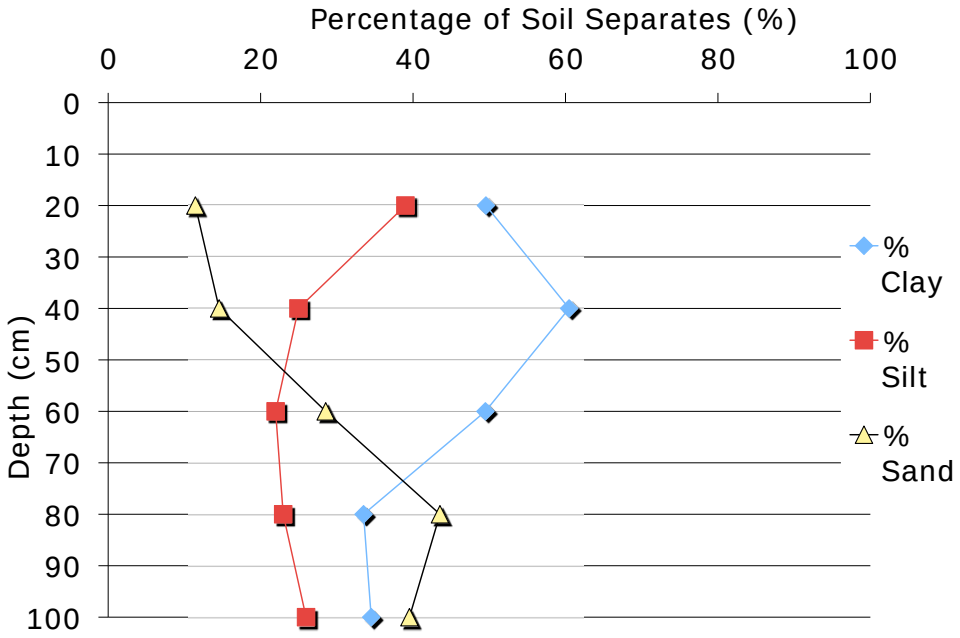

Figure A.4. Soil Organic Matter

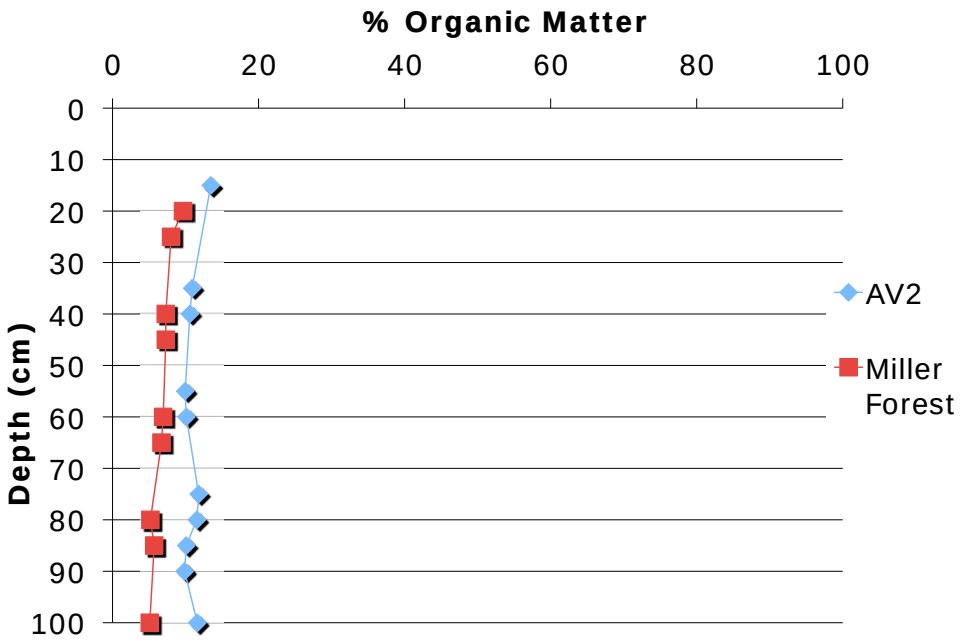

Figure A.5. Soil pH

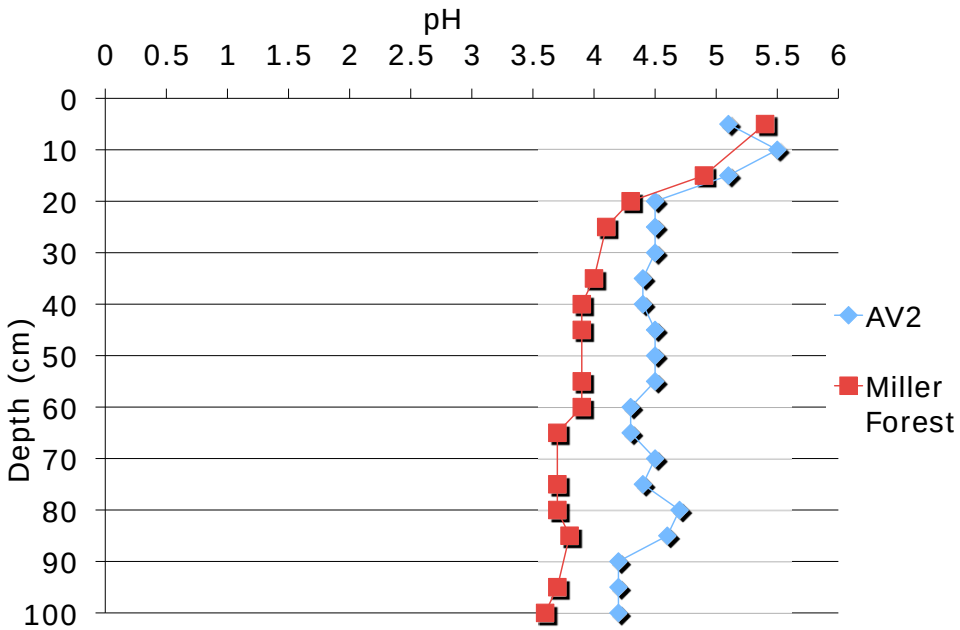

Appendix B: Cu-Substituted Iron Oxide Synthesis & Methanobactin-promoted weathering of Cu-doped ferrihydrite

IRON OXIDE SYNTHESIS

(Adapted from Cornell and Schwertmann, 2003)

The Cu-doped iron oxides were synthesized as described below, and used in the study by Knapp et al., (2007).

Synopsis

Initially, 74.34 g of $Fe(NO_3)_3.9H_2O$ was combined with 0.02157 g of $CuCl_2.2H_2O$ in 3-L of NANOpure H_2O and bubbled continuously with a stream of N_2 gas at room temperature (25^oC). The starting pH of the reddish brown solution was 1.87 due to the acidity of the ferric nitrate. To promote iron precipitation the solution was titrated slowly with 1 M KOH so that pH increased at increment values ranging between 0.01-0.1 per minute until pH 7 was achieved with a characteristic dark brown colored suspension. The mixture of suspended iron particulate matter with trace amounts of copper was monitored periodically to maintain the pH at 7 for at least 48 hours. The suspension was centrifuged at 4000 rpm for 1 hour using a Sorvall Legend T tabletop centrifuge (Thermo Electron Corporation, Waltham, MA). Upon decanting the supernatant, the iron oxide paste was secured in dialysis tubing and soaked in NANOpure water with a magnetic stirrer for 7 days. The conductivity of the water was monitored regularly and replaced twice daily over the span of the 7 days. The conductivity of the water before removing the iron oxide from the dialysis tubing was as low as 20 μS. The low salt iron oxide was then freeze-dried until all moisture was completely removed. The resulting Cu concentration was estimated to be 108 ppm (mg Cu per kg iron oxide). The same protocol was repeated to yield a dry mass of Cu-substituted iron oxide with a Cu concentration of approximately

800 ppm. Solid phases were characterized by X-Ray diffraction. Sequential extractions (Poulton and Canfield, 2005) were performed on the freeze-dried product to confirm the available copper concentration by ICP-OES analysis (Perkin-Elmer, IL).

METHANOBACTIN-PROMOTED WEATHERING OF CU-DOPED FERRIHYDRITE

Synopsis

Methanobactin promoted-dissolution kinetics of Cu-doped ferrihydrite was performed according to a similar experimental design as for chapter 4 (Kulczycki et al., 2007). Instead of using 30 mg of Cu-substituted borosilicate glasses, duplicate samples of 300 mg of Cu-doped ferrihydrite (108 ppm Cu) were reacted in 100-mL solutions of 0.1 M KCl, buffered with 0.1 M Tris-HCl stock to yield a pH of 5.5. The temperature was fixed at 20^{o}C. The experiments were designed to examine how varying methanobactin concentration would influence Cu solubility hence methanobactin concentrations between zero and 100 μM (0, 5, 10, 20, 50, and 100 μM) were examined. Two-mL samples were sacrificed at chosen intervals between zero and 32 days and prepared for analysis as described in chapter 4 (Kulczycki et al., 2007). The filtered solutions collected from the methanobactin reacted Cu-doped iron oxide samples were compared with a number of blanks, which included a media blank (no mb, no iron oxide), a mb blank (no iron oxide), and a aqueous Cu control (100 μM Cu, no mb, no iron oxide). The results were not encouraging as Cu analysis by Bathocuproine method (Standard Methods, 1989) for all samples at all intervals were below the detection limit (aqueous Cu control excepted).

Tabulated results presented below. It stands to reason that the stability of ferrihydrite has a stronger infuence upon Cu retention compared to methanobactin's high affinity to Cu.

REFERENCES

Clesceri LS, Greenberg AE, Trussell RR. 1989. Standard Methods: For the Examination of Water and Wastewater. Washington, D.C.: American Public Health Association.

Cornell RM, Schwertmann U. 2003. The Iron Oxides: Structure, Properties, Reactions, Occurences and Uses: John Wiley & Sons.

Knapp CW, Fowle DA, Kulczycki E, Roberts JA, Graham DW. 2007. Methane monooxygenase gene expression mediated by methanobactin in the presence of mineral copper sources. Proceedings of the National Academy of Sciences 104: 12040-12045.

Kulczycki E, Fowle DA, Knapp CW, Graham DW, Roberts JA. 2007. Methanobactin-promoted dissolution of Cu-substituted borosilicate glass. Geobiology 5: 251-263.

Poulton SW, Canfield DE. 2005. Development of a sequential extraction procedure for iron: implications for iron partitioning in continentally derived particulates. Chemical Geology 214: 209-221.

RESULTS

Copper: mb-promoted dissolution of iron oxide — Cu — 63.55

STDs (ppb)	Abs	484 nm
0	-0.01	
20	-0.008	
100	0.003	
200	0.019	
300	0.034	
400	0.049	y = 0.0001x - 0.0109
500	0.064	R2 = 0.9996

27-Jun-06

Interval 1	Treatment	Abs.	Conc. (ppb)	Dil'n Factor	Conc. (ppb)	[Cu](umole/L)
1a	Mb5	-0.011	-1	7.14	-7.14	-0.11
1b		-0.011	-1	7.41	-7.41	-0.12
2a	Mb5	-0.01	9	6.89	62.03	0.98
2b		-0.011	-1	7.97	-7.97	-0.13
3a	Mb10	-0.011	-1	9.19	-9.19	-0.14
3b		-0.01	9	8.36	75.26	1.18
4a	Mb10	-0.011	-1	7.89	-7.89	-0.12
4b		-0.011	-1	7.86	-7.86	-0.12
5a	Mb20	-0.011	-1	8.57	-8.57	-0.13
5b		-0.011	-1	7.95	-7.95	-0.13
6a	Mb20	-0.011	-1	7.50	-7.50	-0.12
6b		-0.011	-1	8.06	-8.06	-0.13
7a	Mb50	-0.011	-1	8.07	-8.07	-0.13
7b		-0.011	-1	7.85	-7.85	-0.12
8a	Mb50	-0.01	9	8.11	73.01	1.15
8b		-0.01	9	7.68	69.16	1.09
9a	Mb100	-0.01	9	9.06	81.57	1.28
9b		-0.01	9	7.68	69.12	1.09
10a	Mb100	-0.01	9	7.50	67.50	1.06
10b		-0.01	9	8.15	73.39	1.15
11a	Control	-0.011	-1	8.14	-8.14	-0.13
11b		-0.01	9	9.39	84.54	1.33
12a	Mb Control	-0.01	9	8.80	79.20	1.25
12b		-0.01	9	8.11	73.01	1.15
13a	Blank	-0.011	-1	15.82	-15.82	-0.25
13b		-0.011	-1	14.78	-14.78	-0.23
14a	Copper Control	0.019	299	9.21	2753.69	43.33
14b		0.01	209	12.57	2626.75	41.34

Interval 2	Treatment	Abs.	Conc. (ppb)	Dil'n Factor	Conc. (ppb)	[Cu](umole/L)
1a	Mb5	-0.01	9	8.24	74.19	1.17
1b		-0.011	-1	7.35	-7.35	-0.12

2a	Mb5	-0.01	9	8.10	72.88	1.15
2b		-0.011	-1	7.86	-7.86	-0.12
3a	Mb10	-0.01	9	7.53	67.73	1.07
3b		-0.01	9	8.07	72.63	1.14
4a	Mb10	-0.01	9	7.42	66.76	1.05
4b		-0.01	9	8.15	73.39	1.15
5a	Mb20	-0.01	9	8.14	73.27	1.15
5b		-0.011	-1	7.61	-7.61	-0.12
6a	Mb20	-0.01	9	8.15	73.39	1.15
6b		-0.01	9	7.86	70.78	1.11
7a	Mb50	-0.01	9	8.36	75.26	1.18
7b		-0.01	9	8.91	80.16	1.26
8a	Mb50	-0.01	9	7.60	68.38	1.08
8b		-0.01	9	7.76	69.84	1.10
9a	Mb100	-0.01	9	8.36	75.26	1.18
9b		-0.01	9	8.08	72.75	1.14
10a	Mb100	-0.01	9	8.91	80.16	1.26
10b		-0.01	9	8.36	75.26	1.18
11a	Control	-0.01	9	7.86	70.78	1.11
11b		-0.01	9	9.05	81.43	1.28
12a	Mb Control	-0.01	9	8.80	79.20	1.25
12b		-0.009	19	8.33	158.33	2.49
13a	Blank	-0.01	9	10.20	91.80	1.44
13b		-0.01	9	16.81	151.31	2.38
14a	Copper Control	0.021	319	9.18	2927.60	46.07
14b		0.019	299	9.59	2868.37	45.14

28-Jun-06

STDs (ppb)	Abs	484 nm
0	-0.01	
20	-0.009	
100	0.003	
200	0.018	
300	0.034	
400	0.048	y = 0.0001x - 0.0112
500	0.063	R2 = 0.9994

Interval 3	Treatment	Abs.	Conc. (ppb)	Dil'n Factor	Conc. (ppb)	[Cu](umole/L)
1a	Mb5	-0.01	12	10.44	125.33	1.97
1b		-0.01	12	12.09	145.04	2.28
2a	Mb5	-0.011	2	12.88	25.77	0.41
2b		-0.011	2	8.83	17.66	0.28
3a	Mb10	-0.011	2	10.29	20.58	0.32
3b		-0.011	2	8.53	17.06	0.27
4a	Mb10	-0.011	2	9.10	18.19	0.29
4b		-0.011	2	8.27	16.54	0.26
5a	Mb20	-0.011	2	8.73	17.45	0.27
5b		-0.01	12	8.51	102.18	1.61

6a	Mb20	-0.01	12	8.97	107.63	1.69
6b		-0.01	12	9.39	112.72	1.77
7a	Mb50	-0.01	12	9.10	109.14	1.72
7b		-0.01	12	10.05	120.64	1.90
8a	Mb50	-0.01	12	9.23	110.71	1.74
8b		-0.01	12	9.64	115.73	1.82
9a	Mb100	-0.01	12	11.20	134.40	2.12
9b		-0.008	32	9.52	304.53	4.79
10a	Mb100	-0.01	12	10.43	125.11	1.97
10b		-0.01	12	10.44	125.33	1.97
11a	Control	-0.01	12	9.36	112.33	1.77
11b		-0.01	12	18.62	223.45	3.52
12a	Mb Control	-0.01	12	8.85	106.15	1.67
12b		-0.01	12	8.71	104.55	1.65
13a	Blank	-0.01	12	14.81	177.73	2.80
13b		-0.009	22	9.08	199.75	3.14
14a	Copper Control	0.002	132	12.38	1633.87	25.71
14b		0.004	152	10.46	1590.37	25.03

Interval 4	Treatment	Abs.	Conc. (ppb)	Dil'n Factor	Conc. (ppb)	[Cu](umole/L)
1a	Mb5	-0.01	12	8.94	107.25	1.69
1b		-0.01	12	12.33	148.00	2.33
2a	Mb5	-0.01	12	9.81	117.72	1.85
2b		-0.01	12	10.62	127.47	2.01
3a	Mb10	-0.01	12	8.55	102.63	1.62
3b		-0.01	12	8.29	99.43	1.56
4a	Mb10	-0.01	12	9.24	110.90	1.75
4b		-0.01	12	10.43	125.11	1.97
5a	Mb20	-0.01	12	8.73	104.73	1.65
5b		-0.01	12	7.71	92.53	1.46
6a	Mb20	-0.01	12	8.08	97.00	1.53
6b		-0.01	12	8.08	97.00	1.53
7a	Mb50	-0.01	12	11.22	134.64	2.12
7b		-0.01	12	8.74	104.91	1.65
8a	Mb50	-0.01	12	9.36	112.33	1.77
8b		-0.01	12	8.60	103.16	1.62
9a	Mb100	-0.01	12	10.29	123.49	1.94
9b		-0.01	12	9.19	110.32	1.74
10a	Mb100	-0.01	12	9.96	119.58	1.88
10b		-0.01	12	10.43	125.11	1.97
11a	Control	-0.01	12	8.61	103.34	1.63
11b		-0.01	12	8.97	107.63	1.69
12a	Mb Control	-0.01	12	9.48	113.80	1.79
12b		-0.009	22	9.50	209.00	3.29
13a	Blank	-0.01	12	16.91	202.88	3.19

13b		-0.01	12	16.94	203.25	3.20
14a	Copper Control	0.004	152	9.95	1512.00	23.79
14b		0.007	182	8.86	1612.80	25.38

6-Jul-06

STDs (ppb)	Abs	484 nm
0	0	
20	0.002	
100	0.014	
200	0.028	
300	0.044	
400	0.058	y = 0.0001x - 0.0006
500	0.073	R2 = 0.9997

Interval 5	Treatment	Abs.	Conc. (ppb)	Dil'n Factor	Conc. (ppb)	[Cu](umole/L)
1a	Mb5	0	6	3.93	23.58	0.37
1b		0	6	3.96	23.75	0.37
2a	Mb5	0	6	3.94	23.67	0.37
2b		0	6	4.07	24.43	0.38
3a	Mb10	0	6	4.00	24.00	0.38
3b		0	6	3.78	22.66	0.36
4a	Mb10	0.001	16	3.92	62.67	0.99
4b		0	6	3.76	22.58	0.36
5a	Mb20	0	6	3.92	23.50	0.37
5b		0	6	3.80	22.82	0.36
6a	Mb20	0	6	4.01	24.09	0.38
6b		0	6	3.62	21.70	0.34
7a	Mb50	0	6	3.94	23.66	0.37
7b		0	6	4.80	28.80	0.45
8a	Mb50	0	6	4.06	24.34	0.38
8b		0	6	3.66	21.95	0.35
9a	Mb100	0	6	3.97	23.83	0.38
9b		0	6	4.28	25.69	0.40
10a	Mb100	0	6	3.81	22.88	0.36
10b		0	6	3.96	23.75	0.37
11a	Control	0.002	26	3.74	97.25	1.53
11b		0	6	4.25	25.48	0.40
12a	Mb Control	0	6	3.88	23.26	0.37
12b		0	6	3.96	23.75	0.37
13a	Blank	0	6	8.78	52.67	0.83
13b		0	6	4.77	28.61	0.45
14a	Copper Control	0.067	676	4.22	2849.60	44.84
14b		0.061	616	4.58	2818.98	44.36

Interval 6	Treatment	Abs.	Conc. (ppb)	Dil'n Factor	Conc. (ppb)	[Cu](umole/L)
1a	Mb5	0	6	4.44	26.66	0.42

1b		0	6	6.65	39.89	0.63
2a	Mb5	0	6	4.48	26.90	0.42
2b			6	#DIV/0!	#DIV/0!	#DIV/0!
3a	Mb10	0	6	4.52	27.10	0.43
3b		0	6	4.33	26.00	0.41
4a	Mb10	0	6	4.68	28.11	0.44
4b		0	6	4.82	28.91	0.45
5a	Mb20	0	6	4.98	29.89	0.47
5b		0	6	4.23	25.38	0.40
6a	Mb20	0	6	4.50	27.00	0.42
6b		0	6	7.36	44.18	0.70
7a	Mb50	0	6	5.49	32.94	0.52
7b		0	6	10.59	63.55	1.00
8a	Mb50	0	6	5.14	30.82	0.49
8b		0	6	5.45	32.68	0.51
9a	Mb100	0	6	4.47	26.80	0.42
9b		0	6	4.10	24.62	0.39
10a	Mb100	0	6	4.33	26.00	0.41
10b		0	6	5.12	30.71	0.48
11a	Control	0	6	5.10	30.59	0.48
11b		0	6	4.50	27.00	0.42
12a	Mb Control	0	6	4.46	26.75	0.42
12b		0	6	5.57	33.39	0.53
13a	Blank	0	6	4.98	29.89	0.47
13b		0	6	4.56	27.36	0.43
14a	Copper Control	0.063	636	4.53	2883.20	45.37
14b		0.057	576	4.98	2869.13	45.15

June 28(2), 2006

STDs (ppb)	Abs	484 nm
0	-0.006	
20	-0.004	
100	0.007	
200	0.021	
300	0.037	
400	0.052	y = 0.0001x - 0.0071
500	0.067	R2 = 0.9992

Interval 7	Treatment	Abs.	Conc. (ppb)	Dil'n Factor	Conc. (ppb)	[Cu](umole/L)
1a	Mb5	-0.006	11	11.81	129.89	2.04
1b		-0.006	11	13.70	150.70	2.37
2a	Mb5	-0.006	11	8.58	94.40	1.49
2b		-0.006	11	7.96	87.55	1.38
3a	Mb10	-0.006	11	9.93	109.23	1.72
3b		-0.006	11	7.99	87.85	1.38
4a	Mb10	-0.006	11	8.50	93.50	1.47
4b		-0.006	11	9.33	102.61	1.61

5a	Mb20	-0.005	21	8.17	171.55	2.70
5b		-0.006	11	9.61	105.71	1.66
6a	Mb20	-0.006	11	7.99	87.85	1.38
6b		-0.006	11	9.19	101.13	1.59
7a	Mb50	-0.006	11	13.10	144.05	2.27
7b		-0.005	21	9.59	201.46	3.17
8a	Mb50	-0.005	21	8.58	180.22	2.84
8b		-0.005	21	8.57	179.91	2.83
9a	Mb100	-0.005	21	9.58	201.10	3.16
9b		-0.004	31	7.58	235.12	3.70
10a	Mb100	-0.005	21	8.80	184.80	2.91
10b		-0.005	21	8.31	174.58	2.75
11a	Control	-0.006	11	8.23	90.51	1.42
11b		-0.006	11	8.80	96.77	1.52
12a	Mb Control	-0.005	21	9.76	204.93	3.22
12b		-0.006	11	12.29	135.18	2.13
13a	Blank	-0.006	11	9.61	105.71	1.66
13b		-0.006	11	11.12	122.32	1.92
14a	Copper Control	0.133	1401	8.32	11654.70	183.41
14b		0.081	881	12.52	11032.52	173.61

Interval 8	Treatment	Abs.	Conc. (ppb)	Dil'n Factor	Conc. (ppb)	[Cu](umole/L)
1a	Mb5	-0.006	11	8.54	93.91	1.48
1b		-0.006	11	10.79	118.67	1.87
2a	Mb5	-0.006	11	9.33	102.61	1.61
2b		-0.006	11	8.91	97.97	1.54
3a	Mb10	-0.006	11	9.91	109.04	1.72
3b		-0.006	11	8.77	96.46	1.52
4a	Mb10	-0.006	11	8.67	95.33	1.50
4b		-0.006	11	12.04	132.48	2.08
5a	Mb20	-0.005	21	8.24	173.10	2.72
5b		-0.005	21	8.41	176.65	2.78
6a	Mb20	-0.005	21	8.52	178.97	2.82
6b		-0.005	21	8.78	184.48	2.90
7a	Mb50	-0.005	21	9.76	204.93	3.22
7b		-0.005	21	10.04	210.75	3.32
8a	Mb50	-0.005	21	9.59	201.46	3.17
8b		-0.005	21	8.44	177.26	2.79
9a	Mb100	-0.004	31	9.30	288.15	4.53
9b			71	#DIV/0!	#DIV/0!	#DIV/0!
10a	Mb100	-0.004	31	8.68	269.14	4.24
10b		-0.004	31	8.97	278.02	4.38
11a	Control	-0.006	11	8.52	93.75	1.48
11b		-0.006	11	10.45	114.98	1.81
12a	Mb Control	-0.004	31	9.03	279.98	4.41

12b		-0.005	21	9.54	200.39	3.15
13a	Blank	-0.006	11	20.42	224.65	3.54
13b		-0.006	11	14.70	161.73	2.55
14a	Copper Control	0.095	1021	11.54	11784.04	185.44
14b		0.137	1441	8.13	11710.66	184.29

Appendix C: Methanobactin-promoted dissolution of Gibbsite

Synopsis

Methanobactin promoted-dissolution kinetics of gibbsite ($Al(OH)_3$) was performed according to a similar experimental design as for chapter 4 (Kulczycki et al., 2007). Instead of using 30 mg of Cu-substituted borosilicate glasses, triplicate samples of 30 mg of synthetic gibbsite powder (obtained from Fisher Scientific; size fraction: 125 to 250 μm) were reacted in 100-mL solutions of unbuffered NANOpure DI water. The temperature was fixed at 20^{o}C. The experiments were designed to examine how varying methanobactin concentration would influence Al solubility hence methanobactin concentrations between zero and 90 μM (0, 10, 25, 50, and 90 μM) were examined. Batch samples were sacrificed at chosen intervals between zero and 48 days and prepared for analysis as described in chapter 4 (Kulczycki et al., 2007). The filtered solutions collected from the methanobactin reacted gibbsite samples were compared with a number of blanks, which included a media blank (no mb, no gibbsite), a mb blank (no gibbsite), and a aqueous gibbsite control.

Some variability in solution pH was observed between samples (see below). Controls demonstrated pH values that were generally higher than the methanobactin reacted samples but were within a few decimal places. The departure from neutral pH conditions was expected to enhance gibbsite solubility. However, the solutions became rapidly buffered within the first couple of hours.

The results would suggest that Al solubility is enhanced within the first several days of the experiment prior to partitioning out of solution, either by sorption or precipitation. Due to statistical error between analyses, it was not possible to draw

conclusions about the effect of changing methanobactin concentrations on gibbsite dissolution kinetics. Furthermore, Al solubility for the gibbsite control was comparable to the mb samples in the first interval (t = 0.5 hours); although, a noticeable decline in Al solubility relative to the mb samples was observed thereafter. The role of methanobactin with respect to Al solubility in minerals should not be ruled out. The tabulated results for the first 25 days (603 hours) are presented below with an accompanying figure (figure C.1) that includes data up to the 48th day.

REFERENCES

Kulczycki E, Fowle DA, Knapp CW, Graham DW, Roberts JA. 2007. Methanobactin-promoted dissolution of Cu-substituted borosilicate glass. Geobiology 5: 251-263.

RESULTS

	Al ppm	MW	26.98	
Time (Hours)	A - mb9	error	umoles/L	Uncertainty
0.5	0.012	0.01	0.44	0.26
2.5	0.019	0.00	0.70	0.09
8.75	0.023	0.01	0.85	0.33
25.5	-0.009	-0.01	-0.33	-0.19
34	-0.011	0.00	-0.41	-0.15
46.25	-0.026	-0.02	-0.96	-0.56
52.35	-0.019	-0.01	-0.70	-0.26
69.4	-0.039	-0.01	-1.45	-0.41
453.5	-0.038	-0.01	-1.41	-0.23
603	-0.048	-0.01	-1.78	-0.23

Time (Hours)	B - mb24	error	umoles/L	Uncertainty
0.5	0.026	0.01	0.96	0.28
2.5	0.021	0.01	0.78	0.29
8.75	0.005	0.01	0.19	0.26
25.5	-0.001	0.00	-0.04	-0.14
34	-0.007	-0.01	-0.26	-0.26
46.25	-0.02	0.00	-0.74	-0.17
52.35	-0.012	-0.01	-0.44	-0.20
69.4	-0.02	-0.01	-0.74	-0.53
453.5	-0.028	-0.01	-1.04	-0.42
603	-0.05	0.00	-1.85	-0.16

Time (Hours)	C - mb48	error	umoles/L	Uncertainty
0.5	0.015	0.01	0.56	0.38
2.5	0.017	0.00	0.63	0.17
8.75	0.006	0.01	0.22	0.32
25.5	-0.001	-0.01	-0.04	-0.29
34	-0.005	-0.01	-0.19	-0.30
46.25	-0.006	-0.02	-0.22	-0.64
52.35	-0.012	-0.01	-0.44	-0.23
69.4	-0.012	-0.01	-0.44	-0.37
453.5	-0.023	-0.01	-0.85	-0.37
603	-0.055	-0.01	-2.04	-0.35

Time (Hours)	D - mb90	error	umoles/L	Uncertainty
0.5	0.01	0.00	0.37	0.10
2.5	0.021	0.00	0.78	0.13
8.75	0.013	0.01	0.48	0.33
25.5	0.007	0.01	0.26	0.23

34	-0.001	-0.01	-0.04	-0.23
46.25	0	0.00	0.00	#DIV/0!
52.35	-0.015	0.00	-0.56	-0.15
69.4	-0.011	-0.01	-0.41	-0.32
453.5	-0.029	0.00	-1.07	-0.16
603	-0.063	-0.02	-2.33	-0.56

Time (Hours)	X - Control	error	umoles/L	Uncertainty
0.5	0.022	0.01	0.82	0.24
2.5	0.001	0.00	0.04	0.13
8.75			0.00	#DIV/0!
25.5	-0.013	-0.01	-0.48	-0.31
34	-0.022	-0.01	-0.82	-0.23
46.25	-0.019	-0.01	-0.70	-0.42
52.35	-0.021	-0.01	-0.78	-0.19
69.4	-0.02	0.00	-0.74	-0.10
453.5	-0.019	-0.01	-0.70	-0.19
603	-0.038	-0.01	-1.41	-0.27

Time (Hours)	Blank	error	umoles/L	Uncertainty
0.5	-0.018	-0.01	-0.67	-0.39
2.5	-0.019	-0.01	-0.70	-0.33
8.75			0.00	#DIV/0!
25.5	-0.031	-0.01	-1.15	-0.21
34	-0.022	-0.01	-0.82	-0.30
46.25	-0.033	0.00	-1.22	-0.13
52.35	-0.03	-0.01	-1.11	-0.41
69.4	-0.036	-0.01	-1.33	-0.28
453.5	-0.033	-0.01	-1.22	-0.54
603	-0.039	-0.01	-1.45	-0.34

Time (Hours)	mb blank	error	umoles/L	Uncertainty
0.5	-0.018	0.00	-0.67	-0.16
2.5	0.01	0.07	0.37	2.48
8.75	-0.026	-0.01	-0.96	-0.55
25.5	-0.019	-0.01	-0.70	-0.35
34	-0.029	-0.01	-1.07	-0.23
46.25	-0.024	-0.01	-0.89	-0.46
52.35	-0.036	-0.01	-1.33	-0.30
69.4	-0.035	0.00	-1.30	-0.16
453.5	-0.032	-0.01	-1.19	-0.34
603	-0.04	-0.01	-1.48	-0.20

mb-gibbsite dissolution experiment

	pH						
Time (Hours)	A - mb9	B - mb24	C - mb48	D - mb90	X - Control	Blank	mb blank
0.5	7.68	7.58	7.24	7.14	7.85	5.79	5.89
2.5	7.19	7.06	7.02	6.91	7.06	5.67	5.28
8.75	6.94	6.9	6.78	6.7	6.82	5.5	6.43
25.5	7.57	7.64	7.31	7.24	7.27	5.86	5.96
34	7.42	7.38	7.44	7.54	7.41	6.09	6.2
46.25	7.46	7.43	7.49	7.42	7.38	6.05	6.37
52.35	7.36	7.42	7.47	7.43	7.38	6.21	6.41
69.4	7.27	7.39	7.37	7.32	7.35	6.11	6.29
453.5	7.29	7.2	7.35	7.25	7.32	5.89	6.03
603	7.35	7.45	7.45	7.4	7.46	6.1	6.17

Figure C.1.

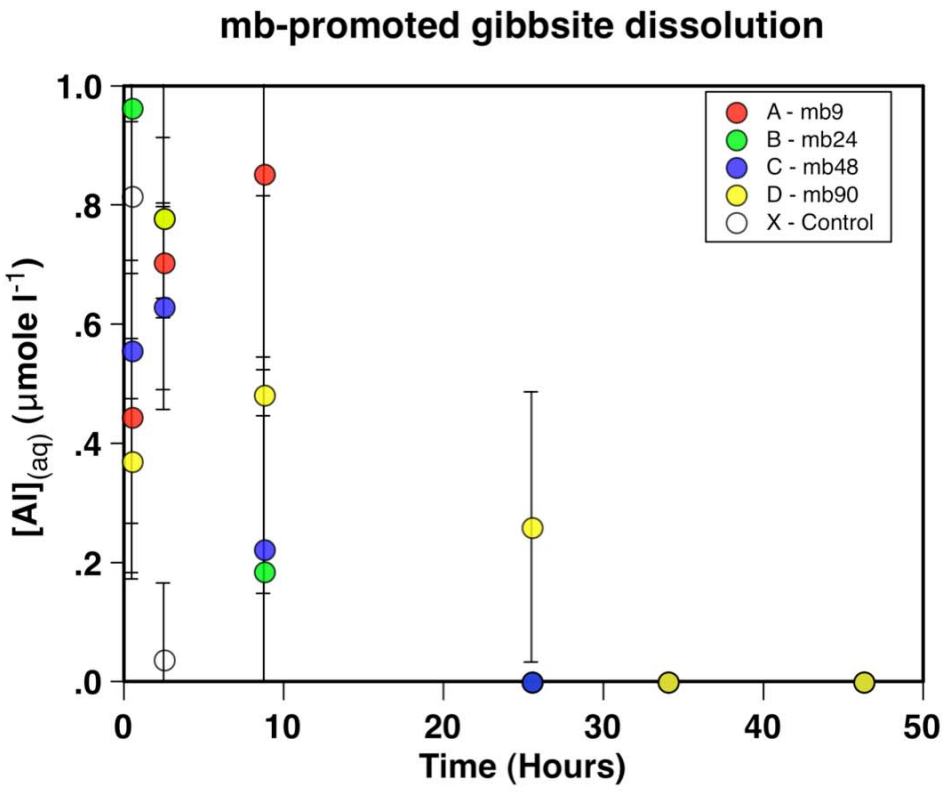
mb-promoted gibbsite dissolution
A - mb9
B - mb24
C - mb48
D - mb90
X - Control
[Al](aq) (µmole l-1)
1.0
.8
.6
.4
.2
.0
0
10
20
30
40
50
Time (Hours)

Appendix D: Analysis of Copper-Methanobactin Complex

i. Chromophore Response to Cu:mb complex formation

The formation of a Cu:mb complex is known to illicit a chromophore response (Kim et al., 2004), and can be detected with varying response across the ultra violet (UV) and visible (Vis) range of the electromagnetic spectrum. The following passage reflects some prelimary analysis examining the chromophore response to the formation of a Cu:mb complex. The intent of this work was to quantify the chromophore response as a function of methanobactin to Cu ratio across the UV-Vis spectrum.

METHODS

To evaluate the chromophore response of during the formation of a Cu:mb complex at different Cu to methanobactin ratios, stock methanobactin solutions were spiked with different Cu concentrations and stored in the dark for 5 minutes to allow the chromopeptide reaction to occur. The pH of the solution was also recorded. Once the incubation was complete, a spectrophotometer (dual-beam Shimadzu UV160U) was used to run a scan of the solutions across a range between 250 and 600 nm. In one set of experiments the ionic strength of stock methanobactin solutions was set at 0.1 M with KCl, while in another set the stock methanobactin solution was made in deionized water. Not all of the data is shown here. In one set of experiments, the methanobactin to Cu ratio increased as follows from experiment to experiment: 0.088:1, 0.18:1, 0.44:1 and 8.79:1. In another set of experiments, the methanobactin to Cu ratio was set at 1:1 and 10:1.

RESULTS AND DISCUSSION

The spectrophotmetric scans of the Cu:mb complex solutions are shown in figures D.1, D.2 and D.3 below. Figure D.1 shows the scans of solution complexes where the methanobactin concentration was fixed at 8 μM in deionized water and the Cu concentration was between 0.91 μM and 91 μM. The highest chromofore response was detected at a wavelength of 340 nm in each case (absorbance of 0.057 to 0.062). The pH decreased with increasing Cu concentration (pH 4.46 to 2.71) due to the acidity of the Cu stock solution. In the 1:1 mb:Cu complex solutions (figure D.2), the highest chromophore response was observed at a wavelength of 330 nm (0.035 absorbance units). The methanobactin concentration was set at 5 μM, and was made in deinized water. The pH was ~6.2. The highest chromophore response was observed for complex solutions with a methanobactin to Cu ratio of 10:1 (figure D.3) at a wavelength of 340 nm (0.08 absorbance units). The solution pHs were between 6.11 and 6.39. When the pH is above 6, it would appear that a higher chromophore response correlates with increasing mb to Cu ratio on a molecule per mole basis. Similar findings by Choi et al., (2006) confirmed the thermodynamics of this relationship and concluded that higher affinity constants were associated with higher mb:Cu ratios.

Figure D.1.

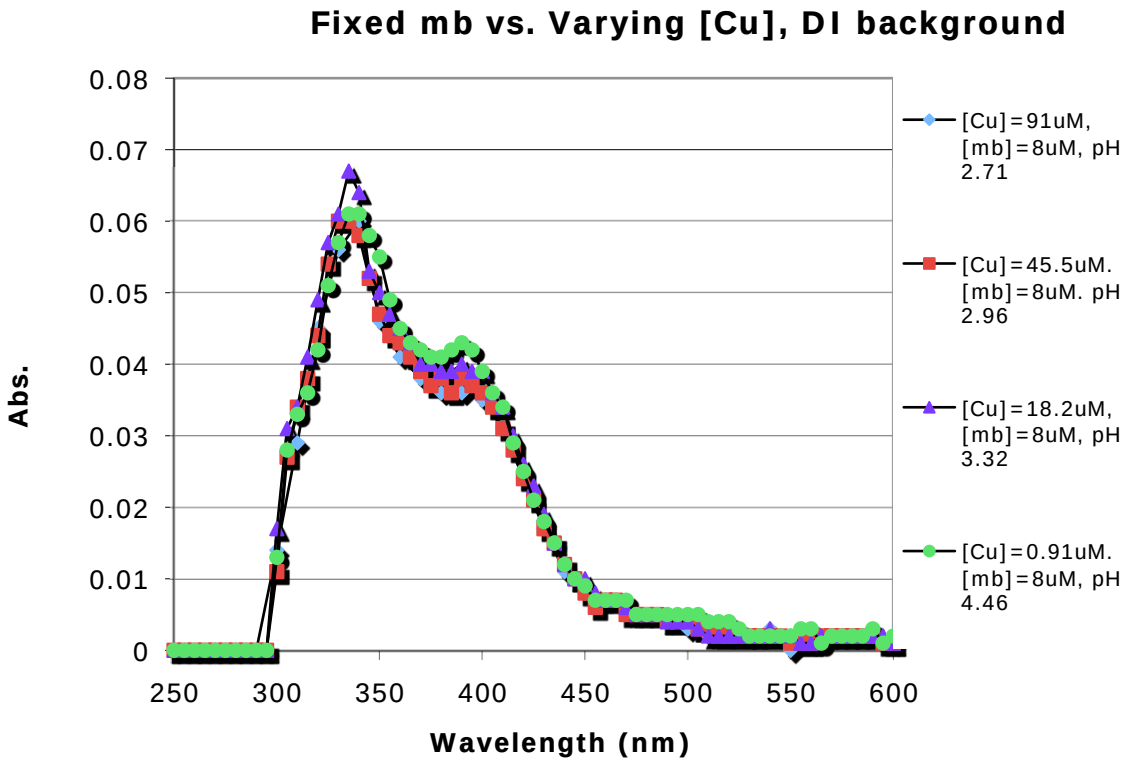
Fixed mb vs. Varying [Cu], DI background
Abs.
0.08
0.07
0.06
0.05
0.04
0.03
0.02
0.01
0
250
300
350
400
450
500
550
600
Wavelength (nm)
[Cu]=91uM, [mb]=8uM, pH 2.71
[Cu]=45.5uM. [mb]=8uM. pH 2.96
[Cu]=18.2uM, [mb]=8uM, pH 3.32
[Cu]=0.91uM. [mb]=8uM, pH 4.46

Figure D.2.

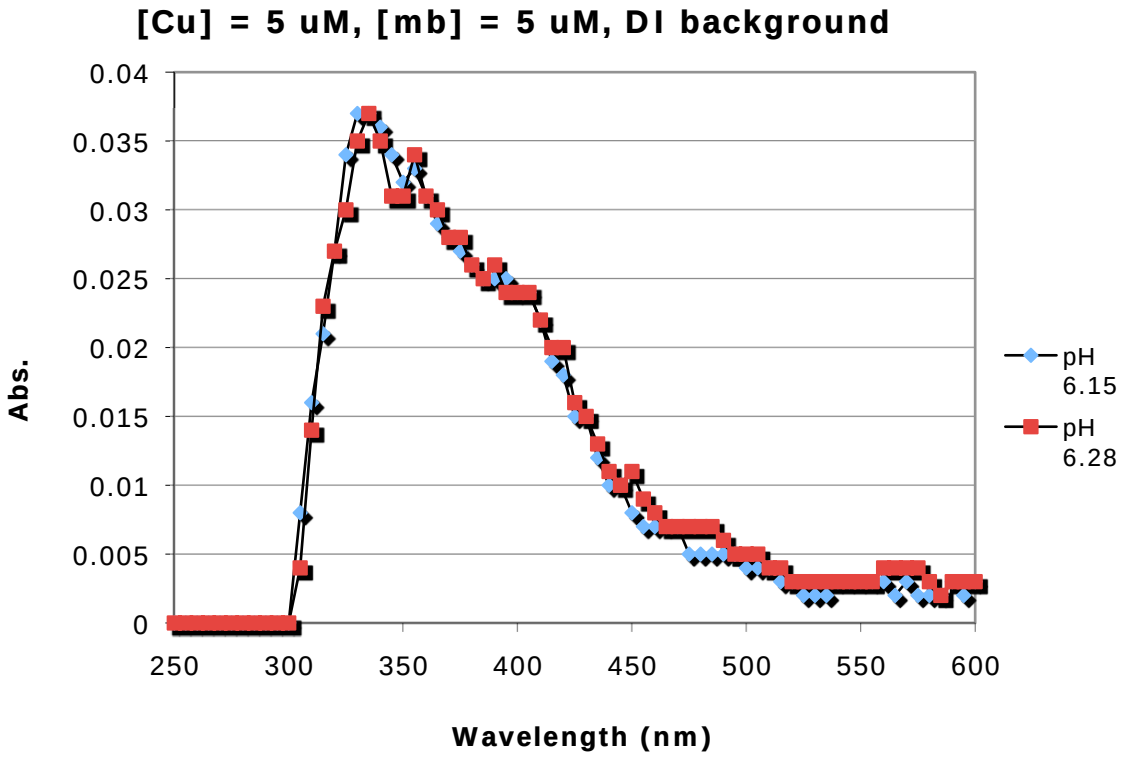
[Cu] = 5 uM, [mb] = 5 uM, DI background
Abs.
0.04
0.035
0.03
0.025
0.02
0.015
0.01
0.005
0
250
300
350
400
450
500
550
600
Wavelength (nm)
pH 6.15
pH 6.28

Figure D.3.

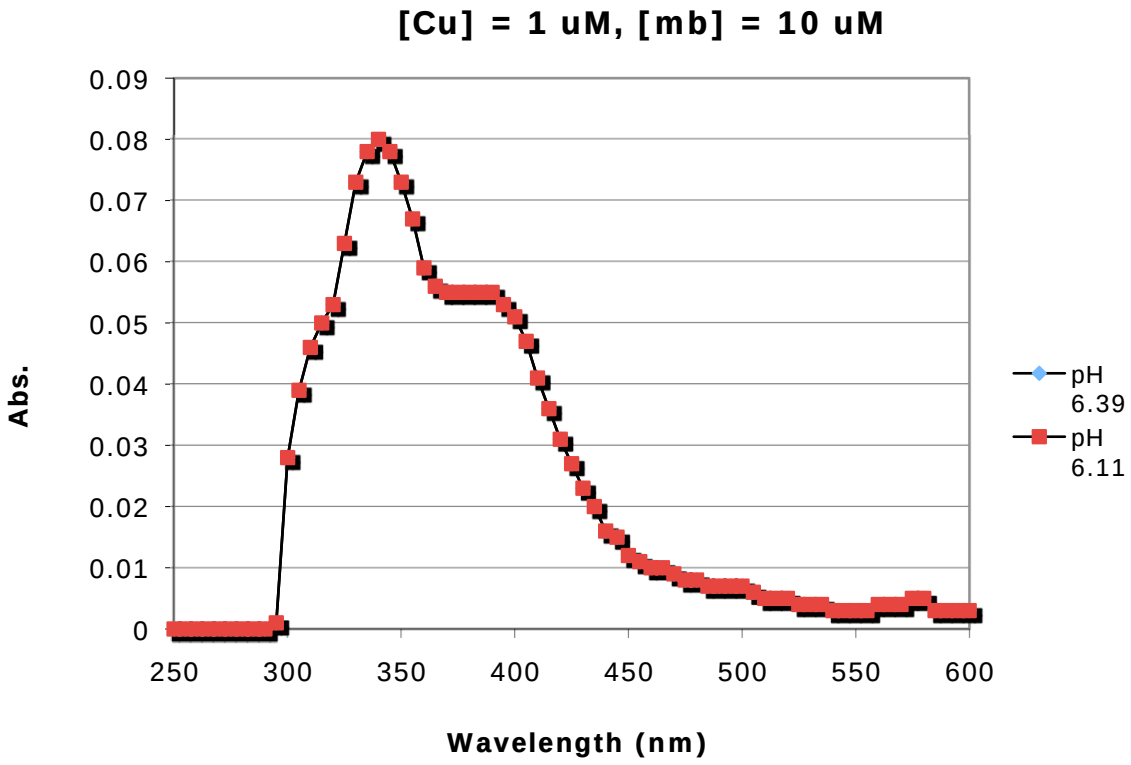
[Cu] = 1 uM, [mb] = 10 uM
Abs.
0.09
0.08
0.07
0.06
0.05
0.04
0.03
0.02
0.01
0
250
300
350
400
450
500
550
600
Wavelength (nm)
pH 6.39
pH 6.11

ii. Methanobactin to Cu ratios

The relationship between methanobactin:Cu ratio was further illustrated by examination of the chromophore response across a range of more discreet intervals.

METHODS

A buffered stock solution (0.1 M Tris-HCl) of methanobactin with an ionic strength fixed at 0.1 M KCl was used to evaluated different ratios of methanobactin to Cu. The Cu:mb ratio was compared at discreet intervals across a range between 0.02:1 to 9:1, including at 10 μM Cu solution with no methanobactin. The chromophore response was recorded at a wavelength of 330 nm.

RESULTS AND DISCUSSION

The results of the chromophore response to increasing Cu:mb ratio are illustrated if figure D.4. As predicted, the chromophore response decreased with increasing Cu:mb ratio. No chromophore response was observed for Cu in the absence of methanobactin. The pH remained fixed at 6.9 ± 0.1 for all Cu:mb combinations. The findings imply that a higher chromophore response exists with higher mb:Cu ratios.

Figure D.4.

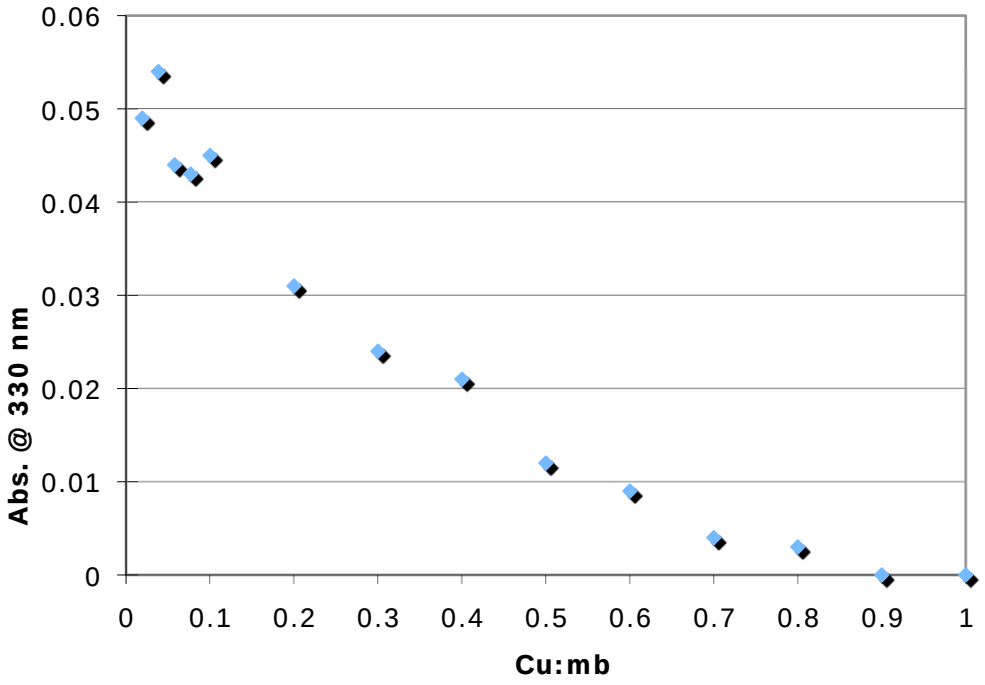
0.06
0.05
0.04
0.03
0.02
0.01
0
Abs. @ 330 nm
0
0.1
0.2
0.3
0.4
0.5
0.6
0.7
0.8
0.9
1
Cu:mb

iii. KOH Titration of Cu:mb

METHODS

A 1:1 Cu:mb complex solution was titrated with 0.01 M KOH at increments of 0.5 mL from an initial pH of 2.5 up to pH 11. The original solution contained 10 μM of Cu and 10 μM of methanobactin. The ionic strength was fixed at 0.1 M KCl. The pH was lowered to 25 using 350 μL of 0.1 N HCl. The intial solution volume was 10 mL after setting the pH to 2.5.

RESULTS AND DISCUSSION

The results of the titration are illustrated in figure D.5, and it would appear that neutrality (pH 7) is achieved after adding 5.04 mL of base. The total acidity of the Cu:mb complex was calculated to be 5 meq L^{-1}. We can conclude that Cu:mb complexes contribute a weak buffering capacity to dilute solutions.

Figure D.5.

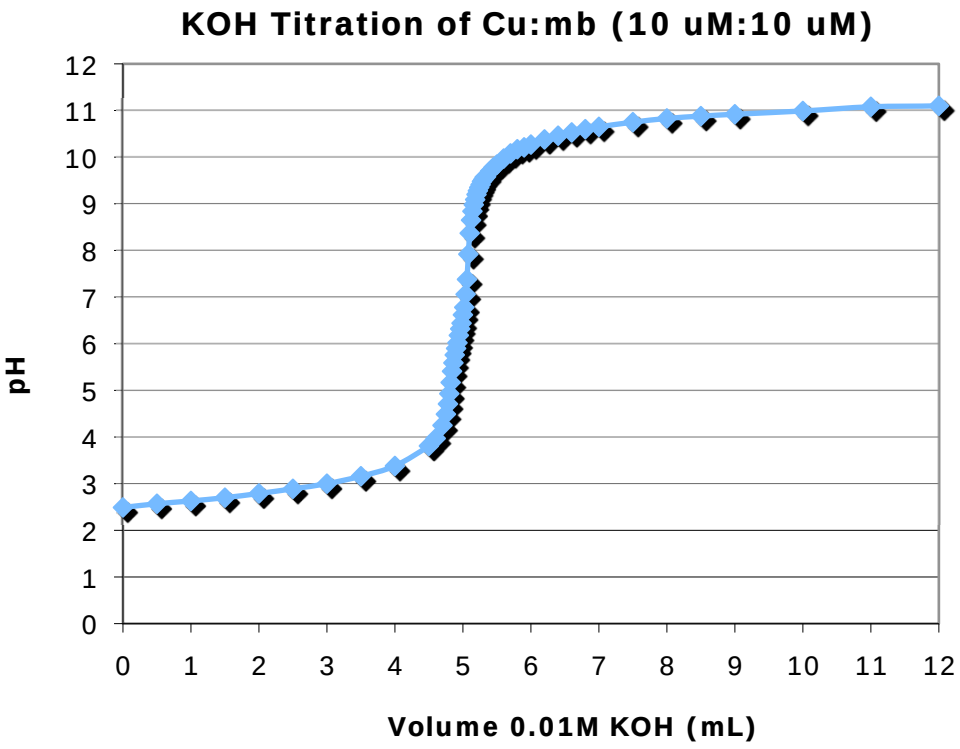
KOH Titration of Cu:mb (10 uM:10 uM)
pH
Volume 0.01M KOH (mL)
0
1
2
3
4
5
6
7
8
9
10
11
12

REFERENCES

Choi D, et al. 2006. Spectral, kinetic, and thermodynamic properties of Cu(I) and Cu(II) binding by methanobactin from Methylosinus trichosporium OB3b. Biochemistry 45: 1142-1453.

Kim HJ, Graham DW, DiSpirito AA, Alterman M, Galeva N, Larive CK, Asunskis D, Sherwood PMA. 2004. Methanobactin, a copper-acquisition compound from methane-oxidizing bacteria. Science 305: 1612-1615.

Appendix E: Cover illustration of PNAS, volume 104, 2007.

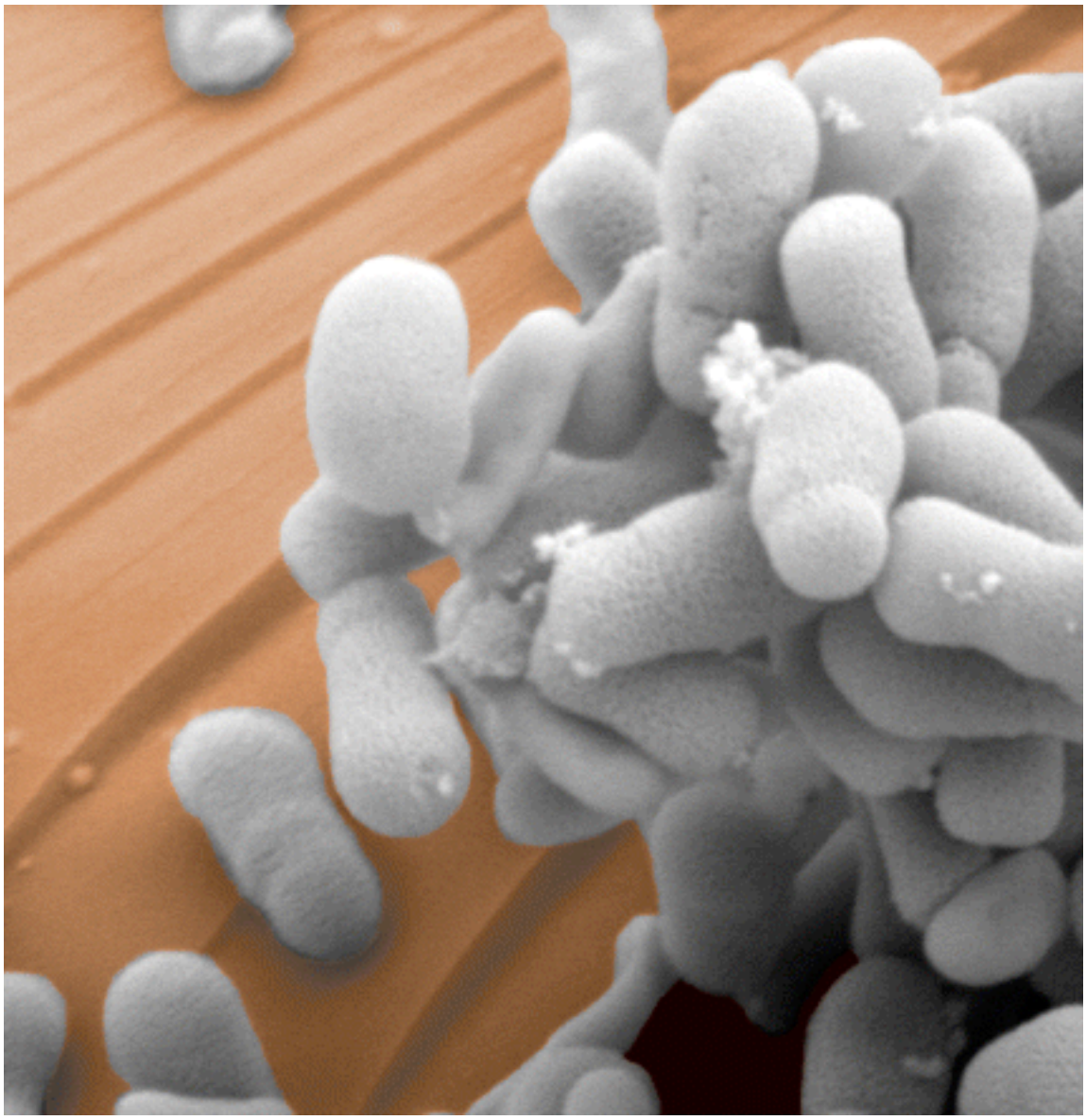

Cover image: Methane-oxidizing bacteria (*Methylosinus trichosporium* OB3b) cluster on copper-doped glass. Methanotrophic bacteria suppress methane, a major greenhouse gas. Expression of the bacterial enzyme methane monooxygenase is regulated by copper. Solid-phase copper geochemistry determines whether the metal is available for use. See the article by Knapp *et al.* on pages 12040–12045. Image courtesy of Ezra Kulczycki.

REFERENCES

Knapp CW, Fowle DA, Kulczycki E, Roberts JA, Graham DW. 2007. Methane monooxygenase gene expression mediated by methanobactin in the presence of mineral copper sources. Proceedings of the National Academy of Sciences 104: 12040-12045.

Appendix F: Scanning electron microscopy images

Figure F.1. SEM image of *Methylosinus trichosporium* OB3b cells colonizing the surface of Cu-substituted borosilicate glass with a Cu concentration of 800 ppm. Cells are coated with Si rich amorphous gel as consequence of 17 hours of reactivity. Silicon rich pricipitates have also formed on the glass surface. Scale bar is 1 μm.

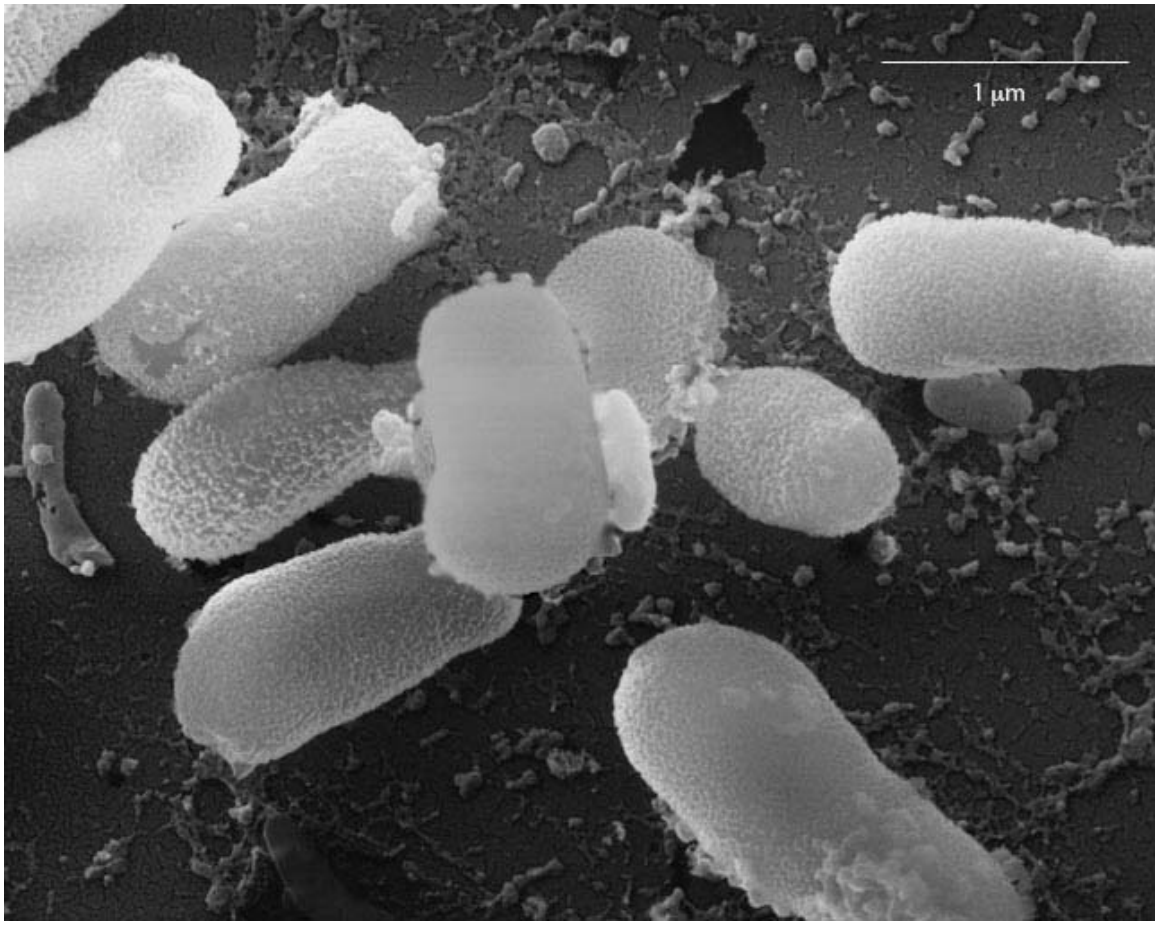

Figure F.2. SEM image of *Methylosinus trichosporium* OB3b cells colonizing the surface of Cu-substituted borosilicate glass with a Cu concentration of 800 ppm. Cells are coated with Si rich amorphous gel as consequence of 17 hours of reactivity. Scale bar is 1 μm.

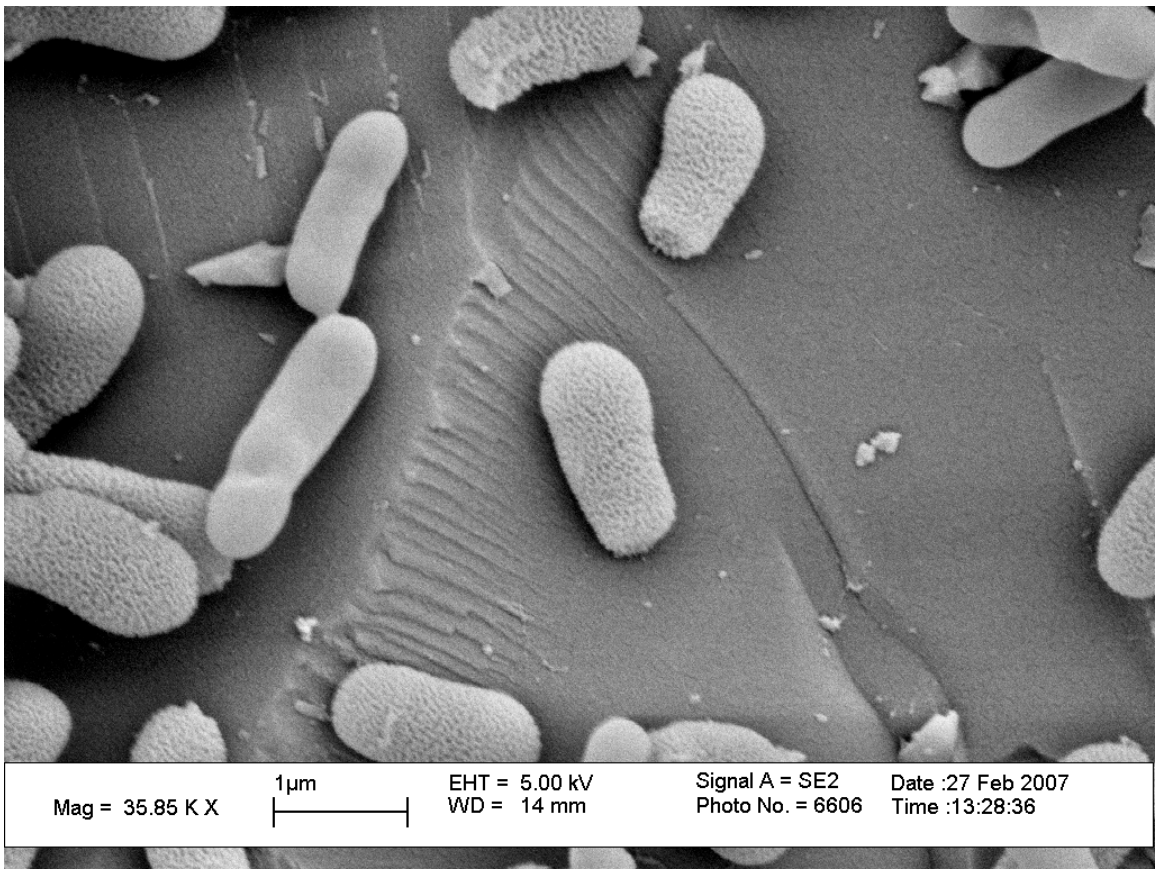

Figure F.3. SEM image of *Methylosinus trichosporium* OB3b cells colonizing the surface of Cu-substituted borosilicate glass with a Cu concentration of 80 ppm after 10 hours of reactivity. Scale bare is 10 μm.

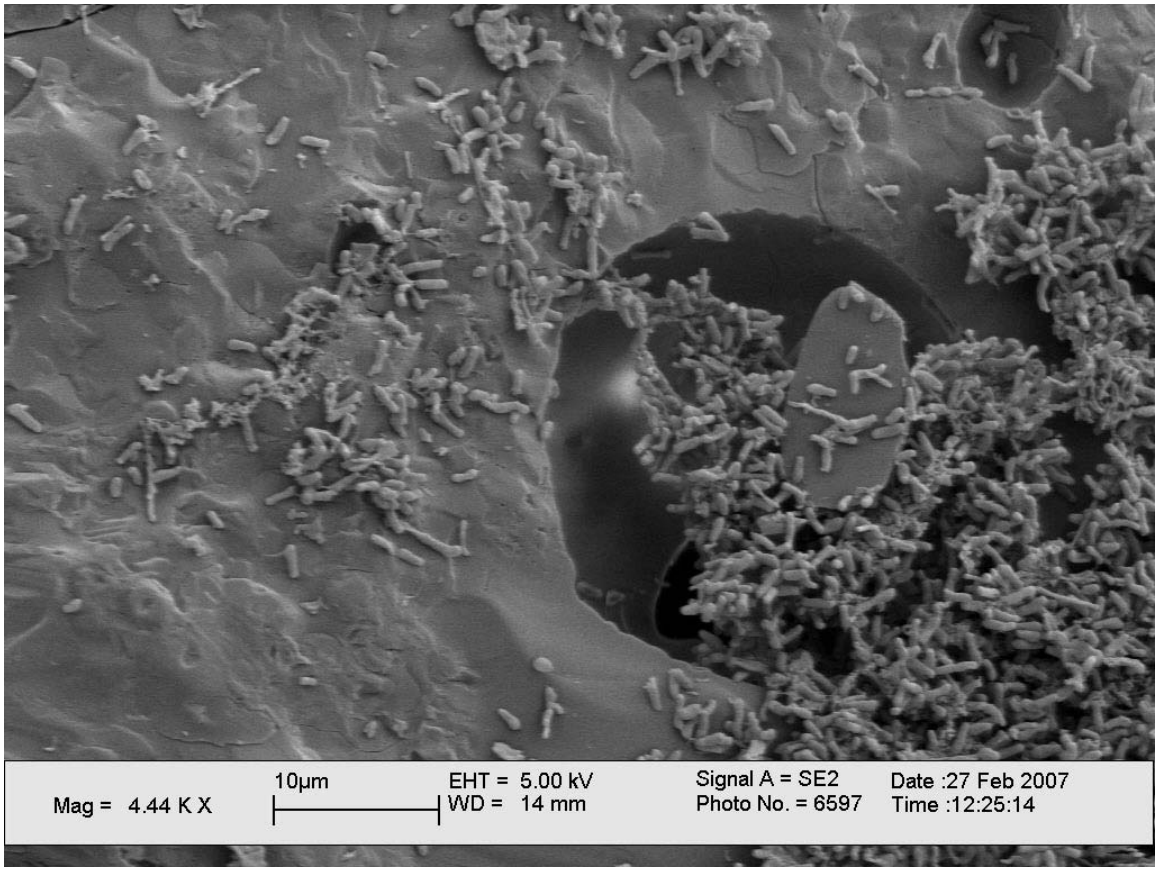

Figure F.4. SEM image of *Methylosinus trichosporium* OB3b cells colonizing the surface of Cu-substituted borosilicate glass with a Cu concentration of 80 ppm after 18.75 hours of reactivity. Scale bare is 1 μm.

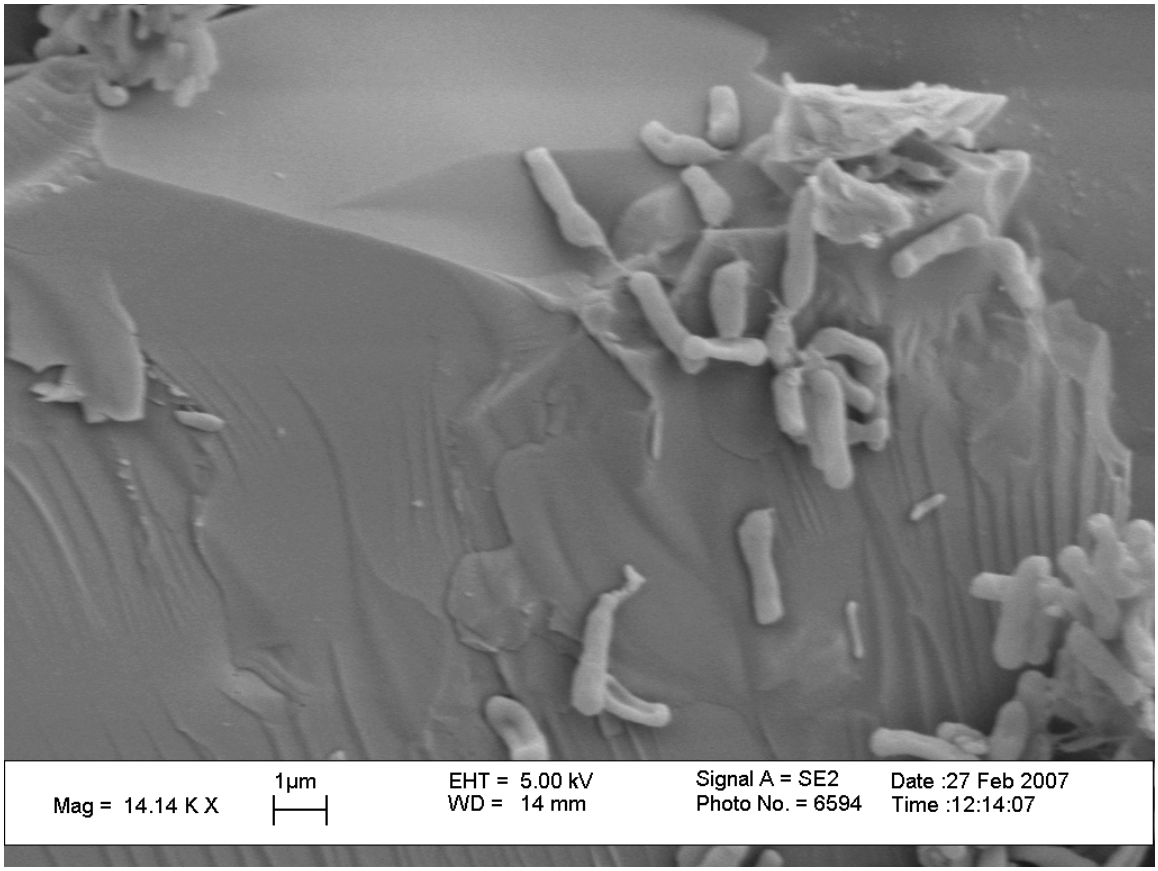

Figure F.5. SEM image of *Methylosinus trichosporium* OB3b cells colonizing the surface of Cu-substituted borosilicate glass with a Cu concentration of 80 ppm after 18.75 hours of reactivity. A heavy Si rich coating has formed on the cells. Scale bare is 1 μm.

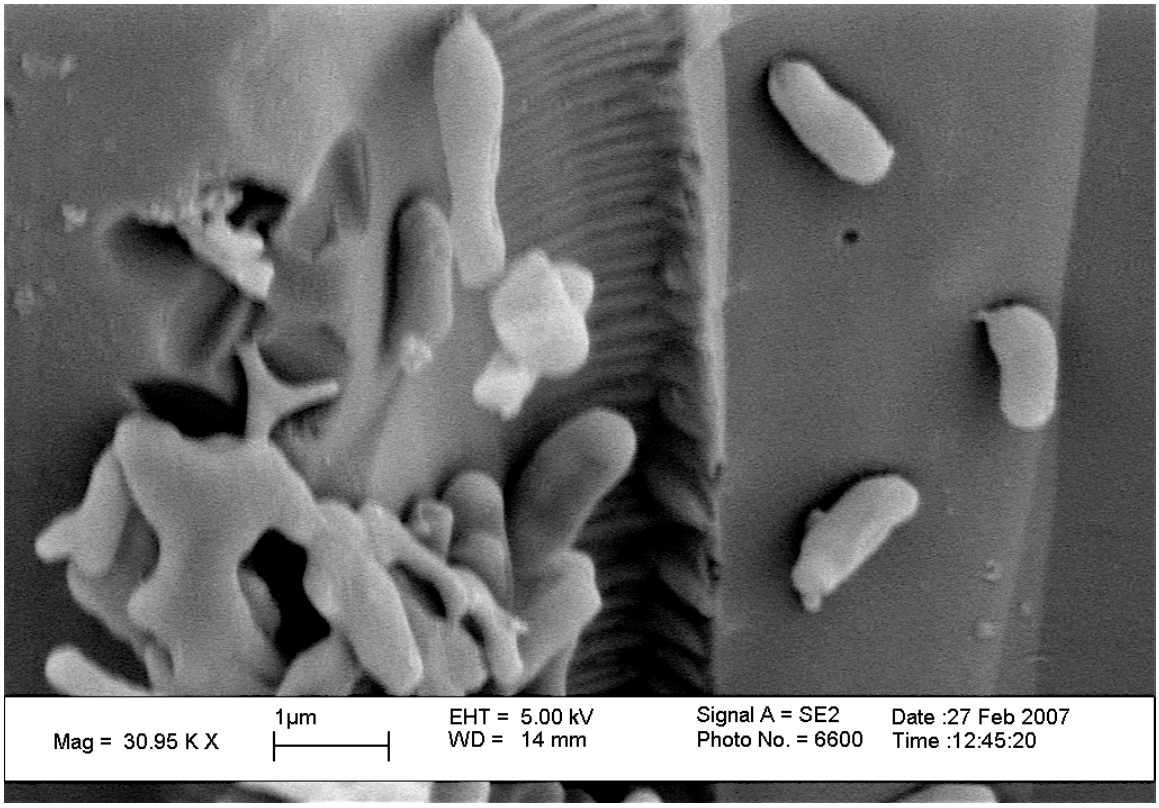

Figure F.6. SEM image of *Methylosinus trichosporium* OB3b cells colonizing the surface of borosilicate glass (Cu concentration of 0 ppm) after 38.5 hours of reactivity. White arrow shows exocellular polymeric material extending from a cluster of cells onto the surface of single location of the glass. Scale bar is 1 μm.

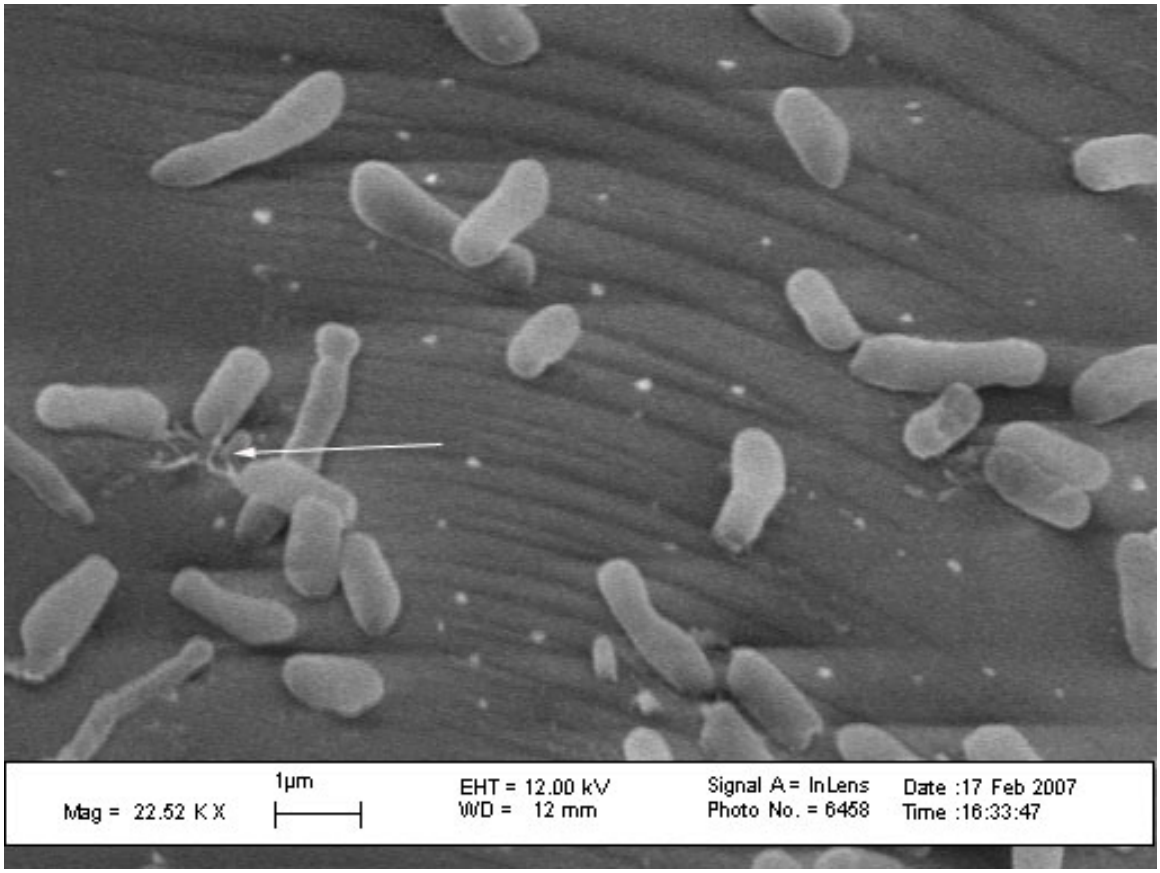

Figure F.7. SEM image of *Methylosinus trichosporium* OB3b cells colonizing the surface of borosilicate glass (Cu concentration of 0 ppm) after 38.5 hours of reactivity. Scale bar is 2 μm.